"DEUTERIUM AND CARBON ISOTOPE EFFECT STUDIES OF THE McLAFFERTY REARRANGEMENT OF SUBSTITUTED BUTYROPHENONES"

A Thesis

Presented for the Degree of

Doctor of Philosophy

in

The University of Adelaide

by

Dennis John Underwood, B. Sc. (Hons)

Department of Organic Chemistry

1980

"This Inquiry, I must confess, is a gropeing in the Dark; but although I have not brought it into a clear light; yet, I can affirm that I have brought it from an utter darkness to a thin mist ....."

John Aubrey, Brief Lives.

CONTENTS

SUMMARY

The objective of the work reported in this thesis was to elucidate the details of the mechanism for the loss of ethylene from molecular cations of various substituted butyrophenones; i.e., the McLafferty rearrangement. Mechanisms proposed for the rearrangement are, (i) stepwise, with hydrogen transfer as the rate determining step, (ii) stepwise, with carbon-carbon bond cleavage as the rate determining step and (iii) concerted.

The approach used in this investigation was to study possible isotope effects for the ion source and first field free region decompositions of 4-($^2H_1$)-*p*-substituted butyrophenones and 4-($^2H_1$)-2-ethyl-*p*-substituted butyrophenones. Deuterium isotope effects were observed for both series of compounds. Trends observed in the isotope effect with Brown's σ_p^+ values are discussed in terms of Westheimer's theory. The possibility that 1,5-hydrogen migration in these systems is an equilibrium situation is also discussed.

In addition, 1-(^{13}C)-butyrophenone, 2-(^{13}C)-butyrophenone, 3-(^{13}C)-butyrophenone and 4-(^{13}C)-butyrophenone were prepared and attempts were made to measure intermolecular carbon-13 isotope effects for loss of ethylene from these compounds. The difficulties involved in such measurements are discussed.

Compounds 3-(^{13}C)-2-ethylbutyrophenone and 4-(^{13}C)-2-ethylbutyrophenone were synthesized and a carbon-13 isotope effect was measured for the field free region reaction of the former. The carbon-13 and deuterium isotope effects and the observation of an α-secondary isotope effect for the reaction of 3-($^{2}H_2$)-2-ethylbutyrophenone are discussed in terms of the possible mechanisms for the process.

Deuterium and carbon-13 isotope effects were calculated using various reactant and transition state models based on the stepwise and concerted mechanisms proposed. The results obtained from the concerted models were shown to reproduce the experimental isotope effects, at least in a semi-quantitative fashion.

Experiments were performed in an attempt to detect the presence of an intermediate in the reaction pathway. Clearly, the existence of such a species precludes the possibility of the operation of the concerted mechanism for the McLafferty rearrangement in this system. Ion-molecule reactions of 4-($^2H_3$)-butyrophenone were investigated but the presence of such an intermediate could not be observed. 2-Allylbutyrophenone was prepared in order to provide an alternative pathway to the McLafferty rearrangement for the proposed intermediate. The mass spectrum of this compound is discussed.

STATEMENT

This thesis contains no material which has been accepted for the award of any other degree or diploma in any University and that, to the best of my knowledge and belief, the thesis contains no material previously published or written by another person except when due reference is made in the text.

D.J. Underwood

ACKNOWLEDGEMENTS

I wish to express my sincere thanks to Dr. J.H. Bowie for his guidance, encouragement, enthusiasm and understanding during his supervision of this work. I would also like to extend my gratitude to the following people; Dr. R.H. Prager for his supervision while Dr. Bowie was on study leave, Dr. P.J. Derrick, Professor A. Fry and Dr. D.E. Lewis for some rewarding discussions and to Mr. T. Blumenthal for his skilful technical advice. In addition, I also wish to express my appreciation of the help given by Dr. K.D. King and Dr. T. Kurucsev in using various computer programs.

My thanks also go to Julie Waite for her patience in typing this manuscript.

Finally, I wish to thank all of my family and friends for their understanding and support. In particular, I am indebted to Lenore, for her encouragement and to Bob and Cathy for their continued support.

CHAPTER 1

AN INTRODUCTION TO ISOTOPE EFFECTS

Much of physical chemistry is concerned with the study of the kinetics, thermodynamics and dynamics of chemical reactions, with the view to delineating as much as possible the potential energy surfaces for these processes. However, many of the experimentally accessible parameters of potential energy surfaces such as equilibrium and rate constants, are of little value by themselves. The procedure of correlating the change in rate or equilibrium constants with changes in molecular structure, for a particular reaction type, adds new meaning to these values. This technique is well known to the physical organic chemist who relies heavily on structure-reacticity relationships such as the Hammett equation[1] and other linear free energy relationships.

The investigation of potential energy surfaces by utilizing the effects of substituents or structural changes on reaction rates and equilibria poses a serious problem in that alteration of the molecular structure necessitates changes in the potential energy surface for the reaction. Thus great care must be used when interpreting relationships between the changes made and the results obtained. In effect, quantitative prediction of substituent effects and structural changes requires a quantum-mechanical analysis of the shifts in electronic potential energy which can then be related to rate constants and thermodynamic parameters. This analysis is generally only feasible for very small molecules and not for polyatomic systems and is therefore of limited application.

A complementary approach to this problem is the measurement and analysis of isotope effects. In general, the effects most usually studied are the changes in rate and equilibrium constants one observes on substituting various atoms with their isotopes. The

unique feature of an isotope effect is that it is determined by a single potential energy surface (Born-Oppenheimer approximation), and consequently isotope effects provide a probe of the nature of a single transition state† which is in contrast to ordinary substituent effects. The technique of combining substituent effects with isotope effects can, for the reasons outlined above, be a powerful aid in the elucidation of reaction mechanisms.

As with reaction rates, there has been less emphasis placed on the absolute magnitude of isotope effects than on correlations describing their variation from one reaction to another. In particular Westheimer's theory concerning the relationship between the magnitude of the isotope effect and the structure of the transition state, has been particularly valuable. This theory has led to much experimental and theoretical work, often leading to particularly illuminating results. In fact it appears that no study of kinetic isotope effects can be complete without resorting to Westheimer's theory.

The remainder of this introduction will be concerned with describing the fundamental origins of isotope effects with the aim of providing the information necessary for interpreting the work described in later parts of this thesis. Much of the basic theory of isotope effects has been extensively reviewed[2-13].

The Origins of Isotope Effects

Isotopic substitution of particular atoms within a molecule

---

† The term activated complex has the same meaning as transition state.

can lead to isotope effects which are either kinetic or thermodynamic in nature. In the case of the kinetic isotope effect, the rate equations are concerned with a reactant system and a transition state that leads to the required products. Equilibrium isotope effects, on the other hand, are concerned only with the properties of reactant and product systems. Since they are by definition thermodynamic in nature, they have no basis in the properties of the transition state which separates the reactant and product regions on a potential energy surface. Equilibrium isotope effects, being concerned only with stable species, are more readily evaluated in terms of structural changes and more amenable to calculation than kinetic isotope effects. Calculation of kinetic isotope effects requires a detailed knowledge of the structure of both reactants and the transition state.

Isotope effects can be considered to be either primary or secondary depending on the position of isotopic substitution relative to the reaction site. Primary isotope effects are observed when a bond to the isotopically substituted atom is either formed or broken during the course of the reaction. Secondary isotope effects result when bonds to the isotopically substituted atom are neither formed nor broken during the reaction. Following Halevi[14], secondary effects can be subdivided into those that result from spatial changes in the isotopic atom and those that do not. The first of these is the α-secondary isotope effect and is due in the main to re-hybridization effects[15]. A distinguishing, but not definitive relationship between primary and α-secondary hydrogen isotope effects is that the latter are usually much smaller in value (around k_H/k_D 1.15).

The second division of the secondary isotope effect (viz.

those not resulting from spatial changes) has as its basis hyperconjugative and inductive effects[16]. Isotopic substitution at sites further from the reaction site than the β position result in much smaller isotope effects which are consequently both difficult to explain and to treat physically.

The Born-Oppenheimer Approximation

The fundamental point of any discussion of the properties of potential energy surfaces in general and isotope effects in particular, is the Born-Oppenheimer approximation[17]. This approximation, which for most practical purposes may be regarded as exact, is based on the very large differences between the masses of nuclei and of the electrons of a molecule. It assumes that the electronic distribution in a molecule can be evaluated within a static nuclear framework. This results from the expectation that the electronic distribution will change instantaneously with nuclear motion (such as in the vibration of a bond or the complex movements of nuclei during rearrangement reations). On this basis it can be seen that the potential energy surface is not a function of isotopic substitution.

As a consequence of this simplifying assumption the notion and calculation of potential energy surfaces becomes meaningful; the nuclear conformation changes can be described with respect to molecular energy changes. If the Born-Oppenheimer approximation were to fail, as in the case of rapidly moving nuclei, then the notion of a potential energy surface would no longer be meaningful.

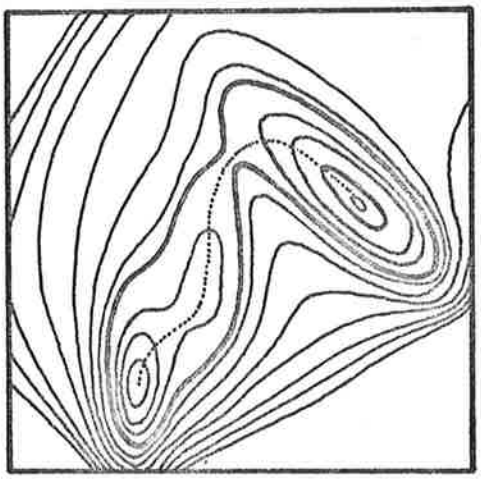

Potential Energy Contour Diagram

Saddle Point

Figure 1-1

Absolute Rate Theory

The formalism of kinetic isotope effect theory is founded in the absolute rate theory (or transition state theory) of Eyring and Polanyi[18,19], which is entirely classical in nature. The basic premise of this theory is the existence of a transition state through which suitable reactant molecules pass to products. A transition state is defined as the configuration of the reacting system at the col or saddle point on a potential energy surface, which is the point of maximum energy along the reaction path. Figure 1-1 shows a portion of a potential energy surface in the form of a contour diagram. The diagram shows the existence of two stable species in potential wells which can interconvert by crossing a high energy col or saddle point. The molecular configuration at the saddle point is

the transition state. This state of the system is a condition of dynamical instability. Motion to one side of the saddle point qualitatively differs in character from motion to the other side. In effect, the choice of the transition state to be the configuration at the maximum of potential energy along the reaction path, is an oversimplified feature of absolute rate theory[20]. A more rigorous treatment which involves considering reactions in terms of free energy surfaces, demands that both entropic and energetic effects be evaluated together. The criterion of maximizing free energy with respect to the atomic coordinate changes for a particular reaction in order to locate the transition state, is the basis for the application of canonical variational theory to generalized absolute rate theory (of which absolute rate theory is a part). The methods of the canonical variational treatment of absolute rate theory are described by Garrett and Truhlar[21,22].

Another assumption of absolute rate theory is the so-called "equilibrium" existing between the reactants and the transition state. Since our only knowledge of the transition state is our preconceived ideas about its location, then any attempt to describe the energy distribution of this state will be met with difficulties. However, in the absence of the desired knowledge about the energy distribution one is forced to make an educated guess. The least-biased guess that can be made is that all partitionings of the given energy of the transition state are equally probable. This allows one to make the least assumptions about the transition state.

The least-biased approach then allows the application of statistical mechanics to the derivation of the absolute rate theory equations[20,23]. Statistical mechanics has been applied extensively

to equilibrium situations which has led to the misunderstanding that its use in absolute rate theory presumes an equilibrium between reactants and the transition state. The least-biased approach, as described above, is part of a general procedure called information theory used for making educated guesses[25].

Consider the generalized bimolecular gas phase reaction in scheme 1-1,

$$A + B \longrightarrow X^{\neq} \longrightarrow D + E$$

Scheme 1-1

where $X^{\ddagger}$ denotes the critical configuration referred to as the transition state. The rate of reaction is simply the product of the concentration of the transition state species and the average velocity of motion of these species over the potential energy barrier from the reactant region to the product region.

By applying standard equilibrium statistical mechanics[24] to the populations of reactants and transition states, the concentration of transition states can be evaluated as shown in equation 1-1,

$$[X^{\ddagger}] = [A][B]. \frac{Q_X^{\ddagger}}{Q_A Q_B} \cdot e^{-\varepsilon_0/k_B T} \qquad \text{Equation 1-1}$$

where [ ] denotes the number per unit volume, Q the partition function per unit volume for each of the species involved, ε_0 is the potential energy at the saddle point, k_B is the Boltzmann constant and T is the absolute temperature. In the transition state, the

degree of freedom corresponding to motion along the reaction path, which is the path requiring the least energy to traverse from reactants to products, is separable from the other degrees of freedom of the transition state and is treated as a one dimensional translational function[19,20,26]. The rate of reaction, being the concentration of transition state species multiplied by the average velocity of passage of these species over the potential energy maximum from reactant to products, is described in equation 1-2[27].

$$\text{rate} = [A][B] \cdot \frac{k_B T}{h} \cdot \frac{Q^{\ddagger}}{Q_A Q_B} \cdot e^{-\varepsilon_0 / k_B T} \qquad \text{Equation 1-2}$$

In equation 1-2, h is the Planck constant and $Q^{\ddagger}$ is the partition function per unit volume for the transition state without the degree of freedom corresponding to the reaction coordinate. As a result, the partition functions Q_A and Q_B describe 3N-6 (or 3N-5 for linear molecules) degrees of freedom whereas $Q^{\ddagger}$ describes 3N-7 degrees of freedom (where N denotes the number of atoms in each species). Consequently, the classical rate constant described in terms of absolute rate theory is given in equation 1-3,

$$k(T) = \kappa \cdot \frac{k_B T}{h} \cdot \frac{Q^{\ddagger}}{Q_A Q_B} \cdot e^{-\varepsilon_0 / k_B T} \qquad \text{Equation 1-3}$$

where κ is the transmission coefficient (omitted from equation 1-2 for simplicity). The transmission coefficient expresses the probability that a reactant system (suitably activated or not) moving towards the product region of a potential energy surface, will in fact reach the product region. There are two components of the transmission coefficient both of which will be discussed in a later section.

The computation of the thermal rate constant is reduced to the

calculation of partition functions for the reactant system and the transition state. These calculations require a knowledge of the potential energy of the reacting system as a function of the particular atomic coordinates which change during the reaction. The transition state configuration, however, is rarely known and therefore must be modelled from stable systems or calculated.

Calculation of potential energy surfaces by solution of the Schrödinger equation (the so-called *ab initio* approach) has received much attention. The results of these calcuations are discouraging, however, for all but the simplest of systems. A limiting characteristic of the *ab initio* approach is the large amount of computing time required for even simple polyatomic species. The computational effort depends not only on the procedures used for localizing the transition state, but also on the complexity of the energy hypersurface. There are other factors contributing to the effort required, such as the availability of suitable starting points for saddle point location (often obtained by using simpler semi-empirical methods), the desired density of path points for the description of the reaction path and the numerical accuracy required for the calculation of molecular structures. Many of these factors are discussed by Müller[28] in a recent review covering the problems of calculating reaction paths on multi-dimensional energy hyper-surfaces.

Due to the inherent difficulties of the *ab initio* approach to potential energy surface calculations, one is often forced to adopt a semi-empirical approach[29] (such as CNDO, complete neglect of differential overlap; INDO, intermediate neglect of differential overlap; or MINDO, modified INDO), or a completely empirical stance

(BEBO, which is the bond energy bond order method of Johnston [4]).

Potential Energy Hypersurfaces

A chemical reaction is conveniently discussed in terms of a reaction potential energy profile covering aspects of mechanism, structure and energy. According to absolute rate theory, as a reactant system evolves with respect to a particular reaction, it passes from the energy minimum of the reactant state through an unstable transition state of higher energy to the energy minimum of the product state. This description is simplistic in that little emphasis is placed on the necessary structural changes taking place in the molecular system which give rise to these potential energy changes.

The reaction coordinate can be visualized as those molecular changes which occur in a particular reaction giving rise to the desired products, while requiring the minimum in energy changes (see figure 1-1). Thus the reaction coordinate is a complex function of structural changes characterizing the chemical transformation and in this respect requires a multidimensional potential energy function.

The theoretical treatment of a chemical reaction requires the detailed knowledge of the potential energy of a molecular system in terms of all internal degrees of freedom. This pre-requisite is independent of whether a static description of the reaction is pursued (e.g., by localizing the minimum energy path), or whether a dynamic treatment of reactivity is attempted (e.g., by computing numerous trajectories over which the molecular system oscillates along the reaction coordinate). Thus, the potential energy of a

system being a function of many parameters does not lend itself to graphic representation. A one parameter potential energy function, such as that describing diatomic systems, can easily be represented by a two dimensional graph. A two parameter potential energy function can be visualized by a three-dimensional relief or by a two-dimensional contour diagram. However, a multi-parameter energy function can only be considered as a hypersurface in multi-dimensional configurational space. Unless the motion of the atoms in a polyatomic system undergoing reaction can be generalized to a one or two parameter reaction coordinate, then a description in terms of the potential energy hypersurface is conceptually quite difficult.

Formally[30], the potential energy hypersurface of an elementary reaction is a set of points in (n+1)-dimensional configuration - energy space; each point represents the energy associated with one of all possible nuclear configurations of the system. The general point on the surface is $(r_1, r_2, \ldots . r_n, V)$ where the coordinates r_i, i=1,2,.....,n represent the n internuclear distances sufficient to describe any configuration and V is the corresponding potential energy. For a reaction involving N nuclei, the dimension n of configuration space is given by equation 1-4.

$$n = \begin{cases} 1 & \text{if } N=2 \\ 3N-6 & \text{if } N \geqslant 3 \end{cases} \qquad \text{Equation 1-4}$$

The Formalism of the Kinetic Isotope Effect

The isotope effect on reaction rates can be expressed in terms of the ratio of the isotopic rate constants for the reaction. By convention, this ratio is expressed as the rate constant for the light isotope relative to the rate constant of the heavy isotope.

The isotopic rate constant ratio, equation 1-5, is derived from equation 1-3 and therefore encompasses all of the basic assumptions of absolute rate theory.

$$\frac{k_1(T)}{k_2(T)} = \frac{\kappa_1}{\kappa_2} \cdot \frac{Q_1^{\ddagger}}{Q_2^{\ddagger}} \cdot \frac{Q_{A2}\, Q_{B2}}{Q_{A1}\, Q_{B1}} \cdot e^{(\varepsilon_{01} - \varepsilon_{02})/k_B T}$$

Equation 1-5

As discussed previously, evaluation of partition functions and transmission coefficients requires a detailed knowledge of the potential energy surface particularly in the reactant and the saddle point regions. This information however is rarely known, and as a direct result of this limiting aspect it becomes necessary to resort to approximate procedures in the evaluation of the partition functions. However, one advantage of studying kinetic isotope effects is that when ratios of rate constants are taken, then the approximations used in the practical application of the theory tend to cancel. Due to this simplification, it then becomes possible to predict isotope effects on the rate constant for a reaction with far greater reliability than prediction of the rate constant itself. It thus becomes reasonable to attempt to evaluate the isotope effect for reactions so complex that the prediction of the rate constant could not be attempted.

The partition functions contained in the kinetic isotope expression (equation 1-5) are particularized in the following conventional manner. The energy of a molecule containing N atoms is described in terms of 3N independent degrees of freedom corresponding to three translations and three rotations (two if the molecule is linear), and 3N-6 internal vibrations (3N-5 for linear molecules). The internal vibrations are described by harmonic oscillator partition

functions while the translations and rotations of the system as a whole are treated as classical degrees of freedom. In deriving the classical absolute rate theory expression one of the internal degrees of freedom of the transition state is separated from the partition function as a translation. This degree of freedom has a zero or imaginary frequency and is designated as $\nu_L^{\ddagger}$. Thus the number of internal degrees of freedom for the transition state is 3N-7, (or 3N-6 for linear transition states).

The rate ratio including the appropriate translational, rotational and harmonic oscillator partition functions is described by equation 1-6[31-34], where separability of energy into translational rotational and vibrational degrees of freedom is assumed.

$$\frac{k_1(T)}{k_2(T)} = \frac{\kappa_1}{\kappa_2} \cdot \frac{\dfrac{S_1}{S_2}}{\dfrac{S_1^{\ddagger}}{S_2^{\ddagger}}} \cdot \frac{\left(\dfrac{M_2}{M_1}\right)^{3/2}}{\left(\dfrac{M_2^{\ddagger}}{M_1^{\ddagger}}\right)^{3/2}} \cdot \frac{\left(\dfrac{IA_2\, IB_2\, IC_2}{IA_1\, IB_1\, IC_1}\right)^{1/2}}{\left(\dfrac{IA_2^{\ddagger}\, IB_2^{\ddagger}\, IC_2^{\ddagger}}{IA_1^{\ddagger}\, IB_1^{\ddagger}\, IC_1^{\ddagger}}\right)^{1/2}} \cdot$$

$$\frac{\prod_{i}^{3N-6} \left(\dfrac{1 - e^{-u_{i1}}}{1 - e^{-u_{i2}}}\right)}{\prod_{i}^{3N-7} \left(\dfrac{1 - e^{-u_{i1}^{\ddagger}}}{1 - e^{-u_{i2}^{\ddagger}}}\right)} \cdot \frac{\exp\left[\sum_{i}^{3N-6} (u_{i1} - u_{i2})/2\right]}{\exp\left[\sum_{i}^{3N-7} (u_{i1}^{\ddagger} - u_{i2}^{\ddagger})/2\right]}$$

Equation 1-6

In equation 1-6, M refers to the molecular mass, IA, IB, IC are the three principle moments of inertia, S is a symmetry number and u_i is defined in equation 1-7,

$$u_i = \frac{h\nu_i}{k_B T} \qquad \text{Equation 1-7}$$

where ν_i is the frequency of the ith internal degree of freedom. The symmetry number is defined as the total number of independent permutations of atoms (or groups) in a molecule that can be arrived at by simple rigid rotations of the entire molecule. When symmetry numbers are omitted from all rotational partition functions, S then becomes the reaction path multiplicity[4,20,35].

Equation 1-6 can be abbreviated in a conventional way to give equation 1-8,

$$\frac{k_1(T)}{k_2(T)} = \frac{\kappa_1}{\kappa_2} \cdot \frac{S_1 S_2^{\ddagger}}{S_2 S_1^{\ddagger}} \cdot \text{MMI} \cdot \text{EXC} \cdot \text{ZPE} \qquad \text{Equation 1-8}$$

where MMI represents the product of the masses and moments of inertia. The EXC or excitation factor includes the product over that part of the harmonic oscillator partition function which accounts for the population statistics of upper levels of vibration. The zero-point energy term ZPE, accounts for the difference in vibrational zero-point energy between the reactants and the transition state.

Within the harmonic approximation, the isotopic sensitivity of the classical translational and rotational partition functions is related to the vibrational frequencies of a molecule according to the Teller-Redlich product rule[36,37]. This rule is stated in equation 1-9,

$$\left(\frac{M_1}{M_2}\right)^{3/2} \cdot \left(\frac{IA_1 IB_1 IC_1}{IA_2 IB_2 IC_2}\right)^{1/2} = \prod_j^N \left(\frac{m_{j1}}{m_{j2}}\right)^{3/2} \cdot \prod_i^{3N-6} \frac{\nu_{i1}}{\nu_{i2}}$$

Equation 1-9

where m_j represents the mass of the isotope. Applying the product rule to equation 1-6 and abbreviation the terms as in equation 1-8 one obtains equation 1-10,

$$\frac{k_1(T)}{k_2(T)} = \frac{S_1 S_2^{\ddagger}}{S_2 S_1^{\ddagger}} \cdot \frac{\kappa_1}{\kappa_2} \cdot \frac{\nu_{1L}^{\ddagger}}{\nu_{2L}^{\ddagger}} \cdot VP \cdot EXC \cdot ZPE \qquad \text{Equation 1-10}$$

where VP refers to the vibrational frequency product and is defined in equation 1-11.

$$VP = \frac{\prod_{\pi}^{3N-6} \frac{u_{2i}}{u_{1i}}}{\prod_{\pi}^{3N-7} \frac{u_{2i}^{\ddagger}}{u_{1i}^{\ddagger}}} \qquad \text{Equation 1-11}$$

The ratio $\nu_{1L}^{\ddagger} / \nu_{2L}^{\ddagger}$ results from the requirement that the product of the vibrational frequencies for the transition state is taken over 3N-7 internal degrees of freedom. One degree of freedom for this product is therefore factored out from equation 1-9.

The harmonic rate ratio (equation 1-10) approaches the ratio $\nu_{1L}^{\ddagger} / \nu_{2L}^{\ddagger}$ at infinite temperatures. Accordingly this ratio is known as the classical rate ratio or the temperature independent factor (TID)[38]. It is the isotopic ratio of the imaginary frequencies corresponding to the negative curvature of the potential energy surface in the direction of the reaction coordinate at the saddle point. The classical nature of the TID factor emphasises Stern and Wolfsberg's dictum[39] that there is no quantum-mechanical isotope

effect unless there are bond force constant changes between the reactants and the transition state.

The value of $\nu_L^{\ddagger}$ is related to the shape of the potential energy surface at the saddle point and hence to the tunnelling factor required to correct the classical absolute rate theory equation. However, some authors have alluded to the quantum-mechanical nature of $\nu_L^{\ddagger}$ [40] which denies its origins in classical absolute rate theory.

The fundamental difference between equilibrium and kinetic isotope effects can be clearly seen in the behaviour of the absolute rate theory equations at infinite temperatures. The limiting form of the kinetic equations at infinite temperatures is the classical ratio $\nu_{1L}^{\ddagger} / \nu_{2L}^{\ddagger}$ as discussed previously. This result is to be contrasted with all equilibrium isotope effects which vanish at very high temperatures. This can be readily understood when one considers that in the derivation of the rate equations, the kinetic situation requires intimate knowledge of the transition state, whereas the equilibrium case, being concerned with thermodynamics does not require knowledge of any transition states or intermediates.

Originally, the upper limit for the TID factor for the simple bond rupture case was thought to be the Slater coordinate value[41] which is the square root of the inverse of the reduced masses of the atoms forming the bond as shown in equation 1-12.

$$\frac{\nu_{1L}^{\ddagger}}{\nu_{2L}^{\ddagger}} = \left(\frac{\mu_2}{\mu_1}\right)^{1/2} \qquad \text{Equation 1-12}$$

This limit, however, is not consistent with the transition state approach excepting when the reaction coordinate involves the motion of two atoms. Consequently Bigeleisen and Wolfsberg[33] proposed

that a more reasonable formulation would be to choose the coordinate which separates the two fragments. This leads to equation 1-13,

$$\frac{\nu_{1L}^{\ddagger}}{\nu_{2L}^{\ddagger}} = \left(\frac{1/\mu_{\alpha_1} + 1/\mu_{\beta_1}}{1/\mu_{\alpha_1} + 1/\mu_{\beta_2}} \right)^{1/2} \qquad \text{Equation 1-13}$$

in which μ_α and μ_β refer to the reduced masses of the separating fragments. Evaluation of this equation leads to the fragment coordinate value. This value will only be approximate however, unless the two separating fragments lie on the extension of the line corresponding to the broken bond[34]. Bigeleisen and Wolfsberg have also considered the TID factor in three centred reactions[42] a discussion of which is given by Melander[2].

The TID factor in equation 1-10 results from the application of the Teller-Redlich product rule (equation 1-9) to equation 1-8. Comparison of equation 1-8 with equation 1-10 yields a relationship between the TID factor and the partition functions VP and MMI given in equation 1-14.

$$\frac{\nu_{1L}^{\ddagger}}{\nu_{2L}^{\ddagger}} = \frac{MMI}{VP} \qquad \text{Equation 1-14}$$

Many computer programs which calculate isotope effects by evaluating the partition functions described in equation 1-8, arrive at the TID factor by the relationship in equation 1-14.

The Heavy Atom Approximation

Equation 1-10 describes the general form of the harmonic rate ratio. A variant of this equation describing heavy atom (carbon and heavier elements) isotope effects was initially introduced by

Bigeleisen and Göeppert-Mayer[31] for isotope exchange equilibria and then carried over to reaction rates by Bigeleisen[32]. Equation 1-15 describes this formulation,

$$\frac{k_1(T)}{k_2(T)} = \frac{S_1S_2^{\ddagger}}{S_2S_1^{\ddagger}} \cdot \frac{\kappa_1}{\kappa_2} \cdot \frac{\nu_1 L^{\ddagger}}{\nu_2 L^{\ddagger}} \left(1 - \sum_{i}^{3N-7} G(u_i^{\ddagger})\, \Delta u_i^{\ddagger} + \sum_{i}^{3N-6} G(u_i)\Delta u_i \right)$$

Equation 1-15

where Δu_i is defined by equation 1-16 and G(u) is a function of u described in the original papers[31,32] and by Melander[2] and Van Hook[10].

$$\Delta u_i = u_{1i} - u_{2i} = \frac{h(\nu_{1i} - \nu_{2i})}{k_B T}$$

Equation 1-16

In deriving equation 1-15, Bigeleisen and Göeppert-Mayer made the assumption that Δu is small compared to u; that is they took the limiting cases of either heavy atom isotope effects (small $\nu_{1i} - \nu_{2i}$) or high temperatures. As a result this equation is in a very convenient form for the qualitative and quantitative evaluation of many heavy atom isotope effects[43].

Zero-Point Energy Terms

Many of the approximate forms of the harmonic rate ratio expression (equation 1-10) assume that the major contributor to the difference in rates of reaction on isotopic substitution is the ZPE term[2]. This is particularly true when considering primary isotope effects on reactions involving hydrogen transfer between two heavy atoms or groups. In these cases the hydrogen isotope is close to the centre of mass and isotopic substitution should lead to effectively no change in molecular mass or moments of inertia. However, it must be

noted that all terms in equation 1-10 may contribute significantly to the isotope effect. This is emphasised in calculations performed by Wolfsberg and Stern[34] indicating that there does not appear to be any simple set of correlations which express the complicated interplay of the various terms in equation 1-10. Nevertheless, the ZPE term appears to be dominant in many cases and its importance demands further discussion.

The existence and magnitude of the zero-point energy follows from any quantum-mechanical treatment of the oscillator and in particular from an understanding of the uncertainty principle. If the system existed in the motionless state represented by the lowest point in the potential energy well describing its oscillation, then both its position and momentum would be known exactly thereby contravening the uncertainty principle. The quantum-mechanical description of the zero point energy level yields probability distributions for both the position and momentum, which then satisfies the uncertainty principle.

In the case of a simple diatomic molecule within the harmonic oscillator approximation, the zero-point energy of a molecular vibration having a frequency of ν_0 (Hertz) is given by equation 1-17,

$$\varepsilon_0 = \tfrac{1}{2} h\nu_0 \qquad \text{Equation 1-17}$$

where ε_0 is the zero point energy, h is the Planck constant and c the velocity of light. The frequency of vibration is related to the bond force constant f, and the effective mass of the vibration m* by equation 1-18.

$$\nu_0 = \frac{1}{2\pi} \left(\frac{f}{m^*}\right)^{1/2} \qquad \text{Equation 1-18}$$

The effective mass is determined by only those atoms which are in motion with respect to the reaction coordinate. Johnston has defined the effective mass for situations ranging from a simple translation of a non-rotating, non-vibrating molecule to the general case of a rotating, translating, vibrating, linear triatomic[4].

The bond force constant is a characteristic of the potential energy surface for the molecule and is a measure of the change in potential energy which occurs with changes in the position of the atoms involved in a vibration. For small displacements of the atoms Δr from their equilibrium internuclear distance r_e, the two dimensional potential energy curve (diatomic case) can be approximated by a parabola. Figure 1-2 shows that for small displacements, the simple parabolic function adequately approximates the Morse function[4],

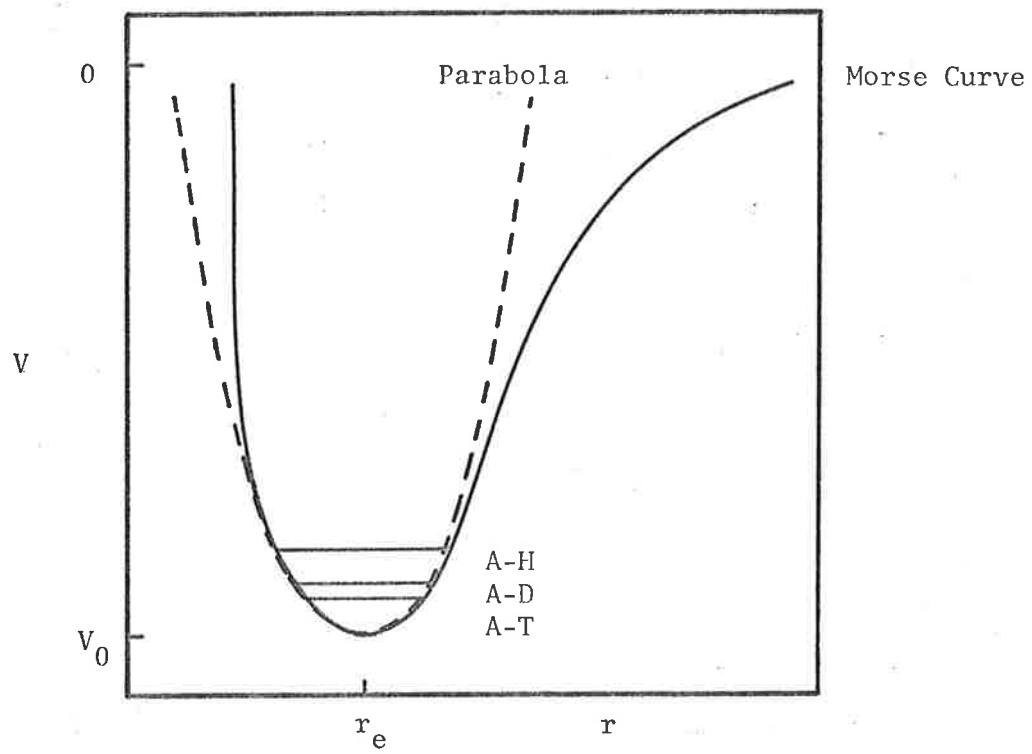

Figure 1-2

which is a better description of the change in potential energy with bond distance for the diatomic molecule. In figure 1-2, V is the potential energy, V_0 the energy at the bottom of the potential well, r is the internuclear distance in the diatomic A-H and r_e is the equilibrium internuclear distance. Equation 1-19 describes the parabola in terms of the change in potential energy accompanying change in internuclear separation for a particular bond force constant.

$$\Delta V = V - V_0 = \tfrac{1}{2} f \Delta r^2 \qquad \text{Equation 1-19}$$

The bond force constant corresponds to the curvature of the potential energy curve at its minimum and is therefore defined by equation 1-20.

$$f = \left(\frac{\partial^2 V}{\partial \Delta r^2}\right)_{r_e} \qquad \text{Equation 1-20}$$

The potential energy, and hence the force constants of a molecule are, by virtue of the Born-Oppenheimer approximation, unaffected by isotopic substitution. The zero-point energy, on the other hand, changes with isotopic substitution since there is a change in effective mass (see equation 1-18 and 1-17). For a simple diatomic hydride A-H, or more generally a system which can be approximated to one, the effective mass is equivalent to the reduced mass μ as defined in equation 1-21. For more complex systems involving for example non-linear motion of the isotope or rotations, this relationship is not necessarily valid.

$$\frac{1}{\mu} = \frac{1}{m_A} + \frac{1}{m_B} \qquad \text{Equation 1-21}$$

A simplifying feature of hydrogen isotope effects is that the mass of the atom (or group) to which the hydrogen is bound, is usually much larger than that of the hydrogen isotope which results in the effective mass of the vibration reducing to the mass of the isotope. This simplification takes into account the fact that with large atoms (or groups), most of the motion of the vibration is by the hydrogen isotope. As a result of this the change in zero-point energy on substitution of hydrogen for deuterium is given by equation 1-22.

$$\Delta\varepsilon_0\ (H,D) = \tfrac{1}{2}h\ (\nu_H - \nu_D) = \frac{hf^{1/2}}{4\pi}\left(\frac{1}{m_H^*} - \frac{1}{m_D^*}\right)^{1/2}$$

Equation 1-22

From equation 1-22 it is clear that the magnitude of the change in zero-point energy on isotopic substitution is dependent on the size of the force constant. It is the possibility of a difference in force constant between the reactants and transition state (kinetic situation) or between reactants and products (equilibrium situation) that leads to isotope effects on rates and equilibria. This re-emphasises Wolfsberg and Sterns dictum[39] mentioned previously.

In many respects, hydrogen vibrations in polyatomic molecules are similar to those of diatomics. Polyatomic molecules however, possess bending as well as stretching vibrations. Assuming that the effective mass for the bending vibration is again equal to the mass of the hydrogen isotope, and that the bond lengths to the isotope are approximately the same for all of the hydrogen isotopes[44] then the shift in zero point energy is again $2^{-1/2}$ as shown in equation 1-22.

The validity of the assumptions used in deriving the simplistic zero-point energy equation (equation 1-22) can be estimated by consideration of the experimental vibrational frequencies of chloroform and deuterochloroform[45]. This comparison indicates that the isotopic shift for both stretching and bending frequencies is slightly less than $2^{-1/2}$. There are probably two major reasons for this. The first is attributable to the inaccuracy of assigning the mass of the hydrogen isotope to the effective mass. Secondly, and possibly more importantly, the inconsistency is due to mechanical coupling of hydrogen motions with other atomic motions resulting in the "spreading" of isotopic sensitivity between all of the molecule's vibrations. Anharmonic effects, although present, are expected to be very small for zero-point energy differences.

The Westheimer Effect

Primary hydrogen kinetic isotope effects typically vary from k_H/k_D 2 to 10 from one reaction to another. Prior to 1961 there was no satisfactory reason for why this should be so. It was realized, however, that the larger values of the isotope effects that were observed roughly corresponded to the difference in zero-point energy between the stretching vibrations of the hydrogen isotopes in the reactant. However, there was no rationale that related this observation to aspects of the potential energy surface which would enable an explanation of the lower values that were often seen.

The first explanation of the variability of hydrogen kinetic isotope effects was by Westheimer[3], who related the magnitude of the isotope effect to the structure of the transition state. Westheimer's theory assumes a linear three-centred transition state

in which the hydrogen isotope is transferred between two atoms or groups. This situation can be represented by the general reaction in scheme 1-2,

$$A + H{-}B \longrightarrow [A\overset{f_1}{\cdots}H\overset{f_2}{\cdots}B]^{\neq} \longrightarrow A{-}H + B$$

Scheme 1-2

where A and B are assumed to be large atoms or structureless groups. In the transition state defined above, there are two stretching vibrations; the symmetrical ν_s, and the asymmetrical ν_a. These vibrations are shown in figure 1-3.

ν_s ν_a

Figure 1-3

When the stretching bond force constants f_1 and f_2 are equal, there is no motion of the hydrogen isotope in the symmetrical stretching vibration ν_s. As a direct result of this motionless state of the hydrogen atom, there is no change in zero-point energy on isotopic substitution (this result can be seen from equation 1-22).

A system that is analogous to the transition state described

above for hydrogen transfer reactions, is the stable linear triatomic bifluoride ion HF_2^- [46,47]. The hydrogen bond in this ion is believed to be symmetrical (there is some evidence that this may not be the case[47]). In this ion the symmetrical stretching vibration is not isotopically sensitive. In the asymmetrical stretching vibration, the bond force constants are no longer equal, and the hydrogen is in full motion resulting in an isotopically sensitive frequency.

The analogy between the stable bifluoride ion and the unstable hydrogen transfer transition state of Westheimer ends with the symmetrical stretching vibration. The asymmetrical stretching vibration of the bifluoride ion now corresponds to a motion of the atoms of the transition state without a restoring force. This motion now corresponds to a translational motion along the reaction coordinate and across a potential energy maximum. As a translation it possesses no zero-point energy and is therefore isotopically insensitive.

The effects of the isotopically insensitive symmetrical and asymmetrical stretching vibrations of the transition state on the primary kinetic isotope effect can now be readily understood. If there is no change in the zero-point energy levels for the bending vibrations between the reactants and the transition state, then the full effect of the loss of the difference between zero-point energy levels for isotopic species in the symmetrical transition state, will be realized in the isotope effect. Further if there were a weakening of bending vibrations or contributions due to tunnelling then larger values of the isotope effect would be observed.

The potential energy surface for the generalized hydrogen transfer reaction shown in scheme 1-2 can be represented by a two-

dimensional contour diagram as in figure 1-4.

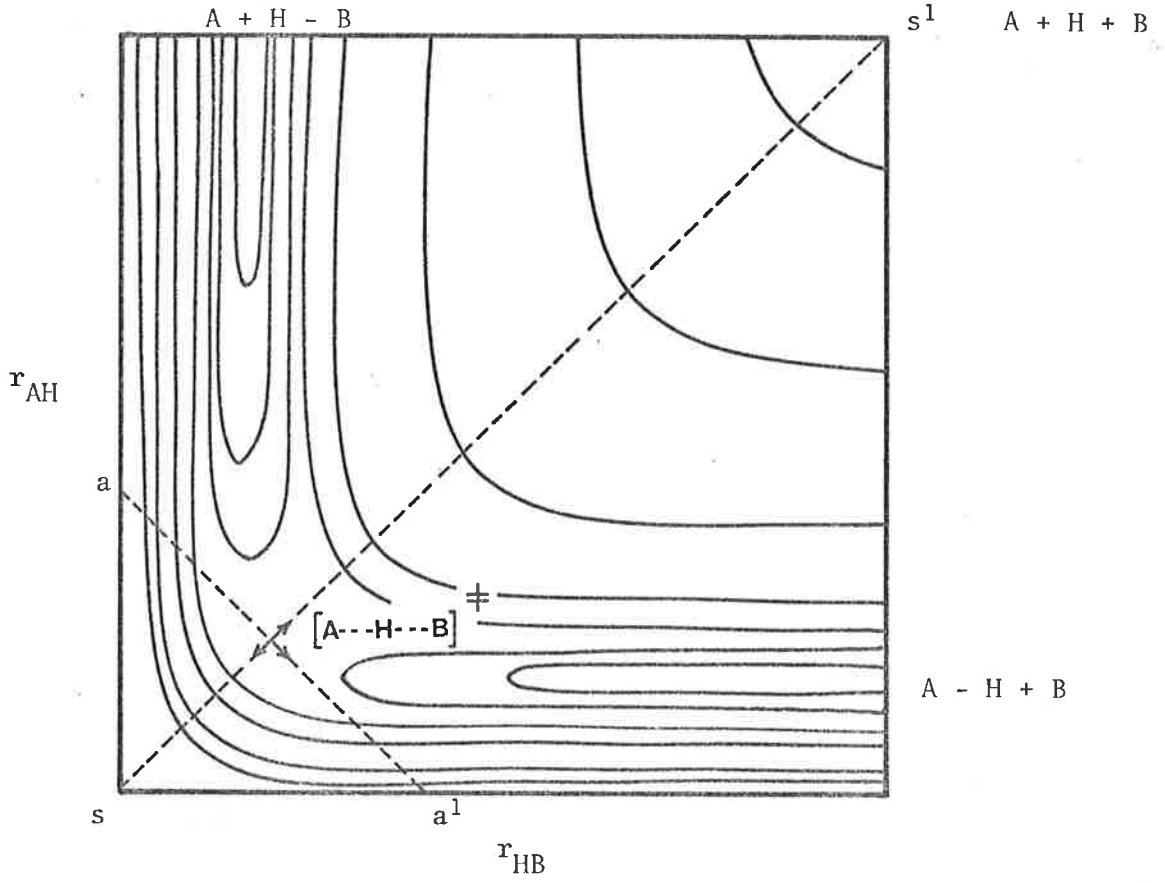

Figure 1-4

The transition state is represented by the configuration at the maximum of potential energy; at the intersection of the lines a,a^1 and s,s^1. The normal coordinates[4,13], Δa and Δs, involve simultaneous extension and contraction of both bonds to the hydrogen in the transition state. The potential energy curves corresponding to the normal coordinates Δa and Δs are given by sections through the surface along the lines a,a^1 and s,s^1 and the harmonic force constants by the curvatures at their minima. The sections through the potential energy surface along the normal modes are shown in figure 1-5.

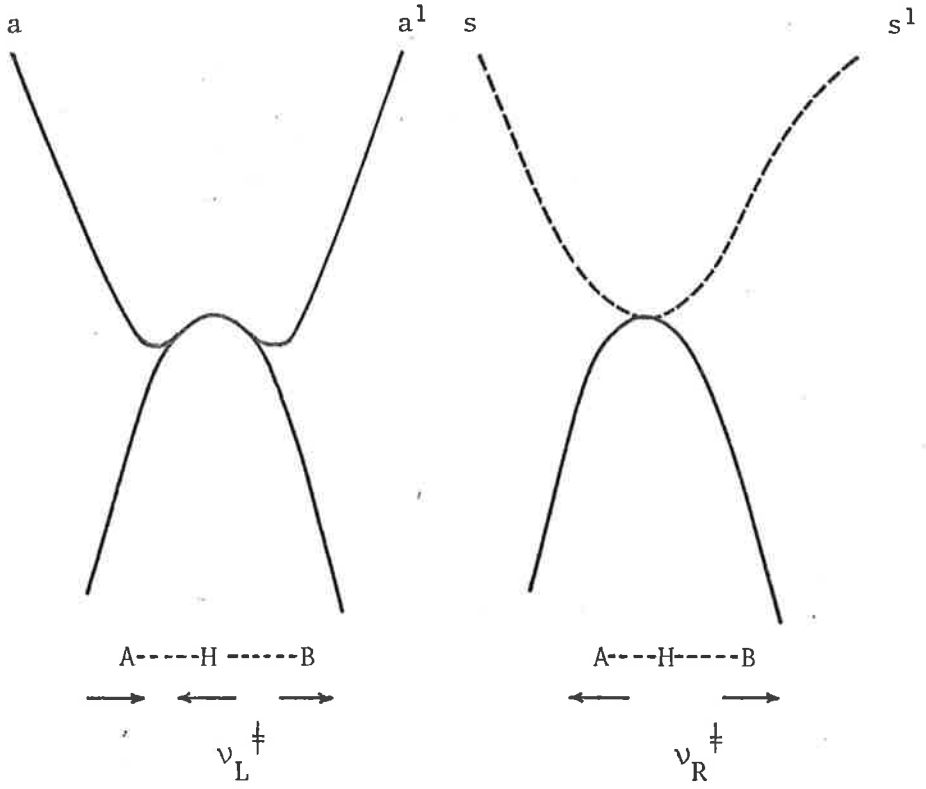

Figure 1-5

Also shown in figure 1-5 are the motions of the atoms involved in each of the normal modes of vibration. The sections described above yield the force constants $\partial^2V/\partial\Delta s^2$ and $\partial^2V/\partial\Delta a^2$, and the frequencies for these normal modes of vibration can be obtained by application of equation 1-18.

The frequency of the normal vibration at the saddle point and in the direction of the reaction coordinate (a-a^1), is denoted by $\nu_L^{\ddagger}$. The potential energy curve can be seen to be concave downwards (figures 1-4, 1-5) resulting in a negative force constant and thus an imaginary frequency for this vibration (see equation 1-18). This frequency is best thought of as a classical frequency defining motion along the reaction coordinate and describing an unstable vibration[4].

The normal mode at the saddle point perpendicular to the reaction coordinate (s-s^1), is described by a potential energy curve which is

concave upwards (figures 1-4, 1-5). As a result this vibration has a positive force constant resulting in a real vibrational frequency $\nu_R^{\ddagger}$. The concept of a vibrating transition state is of course notional since the time required for a vibration is longer than the lifetime of the transition state. None the less, $\nu_R^{\ddagger}$ determines the magnitude of the difference in zero-point energy on isotopic substitution which when added to the classical barrier height determines the minimum energy required for reaction.

To this point the discussion has been concerned with a symmetrical transition state defined by equal force constants f_1 and f_2. In transition states in which f_1 and f_2 are not equal, the transferring hydrogen isotope will move in the real stretching vibration leading to isotopic sensitivity of this motion. As a result, the change in zero-point energy on isotopic substitution will offset some of the zero-point energy difference in the corresponding vibration of the reactants. As the asymmetry of the transition state increases, the degree of cancellation of zero-point energy differences will increase and the value of the kinetic isotope effect will diminish. This is the basis of Westheimer's prediction of the magnitude of the kinetic isotope effect.

One limiting configuration of the asymmetric hydrogen transfer transition state will be the reactant-like case in which the magnitude and isotopic sensitivity of $\nu_R^{\ddagger}$ will approach that of the corresponding stretching frequency of the reactants. The reaction coordinate in this case could be simply described as the translational approach of reactants and the limiting value of the isotope effect would be unity. The other limiting configuration of the transition state is the product-like situation in which $\nu_R^{\ddagger}$ will resemble the stretching

frequency of the product. As a result the kinetic isotope effect would be expected to approach the value of the equilibrium isotope effect.

Westheimer's theory can be seen to be extremely useful in explaining the observation of less than maximum kinetic isotope effects. On the basis of this theory one would predict that the experimental kinetic isotope effect should pass through a maximum value as the symmetry of the transition state for hydrogen transfer is changed from reactant-like to symmetrical to product like[48]. This prediction has led to a great deal of both experimental and theoretical work in an effort to initially observe this trend in isotope effects and then to determine whether this trend has any basis in the above theory. This investigation is of some importance since a corollary of Westheimer's theory is that the observation of such trends in isotope effects is due to the change in symmetry of the transition state. Thus the magnitude of an isotope effect is directly related to a particular transition state structure.

Isotope effects on the ionization of nitroalkanes and ketones using a variety of oxygen and nitrogen bases were first investigated by Bell and Goodall[49] and then by others[50-52]. Although a graph of the isotope effect versus ΔpK (the difference in pKa's of reactant and product) shows considerable scatter (which is perhaps due to the diversity of acids and bases chosen), a maximum in k_H/k_D at ΔpK = 0 can be observed.

Maxima in the kinetic isotope effect for hydrogen atom transfer reactions from a number of thiols to a variety of carbon radicals have also been observed. Lewis[53] has collated much of this data from his own laboratories[54-57] and from others[58]. A plot of

isotope effect versus change in enthalpy for the reaction (as calculated from bond dissociation energies) cannot be adequately fitted by a smooth curve but the trend and the maximum, occurring at about $\Delta H = 0$, is clear.

Hydrogen atom transfer reactions from carbon centres to halogen atoms and from hydrogen halides to carbon centred radicals have also been studied[53,57,59-62]. The kinetic isotope effects for these reactions show a trend when compared with the enthalpy changes for the reaction, which is consistent with the Westheimer effect.

Lewis[63] has also made a systematic study of the tritium kinetic isotope effects for the carbon radical abstraction of hydrogen atoms from trialkyl tin hydrides. The values of the isotope effects were small, ranging from 2.1 to 6.3 with the expected maximum being at 4.7. Generally the isotope effects increase as the new carbon-hydrogen bond strength weakens, but the correlation is poor.

Based on a very wide range of hydrogen atom transfer reactions, Lewis has concluded[64] that for thermoneutral reactions the isotope effect will not be less than the maximum value calculated for complete loss of the stretching vibration zero-point energy of the breaking bond. Larger values than the maximum are then due to tunnelling. For exothermic reactions, the isotope effect will fall from the maximum value as the exothermicity increases. The effect of exothermicity changes on the isotope effect will be modified by steric factors[55,65] and contributions of polar structures[59] to the transition state. Steric hinderance raises the energy of the transition state, compared to a similarly exothermic unhindered model, thereby increasing the isotope effect. The contribution of polar

structures reduces the barrier (stabilizes the transition state) resulting in a reduction in the isotope effect for non-thermoneutral reactions. The above conclusions follow from consideration of the direct relationship between the variation in isotope effect with exothermicity and the ratio of activation energy to the enthalpy of reaction. All of these conclusions are in complete accord with the theory advanced by Westheimer.

There are many examples of isotope effect studies which can be understood in terms of Westheimer's basic theory. Many of these are included in the review by More O'Ferrall[13]. It is clear from much of this data that the best correlations of isotope effect and transition state symmetry (measured by enthalpy of reaction, ΔpK etc.) are for those reactions bearing a close relationship; for example a single substrate with a series of bases. Examples of this can be seen in the work of Bell and Barnes[52] on the ionization of ethyl-nitroacetate in which the effective pKa of a single base was varied by effecting solvent changes[66-70]. There are probably many other reasons why smooth correlations are not always observed. One such factor is possibly due to solvent effects which may be minimized by the study of hydrogen atom transfers, since neither reactants nor products are necessarily charged. Solvent effects may be precluded altogether by the study of gas phase reactions. Another factor which may contribute to the problems of such correlations is the need to correct the isotope effect for the presence of tunnelling. An example of this occurs in the investigations of hydrogen atom transfer from thiols in which the large isotope effect obtained for the reaction of the trityl radical with mesitylene thiol[53,55] (k_H/k_D 9.4) requires a substantial tunnelling correction. The

presence of secondary isotope effects, which cannot be compensated for in a uniform manner, within a homogeneous family of reactions must also lead to problems in isotope effect correlations[51].

There are fewer examples of correlations involving isotope effects and transition state structure for gas phase reactions when compared to those obtained for solution reactions. One such study investigated the variation in kinetic isotope effect with the Hammett σ_p^+ factor[71] for the unimolecular loss of keten from a series of substituted acetanilide and phenyl acetate radical cations[72]. A maximum was not observed in the series but a clear trend of the value of the isotope effect with the ability of the substitutent to stabilize the transition state (or reduce the barrier) was observed. This is in accord with the effect of polar contributing structures on the isotope effect as described by Lewis[53,59].

Wellman and co-workers[73] have made a preliminary study of the gas phase proton-transfer reactions of a variety of substituted toluenes with a series of oxygen bases (e.g., the methoxide anion etc.). The range of isotope effects observed is small (k_H/k_D, varying from 0.7 to 1.6) but the correlation with the exothermicity of the reaction is clear. These results, when considered in terms of Hammond's postulate[74], are comprehensible within Westheimer's basic framework. Jasinski and Brauman[75] have studied the gas phase proton transfer reactions of various pyridine bases. The reaction efficiency was found to be reduced by increasing the bulk of the alkyl substituents at the 2 and 6 position of the pyridine ring. As the reaction efficiency decreased they found that the hydrogen isotope effect increased (k_H/k_D 1.0 to 1.8). The effect of increasing the steric hinderence to reaction is to raise the energy of the transition

state thereby reducing the reaction efficiency and increasing the isotope effect as discussed previously. The increased barrier height correlates with larger interaction force constants and therefore greater tunnelling corrections[53]. Since the range of isotope effect values in this case is small then the importance of the magnitude of the tunnelling correction is unclear.

Other Factors Contributing to Kinetic Isotope Effects

There have been many reservations expressed by authors about Westheimers basic theory[22,76-84]. Many of these critiques are theoretical and are concerned with some of the assumptions made by Westheimer in his simplified treatment. These factors include the consideration of bending vibrations, the tunnelling correction to the reaction coordinate motion, and non-zero imaginary frequency vibrations ($\nu_L^{\ddagger}$). Westheimer's treatment however, still remains as the simplest and most effective rationale for isotope effect behaviour, but it is now clear that other effects, such as those mentioned above, must be considered as overlays to the basic stretching vibration considerations.

Westheimer only briefly considered bending vibrations and assumed that the zero point energy changes on isotopic substitution cancelled between the reactants and the transition state. Similarly, Bigeleisen[85] in his theoretical treatment of the symmetry of the transition state and isotope effects ignored the effect of bending vibrations on the basis that, to a first approximation, the tunnel effect exactly cancels the contribution of the bending vibration[86]. The importance of bending vibrations, or more correctly the zero-point energy for these vibrations, in their contribution to the isotope

effect should not be underestimated. Kresge and Chiang found in their study of the proton transfer from hydrogen fluoride to ethyl vinyl ether that the hydrogen isotope effect was small (k_H/k_D 3.35) when compared to the maximum isotope effect expected from uncompensated loss of the H-F stretching frequency[87]. The rationale they proposed to account for this observation was the presence of an uncompensated hydrogen bending vibration in the transition state, accounting for some of the difference in zero-point energy in the isotopic reactants. Similarly, Lewis and Kozuka[62] suggested that the low hydrogen isotope effects obtained (k_H/k_T 1.04 - 4.14) for atom transfer from hydrogen bromide to a variety of substituted 2-bromoethyl radicals was due to an uncompensated hydrogen bending vibration in the transition state.

Calculations[80,88] have shown that incorporation of bending vibrations, in four and five-centred transition state models, does not fundamentally alter the conclusions based on Westheimer's three-centred model. In particular, the calculations indicated that when the reactant contains bending vibrations, the effect of isotopic substitution on zero-point energy levels cancel between reactant and transition state. This is in accord with Westheimer's assumptions. In the case where only the transition state possesses bending vibrations the calculated isotope effect is small. An example of this situation occurs with the reactions of hydrogen halides mentioned previously. When the reaction involves loss of reactant bending vibrations (such as in the case of the reaction of polyatomic species with the halide anions), the calculated isotope effect has a much broader maximum encompassing asymmetrical transition states. In addition, the values are much larger than expected for

product-like transition states. This effect correlates with a decrease in the zero-point energy contribution to the isotope effect and a simultaneous increase in contribution from the bending vibrations as the transition state structure is varied from symmetrical to product-like.

Westheimer's basic model was that of a three-centred linear transition state. It was necessary to consider a linear system in order to simplify the treatment of the forces to the isotope which would lead to a symmetrical transition state and hence isotopic insensitivity of its vibrations. If the transition state is not linear, then there cannot be a balance of forces resulting in immobility of the isotope. Figure 1-6 shows the forces acting on the isotope in a symmetrical non-linear transition state.

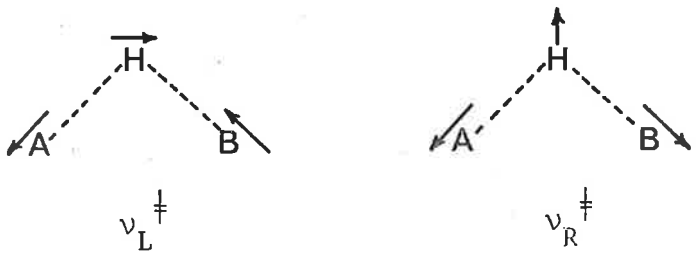

Figure 1-6

Calculations on non-linear transition states[89-91] show that the isotope effect falls as the angle between the partial bonds to the hydrogen decreases. In particular, More O'Ferrall[89] has shown that the calculated hydrogen isotope effect value for a symmetrical transition state decreases from 7.9, at an angle of 180° (linear three-centred model) to 0.9 at 60°. The calculations also indicated

that the variation of the isotope effect with transition state symmetry was only slight for small angles (< 90^{o}). Recent experimental evidence for the effect of bent transition states on the isotope effect comes from a study of allylic hydrogen abstraction by tert-butoxyl radicals[92] and singlet oxygen hydroperoxidation of 4-methyl-2,3-dihydro-γ-pyran[93].

Bell considered that when proton transfer is concomitant with displacement of a heavy atom or group, (such as in elimination reactions and some rearrangement reactions), electronic coupling of the hydrogen and heavy atom or group motion in the reaction coordinate may occur[78]. The effect of this coupling would be to decrease the importance of hydrogen motion in the reaction coordinate leading to some loss in isotopic sensitivity, even in symmetrical transition states. Figure 1-7 shows the atomic motions in a β-elimination reaction.

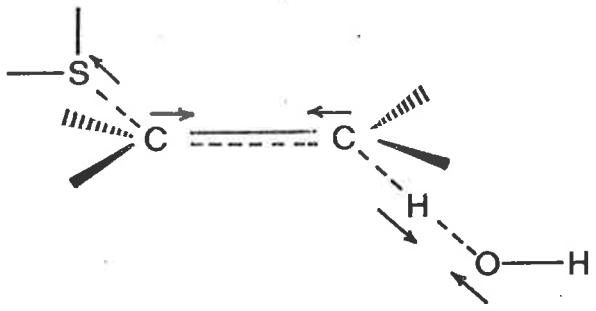

Figure 1-7

Katz and Saunders, in their theoretical study of hydrogen and sulphur isotope effects on the E_2 elimination reaction of hydroxide ion with the ethyl dimethyl sulphonium ion (see figure 1-7), concluded that the hydrogen isotope effect is strongly influenced by the extent of coupling of the proton transfer with the other atomic motions[94]. This result arose from the sensitivity of the isotope effect values on the value of the interaction force constant[4]. As the value of the interaction force constant decreases, the proton transfer motion becomes less important as a component of the reaction coordinate frequency and a more important component of the real frequencies of the transition state. Consequently, there is a cancellation of at least part of the zero-point energy differences between the reactants and transition state leading to a reduced isotope effect. Experimentally however, this effect is difficult to observe. Large isotope effects (k_H/k_D 6 - 10) for concerted reactions are common[6], and isotope effect maxima have been observed in β-eliminations[67].

The role of the interaction force constant on both the magnitude of hydrogen isotope effect and on the observation of maxima for symmetrical transition states is very important. Willi and Wolfsberg[77] and later Motell and co-workers[84] found that the interaction force constant can almost negate the effect of asymmetry on the magnitude of the kinetic isotope effect. A wide variety of asymmetric transition states may give rise to large isotope effects providing that the interaction force constant is sufficiently large. This is due to the end group motion in a three-centred transition state model. This motion dominates the real vibrational frequency diminishing the effect of differences in mass of the central atom

(hydrogen or deuterium) on the isotope effect.

Another area of kinetic isotope effects not dealt with by Westheimer concerns the effect of tunnelling on the isotopic rate ratio. Tunnelling corresponds to a quantum mechanical correction to the reaction coordinate and is highly approximate in nature. There are two corrections to the absolute rate theory equations (equations 1-6, 1-8) which are combined to form the transmission coefficient (κ). The first type of correction factor, denoted by K, describes the probability that systems possessing energies greater than that of the transition state may not pass over the barrier to products. Such systems are reflected back into the reactant valley. As with the tunnelling correction, K is a quantum mechanical correction to the barrier passage process. This factor is always less than unity and to a first approximation is isotope independent. As a result K cancels from the isotopic rate ratio equations leaving them to be corrected only for tunnelling.

The problem of the tunnelling correction is large and has been considered extensively elsewhere[4,12,13,95-98], and only some of its relationships to hydrogen kinetic isotope effects will be discussed here. The tunnelling correction, denoted by Γ, arises in a very direct way from the basic tenets of quantum theory as expressed by the uncertainty principle. Due to the wave-particle duality of matter, the hydrogen isotopes can be described in terms of wavelengths. Under normal conditions, their effective wavelengths are of the order of magnitude of 10^{-9} - 10^{-8}cm, which is comparable with the distances nuclei move during chemical reactions. As a result, the uncertainty in the position of the hydrogen isotope (or its effective wavelength, which amounts to the same thing) is of the

same order of magnitude as the dimensions of the barrier to reaction. This leads to a finite probability of the particle being on either side of the barrier. It is clear from the uncertainty principle that the lighter particle will have a greater uncertainty in its position with relation to the barrier. Also, the presence of a thin barrier tends to increase the need and magnitude of the tunnelling correction. Two other characteristics of the tunnelling correction are firstly that its value is always greater than unity and secondly that it is temperature dependent; Γ decreases with increasing temperature.

These characteristics are expected to correlate with the following properties of the transition state; (i) the curvature of the potential energy surface along the reaction coordinate, (ii) the sensitivity of motion along the reaction coordinate to the isotopic mass of hydrogen, and (iii) the activation energy of the reaction in the thermodynamically favoured direction[97].

The contribution of (i) and (ii) to the tunnelling correction is conveniently expressed in terms of the reaction coordinate frequency $\nu_L^{\ddagger}$ which is defined by the relationship in equation 1-23.

$$\nu_L^{\ddagger} = \frac{1}{2\pi} \left(\frac{f_a}{m^*}\right)^{1/2} \qquad \text{Equation 1-23}$$

As discussed previously, if f_a is negative, an imaginary value for $\nu_L^{\ddagger}$ is obtained. A large isotopically sensitive value of $\nu_L^{\ddagger}$ will be associated with a large degree of tunnelling. In Westheimer's treatment of kinetic isotope effects, f_a and $\nu_L^{\ddagger}$ were assumed to be zero corresponding to a flat-topped energy barrier and no tunnelling correction. A more realistic model may be deduced from a consideration of the symmetry of the transition state in terms of reactant and

product-like structures implied by Hammond's postulate[30,74,99].

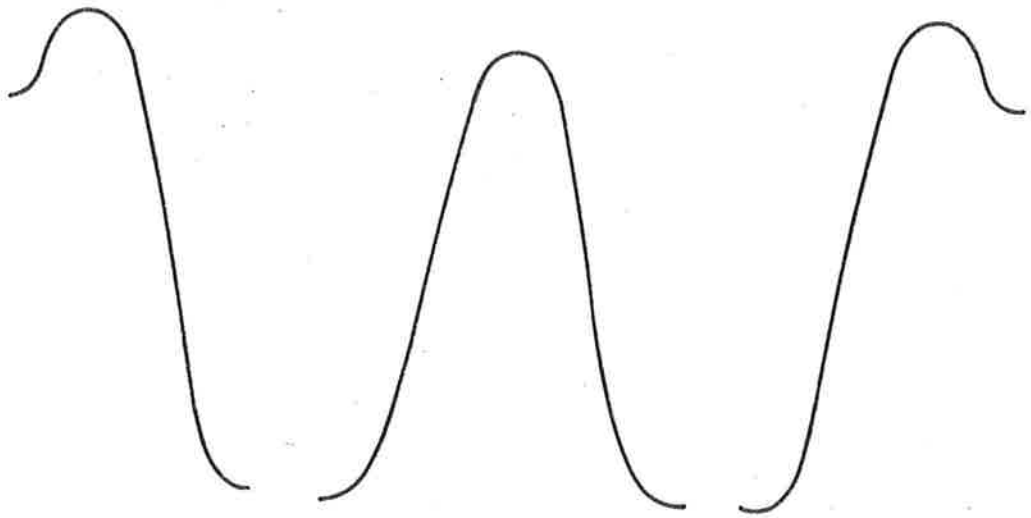

reactant-like	symmetrical	product-like
$\nu_L^{\ddagger} \rightarrow 0$	$\nu_L^{\ddagger} \rightarrow 0$	$\nu_L^{\ddagger} \rightarrow 0$
$\frac{\nu_L^{\ddagger}}{\nu_{2L}^{\ddagger}} \rightarrow 1$	$\frac{\nu_{1L}^{\ddagger}}{\nu_{2L}^{\ddagger}} \rightarrow \sqrt{2}$	$\frac{\nu_{1L}^{\ddagger}}{\nu_{2L}^{\ddagger}} \rightarrow 1$

Figure 1-8

As can be seen from figure 1-8, a flat-topped barrier will only arise in the limiting cases of a highly exothermic or endothermic reaction. As a result, a minimum tunnelling correction is expected for extreme reactant or product-like transition states and a maximum correction is required for a symmetrical transition state. The factors mentioned previously which correlate with the tunnelling correction, suggest that its contribution to the kinetic isotope effect will show the same qualitative variation with transition state structure as Westheimer predicted on the basis of zero-point energy changes above.

The first estimate of the tunnelling correction was made by Wigner[100,101] for a one-dimensional barrier of arbitrary shape. This

relationship is shown in equation 1-24

$$\Gamma = 1 - \frac{u_i^{\ddagger 2}}{24} \qquad \text{Equation 1-24}$$

where $u_i^{\ddagger} = h\nu_i^{\ddagger}/k_B T$. This equation is believed to give the tunnelling correction for those cases in which the correction is expected to be small.

To estimate larger tunnelling corrections, some detail of the barrier must be considered. The first approach approximating the barrier for a symmetrical transition state was made by Bell[9,12,102,103]. The Bell tunnelling correction is given in equation 1-25.

$$\Gamma = \frac{\frac{1}{2}u_i^{\ddagger}}{\sin \frac{1}{2}u_i^{\ddagger}} \qquad \text{Equation 1-25}$$

This is the first term of a series and suffices for high barriers and small values of $u^{\ddagger}$, but for larger tunnelling corrections later terms in the series are required.

CHAPTER 2

AN INTRODUCTION TO MASS SPECTROMETRY

The field of mass spectrometry covers a diverse range of research interests each of which has been extensively reviewed. General reviews covering all aspects of mass spectrometry appear regularly[104-108]. A large number of reviews have appeared on specific areas of mass spectrometry; these include the evaluation of potential energy surfaces[109,110], metastable ions and gaseous ion thermochemistry[111,112], fundamental rate theories[113,114], energy distribution in the unimolecular decomposition of ions[115], molecular orbital calculations for ionic species[116] and unimolecular chemistry of positive ions[117]. Other techniques in the study of gas phase ion chemistry which have been reviewed include isotopic labelling and kinetic isotope effect studies[118,119], collisional activation[120], ion-molecule reactions[121] and new ionization techniques[122,123].

Ions formed in the Mass Spectrometer

Figure 2-1 shows the arrangement of the electric and magnetic sectors in a double focusing mass spectrometer of Nier-Johnson geometry[124]. The main ion beam entering the electric sector has kinetic energy given by equation 2-1,

$$\tfrac{1}{2}\, mv^2 = eV \qquad \text{Equation 2-1}$$

where m is the mass of the ions, v their velocities and V the accelerating voltage. The radius of the path taken by the beam of ions in the electric sector (r_e) is given by equation 2-2,

$$\frac{mv^2}{r_e} = zF \qquad \text{Equation 2-2}$$

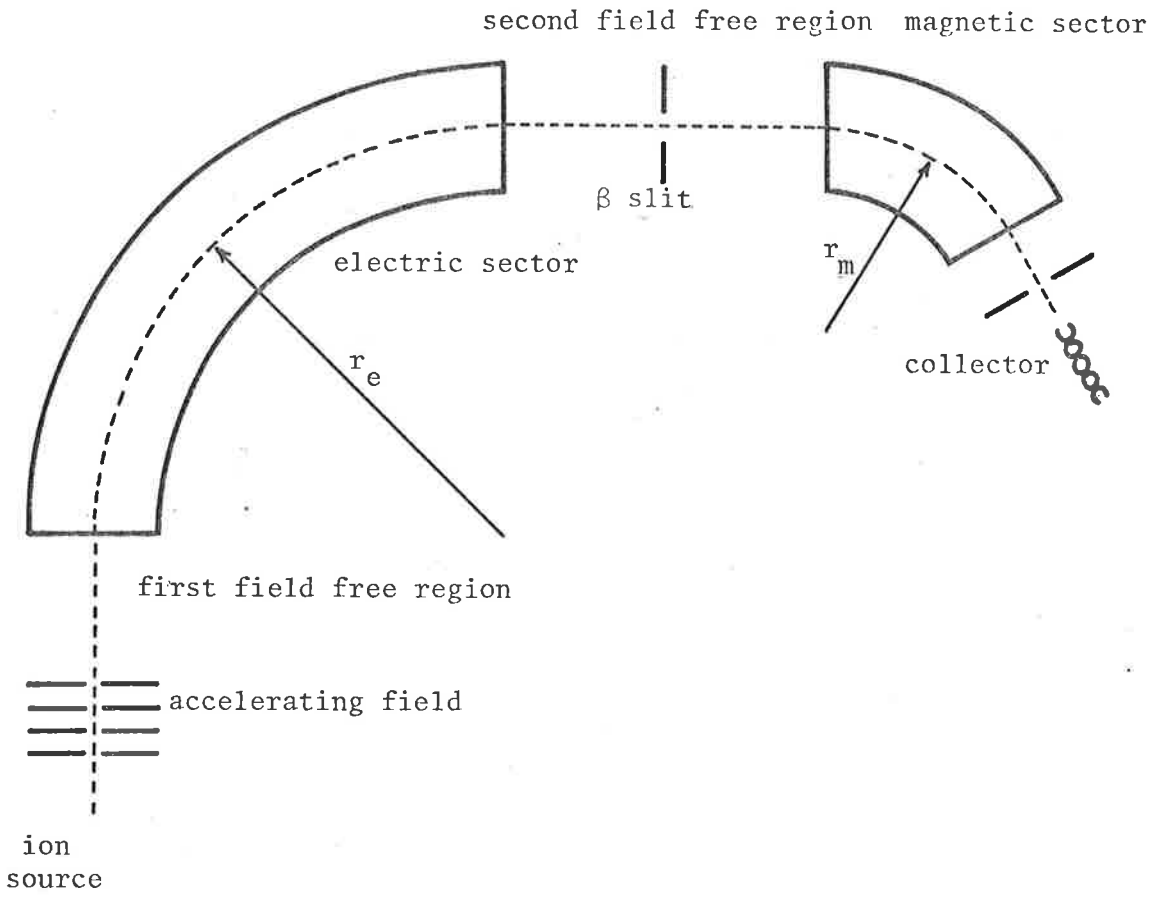

Figure 2-1

where F is the electrostatic field strength and z the charge on the ions. Ions in the magnetic sector will travel a path of radius r_m defined by equation 2-3,

$$r_m = \frac{mv}{zB} \qquad \text{Equation 2-3}$$

where B is the magnetic field strength.

Three types of ions can be recognised in a normal mass spectrum; molecular ions ($M^{+\cdot}$), fragment ions ($F^{+\cdot}$) and metastable ions (m*). In the ion source ions are produced with a range of internal energies

(distributed among the electronic, vibrational and rotational degrees of freedom). To a first approximation it is the amount of internal energy an ion contains which determines its rate of decomposition, and as a result the region of the mass spectrometer in which the ion will decompose. Figure 2-2 generalizes the relationship between the type of ion seen in a normal mass spectrum and the typical range of rate constants required to produce these ions[125].

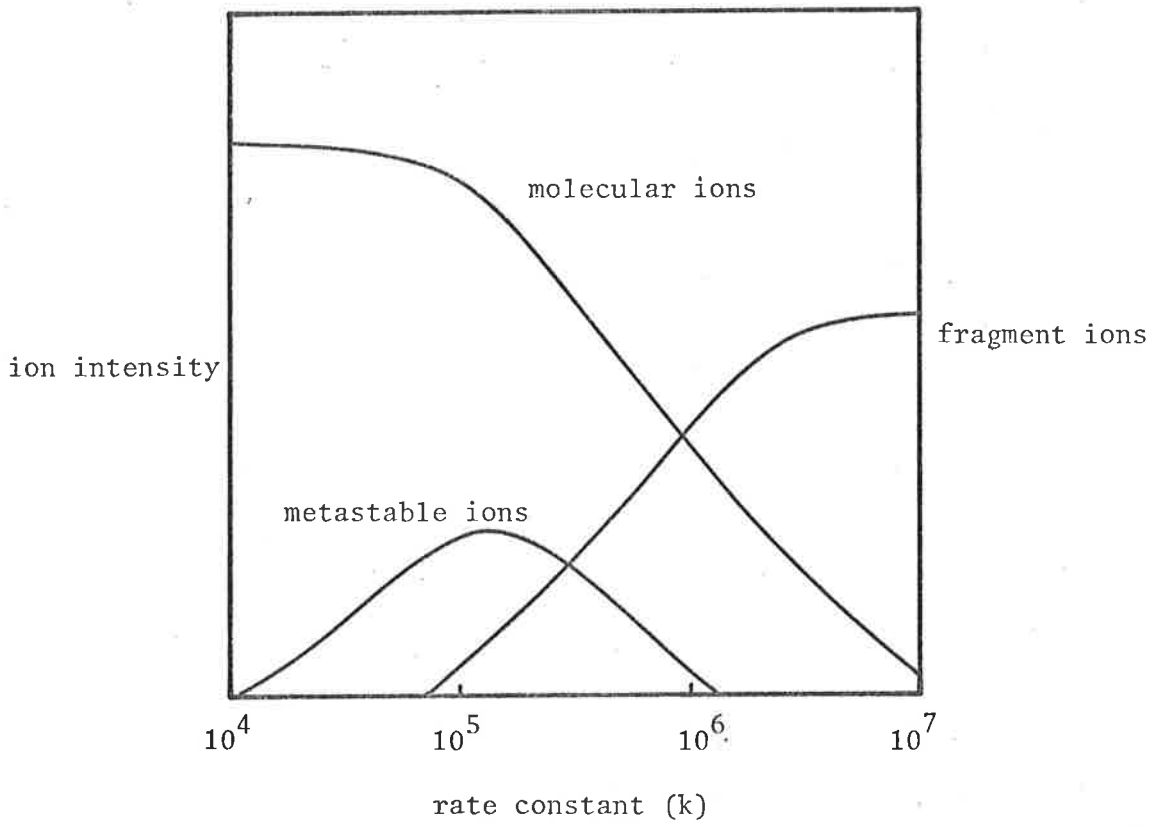

Figure 2-2

Molecular ions are defined as ions which are formed in the ion source with an internal energy which is low enough to ensure that they reach the collector without fragmenting some 10^{-5}sec. after their formation. The ions contributing to the molecular ion peak in the spectrum will have a distribtuion of internal energies. The mean of this distribution corresponds to a rate constant for

fragmentation which is small compared to the mass spectrometer time scale (typically $k \leqslant 10^5$ sec^{-1}). The ions composing the molecular ion peak may not be homogeneous in that some may have sufficient energy to undergo isomerization reactions but insufficient energy to fragment. Such ions will not be distinguishable from the other molecular ions which have insufficient energy to undergo isomerisation.

Fragment ions are ions which are formed by the unimolecular reactions of molecular ions in the source. The residence time of ions in the ion source is of the order of 10^{-6} sec. This means that providing a molecular ion has sufficient energy to react, then it must do so with a rate constant $k \geqslant 10^6$ sec^{-1} to enable observation of fragment ions in the mass spectrum (see figure 2-2). If the fragment ions are formed with significant internal energy then these ions may also undergo unimolecular fragmentation reactions in the ion source.

Molecular and fragment ions that undergo unimolecular reactions in the ion source can be called unstable ions since their lifetimes are $< 10^{-6}$ sec. Since ions are formed with a distribution of internal energies, ranging from zero to $\varepsilon(e) + \varepsilon(T) - IP_v$ where $\varepsilon(e)$ is the electron beam energy, $\varepsilon(T)$ is the maximum initial thermal energy of the molecules and IP_v is the (vertical) ionization potential, then decomposition of these ions will be expected to occur along the entire ion path of the mass spectrometer. The ion source reactions occur from ions in the higher energy region of this distribution; the lower energy regions leading to ions of longer lifetime. Figure 2-5(a) indicates the energy distribution function, $P(\varepsilon)$, of the ions in the source and the relative proportions of the distribution giving rise

to each type of ion.

Metastable ions (m*) correspond to ions that decompose in the regions outside of the ion source of a mass spectrometer. In particular they correspond to the ions that fragment in the field free regions of the instrument (see figure 2-1). In the normal mass spectrum, peaks due to ions resulting from metastable ion transitions in the second field free region can be observed. They are usually identified by being broader than normal peaks (due to the kinetic energy released in the metastable ion transition), being of low abundance and most importantly occurring at non-integral mass to charge (m/z) ratio. The non-integral m/z values of metastable ion peaks can be understood if one considers the second field free reaction in scheme 2-1.

$$m_1 \longrightarrow m_2 + m_3 \qquad \text{Scheme 2-1}$$

The ions m_1^+ and m_2^+ are the metastable ion and its fragment ion respectively and m_3 is the neutral fragment. The kinetic energy of the metastable ion (defined by the electric sector; see equation 2-2) will be partitioned between the fragment ion and the neutral fragment; the fragment ion will possess a fraction m_2/m_1 of the kinetic energy. As a result, the fragment ions are deflected more readily by the magnetic field in the magnetic sector and will appear at $m_2^2/(m_1 z)$ in the mass spectrum[126]. Metastable ion transitions in the first field free region are also of interest but due to the partitioning of kinetic energy, the fragment ion is not transmitted through the electric sector with the main ion beam. As a result ions produced from reactions in the first field free region are not observed in normal mass spectra. These ions can be observed by the use of special

defocusing techniques.

Ions formed in the first field free region can be transmitted through the electric sector at the voltage used to transmit the main ion beam (E_1) if their kinetic energy is increased in the ratio m_1/m_2. To increase the kinetic energy of these ions, the accelerating voltage is raised from its normal value V_1 to V_2 according to the relationship in equation 2-4.

$$V_2 = \frac{m_1}{m_2} V \qquad \text{Equation 2-4}$$

At V_2 the main ion beam has higher kinetic energy than is required for traversing the path of equi-potential of the electric sector and will therefore not be focused at the β-slit. The ions formed in the first field region which satisfy equation 2-4 will now have sufficient kinetic energy to pass through the electric sector and will be focused at the collector after mass analysis. If the magnetic sector is pre-set to allow ions of mass m_2 to reach the collector, and the accelerating voltage is scanned upwards from V_1, then all ions of mass m_2 formed from various parent ions will be collected in turn. The ratio of V_1 to V_2 for each peak will define the ratio of daughter to parent ions. This is the basis of the high-voltage (HV) scanning technique[127-129].

An alternative defocusing technique focuses the ions formed in the first field free region by lowering the electric sector voltage from its original value E_1 to E_2. The voltage is decreased to the value defined by equation 2-5.

$$E_2 = \frac{m_2}{m_1} E_1 \qquad \text{Equation 2-5}$$

The daughter ions transmitted through the electric sector in such a

manner will be recorded at a mass to charge ratio $m_2^2/(m_1 z)$ in the mass spectrum.

One advantage of studying metastable ion reactions in the first field free region is that each transition is unequivocally identified in terms of the masses of the parent and daughter ions by equations 2-4 and 2-5. In addition, all of the parent ions for each daughter ion may be found by scanning the accelerating voltage at a set magnetic field (this is not possible in the electric sector defocusing technique as described above). Another advantage is that in the absence of the main ion beam the ion collector sensitivity can be increased so that weak metastable ion transitions can be detected.

When a collector electrode is mounted at the β-slit and either the accelerating voltage or the electric sector voltage is scanned, the spectrum obtained is known as an ion kinetic energy (IKE) spectrum[130-132]. However to unequivocally assign each peak in such a spectrum with a particular metastable ion transition, mass analysis of the daughter ion is required. This is necessary since the relationship in equations 2-4 and 2-5 may be satisfied by more than one pair of values for m_1 and m_2. As mentioned previously, the daughter ion will appear at $m_2^2/(m_1 z)$ for electric sector defocusing and m_2/z for accelerating voltage defocusing.

In order to obtain unequivocal information concerning ion fragmentations from an electric sector scanning technique it is desirable to carry out mass separation of the swarm of ions leaving the accelerating field, prior to energy analysis. This is the basis of reverse sector instruments in which the magnetic sector precedes the electric sector[133,134]. An ion of any mass to charge ratio can then be selected by the magnetic sector and its subsequent

fragmentations (occurring now in the second field free region) can be investigated by scanning the electric sector voltage. The spectrum so obtained is known as a mass analysed ion kinetic energy (MIKE) spectrum.

A new development which is useful in identifying all of the unimolecular fragmentations of an ion is the technique of linked scans in which two of the three fields of the mass spectrometer, accelerating, electrostatic or magnetic, are scanned simultaneously[135]. The most important of these techniques is scanning of both the electrostatic and magnetic fields[136]. The initial values of the fields are such that the parent ion of interest is transmitted and the scan then involves decreasing the fields in a constant ratio. As the scan progresses all daughter ions formed from this parent in the first field free region are transmitted in succession.

Ionization and Energy Transfer

There are many methods of ionizing a neutral molecule for mass spectrometric study. These include chemical ionization[137], field ionization and field desorption[138,139], electrohydrodynamic ionization[140], atmospheric pressure ionization[141], photoionization[142] and radionuclide ionization[143]. The most common method for producing molecular ions is by electron impact in which gaseous neutral molecules interact with electrons from an electron beam. The energy of the electron beam is generally greater than the ionization potential of the neutral molecule and therefore excess energy remains in the molecule after ionization. Under the conditions usually employed in the electron impact source, molecular anions can be formed by the acceptance of low energy photoelectrons (resonance capture process).

These ions are formed in low abundance and are the species studied in negative ion mass spectrometry[144].

In the ion source the bombarding electrons interact with the neutral molecule to varying extents thereby transferring non-fixed amounts of energy to the molecule. In addition, the electron beam is not mono-energetic and as a result the molecular ions will have a distribution of internal energies as shown in figure 2-5(a). When only a small amount of energy is transferred from the electron to the molecule excitation rather than ionization may occur.

The interaction time between an electron in the electron beam and a neutral molecule is of the order of 10^2sec. less than the time required for the fastest vibration. As a result the position of the nuclei will not change during the interaction and the removal of a valence electron from the molecule will occur by a vertical rather than an adiabatic ionization process. That is to say, the transition will follow the Franck-Condon rule[145,146] which requires that the configuration and momenta of the nuclei do not change during the ionization process.

As a result of the vertical ionization process the molecule is not only in an electronically excited state but is also vibrationally excited. This is in contrast to adiabatic ionization potentials (IP_{ad}) which correspond to the energy required to remove an electron from a molecule in its lowest vibrational level, leaving the resultant ion in its lowest vibrational level. Electron impact ionization potentials are frequently larger than spectroscopic values since the former may produce vibrationally excited ions even at the threshold electron energy.

The quantum mechanical basis of this principle lies in the overlap

between the vibrational wavefunctions of the two electronic states. Transitions occur most strongly between vibrational states that have the most overlap since these will have similar characteristics. The ground vibrational wavefunction is a bell shaped curve with its maximum near the equilibrium nuclear configuration (see figure 2-3). Many of the vibrational wave functions of the excited electronic states overlap this function, but the greatest overlap occurs with functions that reach a maximum in the same region of space. If the potential energy surfaces for the ground state of the neutral and the electronic state of the ion are displaced, then the maxima of the wavefunctions that are most important will be at the edge of the potential well. As a result the vertical transition will result in the strongest overlap between the functions. These principles are shown in figure 2-3.

As the energy of the electron beam is increased, electronically excited molecular ions may be formed. At the ionization potential (IP_v) the energy of the bombarding electron is sufficient to produce molecular ions in their ground state with varying degrees of vibrational excitement. The distribution of energy for molecular ions will extend from those ions which have almost no vibrational energy to those which were initially highly thermally excited and received all of the electron's energy. As stated previously, the formal limits of the internal energy distribution are zero to $\varepsilon(e) + \varepsilon(T) - IP_v$. The energy distribution is shown in figure 2-5(a).

The behaviour of molecular ions possessing defined amounts of internal energy is of much interest since, for example, the variation in reaction rate as a function of excess energy can then be compared with theory on a firm basis. The earliest experimental approach

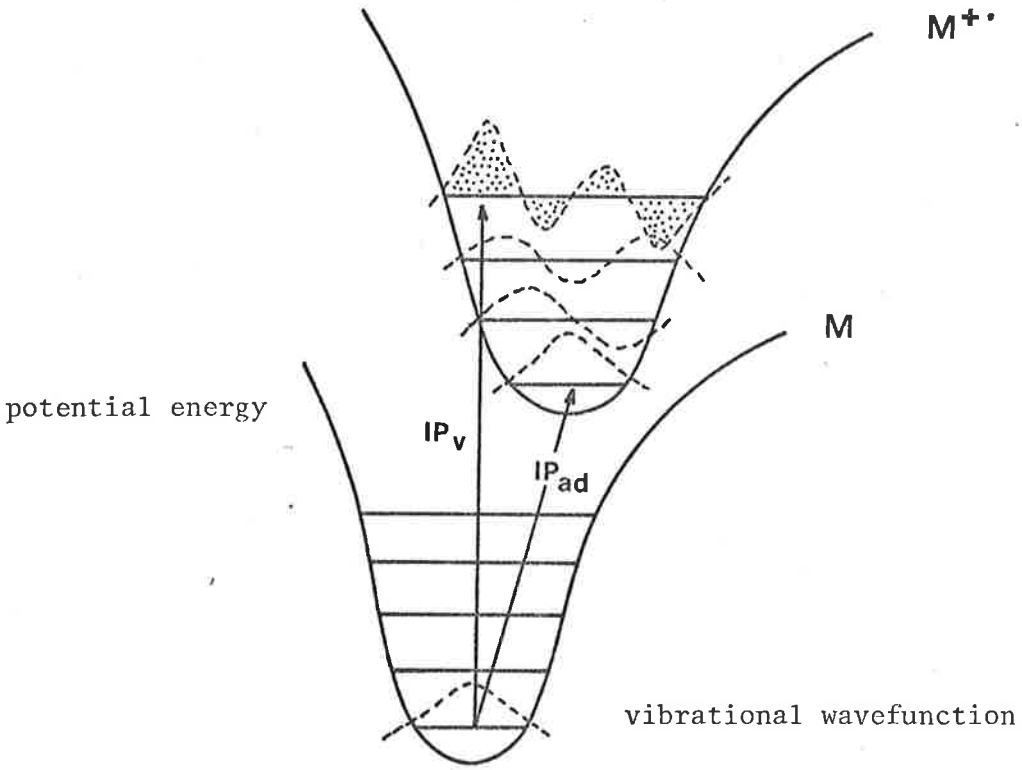

Figure 2-3

to the problem of forming mono-energetic molecular ions was charge-exchange mass spectrometry[147]. A more recent procedure is photo-electron-photoion coincidence mass spectrometry[123,142,148]. In this technique ions are detected in coincidence with energy analysed photoelectrons. This determines the energy balance in photoionization and as a result, ions of known internal energy can be investigated.

The electron impact source of a mass spectrometer is usually operated at a pressure of around 10^{-6} torr and as a result the ions produced will not undergo intermolecular collisions. In the absence of both intermolecular energy transfer and radiative

transitions, the internal energy of each ion is fixed at the value produced in the initial excitation. This situation should be contrasted with condensed phase thermal, photochemical and electrochemical reactions where collisional deactivation produces a Maxwell-Boltzmann distribution of energies. Gas phase techniques in which the ions can be thermalized include high-pressure mass spectrometry[149], flowing-afterglow[150] and ion cyclotron resonance (icr) mass spectrometry[121].

The internal energy of the molecular ion can be divided into electronic, vibrational and rotational states. Vibrational and rotational energy are not interconvertible in the absence of collisions. Electronic and vibrational energy can be interconverted by the reversible process of internal conversion; if the density of electronic states is high then it is possible to populate low-lying electronic states from higher ones by the crossing of potential energy surfaces. The principle of internal conversion is shown in figure 2-4.

There is no information about the numbers of electronic states and associated vibrational states to which excitation may occur in complex molecules. However it is expected that the density of states will increase with energy which will result in an increase in the number of potential energy surface crossings. As the energy is increased then the effects of the anharmonicity of vibrations results in greater overlap of vibrational states between electronic states. In this way vibrational quanta originally localized in particular bonds can be randomised throughout the vibrational modes of the entire molecule. The randomization of internal energy throughout the ion is assumed to occur at a rate which is rapid in

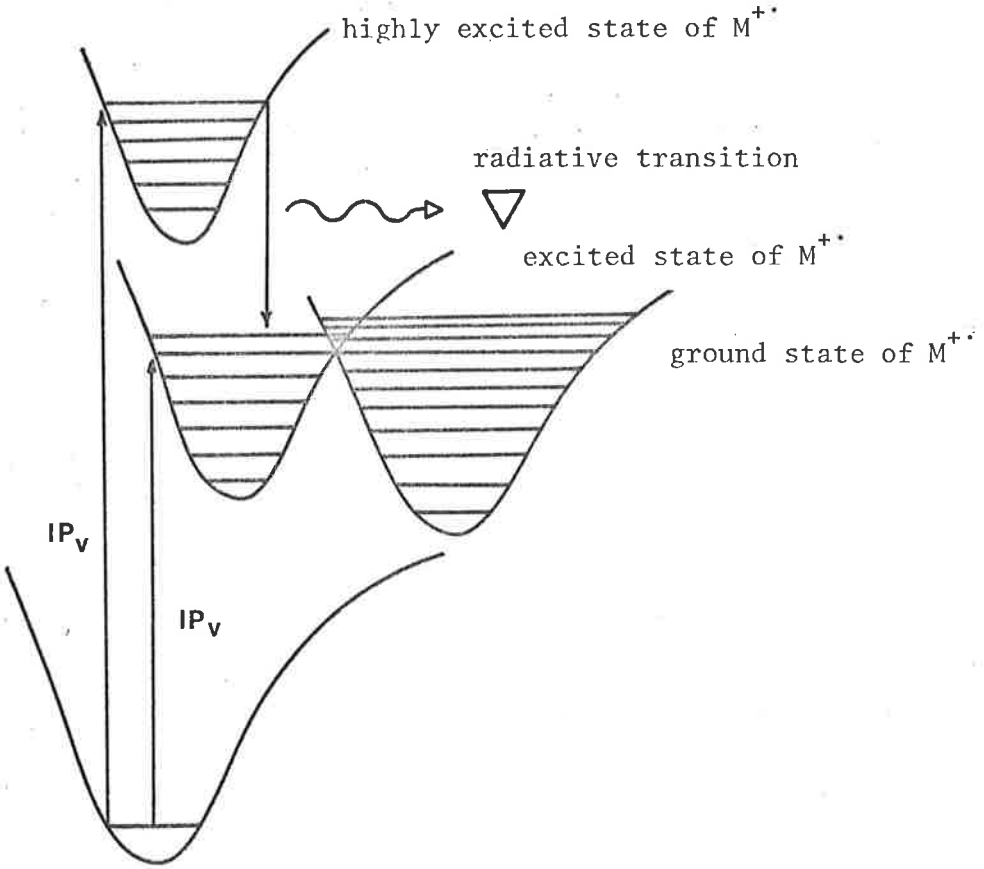

Figure 2-4

comparison with fragmentation. This is one of the basic tenets of the statistical theory of unimolecular reaction rate theory.

Statistical Unimolecular Rate Theory

Statistical theories have been developed with the aim of predicting reaction rate constants and breakdown diagrams for the unimolecular reaction of gas phase ions. Such theories determine the reaction rate by determining the probability of reaction proceeding from a reactant, with its internal energy distributed throughout its electronic states, to a transition state with its

own electronic distribution. As with absolute rate theories a critical point on the potential energy surface is examined and this transition state dominates the magnitude of the rate constant. In evaluating rate constants using statistical theories one must guess the structure of the transition state and estimate its vibrational frequencies by comparison with known stable molecules. To make educated guesses of transition state structure, a detailed knowledge of structure of both the reactants and products and of the mechanism of their interconversion is required. In this sense statistical theories in their present quasi-equilibrium theory (QET)[151] and Rice, Ramsperger, Kassel and Marcus (RRKM)[152-155] forms are not truly predictive. For systems in which the statistical theories show good agreement with the observed rates of reaction, then these numerical methods can then be used to probe the finer details of reaction kinetics (such as kinetic shifts).

The most important of the assumptions of QET is that the molecular processes leading to the formation of a mass spectrum consist of a series of competing, consecutive unimolecular reactions of energetically excited ions. Further, as mentioned previously, it is assumed that the initial excess energy gained in ionization randomises throughout the entire molecule at a rate which is rapid relative to the rate of reaction of the ion: the energy flow from one electronic state to another occurs in times comparable with those required for molecular vibrations. The QET recognises that rates of unimolecular reactions depend on the energies and entropies of activation and the rate constant for the reaction is most simply related to the internal energy (ε) of the decomposing ion by equation 2-6[151,156,157].

$$k(\varepsilon) = \nu \left(\frac{\varepsilon - \varepsilon_o}{\varepsilon}\right)^{s-1} \qquad \text{Equation 2-6}$$

In equation 2-6 the activation energy is denoted by ε_o, ν is a frequency factor and s represents the number of effective harmonic oscillators.

When the internal energy of the ion is high relative to the activation energy for the process, then the rate constant approaches the frequency factor for the reaction. In the case of simple bond cleavages, the frequency factor approaches the vibrational frequency of the bond in question (of the order of 10^{14} $sec.^{-1}$). For rearrangement reactions, the frequency factor is several orders of magnitude lower than for simple cleavage reactions reflecting the entropic factors of the transition state. As a result, even though rearrangement reactions usually have lower activation energies and the ratio $(\varepsilon - \varepsilon_o)/\varepsilon$ may be close to unity their rate constants are usually lower than for simple cleavage reactions.

If the internal energy of the ion is of the same order of magnitude as the activation energy, then the reaction will not occur at the rate given by the frequency factor. The rate will depend on the time taken for sufficient vibrational quanta to gather in the reaction coordinate. This will in turn depend on the total number of vibrational quanta available, the activation energy and the number of vibrational states available in the molecule (related to molecular size). In equation 2-6, s is the number of internal degrees of freedom (3N-6 for non-linear molecules, 3N-5 for linear molecules). In practise however, s is taken as the effective number of oscillators which may be as low as one fifth of the total number. Figure 2-5(a) and (b) relates the rate constant versus internal energy plots for a

simple cleavage ($M^{+\cdot} \longrightarrow A^{+\cdot} + N_1$) and a rearrangement reaction ($M^{+\cdot} \longrightarrow B^{+\cdot} + N_2$) to the energy distribution function $P(\varepsilon)$ for the molecular ion. The energy distribution plot shows the relative proportions of the molecular ions which give rise to each type of ion at the collector.

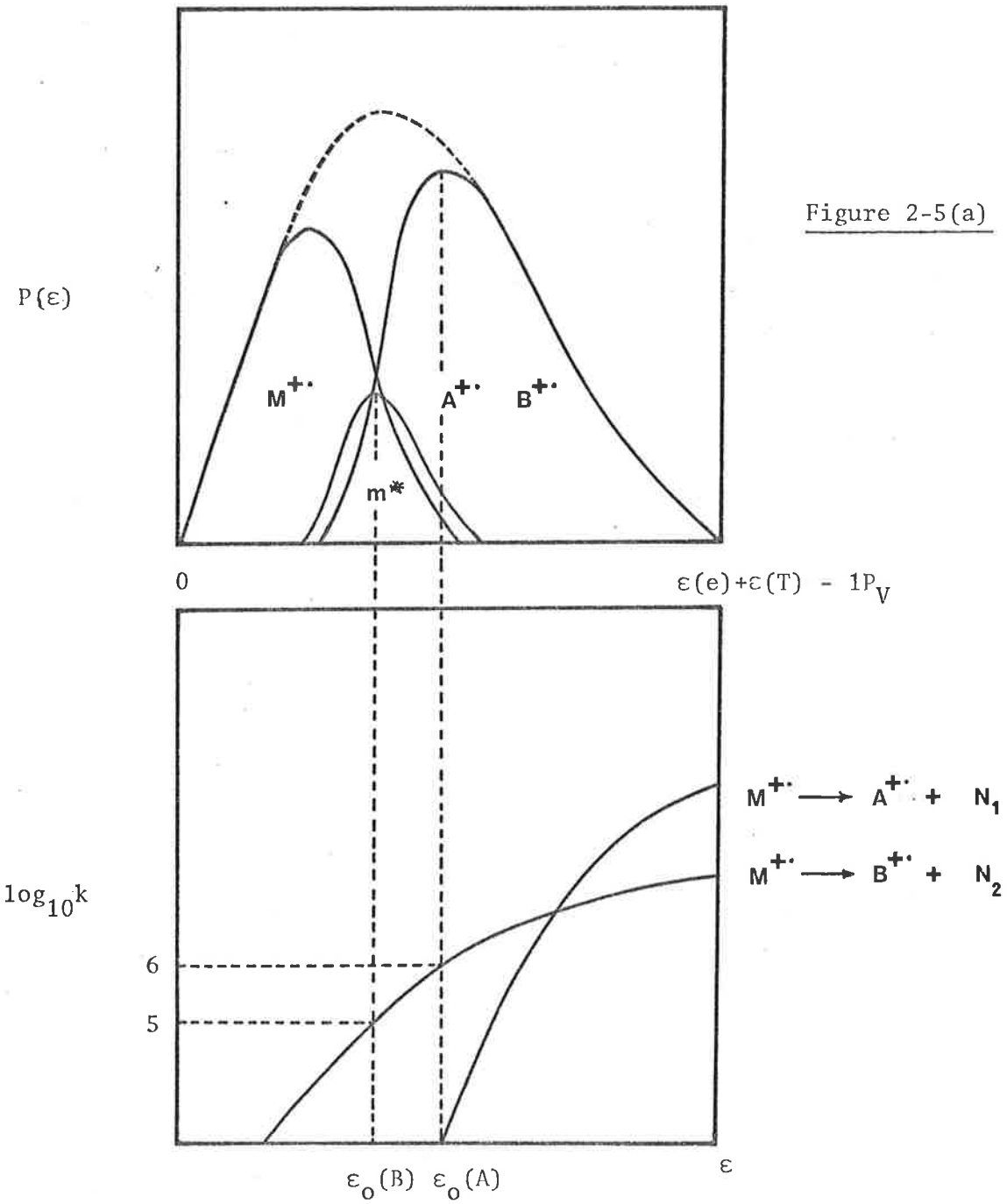

Figure 2-5(a)

Figure 2-5(b)

Equation 2-7 is the RRKM statistical equation[152-155,157-160]. This equation, although formally quite different from

$$k(\varepsilon) = \frac{1}{h} \frac{Z^{\ddagger}}{Z^*} \frac{\Sigma P^{\ddagger}(\varepsilon - \varepsilon_o)}{N^*(\varepsilon)} \qquad \text{Equation 2-7}$$

the QET equation in its simplistic form (equation 2-6), encompasses all of its essential features in a more readily assimilable form. The terms $Z^{\ddagger}$ and Z^* in equation 2-7, describe the products of the partition functions for the adiabatic degrees of freedom of the transition state and the activated reactant respectively. The term $\Sigma P^{\ddagger}(\varepsilon - \varepsilon_o)$ is the total sum of the degeneracies of all possible energy eigenstates of the active degrees of freedom for the transition state at total energy $\varepsilon - \varepsilon_o$ $(=\varepsilon^{\ddagger})$. The $N^*(\varepsilon)$ factor is the number of eigenstates per unit energy of the active degrees of freedom for the activated molecule at energy ε. The degrees of freedom in RRKM theory are considered to be either active or adiabatic. The vibrational and internal rotational degrees of freedom are considered as active and only the overall molecular rotations are adiabatic. The terms corresponding to the translational degrees of freedom of the activated molecule and transition state always cancel. Expressions for $\Sigma P^{\ddagger}(\varepsilon - \varepsilon_o)$ and $N^*(\varepsilon)$ have been developed by Marcus and Rice[152-155].

The RRKM theory enables calculation of unimolecular rate constants using a knowledge of molecular structure and thermochemistry. Unlike QET there are no adjustable parameters such as the effective number of oscillators or the frequency factor. However in practice, there are two semi-empirical aspects; (i) assignment of structure and frequencies to the transition state and (ii) the degree of

anharmonicity in the molecular vibrations at high energies[158].

Recently the RRKM theory has been incorporated into phase-space formalism[114,161-163]. Phase-space theory conserves the total angular momentum of the transition state and probes the channels available for reaction products. This, in effect, moves examination of the potential energy surface for the reaction away from the transition state and into the region of product separation. When the transition state resembles the products then both RRKM and phase-space theories predict similar rate constants. As the transition state becomes more reactant-like phase-space theory then provides the upper limit to the reaction rate constant.

Comparison of experimental results and rate constants calculated using RRKM theory for ions with an imprecise amount of internal energy has only been modestly successful[114]. Studies of metastable ions with their small distribution of excess internal energy has alleviated this problem to an extent. Although the excess energy is more closely defined in these ions there is still an energy distribution and variation of the rate constant as a function of excess energy remains largely unexplored. Charge-exchange and photoelectron-photoion coincidence mass spectrometry have transformed this area. Either technique imparts precise amounts of excess internal energy to the ion so that variation of reaction rate constant with energy can be compared with theory on a firm basis. The review by Chesnavitch and Bowers[114] summarizes the results obtained in the application of statistical rate theories to ionic systems where mono-energetic data have been obtained.

The lack of success of the statistical theories has been demonstrated by Eland and coworkers[164-167] by using photoelectron-

photoion coincidence mass spectrometry. In particular, in their study of the fragmentations of methyl halide molecular ions they found that the ions undergo specific reactions to various products, depending on their electronic state[167]. In addition they found that some internal conversion did occur, to an extent which correlated with the energy difference between the states concerned. However the vibrational energy did not statistically re-distribute between certain states. Results such as these are not in accord with the basic tenets of statistical theories. In contrast to these results, Eland has also shown that in the fragmentation of propane and neo-pentane molecular ions the statistical fragmentation model is probably correct[168]. Charge-exchange mass spectrometry of iso-butane[169] yielded a breakdown diagram which when compared with the calculated curve (QET) yielded good agreement up to 17eV.

Energetics of Ion Decomposition

In the study of unimolecular fragmentations of ions, the mechanism and energetics of the process can only be fully understood when the structure and electronic identity of the reactants, transition state and products are known (i.e., the potential energy surface for the reaction is known in detail). Some of the information required is the heat of formation of the reactants and products, the activation energy (or critical energy) for the process and how the excess energy of the products is distributed amongst the vibrational, rotational and translational degrees of freedom. Much of this information is not available for the gas phase ion chemistry of polyatomic systems. Even the assignment of the structure of the reactant ion may be highly tenuous. Structures of ions are usually

inferred from the structure of the neutral molecule and from consideration of the reaction channels which are open to the ion. Inferences gained by this type of indirect study may often be contradictory and misleading. In fact the structure of the non-decomposing ion may well be different from that of the decomposing ion[162].

Figure 2-6 shows a schematised potential energy curve for the formation and decomposition of a molecular ion. Shown in the figure are some of the thermochemical parameters which describe this

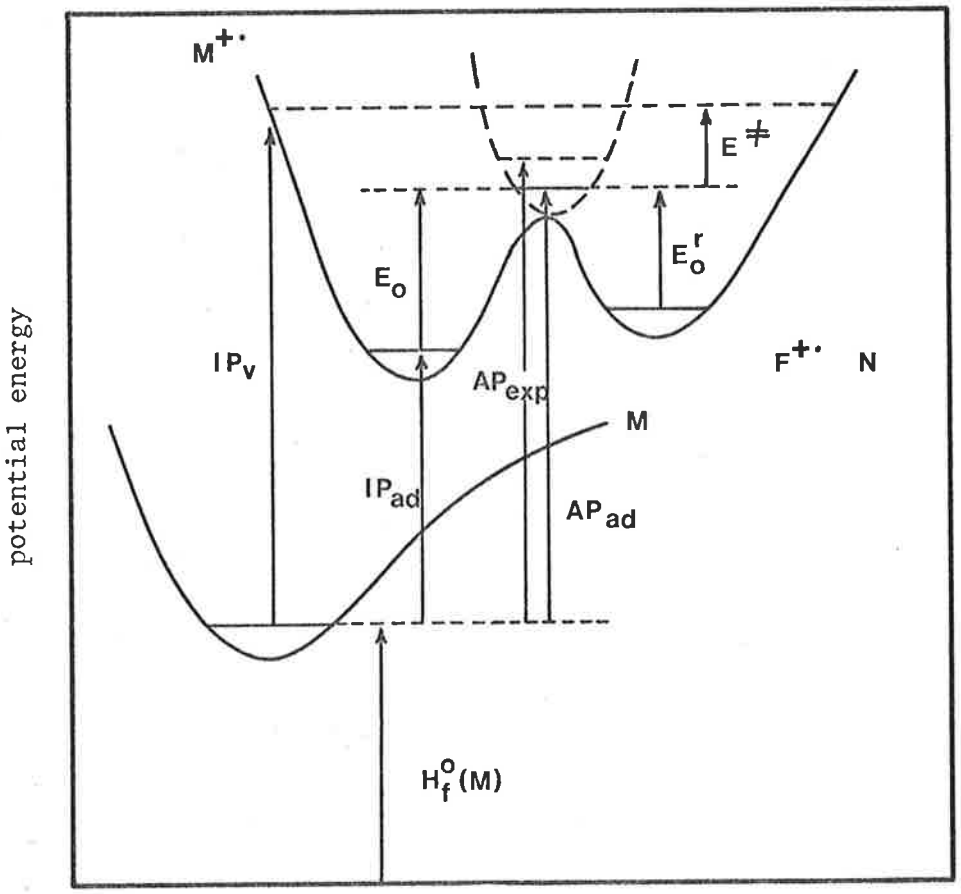

Figure 2-6

fragmentation. The minimum energy required by the molecular ion for fragmentation to yield the daughter ion ($F^{+\cdot}$) is the appearance potential and is denoted by AP. The experimental value of the appearance potential (AP_{exp}) differs from the adiabatic value (AP_{ad}) by an amount which varies with the time limits imposed on the reaction by instrumental factors and on the presence of competing reactions which may also occur at the threshold electron energy. In order to observe daughter ions as stable ions in a mass spectrum, they must be formed by reactions that occur in the ion source. Typically, an ion spends around 10^{-6} sec. in the source before being accelerated into the analyser region of the mass spectrometer. As a result, the experimental appearance potential for stable ions corresponds to an energy at which a large number of parent ions are decomposing with a rate constant of $\geqslant 10^{6}$ sec.$^{-1}$. The difference between the experimental and adiabatic appearance potentials is the excess energy required to achieve this rate of reaction and is termed the kinetic shift[170]. This difference can be reduced by sampling ions with longer lifetimes such as metastable ions[171]. Ions with longer lifetimes will have a lower (mean) internal energy and their reaction in later sections of the mass spectrometer means that there is a lower kinetic shift operative. Kinetic shifts can be estimated by the photoelectron-photoion coincidence technique using a delay between electron detection and ion extraction[172,173] and by calculation [174,175].

The other factor affecting the experimental appearance potential is the competitive shift. If competing reactions are occurring at the threshold electron energy of the reaction understudy, the rise in the number of daughter ions with electron energy may be slow. This may cause up to 2eV difference between AP_{exp} and AP_{ad}[176].

The activation energy in figure 2-6 is denoted by ε_o and is equal to $AP_{ad} - IP_{ad}$. The activation energy for the reverse process is ε_o^r, the internal energy of the transition state is $\varepsilon^{\ddagger}$ and the sum of these parameters is the excess internal energy of the products denoted by ε_{excess}.

The excess energy must be distributed among the degrees of freedom of the products as the system passes from the saddle point to the product region of the potential energy surface. This energy may appear in electronic, vibrational, rotational or translational states or any combination of these. If the energy of the reacting ions is more than sufficient for reaction (considering not only the activation energy but also the kinetic shift), then this additional energy ($\varepsilon^{\ddagger}$) will also be partitioned amongst the product's degrees of freedom. The manner in which ε_{excess} is partitioned is naturally a function of the potential energy surface for the reaction and knowledge of the re-distribution is essential if the thermochemistry of a reaction is to be properly delineated.

The portion of the excess energy which is partitioned into the translational degrees of freedom of the products can be determined indirectly by analysis of the peak shape of both normal and metastable ions. The kinetic energy which is released may have originated from either the activation energy for the reverse process alone or from the internal energy of the transition state ($\varepsilon^{\ddagger}$) as well. The distinction between the dual origins of the kinetic energy release arises from the variable nature of the energy of the transition state (the so-called non-fixed energy). The reverse activation energy is fixed and dependent on the nature of the potential energy surface for the reaction. The energy of the transition

state, on the other hand, is dependent on the energy imparts to the reacting ion during the initial ionization process. As a result, ions reacting in different regions of the mass spectrometer (ions of different lifetimes) will release varying amounts of kinetic energy[177]. If the kinetic energy release by metastable ion transitions is studied, then it is found that it is dependent to a greater extent on the reverse activation energy than on the energy of the transition state. This result is expected since the contribution of $\varepsilon^{\ddagger}$ to the excess energy of the products is small for ions of long lifetimes. As a consequence, the kinetic energy released from metastable ion transitions is more characteristic of the potential energy surface for the reaction than releases from ion source reactions.

The kinetic energy release is measured from the width of the metastable peak at either 50% or 20% of peak height. Equation 2-8 shows the relationship between the kinetic energy release (T) and the masses of the daughter ion (m_2), the neutral (m_3) and the parent ion (m_1), the voltage at which the peak maximum occurs (E) and the width of the metastable peak (ΔE)[178].

$$T = \frac{m_2{}^2}{16.m_1.m_3.} \left(\frac{\Delta V}{V}\right)^2 \qquad \text{Equation 2-8}$$

Since the kinetic energy released during metastable ion transitions can be measured with high precision[179], attempts have been made to understand the partitioning of the reverse activation energy between the translational and internal degrees of freedom of the products. Recently model calculations, which were based on a dynamical model, showed good agreement with experimental results for the release of kinetic energy for a number of ionic reactions[180].

The calculations showed that if the transition state coordinate corresponded to a translational motion separating the products of the reaction, then the reaction coordinate from the transition state to products is a straight line on the hypersurface (repulsive surface[181]). As a result the kinetic energy released along this path is expected to initially appear almost entirely as kinetic energy of separation and the absence of reaction coordinate curvature means that little of this energy will be lost subsequently to other modes of product motion. This situation is most likely to arise with "late" transition states which tend to occur with endothermic reactions. As a result, it is expected that a relatively large proportion of the reverse activation energy will appear as kinetic energy of product separation in endothermic reactions.

On the other hand, if the reaction coordinate at the transition state is composed of atomic motions which differ from those required for product separation, the minimum energy path on the reaction hypersurface will be curved. The curvature of the reaction path will tend to have the effect of channelling the excess energy into motions other than translations. This will happen in two ways. Firstly, the initial momentum gain associated with loss of potential energy will pass largely into product motions other than translation particularly over the early part of the trajectory. Secondly, the curvature of the path will provide a mechanism for a greater degree of "scrambling" of kinetic energy among all product modes. Consequently "early" transition states (corresponding to attractive surfaces[181]) should favour partitioning of the reverse activation energy into product vibration. "Early" transition states tend to

occur with exothermic reactions.

The above qualitative arguments based on the trajectory calculations[180] are entirely reasonable when one considers the energy requirements of the reverse processes. In an almost thermoneutral process in which two fragments associate to form a transition state, it has been shown that an "early" saddle point is surmounted most effectively by translational energy in the approach coordinate. Alternatively with a "late" saddle point, vibrational energy in the reactions is more effective[182].

As an example, it is found that the ratio of the kinetic energy released to the reverse activation energy (1.1) for the loss of molecular hydrogen from the ethane radical cation suggests that most of the reverse activation energy passes into translational degrees of freedom. Since the ratio is greater than unity then it appears that some of the vibrational energy of the transition state also passes into kinetic energy of product separation. The loss of hydrogen occurs exclusively by a 1,2 elimination process[183] through a four-centred transition state. The product separation occurs along a plane of symmetry thereby not necessitating the partitioning of excess energy into rotational degrees of freedom. The elimination is endothermic as calculated from appearance potential and ionization potential measurements and the heats of formation of products. Therefore the transition state is expected to be "late". The calculated T/ϵ_o^r ratio is in satisfactory agreement with the experimental ratio when the simplicity of the transition state model is considered[180].

Release of kinetic energy in metastable ion reactions has been attributed to the process being "forbidden" on the grounds of orbital

symmetry[109,184,185]. The 1,2 elimination of molecular hydrogen from $CH_3CH_3^{+\cdot}$, CH_2OH^+, $CH_2NH_2^+$, CH_2SH^+ and $CH_3NH_2^{+\cdot}$ all proceed with significant release of kinetic energy[186]. Construction of a formal correlation diagram (for the loss of hydrogen from the ethane radical cation) shows that as the transition state is passed, the electronic reorganization which occurs is characterised by a molecular orbital in which there is mutual repulsion between the products. Alternatively the negligible kinetic energy released in 1,1 hydrogen eliminations from $C_6H_7^+$, $C_2H_5^+$ and $C_2H_4^+$ is due to the reactions being "allowed" on orbital symmetry grounds[187]. The occurrence of 1,1 eliminations have been supported by a study of deuterium kinetic isotope effects[188].

The dynamical approach to energy partitioning suggests that it is the curvature of the potential energy surface that is the basis to the partitioning process and that orbital symmetry correlations only give an account of the size of the reverse activation energy. Theoretical studies also suggest that the greater the curvature of the reaction coordinate in the region of the transition state the greater the partitioning of ε_o^r into kinetic energy[189,190].

CHAPTER 3

EXPERIMENTAL RESULTS AND DISCUSSION OF SYNTHETIC METHODS

The work contained in this thesis is aimed at elucidating, as far as possible, the details of the mechanism of the McLafferty rearrangement occurring from the radical cations of various aryl alkyl ketones. The particular molecular system chosen for this work was 1-phenyl-1-butanone (butyrophenone) and its various substituted analogues.† There are many reasons for choosing this system; (i) the simplicity of the molecular system with respect to synthetic considerations, (ii) the relatively high intensity of the McLafferty rearrangement product ion in the mass spectra of these compounds, (iii) the relative lack of competing molecular fragmentations of the molecular ion and (iv) the position of the carbonyl functional group in relation to the aromatic ring, which allows aromatic ring substituent changes to be made which presumably affect the reaction electronically without interfering directly with the reaction centre.

A mechanistic problem, such as this, is in essence a problem which concerns delineation of the potential energy surface for the reaction. In general, there are two independent approaches to problems of this kind which are not mutually exclusive in that the use of one generates the need for the other. One approach is to carry out detailed molecular orbital calculations which define the potential energy surface for the reaction. The problems associated

---

† The compounds mentioned in this thesis are named according to the rules and guidelines put forward by IUPAC Commission on Nomenclature of Organic Chemistry (1979)[191]. The systematic name of each compound appears in the experimental section, but for simplicity, trivial names will be used in the general text.

with this approach have been briefly discussed in Chapter 1. Another approach is to attempt to identify gross aspects of the potential energy surface (such as the existance of potential energy wells between those of the reactants and the products) by means of experimental investigations.

The experimental approach is used primarily in this thesis and the objectives are to gain sufficient data to permit a choice between a variety of proposed mechanisms for the McLafferty rearrangement. Theoretical calculations have also been performed in an attempt to define the mechanism for the rearrangement of the butyrophenones in greater detail. As will be discussed at greater length in Chapter 4, the calculations rely to a large extent on the experimental data obtained.

In the main, the experimental approach has been to measure the isotope effects on the rates of the McLafferty rearrangement for the various butyrophenones and to compare these results within the framework of the theory of isotope effects as outlined in Chapter 1. The calculations that were performed on this system serve to facilitate the application of isotope effect theory to this particular system under study.

The format of the remainder of this thesis is, (i) to present the experimental results that were obtained and to discuss the problems encountered, and also to discuss the synthetic procedures in this chapter (Chapter 3), (ii) to detail the calculations and provide a critique of the calculational methods that were used in Chapter 4, (iii) to discuss in Chapter 5 the results described in Chapters 3 and 4 and (iv) to detail the experimental procedures used in the synthesis of each compound studied in Chapter 6.

Mechanistic Considerations

The McLafferty rearrangement[192-194] is by far the most widely studied fragmentation in organic mass spectrometry. One reason for such interest is that it is a major fragmentation pathway from the molecular ions of a wide variety of different compounds. The importance of the McLafferty rearrangement can be gauged by the review by Kingston, Bursey and Bursey[195] which covers the literature up to 1972 and contains 651 references. Meyerson and McCollum[196], Budzikiewicz, Djerassi and Williams[197], Bowie[198] and Holmes[118,119] have also reviewed this type of rearrangement. In view of these extensive reviews of the literature, it is my intension to summarize the important mechanistic aspects from the earlier work, and to describe some of the recent literature which I find particularly relevant.

The rearrangement can be described as a 1,5-hydrogen migration via a six-membered transition state. Cleavage of the 3,4 bond

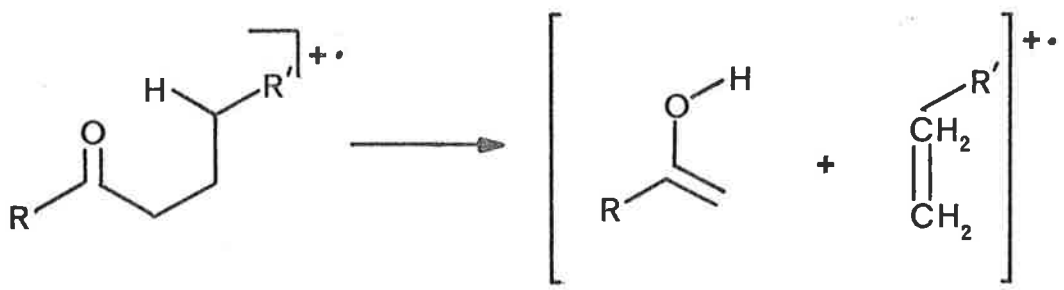

Scheme 3-1

occurs either at the same time as the hydrogen migration (concerted mechanism) or at some later stage (stepwise mechanism). The process is shown in scheme 3-1 for the particular case of the rearrangement occurring with a compound containing a carbonyl functional group. The rearrangement is facile and occurs in the majority of molecules that fulfil the requirement detailed in scheme 3-1[195,197]. The migrating terminus can be oxygen in which case the reaction is observed for ketones, aldehydes, carboxylic acids, esters and amides. If the terminus is carbon, the rearrangement can occur in olefins, acetylenes and aromatic compounds. It is also observed in nitrogen derivatives of carbonyl compounds, in alkaloids, amino acids and nitrogen heterocycles. The terminus can also be sulphur and phosphorus.

If there are two positions containing hydrogens in a 1,5 relationship to the migrating terminus, then the possibility arises that two successive McLafferty rearrangements may occur. The second McLafferty rearrangement is shown in scheme 3-2 for the enol isomer derived from the McLafferty rearrangement of 4-nonanone[197]. The participation of the enol form rather than the keto form in the second McLafferty has been shown by several ion cyclotron resonance experiments[199,200].

Scheme 3-2

The specificity of 1,5-hydrogen transfer has been determined by isotopically labelling a number of ketones, aldehydes and esters[195]. While there can be no doubt that the simple site specific mechanism predominates in conventional 70eV spectra, the behaviour of low energy ions is less clear. Intramolecular scrambling of isotopic labels has been observed in the 10eV spectra of 3-octanones[201,202]. 3-Hexanone and 3-heptanone and their 2,2,4,4-($^2H_4$) analogues have also been studied. These investigations have shown that little or no hydrogen-deuterium scrambling occurs in the 70eV spectrum, whereas the 10eV spectrum shows considerable loss of positional identity for the hydrogen isotopes[202,203]. For ions of increasing lifetime, as sampled by observing reactions occurring in the first and second field free regions, the degree of hydrogen-deuterium scrambling has been shown to increase[202,203]. Non-specific hydrogen transfer has also been observed in the mass spectra of butyric acid[204], propylbenzoate[205] and 4-heptanone[206]. Field ionization studies of hexanal and 3-methyl pentanal and deuterated analogues show that the specificity of the 1,5-hydrogen migration decreases with increasing ion lifetime[207-209].

In order to attain the six membered transition state necessary for the McLafferty rearrangement, two major stereochemical factors need to be satisfied. Firstly, Djerassi and co-workers[210-213] have determined from the study of a series of steroids, that the rearrangement does not occur unless the migrating hydrogen is less than 1.8Å from the migrating terminus. The spectra of the exo and endo isomers of 2-acetyl norbornane support this result[214]. Secondly, the highly directional nature of the orbital containing the unpaired electron on oxygen for radical cations of carbonyl compounds, defines

the direction from which the hydrogen must approach. If the angle between the plane of the carbonyl function and the γ-hydrogen is appreciably greater than zero then it is predicted by molecular orbital calculations that the McLafferty rearrangement will be of reduced importance[215]. However, experimental evidence for this effect from the study of a series of bicyclic ketones, suggests that this stereochemical requirement may not be as critical as the calculations suggest[216]. The spectrum of 2,5-dimethyl-4-isopropyl-3-hexanone provides an example of how steric hinderance can prevent the attainment of the optimal conformation for the 1,5-hydrogen rearrangement, thereby reducing the importance of this reaction in this instance[217].

There has been considerable effort devoted to the determination of the structure of the product ion of the McLafferty rearrangement of carbonyl compounds. The reaction, as depicted in scheme 3-1, requires the formation of the enol isomer of the product ion. The question that must be asked is whether the enol form of the product isomerizes to the keto form.

Studies of the keto-enol tautomerism of carbonyl compounds in solution indicate that the keto isomer is the preferred species, and that there is a high proportion of the enol isomer only if this latter species is stabilized (by increased conjugation, for instance)[218]. Radom and co-workers[219] have shown by molecular orbital calculations, that the potential energy barrier to unimolecular enol to keto transformation is around 80 kcal/mol for acetaldehyde and that the keto form is more stable than the enol form by 11.7 kcal/mol. This barrier is sufficiently high to prevent tautomerization of all but the most highly energized molecules. It is apparent then that the

condensed phase keto-enol tautomerism proceeds by a bimolecular mechanism. Pollack and Hehre[225] have determined by ICR spectroscopy, that the keto form of acetone is more stable by around 13.9 kcal/mol than the enol form. This contrasts the work by Holmes, Lossing and co-workers[226-229] who have determined that the enol form of the ions of aliphatic aldehydes, ketones, acids and esters is 14-31 kcal/mol more stable than the keto form of the ion.

With such a large potential energy barrier to tautomerism, it is difficult to see how the enol ion formed from the McLafferty rearrangement can convert to the keto form via a unimolecular mechanism. Earlier experimental work on ionization potential measurements[196] and a combination of photoionization studies and thermochemical calculations[220,221], concluded that the enol form of the McLafferty rearrangement product ion was the more probable structure. Collisional activation studies of acetaldehyde and its enol isomer[222], acetone and its enol form[223] and acetic acid and its enol form[224] have shown that both the keto and enol ions are stable entities at lifetimes of around 10^{-5}sec. Thermochemical calculations from ionization and appearance potential measurements for a variety of enol and keto radical cations in the gas phase have been carried out by Holmes and Lossing[226-229]. Their conclusions support the above findings in that generally the enol ion is around 14 kcal/mol more stable than the corresponding keto form.

An alternative approach to this problem has been to investigate the further unimolecular reactions of the McLafferty rearrangement product ion and to analyse these in terms of either enol or keto structure. The decomposing $(M-C_3H_6)^{+\cdot}$ ions from menthone[196], 2-isopropyl-3-methylcyclohexanone[196] and piperitone[230] have structures

consistent with the enol form. It has been determined that at least for some aliphatic ketones, the metastable McLafferty product ion, decomposing by the loss of a methyl radical, scrambles in such a way as to suggest re-ketonization of the enolic form[231-233]. In the case of butyrophenone, the $(M-C_2H_4)^{+\cdot}$ ion has been shown by deuterium labelling studies, not to tautomerize in 10^{-5} sec[234,235]. Again, this conclusion arises from the investigation of the loss of a methyl radical from this ion and the observation that hydrogen scrambling does not take place. Elimination of a methyl radical from the $(M-C_2H_4)^{+\cdot}$ ion from butyrophenone, is presumed to occur from the rearranged ion produced by the migration of an aromatic ring hydrogen to the α-carbon, followed by transfer of the enolic hydrogen to the aromatic ring. In both hydrogen migration steps there is expected to be a large activation energy[236]. This mechanism differs from that suggested for the loss of a methyl radical from 0-hydroxybutyrophenone in which the enol-keto tautomerism is "catalysed" by the hydroxy moiety[236].

The structure of ions in general and the McLafferty rearrangement product ions in particular have been investigated on the basis of their reaction with neutral molecules in the cell of an ion cyclotron resonance (ICR) mass spectrometer. In this way, the $(M-C_3H_6)^{+\cdot}$ ion from 2-hexanone has been shown to react in the same manner as the enol ion of acetone (generated from the retro-ene reaction of 1-methyl-cyclobutane) and react differently to ionized acetone itself[237]. This result is not, however, conclusive and cannot be generalized to all McLafferty rearrangements[239,240]. Tautomeric conversion of the enol to the keto form of the $(M-C_3H_6)^{+\cdot}$ ion from 2-propylcyctopentanone has been suggested to occur in an ICR spectrometer modified to allow

long ion residence times[240].

As previously mentioned, the 1,5-hydrogen migration can conceptually occur via a stepwise or a concerted mechanism. If the hydrogen migration and the 3,4-bond cleavage occurs at the same time then the potential energy surface for the reaction consists of the reactant and product potential wells and the transition state at the saddle point which divides them. In this case the reaction coordinate is composed of changes in the atom coordinates for each member of the six-membered transition state. Scheme 3-3 describes the concerted mechanism for hydrogen atom transfer.†

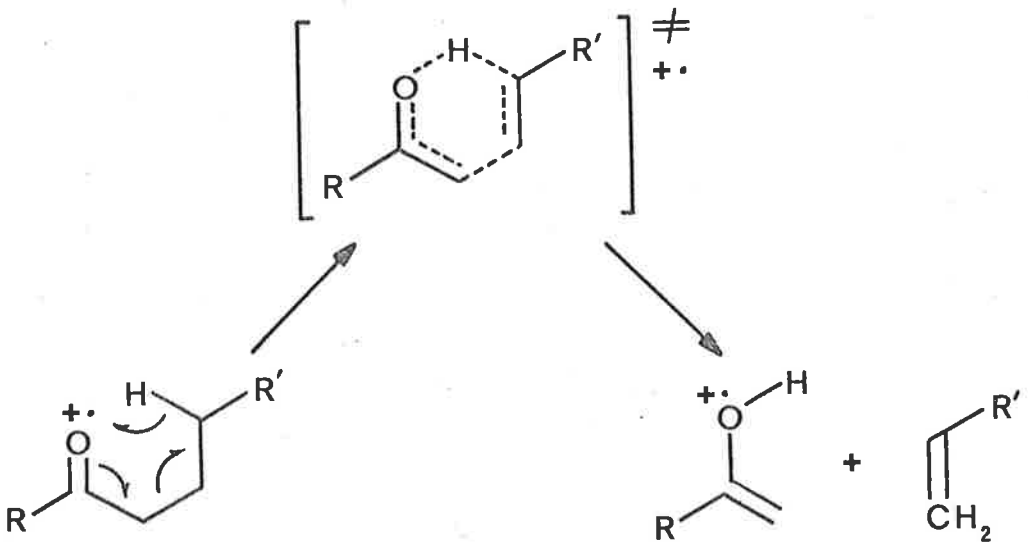

Scheme 3-3

Since all of the atoms in the six-membered transition state are involved in the reaction coordinate, then isotopic substitution of any of them should result in a kinetic isotope effect on the

---

† The rearrangement is depicted as a hydrogen atom transfer for simplicity; hydride ion and proton transfer are also possibilities.

observed rate of reaction.

Alternatively, if the potential energy surface contains a potential well between the reactant and products, then the mechanism is said to be stepwise. In this case the hydrogen migration precedes the cleavage of the 3,4-bond. This process is shown in scheme 3-4, again for hydrogen atom transfer. For the stepwise mechanism, the overall process is composed of two elementary steps (steps (i) and (ii) shown in scheme 3-4), each with its own transition state. The rate of the overall process will be dependent on the elementary step which

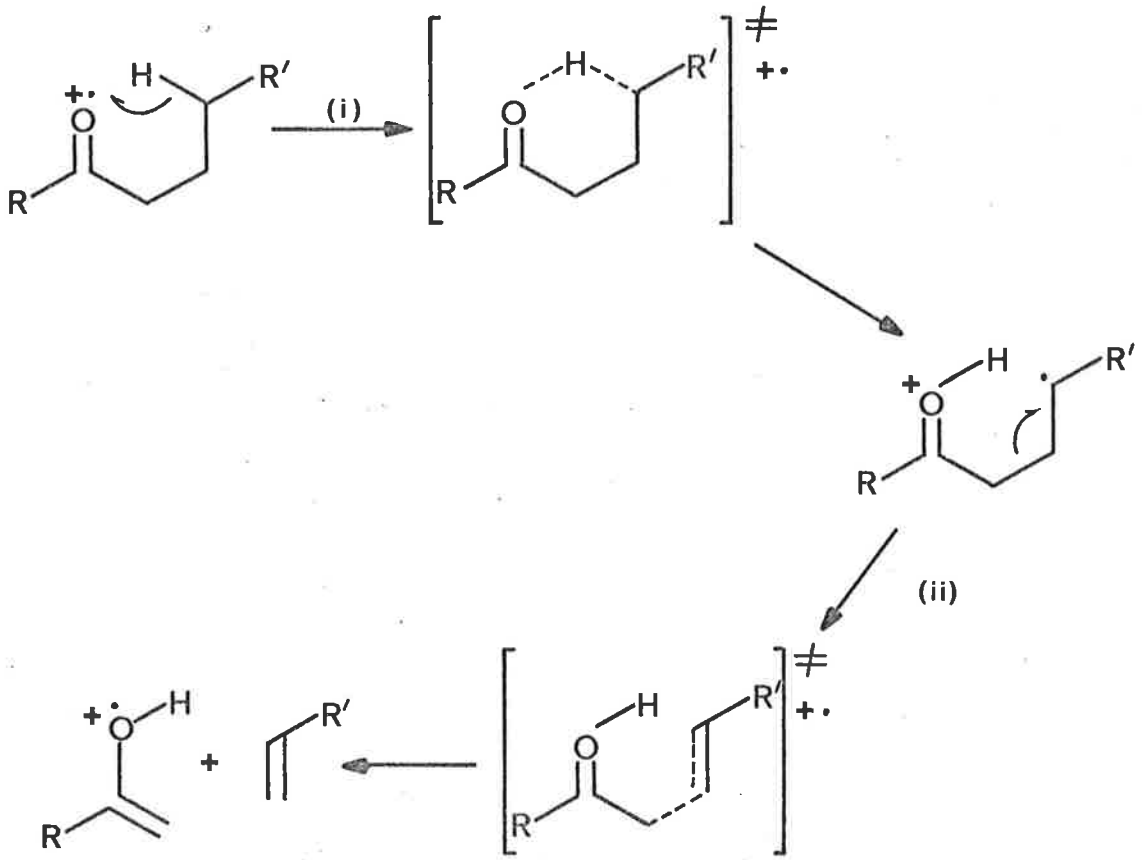

Scheme 3-4

occurs with the lowest rate constant, i.e., dependent on the step involving the transition state of highest energy. If hydrogen migration is the rate determining step, then bonding changes which occur further along the reaction coordinate will have no effect on the reaction rate. As a result of this, one would expect that a hydrogen kinetic isotpe effect would be observed from isotopic labelling at the 5-position. Moreover, since bonding changes occurring after this step have no effect on the overall rate of the process, isotopic labelling of atoms involved in step (ii) will not lead to observation of a kinetic isotope effect on the observed rate of reaction.

Alternatively, if step (ii) in scheme 3-4 is the rate determining step of the stepwise mechanism then isotopic substitution of the 5-hydrogens will not lead to a kinetic isotope effect. However, if step (i) is rapid when compared to step (ii), an equilibrium situation may be encountered and it is therefore possible that a hydrogen isotope effect (equilibrium) will be observed for the reaction[241,242]. Naturally, isotopic substitution of any of the atoms directly involved in step (ii) will lead to kinetic isotope effects on the overall rate for the process[43].

As a result, any investigation of the McLafferty rearrangement utilizing the technique of isotopic labelling to delineate the mechanism, must attempt to distinguish between the mechanistic types outlined above. It is clear that the observation of an isotope effect on the rate for the reaction is not a necessary condition for that atom being involved directly in the rate determining step, i.e., kinetic isotope effect. Not only can the difference in rates on isotopic substitution be due to kinetic reasons but they may rely on thermodynamic factors leading to equilibrium isotope effects or even

hybridization changes or other factors which lead to secondary isotope effects. Clearly, mechanistic arguments based solely on simple labelling experiments must be treated with caution.

The photochemical analogue of the McLafferty rearrangement is the Norrish type II photoelimination[243]. The mechanistic details of this reaction are of some interest to any consideration of the McLafferty rearrangement since the two reactions are formally alike; both involve (i) initial excitation of the reactant molecule and (ii) specific 1,5-hydrogen migration and cleavage of the 3,4 bond. Infrared studies[244] indicate that the type II photoelimination occurring with 2-pentanone in the gas phase, produces propen-2-ol which slowly tautomerizes to acetone. This result is entirely reasonable when one considers the mechanism offered for this elimination reaction.

With aryl alkyl ketones, the type II photoelimination process occurs from the n,π* triplet state[245,246] and there is little doubt that there is a 1,4-biradical as an intermediate in the reaction[247,248]; i.e., the reaction proceeds by a stepwise mechanism in which the 1,5-hydrogen migration is involved in the rate determining step. Reaction rate studies of the Norrish type II photoelimination of para-substituted butyrophenones by Pitts and co-workers[246] and Wagner[247] have indicated that the rate of 1,5-hydrogen migration increases with the ability of the para-substituent to diminish the electron density at the reaction site.

McLafferty and Wachs[249] have studied the effects of substituents on the McLafferty rearrangement of a number of substituted butyrophenones. Their results indicate that the effect of the substituent

on the rate of formation of the $(M-C_2H_4)^{+\cdot}$ ions, as determined by log (Z/Z_o) values[†250], was the following; electron withdrawing substituents strongly enhance the formation of the rearrangement product ion thereby having larger log (Z/Z_o) values than electron donating substituents which tend to diminish the extent of the rearrangement. A plot of log (Z/Z_o) against the Hammett σ values[1] for the substituted butyrophenones exhibited a positive slope indicating that the reaction is; (i) sensitive to substituent changes on the aromatic ring and (ii) the reaction is enhanced by decreased electron density at the reaction site. These observations are consistent with those of Pitts and co-workers[246] and Wagner[247] in their studies of the effects of substituents on the Norrish type II photoelimination in this system.

However, as McLafferty has discussed[251], studies utilizing changes in log (Z/Zo) values with substituent changes must be considered carefully. The abundances of parent and daughter ion peaks not only depend on the rate for the reaction producing the particular daughter ion but also on the rates of all other reactions from each ion and the proportions of non-decomposing forms of each ion. Many of the objections to this type of study can be reduced in importance by viewing the results qualitatively rather than quantitatively. In this way, the correspondence between the effects of substituents on the rate of both the McLafferty rearrangement of butyrophenones and the Norrish type II photoelimination in this

---

† For a process $M^{+\cdot} \rightarrow F^{+\cdot} + N$, where M is a substituted molecular ion, Z = [F]/[M] and Z=Zo when the molecular ion is unsubstituted.

system is clear.

Gooden and Brauman[252] have studied the photodissociation of the butyrophenone molecular ion utilizing an ICR mass spectrometer fitted with an arc lamp and a grating monochromator. Their results indicate that the molecular ion undergoes both photochemical α-cleavage and elimination of ethylene and suggests that these photoprocesses occur from isolated electronic states (thereby violating the basic assumptions of QET as described in Chapter 2). The conclusion of the state specific reactivity of the butyrophenone molecular ion arises from the observation of a sharp transition between the formation of the enol radical cation of acetophenone (type II process) and the butanoyl cation at a photon energy of around 3.3eV.

McLafferty and co-workers have investigated the unimolecular dissociation of both the butyrophenone molecular ion and the protonated form of this ion using the techniques of ion photodissociation in the ICR spectrometer[253] and collisional activation (CA) in the double focusing mass spectrometer[254]. Scheme 3-5 summarizes the unimolecular and ion-molecule chemistry that was elucidated by these techniques. The chemistry described in scheme 3-5 provides an alternative explanation to the state specific photodissociation of the butyrophenone molecular ion proposed by Gooden and Brauman. Using double resonance ICR techniques, McLafferty and co-workers[253] showed that much of the ion at m/z 149 was produced from the ion-molecule reaction between the ion at m/z 120 and butyrophenone. Double resonance techniques and the CA spectrum indicate that the ion at mass m/z 71 arises from the ion at m/z 149 and not from the butyrophenone molecular ion.

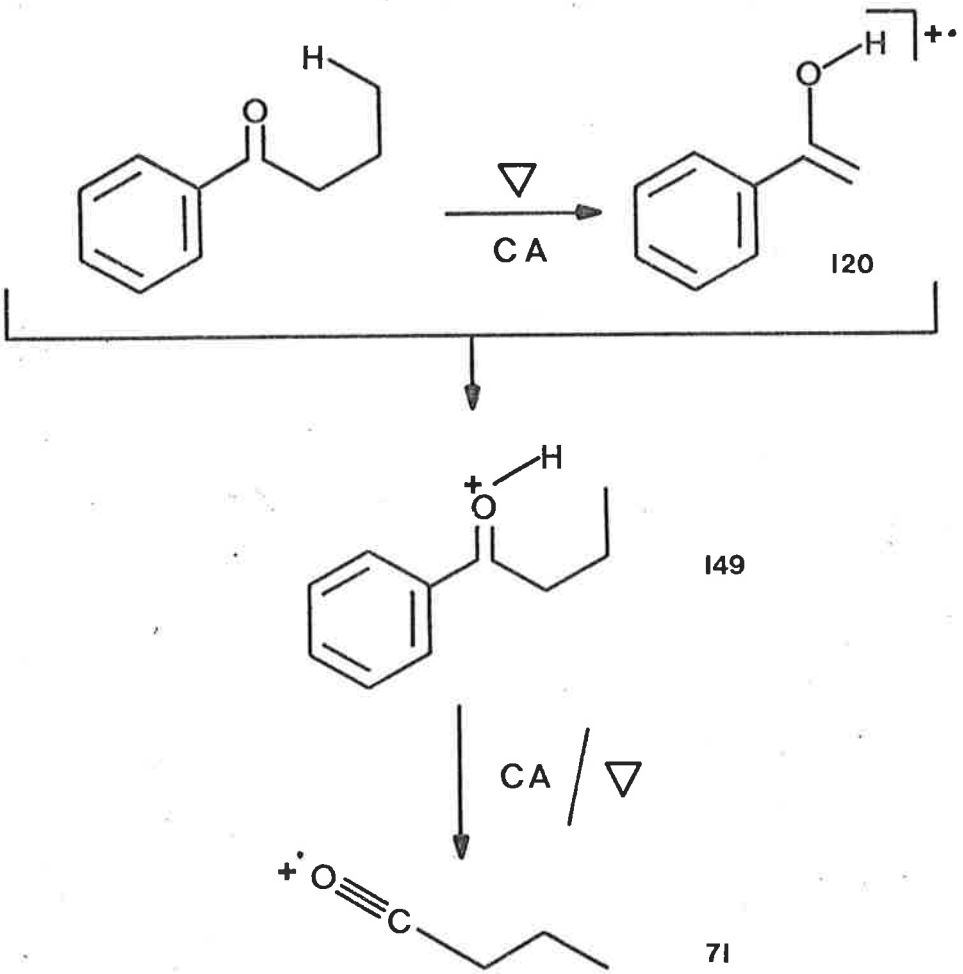

Scheme 3-5

Anodic oxidation of ketones produces a radical cation which can then act as the terminus for a 1,5-hydrogen atom migration, and in this way is formally similar to the McLafferty rearrangement. Comparison of the deuterium isotope effects obtained for the 1,5-hydrogen migration of radical cations generated by both anodic oxidation and electron impact with the isotope effects from the reactions of neutral species (free radicals, and photochemically excited species) imply that radical cations are more reactive[255-257]: in general the deuterium isotope effects for neutral species are

higher than those of the charged species. Furthermore, the isotope effects for the reaction of radical cations generated by either anodic oxidation or electron impact are surprisingly similar. This is emphasized by the results obtained for the rearrangement of 5-($^2H_1$)-2-hexanone radical cation generated by the two processes; the highest isotope effect for anodic oxidation was 1.47 (20°C), whereas the highest mass spectral value was 1.6 (50°C, 70eV)[258]. This suggests that the low isotope effects observed in mass spectral reactions derives from the nature of the radical cation rather than their formative history.

Isotope effects for the McLafferty rearrangement have been reported for ketones, esters, thioketones, aromatic hydrocarbons and aryl alkyl ethers and amines[259-261]. In general, the range of deuterium kinetic isotope effects reported is k_H/k_D 0.70 - 2.17.

Results and Synthetic Methods

The work described in this thesis could be presented in a number of different ways: the most usual way is to discuss the results within the chapter in which they appear. However, due to their reliance on both the experimental and computational data, *any discussion and conclusions will be postponed until all of the results have been presented (Chapter 5).* An exception to this will occur when an experimental approach has proved unsuccessful, in which case the procedure and the problems encountered will be discussed in this chapter.

In addition, the experimental results and synthetic procedures will be presented in chronological order. This is done in an attempt to emphasize the scientific method used in this investigation.

An obvious disadvantage with this approach is that on occassion some of the work may appear disjointed. Any difficulties that may arise due to this will be rectified in Chapter 5.

(a) Para-Substituted Butyrophenones

Initially, the effect of changing the substituent para to the carbonyl group of butyrophenones on the kinetic energy release was investigated. This required the synthesis of a series of para-substituted butyrophenones.

The second part of this investigation was to determine the effect of substituents on the deuterium isotope effect for a series of butyrophenones isotopically labelled at carbon-4. It was therefore necessary to design a synthetic route utilizing a common precursor to incorporate the deuterium label into a number of para-substituted butyrophenones. Since both the isotopically labelled and un-labelled series were required, the most suitable of the synthetic routes available was determined using isotopically un-labelled precursors.

The initial route attempted was the alkylation of para-substituted benzonitriles with propylmagnesium bromide and the subsequent hydrolysis of the imine formed[262]. Preparation of the compounds *p*-methylbutyrophenone, (1-(4-methylphenyl)-1-butanone)† (1); butyrophenone (1-phenyl-1-butanone)(2); and *p*-chlorobutyrophenone (1-(4-chlorophenyl)-1-butanone)(3), was attempted by this method. The reaction is shown in scheme 3-6. The isolated yield of ketone(1) was 40%; the remainder of the product mixture was *p*-methylbenzonitrile.

---

† In this text, the first time that a compound is named, both the trivial and systematic names will be used, with the latter in brackets.

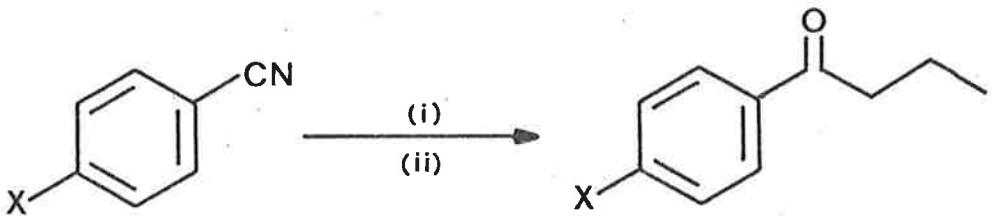

X = CH_3 (1)
H (2)
Cl (3)

(i) n-PrMgI/Et_2O/Δ
(ii) HCl/H_2O

Scheme 3-6

Similarly, the formation of ketones (2) and (3) was shown to be incomplete after heating the reaction mixtures under reflux for 24 hours. Due to the sluggishness of the reaction between the nitriles and propylmagnesium bromide[263], it was decided to approach the synthesis from another route.

The second synthetic route used involved the alkylation of para-substituted benzaldehydes with propylmagnesium bromide, followed by oxidation of the un-purified benzylic alcohols using sodium acetate buffered pyridinium chlorochromate[264]. Generally, the yields of para-substituted butyrophenones for this two-step preparation were 50-80%. The butyrophenones that were prepared by this method were; *p*-methylbutyrophenone (1); butyrophenone (2); *p*-chlorobutyrophenone (3); *p*-bromobutyrophenone, (1-(4-bromophenyl)-1-butanone) (4); *p*-fluorobutyrophenone, (1-(4-fluorophenyl)-1-butanone) (5); *p*-methoxybutyrophenone, (1-(4-methoxyphenyl)-1-butanone) (6); and *p*-cyanobutyrophenone, (1-(4-cyanophenyl)-1-butanone) (7).

p-Hydroxybutyrophenone, (1-(4-hydroxyphenyl)-1-butanone) (8) was prepared in 55% yield by heating *p*-methoxybutyrophenone (6) with anhydrous pyridine hydrochloride according to the method of Prey[265].

p-Cyanobutyrophenone (7) was converted to *p*-amidobutyrophenone, 4-butyrylbenzamide (9) in 91% yield by heating with a hydrogen peroxide and potassium hydroxide solution. This procedure is described by Buck and Ide[266].

The kinetic energy releases for the loss of ethylene from the molecular ions of the para-substituted butyrophenones were measured by the electric sector defocusing technique described by equation 2-5. The instrument used for these measurements was the Hitachi Perkin-Elmer RMU-7D mass spectrometer. Kinetic energy releases were calculated using equation 2-8 which requires the voltage at which the peak maximum occurred (V)† and the width of the peak at half height (ΔV) corrected for the width at half height of the main ion beam. Table 3-1 lists the values of the kinetic energy release for the para-substituted butyrophenones.

The synthesis of the deuterium labelled para-substituted butyrophenones follows the same procedure as described for the unlabelled compounds. The Grignard reagent was prepared from 1-bromo 3-($^2H_1$)-propane(10) which was prepared in 70% yield from 1-($^2H_1$)-3-propanol (11) using phosphorus tribromide by the method of Noller and Dinsmore[267]. The preparation of the alcohol (11) was achieved in 70% yield by the reduction of oxetane by lithium aluminium deuteride[268]. Initially, oxetane was prepared by the

---

† This value was obtained by maximizing the metastable peak height by scanning the peak at voltages around the calculated value of V (obtained from equation 2-5).

Table 3-1

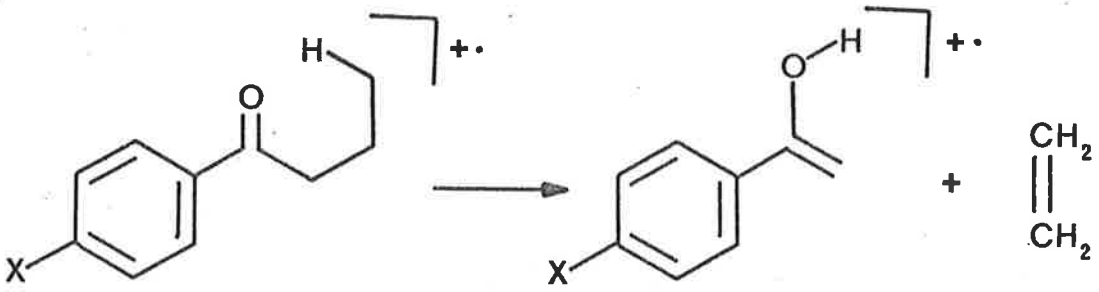

p-X Butyrophenone		$\sigma_p^{+a.}$	T_{50}
p-OH	(8)	-0.92	0.020
p-OCH_3	(6)	-0.78	0.027
p-CH_3	(1)	-0.31	c.
p-F	(5)	-0.07	0.007
p-H	(2)	0.00	0.010
p-Cl	(3)	0.11	0.014
p-Br	(4)	0.15	c.
p-Co.NH_2	(9)	0.45[b]	0.021
p-CN	(7)	0.66	0.015

Notes:

(a) Brown's σ_p^+ value[270]
(b) estimated σ_p^+ value
(c) very small metastable peak; measurement of T too inaccurate.

method of Noller[269] but later purchased. The synthetic route is shown in scheme 3-7†.

The compounds prepared by this method were; 4-($^2H_1$)-*p*-methoxybutyrophenone, (4-($^2H_1$)-1-(4-methoxyphenyl)-1-butanone)(12); 4-($^2H_1$)-*p*-methylbutyrophenone, (4-($^2H_1$)-1-(4-methylphenyl)-1-butanone)(13); 4-($^2H_1$)-*p*-fluorobutyrophenone, (4-($^2H_1$)-1-(4-fluorophenyl)-1-butanone)(14); 4-($^2H_1$)-butyrophenone, (4-($^2H_1$)-1-phenyl-1-butanone)(15); 4-($^2H_1$)-*p*-chlorobutyrophenone, (1-(4-chlorophenyl)-4-($^2H_1$)-1-butanone)(16); 4-($^2H_1$)-*p*-bromobutyrophenone, (1-(4-bromophenyl)-4-($^2H_1$)-1-butanone)(17); and 4-($^2H_1$)-*p*-cyanobutyrophenone, (1-(4-cyanophenyl)-4-($^2H_1$)-1-butanone)(18).

4-($^2H_1$)-*p*-Hydroxybutyrophenone (4-($^2H_1$)-1-(4-hydroxyphenyl)-1-butanone)(19), was prepared in 60% yield from ketone (12) as described previously for compound (8)[265].

Preparation of 4-($^2H_1$)-*p*-amidobutyrophenone (4-(4-($^2H_1$)-butyryl) benzamide)(20) from the ketone (18) was as described for the preparation of compound (9)[266].

The deuterium kinetic isotope effects for loss of ethylene from the molecular ions of compounds (12) - (20) were measured using the Hitachi Perkin-Elmer mass spectrometer at 70eV electron energy. The ratio, k_H/k_D, was obtained by measuring the intensity of both the $(M-CH_2CH_2)^{+\cdot}$ peak and the $(M-CH_2CH(^2H_1))^{+\cdot}$ peak and correcting the former for the natural abundance ^{13}C contribution from the latter.

---

† For simplicity, in schemes and figures, deuterium will be represented by the symbol D rather than the correct symbol ^2H.

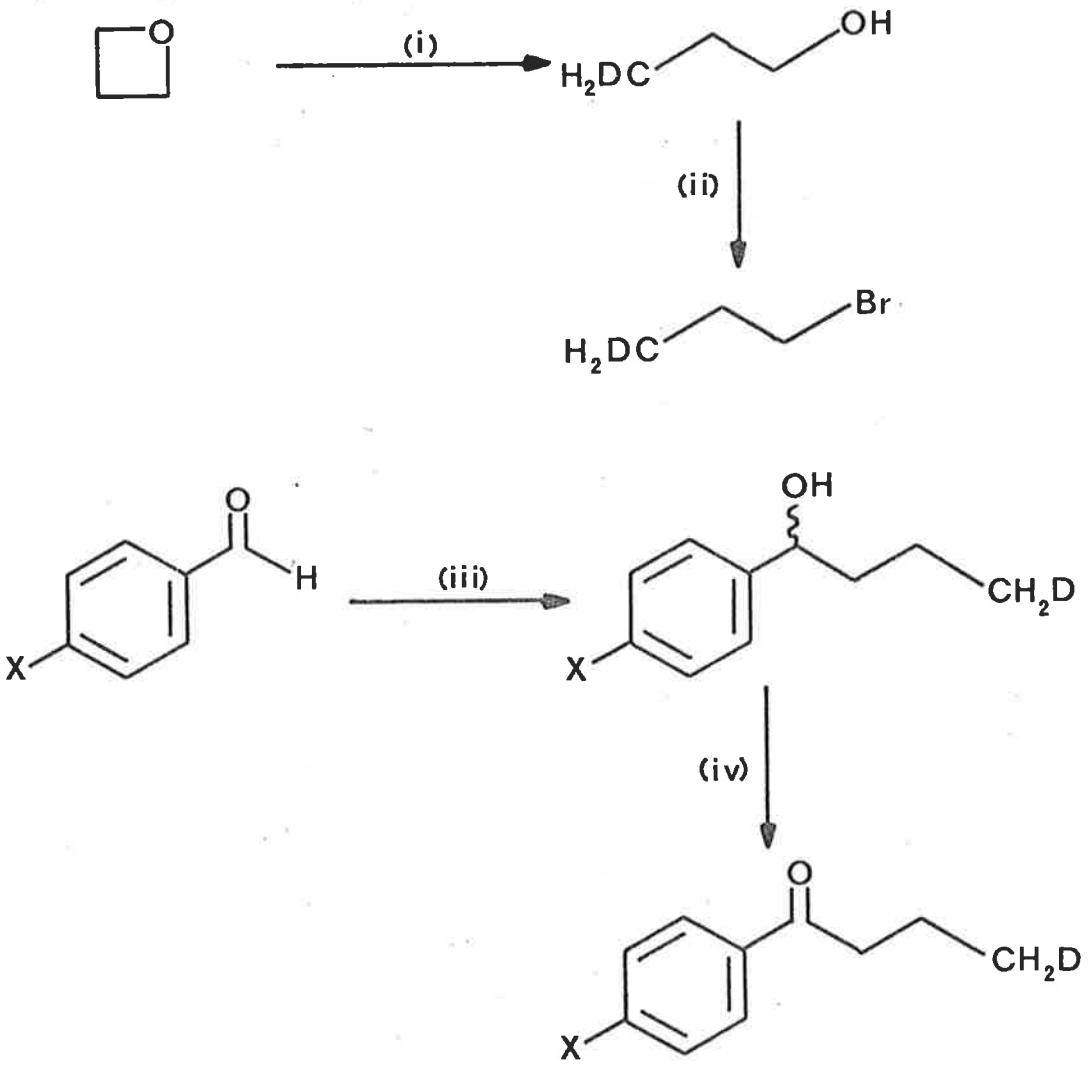

(i) LAD/Et_2O
(ii) PBr_3
(iii) $CH_2DCH_2CH_2MgI/Et_2O$
(iv) pyridinium chlorochromate/NaOAc/CH_2Cl_2

X =		
	OCH_3	(12)
	CH_3	(13)
	F	(14)
	H	(15)
	Cl	(16)
	Br	(17)
	CN	(18)

Scheme 3-7

Both ion source and first field free region (FFR) reactions were investigated. The first FFR metastable ion decompositions were investigated using the electric sector defocusing technique described in Chapter 2 (equation 2-5). Table 3-2 shows the deuterium isotope effects obtained from both regions of the mass spectrometer and compares them to Brown's σ_p^+ values[270]. The σ_p^+ values can in general, be used for the correlation of the rates of any reaction in which direct conjugation between substituents and electron deficient reaction centres is possible. The isotope effect ratio shown in table 3-2 is the average of ten measurements with the standard deviation (SD) as shown.

Due to the strong electron withdrawing capabilities of the nitro group ($\sigma_p^+ = 0.79$), considerable interest was aroused in measurement of the deuterium isotope effect for the McLafferty rearrangement from the molecular ion of 4-($^2H_1$)-*p*-nitrobutyrophenone. Since Grignard reagents react with nitro functional groups to form reduction products (disubstituted amines, hydroxylamines)[271], the previous synthetic route (scheme 3-7) could not be used. However, all attempts at synthesizing this compound via other routes were fruitless.

Initially, synthesis of *p*-nitrobutyrophenone was attempted via the reaction of an organocadmium reagent with an acid halide. This route is based on the observation that organocadmium reagents do not react with the nitro group of aryl nitro compounds[272]. *p*-Nitrobenzoyl chloride was prepared in 82% yield from the reaction of the sodium salt of *p*-nitrobenzoic acid with oxalyl chloride by the method of Adams and Ulich[273]. The reaction between *p*-nitrobenzoyl chloride and dipropylcadmium resulted in the isolation of

Table 3-2

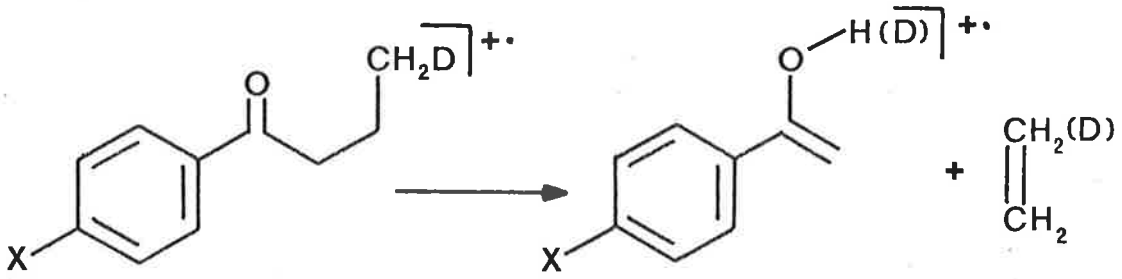

p-X Butyrophenone		σ_p^{+a}	k_H/k_D ion source	k_H/k_D first FFR
p-OH	(19)	-0.92	1.08 ± 0.07	1.0 ± 0.05
p-OCH_3	(12)	-0.78	1.25 ± 0.03	1.04 ± 0.05
p-CH_3	(13)	-0.31	1.17 ± 0.04	1.26 ± 0.05
p-F	(14)	-0.07	1.04 ± 0.02	1.20 ± 0.05
p-H	(15)	0.00	1.30 ± 0.02	1.35 ± 0.05
p-Cl	(16)	0.11	1.21 ± 0.01	1.28 ± 0.05
p-Br	(17)	0.15	1.22 ± 0.03	c
p-$CO.NH_2$	(20)	0.45[d]	1.36 ± 0.01	1.35 ± 0.1[c]
p-CN	(18)	0.66	1.18 ± 0.07	1.37 ± 0.05

NOTES

(a) Brown's σ_p^+ value
(b) Standard deviation
(c) Low intensity metastable ion peak
(d) Estimated σ_p^+ value.

two major products neither of which were the desired ketone. The reaction was repeated under the same conditions using benzoyl chloride; butyrophenone (2) was isolated from the reaction mixture in 60% yield.

An alternative approach to *p*-nitrobutyrophenone involved alkylation of *α*-bromo-*p*-nitroacetophenone, (2-bromo-1-(4-nitrophenyl) -1-ethanone) (21), with 9-ethyl-9BBN, (9-ethyl-9-borabicyclo[3.3.1] nonane) (22) according to the method of Brown and co-workers[274,275]. The reaction sequqnce is shown in scheme 3-8.

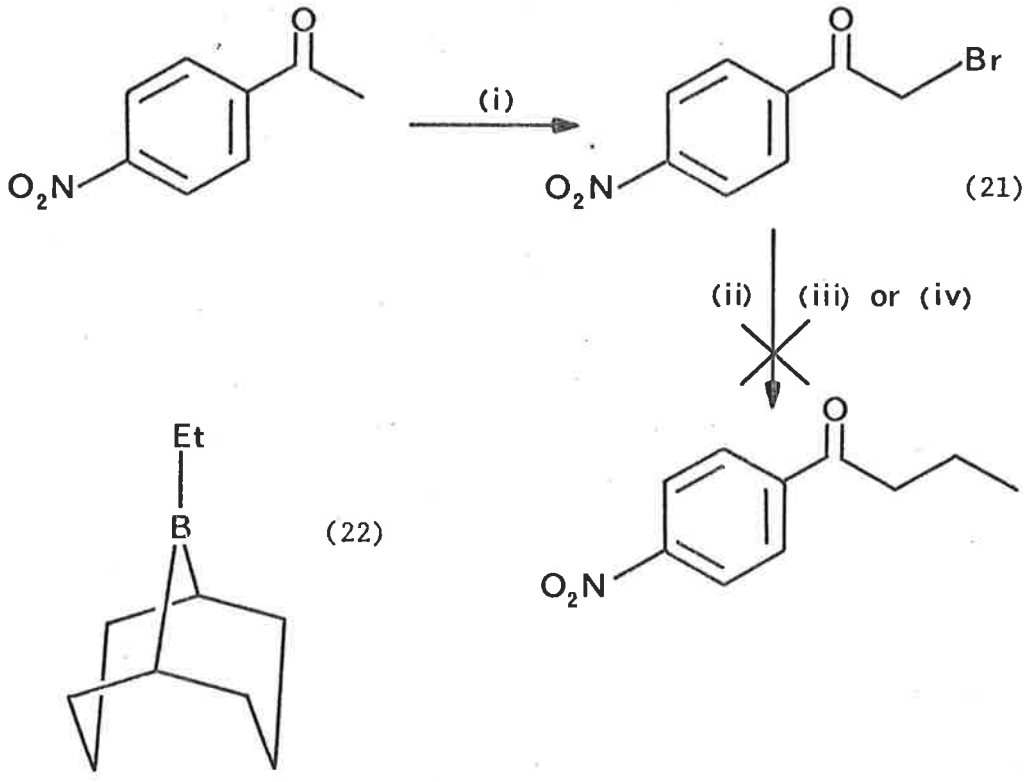

(i) $CuBr_2/CHCl_2/EtOAc$
(ii) 9-ethyl-9-BBN/THF/0°C
(iii) $^tBuOK/^tBuOH$
(iv) potassium 2,4,6-tri(*tert*-butyl)phenoxide

Scheme 3-8

The bicyclo ethyl borane (22) was prepared by bubbling ethylene into a standard solution of 9-BBN (9-borabicyclo[3.3.1]nonane). To this solution was added the α-bromo ketone (21) followed by either potassium *tert*-butoxide or potassium 2,4,6-tri(*tert*-butyl) phenoxide. On the addition of the base, the reaction mixture changed to a dark red colour. With either base, the isolated product was a complex mixture containing none of the desired ketone. Due to the problems encountered in the attempted synthesis of a *p*-nitrobutyrophenone, the preparation of this compound was abandoned.

(b) ICR Experiments

The major difference between the stepwise and concerted mechanism, as shown in schemes 3-3 and 3-4, is the presence of an intermediate in the former case. The nature of the intermediate is that it resembles a protonated carbonyl species (i.e., the 1,5-hydrogen migration produces a species in which the radical centre and charged site are separated). One would expect that if the intermediate has a sufficiently long lifetime, it should be possible to distinguish it from the reactant and product ions. This can be expected to be done on the basis of the specific reactions that each species could undergo; in particular, their ion-molecule reactions. One of the simplest ion-molecule reactions that can be investigated using the ICR mass spectrometric technique, is proton transfer. The advantage of the ICR technique lies in the cyclotron ejection[276] or double resonance experiments[277] in which each charged member of a reaction process can be unequivocally identified in terms of their m/z values.

On this basis, it was proposed to synthesize 4-($^2H_3$)-butyrophenone, (4-($^2H_3$)-1-phenyl-1-butanone) (23). The molecular ion of this compound undergoes the McLafferty rearrangement, producing the enol radical

cation of acetophenone. This product ion has an O-$^2H_1$ bond resulting from 1,5-deuterium migration. If one considered the McLafferty rearrangement to be stepwise, then the intermediate formed by 1,5-deuterium migration would similarly contain an O-$^2H_1$ bond. Potentially, the McLafferty product ion and the intermediate could undergo deuteron transfer reactions with a neutral base. If this occurred within the cell of an ICR mass spectrometer, the source of the deuterium could be unequivocally identified.

The reaction scheme proposed for the synthesis of compound (23) was the same as was used for the preparation of the para-substituted butyrophenones. Effectively, the synthetic problem then reduced to investigating synthetic routes to 1-bromo-3-($^2H_3$)-propane (24). Initially, the alkylation of ethylene oxide with ($^2H_3$)-methylmagnesium iodide seemed the simplest route to a precursor of bromide (24). This procedure is described by Huston and D'Arcy[278]. It was found, however, on repeating the reaction several times with isotopically un-labelled precursors, that the yield of propanol varied greatly (as determined by gas liquid chromatography - GLC). Due to the fickle nature of this reaction, another synthetic route was planned.

An alternative route involved alkylation of acetic acid with ($^2H_3$)-iodomethane. The procedure used was an adaption of the method described by Pfeffer and Silbert[279], and Creger[280]. The di-lithium salt of acetic acid was prepared in tetrahydrofuran at -78^oC using lithium isopropylcyclohexylamide. This base was used due to its solubility in tetrahydrofuran at low temperatures. To solubilize the dianion formed, hexamethylphosphoramide was added to the reaction mixture. Analysis of the crude product, obtained after work-up of the reaction mixture, by GLC indicated that propionic

acid had been formed in only 30% yield. When the reaction was repeated using lithium di-isopropylamide as the base and a reaction temperature of $0^{o}C$, none of the required product was obtained[279,280].

1-Bromo-3-($^{2}H_{3}$)-propane(24) was eventually prepared by the synthetic route outlined in scheme 3-9. Also shown in this scheme is the preparation of 4-($^{2}H_{3}$)-1-phenyl-1-butanone (23). *tert*-Butyl acetate was prepared in 50% yield by the method of Vogel[281]. Preparation of *tert*-butyl 3-($^{2}H_{3}$)-propionate (25) was achieved in quantitative yield (crude) by the procedure outlined by Rathke and Lindert[282]. Initially, in a trial reaction using isotopically unlabelled reactants, hexamethylphosphoramide was added to the lithium salt of *tert*-butyl acetate in tetrahydrofuran. This was an attempt to increase the solubility of the salt in the solvent system. However, the addition of hexamethylphosphoramide had no effect on the overall yield of *tert*-butyl propionate and was therefore omitted from the procedure.

tert-Butyl propionate, required for GLC comparison purposes was prepared in 60% yield from propionyl chloride by the method of Vogel[281].

Reduction of the propionate (25) with lithium aluminium hydride yielded 1-($^{2}H_{3}$)-3-propanol (26) in 65% yield. The bromide (24) was prepared, however, in surprisingly low yield (14%) from the alcohol (26) using phosphorus tribromide[267]. Preparative GLC was used to purify the bromide (24). Preparation of ketone (23) was achieved in 77% yield, based on the starting bromide (24), by methods described previously.

Figure 3-1 shows a portion of the ICR spectrum of a mixture of ketone (23) and 3,5-dimethylpyridine. The ketone (23) was introduced into the cell of the ICR spectrometer via the direct-probe (absorbed onto diatomaceous earth), and the pyridine was introduced via the

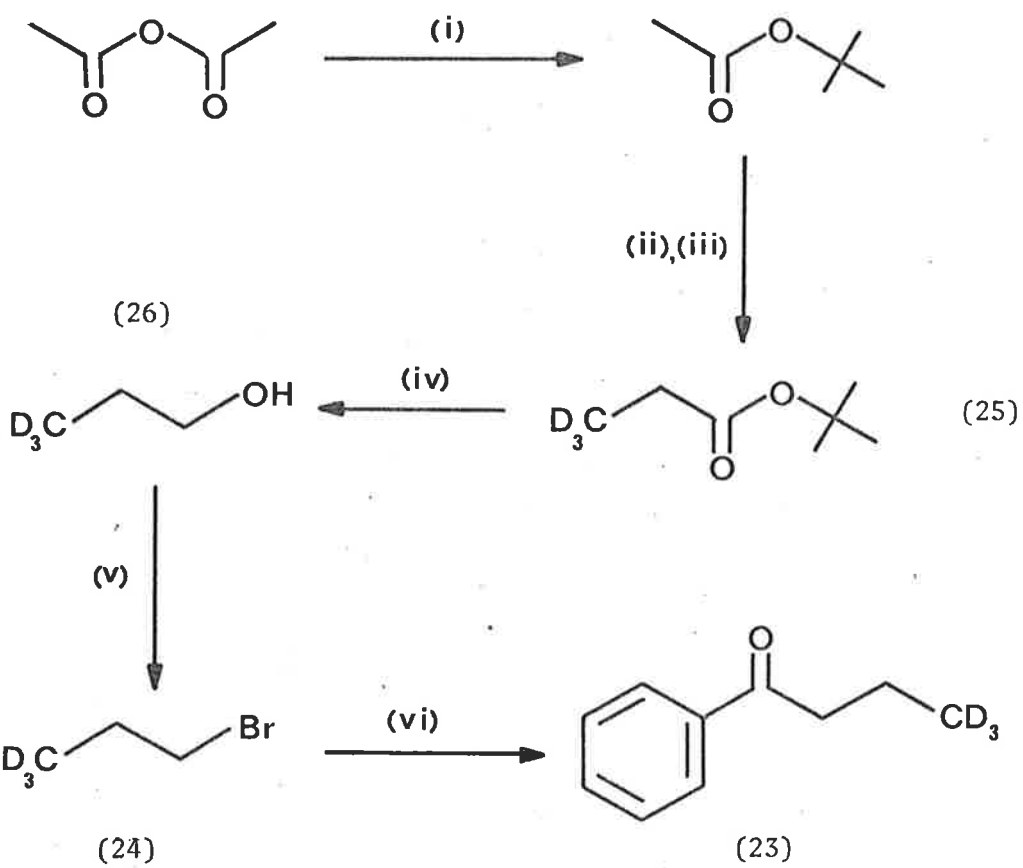

(i) $^{t}BuOH/ZnCl_2$
(ii) lithium isopropylcyclohexylamide
(iii) CD_3I
(iv) LAH/Et_2O
(v) PBr_3
(vi) $CD_3CH_2CH_2MgBr/Et_2O$
(vii) pyridinium chlorochromate/NaOAC/CH_2Cl_2

Scheme 3-9

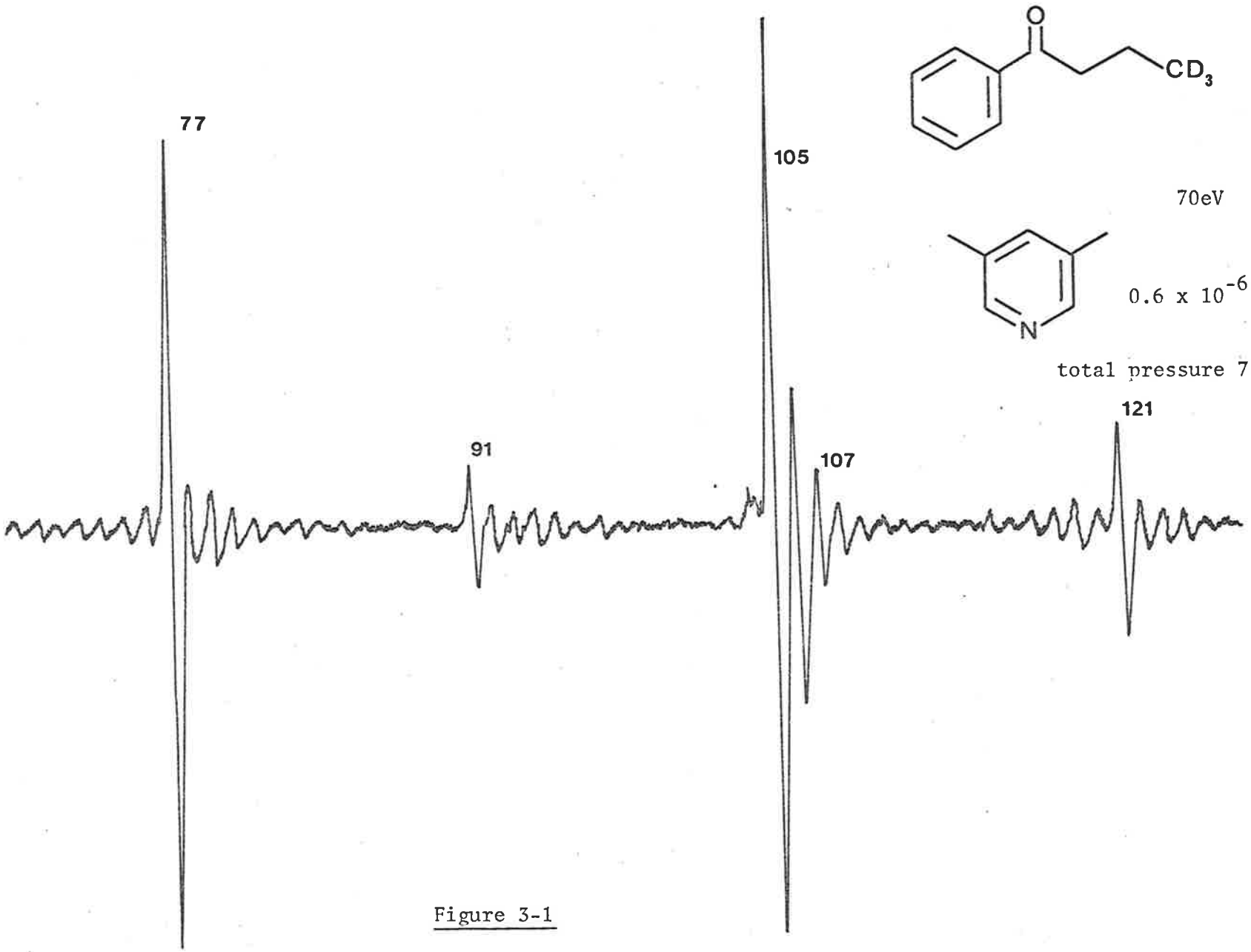
77
105
91
107
121
O
CD3
N
70eV
0.6 x 10-6 torr
total pressure 7.0 x 10-6 torr

Figure 3-1

liquid inlet port.

The ICR spectrum of 3,5-dimethylpyridine, shows large $(M-1)^+$, $M^{+\cdot}$ and $(M + 1)^+$ peaks occurring at m/z values 106, 107 and 108 respectively. The $(M - 1)^+$ and $(M + 1)^+$ ions represent 83% and 38%† of the molecular ion peak respectively. In addition, there is a peak of m/z 109 representing 5%† of the $M^{+\cdot}$ peak. Introduction of the ketone (23) produced a slight increase in the ratio of m/z 109: m/z 108 from 0.13 to 0.23. However, increasing the pressure due to 3,5-dimethylpyridine did not affect this ratio. Cyclotron ejection experiments indicated that the peak at m/z 109 was not produced from the molecular ion of ketone (23), or any other species having m/z 151, but was coupled to the peak at m/z 121. (Enol form of the molecular ion of acetophenone; the product ion of the McLafferty rearrangement from the molecular ion of ketone (23)). Scheme 3-10 shows the

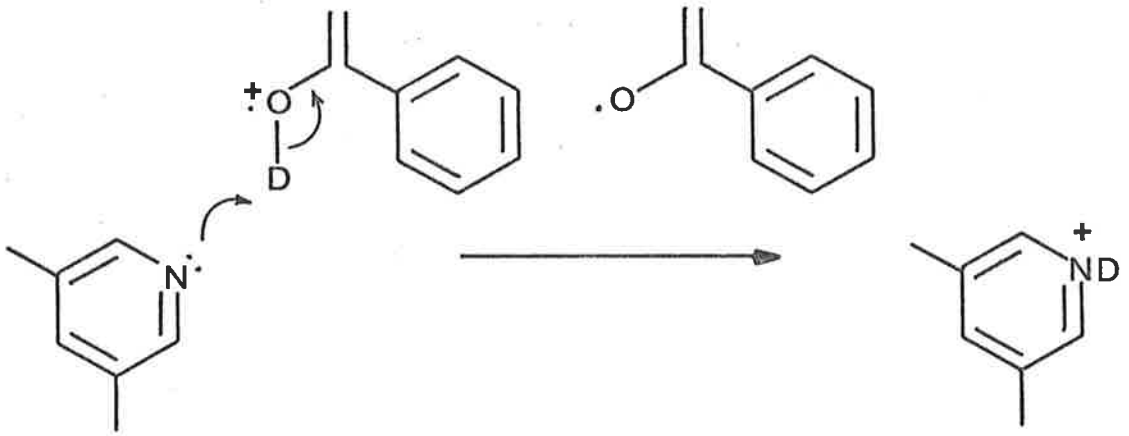

Scheme 3-10

---

† This percentage is not corrected for the natural abundance ^{13}C content due to the preceeding peak.

proposed chemistry for production of m/z 109 in the reaction of ketone (23) with 3,5-dimethylpyridine.

Analysis of the mass spectrum of 4-($^2H_3$)-butyrophenone (23) indicates that the McLafferty rearrangement is site specific for this compound. The ion source and the first FFR reactions of the molecular ion of compound (23) indicate that the 1,5-hydrogen transfer is specific and proceeds without hydrogen scrambling: the McLafferty rearrangement eliminates only ($^2H_2$)-ethylene.

(c) 4-Substituted Butyrophenones

It is clear from the previous section that a deuterium isotope effect is observed for the McLafferty rearrangement of butyrophenones. Moreover, changing the para-substituents of these compounds causes a change in the isotope effect for the process. Presumably, the substituent has its effect on the isotope effect through the forming O-H bond. It is of interest therefore, to examine the change in the deuterium isotope effect due to substitution at the carbon-4 of butyrophenone. In this case, the substituent is expected to have its effect through the change in the strength of the C_4-H bond. The effect of substituents on C-H bond dissociation energies can be obtained from various tables[283].

An initial investigation of this effect involved the study of the following compounds; 4-bromo-4-($^2H_1$)-butyrophenone, (4-bromo-4-($^2H_1$)-1-phenyl-1-butanone)(26), and 4-chloro-4-($^2H_1$)-butyrophenone, (4-chloro-4-($^2H_1$)-1-phenyl-1-butanone)(27). The method used in their synthesis is summarized in scheme 3-11.

The required ketones (26) and (27) were prepared in 94% and 90% yields respectively from 1-($^2H_1$)-4-oxo-4-phenylbutyl 4-toluene sulphonate (28). Their preparations follow the method of Beckwith

Scheme 3-11

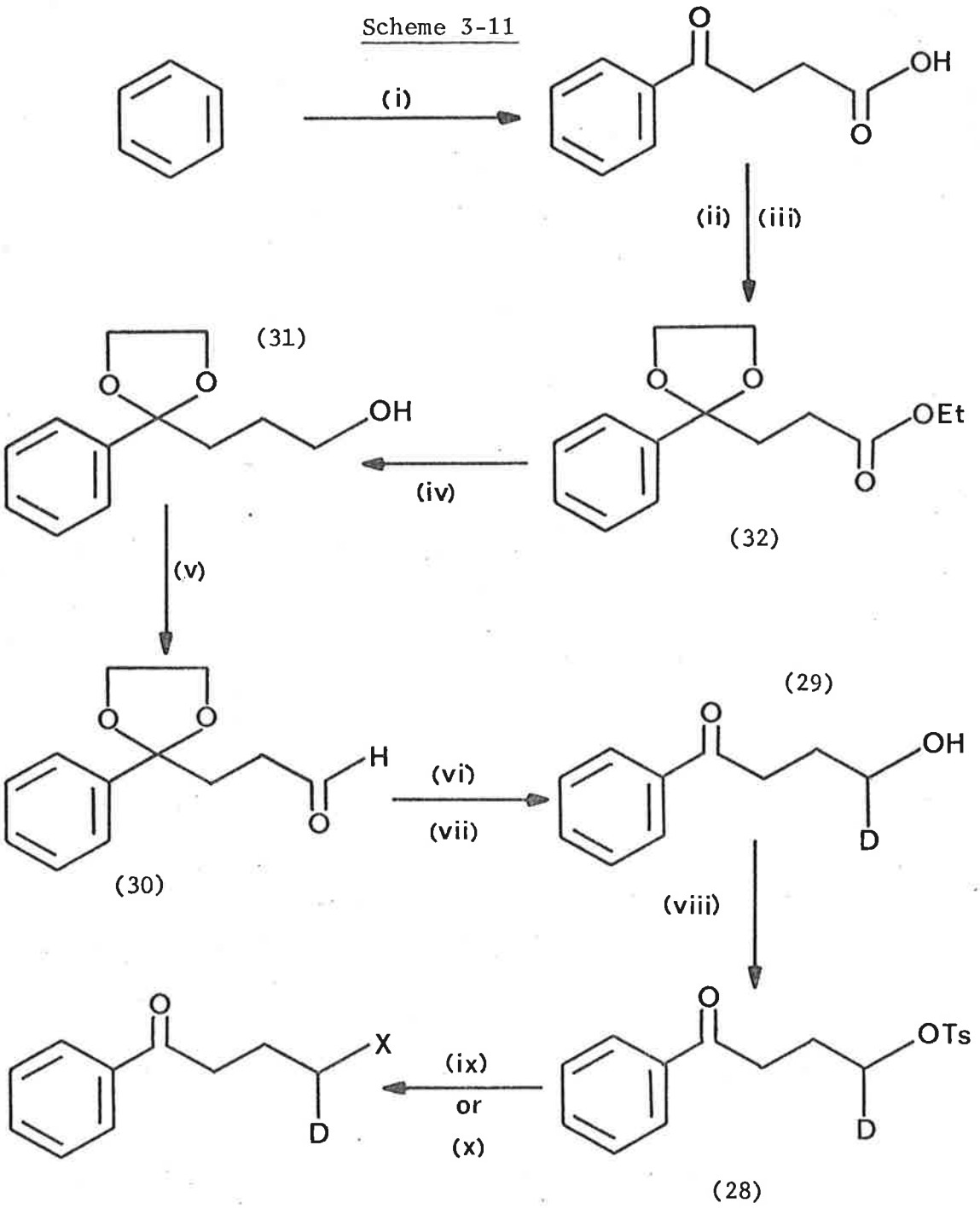

x = Br (26)

Cl (27)

(i) succinic anhydride/$AlCl_3$
(ii) EtOH/TsOH (cat)
(iii) 1,2-dihydroxyethane/TsOH(cat)/benzene/Δ
(iv) LAH
(v) pyridinium chlorochromate/CH_2Cl_2
(vi) LAD
(vii) TsOH/THF/H_2O
(viii) TsCL/pyridine/0°C
(ix) LiBr/HMPA
(x) LiCl/HMPA

and Moad[284] using the appropriate anhydrous lithium halide. The tosylate (28), was prepared in 98% yield from 4-($^2H_1$)-*p*-hydroxybutyrophenone, (4-($^2H_1$)-4-hydroxy-1-phenyl-1-butanone)(29) by conventional means[285]. Preparation of the deuterated alcohol (29) was achieved by reduction of 4,4-ethylenedioxy-4-phenyl-butanal (30) with lithium aluminium deuteride in anhydrous ether, followed by removal of the acetal function using *p*-toluenesulphonic acid in a tetrahydrofuran, water mixture. The overall yield of this process, based on the aldehyde (30), was 88%. The aldehyde (30) was prepared in 78% yield by oxidation of 4-hydroxy-1-phenyl-1-butanone ethylene acetal (31) using pyridinium chlorochromate according to the method of Corey and Suggs[264].

Synthesis of the alcohol (31) follows the procedure described by Ward and Sherman[286]. Ethyl 4,4-ethylenedioxy-4-phenylbutyrate (32) was prepared from 4-benzoylbutanoic acid in quantitative yield (crude) by initially preparing the ethyl ester and then forming the ethylenedioxy acetal of this compound.

The mass spectrum of the chloride (27) unfortunately showed small metastable peaks for the loss of chloroethylene and 1-($^2H_1$)-1-chloroethylene and a deuterium isotope effect for this process could not be estimated. The major fragmentation from the molecular ion of this compound, was loss of HCl.

The metastable ion transition for the loss of bromoethylene and 1-($^2H_1$)-1-bromoethylene from the molecular ion of bromide (26), proceeded with reasonable efficiency. As a result, the deuterium isotope effect for this process was measured as k_H/k_D 1.25 ± 0.12.

(d) Carbon-13 Labelled Butyrophenones

Considering the mechanisms proposed for the McLafferty rearrangement (stepwise versus concerted, schemes 3-3 and 3-4) in the light of the results that were obtained from the deuterium labelling experiments, then a natural progression would be to study the effects of carbon-13 labelling on this process. As mentioned previously, the observation of an isotope effect for a process is not a necessary condition for that atom being involved directly in the rate determining step. Also, isotopic labelling of atoms directly involved in the reaction is required to enable definite conclusions to be made about the nature of the mechanism (stepwise or concerted).

The aim of these studies was to attempt to measure, with sufficient accuracy, differences in the rate of the McLafferty rearrangement due to carbon-13 labelling at carbons 1,2,3 and 4 of butyrophenone. By the very nature of the molecular system chosen, the measurements are of comparative *intermolecular* rates. This requires isotopic carbon-13 incorporation of >90% and the mass spectrometric measurements to be carried out on a mixture of labelled and un-labelled material.

The compounds required for this study were; 1-(^{13}C)-butyropheone, (1-(^{13}C)-1-phenyl-1-butanone)(33); 2-(^{13}C)-butyrophenone, (2-(^{13}C)-1-phenyl-1-butanone)(34); 3-(^{13}C)-butyrophenone, (3-(^{13}C)-1-phenyl-1-butanone)(35); and 4-(^{13}C)-butyrophenone, (4-(^{13}C)-1-phenyl-1-butanone)(36). The synthetic route proposed was to alkylate acetophenone with iodoethane incorporating the carbon-13 label into butyropheonone via these species. This type of reaction is well known and usually procedurally simple. However, in this case the alkylation

of acetophenone was found to be difficult; in most of the alkylations attempted, the yield of monoalkylated product (butyrophenone) was less than that of the dialkylated product.

The first route attempted was the alkylation of the potassium salt of acetophenone; formed in dimethyl sulphoxide from potassium *tert*-butoxide, with iodoethane. This follows the procedure of Heiszwolf and Kloosterziel[287]. Analysis of the reaction mixture by GLC indicated that butyrophenone was formed in only 10% yield; the remainder of the product mixture being 2-ethylbutyrophenone (2-ethyl-1-phenyl-1-butanone)(37), (40%) and acetophenone (50%).

To overcome the problem of dialkylation, it was proposed to use a catalytic phase transfer procedure[288].

Table 3-3 summarizes the conditions used for the phase transfer alkylations and the product composition obtained from them.

Table 3-3

Phase Transfer Catalyst	Alkylating Agent	Conditions	Products
TEBA[a]	bromoethane	20°C, 24h.	no reaction
TEBA[a]	bromoethane	80°C, 48h.	acetophenone (90%) butyrophenone (10%)
TEBA[a]	diethyl sulphate	80°C, 72h.	no reaction
TBA[b]	iodoethane	80°C, 48h.	acetophenone (55%) butyrophenone (25%) 2-ethylbutyro-phenone (20%)

NOTES:

(a) TEBA - triethylbenzylammonium chloride (catalytic amount).
(b) TBA - tetrabutylammonium hydrogen sulphate (one equivalent).

In each experiment listed in table 3-3, the heterogeneous solvent system was composed of dichloromethane and sodium hydroxide solution. The product mixture in each case was analysed using GLC.

An alternative route to the carbon-13 labelled compounds utilized the potassium enolate of acetophenone, which was formed using potassium hydride. The use of this base has been encouraged by Brown[289,290]. The advantages of potassium hydride are that enolate anions are formed rapidly and irreversibly in tetrahydrofuran at room temperature and that dialkylation is minimized. However, all attempts at obtaining butyrophenone in a yield greater than that of 2-ethylbutyrophenone failed. Table 3-4 shows the experimental conditions used in these attempts.

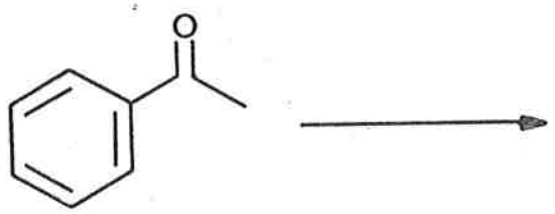

(38) + (2) + (37)

(38)

	Equivalents				Products (%)		
Comments	(38)	iodoethane	Solvent	Temp	(38)	(2)	(37)
normal[a]	1.0	1.0	THF[b]	-78°C	44	19	37
normal	1.5	1.0	THF	-78°C	40	21	39
reverse[a]	1.1	3.0	DMF[c]	0.°C	14	11	75

NOTES

(a) normal addition is the addition of iodoethane to the potassium enolate. reverse addition is the addition of the potassium enolate to iodoethane.
(b) THF - tetrahydrofuran
(c) DMF - dimethylformamide

The presence of starting material in the product mixture indicates that even though the enolate anion is formed irreversibly by potassium hydride, this anion re-protonates in a later step. Since the proportion of the products due to dialkylation is high, it seems that re-protonation of the enolate anion of acetophenone takes place as shown in scheme 3-12.

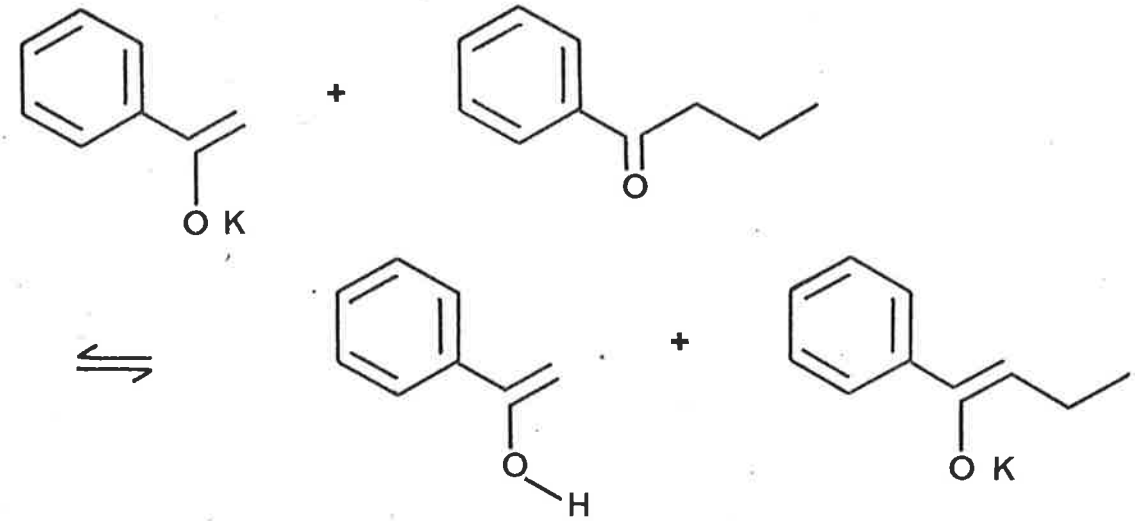

Scheme 3-12

If the equilibrium shown in scheme 3-12 is rapid and lies towards the enolate anion of butyrophenone, this accounts for both the high proportion of acetophenone returned and the presence of dialkylated product.

Since alkylation of the potassium enolate was unsuccessful, it was decided to prepare and alkylate the lithium enolate of acetophenone. To prepare the lithium enolate, the silyl enol ether of acetophenone, ([1-(Phenylvinyl)oxy]trimethylsilane)(39) was prepared[289] and then reacted with methyllithium using 2,2'-bipyridyl as an indicator[291]. Alkylation of the resulting enolate with iodoethane afforded only a 12% yield of butyrophenone; the remainder of the product mixture was acetophenone (81%) and dialkylated product (37) (7%).

The lithium enolate of acetophenone was also prepared using lithium di-isopropylamide in tetrahydrofuran as the base. Alkylation of the enolate at - 78°C with iodoethane yielded the following product distribution; acetophenone (48%), butyrophenone (26%) and 2-ethylbutyrophenone (26%).

In a further attempt to overcome the problems of dialkylation, a procedurally more complex synthetic route was attempted. This route involved the synthesis of the N,N-dimethylhydrazone of acetophenone, preparation of the α-lithiated N,N-dimethylhydrazone and its alkylation with iodoethane, followed by conversion of the N,N-dimethylhydrazone to the ketone. The general procedure is described by Corey and Enders[293]. The advantages of using α-lithiated dimethylhydrazones as enolate anion equivalents are; (i) their efficiency of formation and lack of side reactions, (ii) their stability, (iii) their high reactivity and importantly (iv) their formation of monoalkylated products. The synthetic sequence is summarized in scheme 3-13 for the preparation of 3-(^{13}C)-butyrophenone (35).

Acetophenone dimethylhydrazone (40) was prepared in quantitative yield by the method of Newkome and Fishel[292]. Lithium di-isopropyl amide was used to prepare the α-lithiated acetophenone dimethylhydrazone which was then alkylated at -78°C with 1-(^{13}C)-1-iodoethane. Conversion of 3-(^{13}C)-butyrophenone dimethylhydrazone (41) to the ketone (35) was achieved by using copper^{II} acetate in a mixture of water and tetrahydrofuran[294]. In this way the butyrophenone (33) - (36) were prepared in 60%, 65%, 63% and 65% yields respectively, with isotopic incorporation of >90%.

The carbon-13 kinetic isotope effect experiments were performed

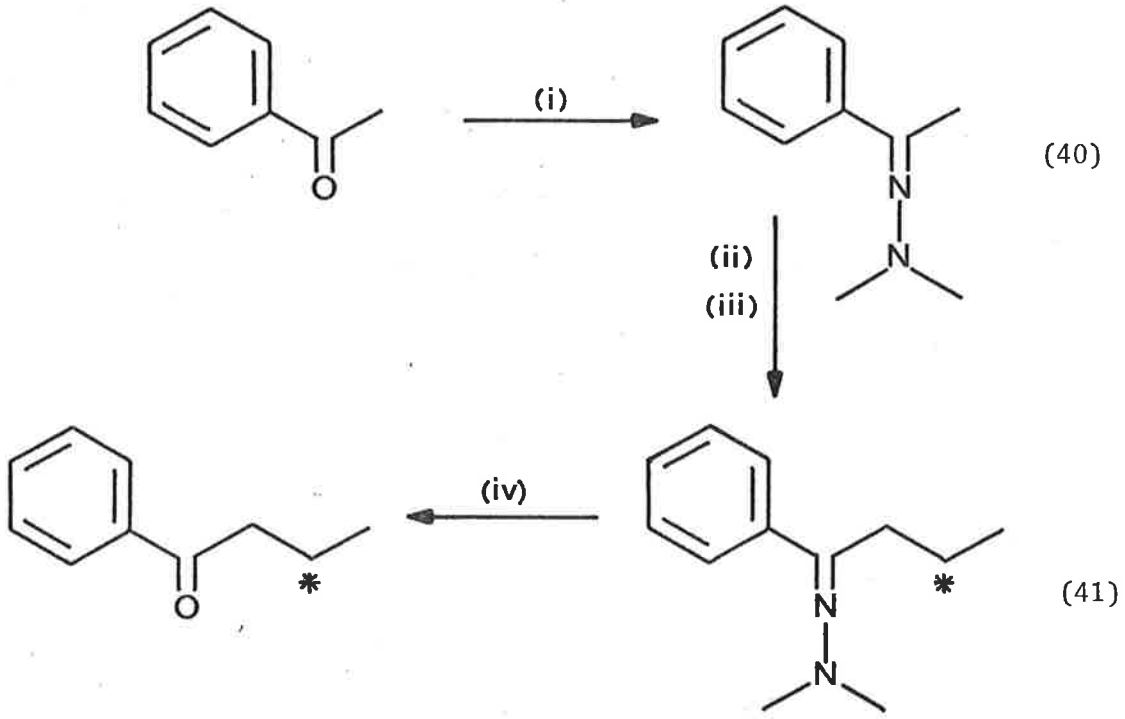

(40)

(41)

(i) $(CH_3)_2N\text{-}NH_2$/EtOH
(ii) lithium di-isopropylamide/0°C
(iii) 1-(^{13}C)-1-iodoethane/-78°C
(iv) $Cu(OAc)_2$/THF/H_2O

Scheme 3-12†

on the new "grand scale" reverse sector instrument designed by Derrick and built at La Trobe University, Victoria[295,296]. The problems encountered in attempting to measure carbon-13 isotope effects for loss of ethylene from carbon-13 labelled butyrophenones arose from two sources. Firstly, there were instrumental and experimental problems in the collection of data of sufficient accuracy to allow the observation of small differences in ion abundances resulting from

---

† The position of the carbon-13 label is indicated by *.

kinetic isotope effects. Secondly, it appeared that there was an isotope effect on the ionization process between butyrophenone and the carbon-13 compounds (33)-(36), which was of the same order of magnitude as the expected kinetic isotope effect. This latter problem will be dealt with more fully in Chapter 5.

The initial experiment involved introducing a mixture of 4-(^{13}C)-butyrophenone (36) and butyrophenone into the reverse sector instrument and measuring the amount of each compound present from the molecular ion peaks. The validity of this method of determining the proportion of each compound in the mixture will be discussed in detail in Chapter 5.

Peak height measurements were made by sampling the voltage output from the peak maximum using a microprocessor. The microprocessor was programmed to collect 20 values of the voltage, average them and to repeat this cycle a number of times elected by the operator. The output consisted of an arbitrary number (directly proportional to the output voltage) representing the total average of the voltages and its standard deviation.

The results obtained for ketone (36) and butyrophenone are shown in table 3-5; $\bar{\chi}$ is the mean and SD is the standard deviation.

Table 3-5

m/z	Sample Number	$\bar{\chi}$ ± SD
149	7000	12771 ± 403
148	7000	12671 ± 368
147	7000	641 ± 6

The ratio of m/z 148/149 (i.e., the ratio of the molecular ions for compounds (2) and (36)) was found to be 1.054 ± 0.06. This ratio is

corrected for natural abundance carbon-13 and the loss of a hydrogen atom from each molecular ion. Clearly, this result is of insufficient accuracy to enable meaningful carbon-13 isotope effect studies to be made.

To determine whether there was an isotope effect on the ionization process, the second FFR metastable ion decompositions, m/z $148^+ \rightarrow 105^+ + 43$ and m/z $149^+ \rightarrow 105^+ + 44$ (α-cleavage) were studied. Since the isotopic label is far removed from the bonds that are breaking, a kinetic isotope effect for this process was not expected. The results obtained for α-cleavage from the molecular ions of 4-(^{13}C)-butyrophenone (36) and butyrophenone are listed in table 3-6.

Table 3-6

Metastable Ion Transition	Sample Number	$\bar{\chi} \pm$ SD	Ratio ± SD
m/z $148^+ \rightarrow 105^+ +43$	20,000	600 ± 72	1.045 ± 0.13
m/z $149^+ \rightarrow 105^+ +44$	20,000	573 ± 2	

The increase in the standard deviation for the ratio in table 3-6 when compared with the ratio of m/z 148/149 from table 3-5 is in part due to the low abundance of the metastable peaks for α-cleavage in the spectrum of butyrophenone. Primarily though, the large standard deviation reflects the problems due to the variation in pressure encountered between successive measurements of the metastable ion process from each compound. The nature of the experiment (i.e., intermolecular comparative process), requires that the magnetic field of the instrument be adjusted between measurements for each compound. This is also expected to be a major problem in attempting to measure carbon-13 isotope effects for the McLafferty rearrangement.

(e) Carbon-13 Labelled 2-Ethylbutyrophenones

The problems that were encountered in attempting to measure carbon-13 isotope effects for the McLafferty rearrangement from butyrophenones, were, in the main, due to *intermolecular* nature of the experiment. The major difficulty was due to the presence of an isotope effect for the ionization process which could not be easily corrected for. Pressure fluctuation problems also led to variability in the data collected resulting in uncertainty in the ratio of peak heights. Clearly, the difficulties encountered in measuring intermolecular kinetic isotope effects cause this method of approach to be uncertain.

The simplest method of overcoming these problems was seen to be the study of a structurally related compound in which *intramolecular* rates could be compared. In such a case, the molecular system would have two sites, one of which is labelled with carbon-13 (>90%), from which the McLafferty rearrangement could occur. This sytem will have one ionization potential and the pressure effects on the peak height would be minimized.

For this reason, the compounds 3-(^{13}C)-2-ethylbutyrophenone, (3-(^{13}C)-2-ethyl-1-phenyl-1-butanone)(42) and 4-(^{13}C)-2-ethylbutyrophenone, (4-(^{13}C)-2-ethyl-1-phenyl-1-butanone)(43) were prepared. Synthesis of compounds (42) and (43) involved alkylation of 3-(^{13}C)-butyrophenone (35) and 4-(^{13}C)butyrophenone (36) respectively with iodoethane by the method of Brown[289,290]. The sequence is summarized in scheme 3-13.

Figure 3-2 shows the mass analysed, ion kinetic energy (MIKE) spectrum of 3-(^{13}C)-2-ethylbutyrophenone (42) and the unresolved peaks due to the metastable ion transitions shown in scheme 3-14.

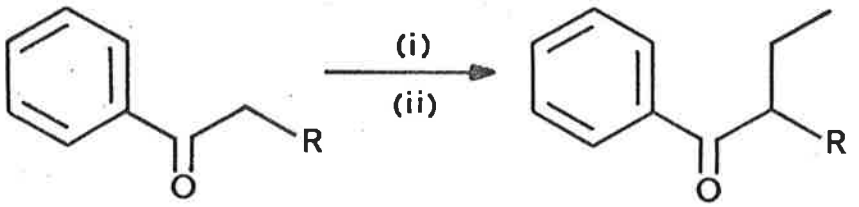

R = $CH_2\overset{*}{C}H_3$ (35)

$CH_2\overset{*}{C}H_3$ (36)

R = $\overset{*}{C}H_2CH_3$ (42)

$CH_2\overset{*}{C}H_3$ (43)

(i) KH/THF

(ii) EtI

Scheme 3-13

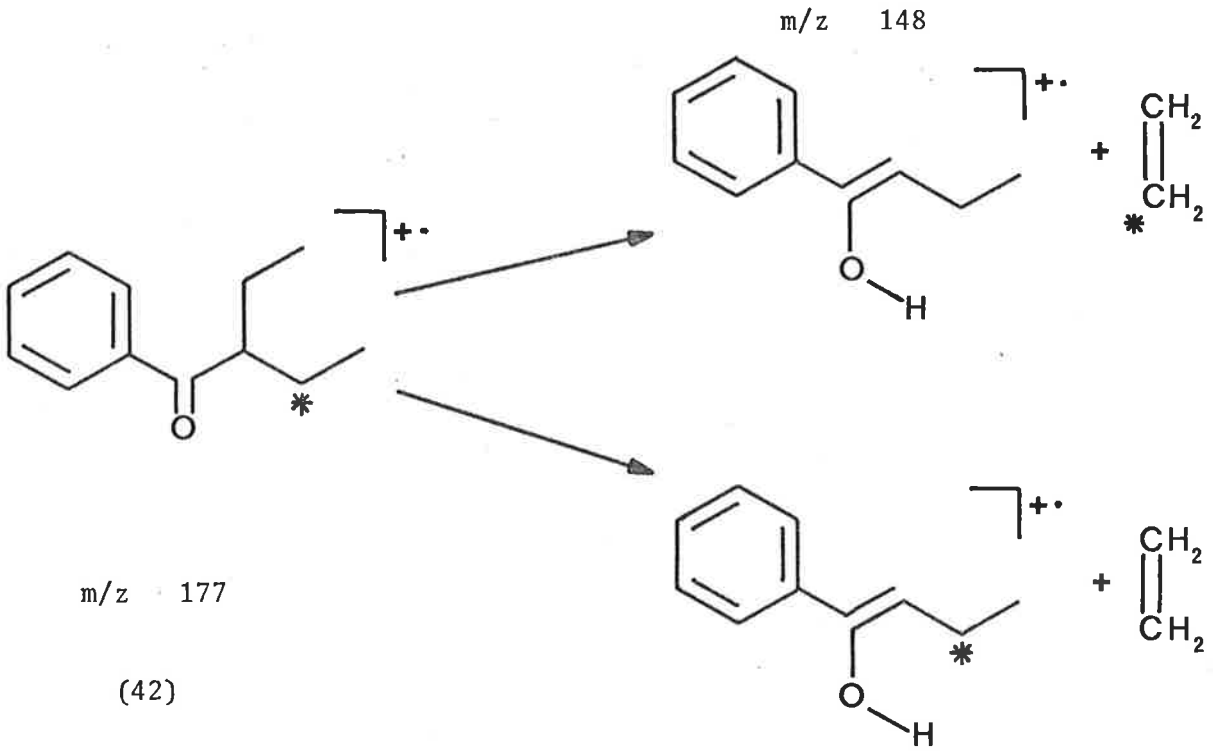

Scheme 3-14

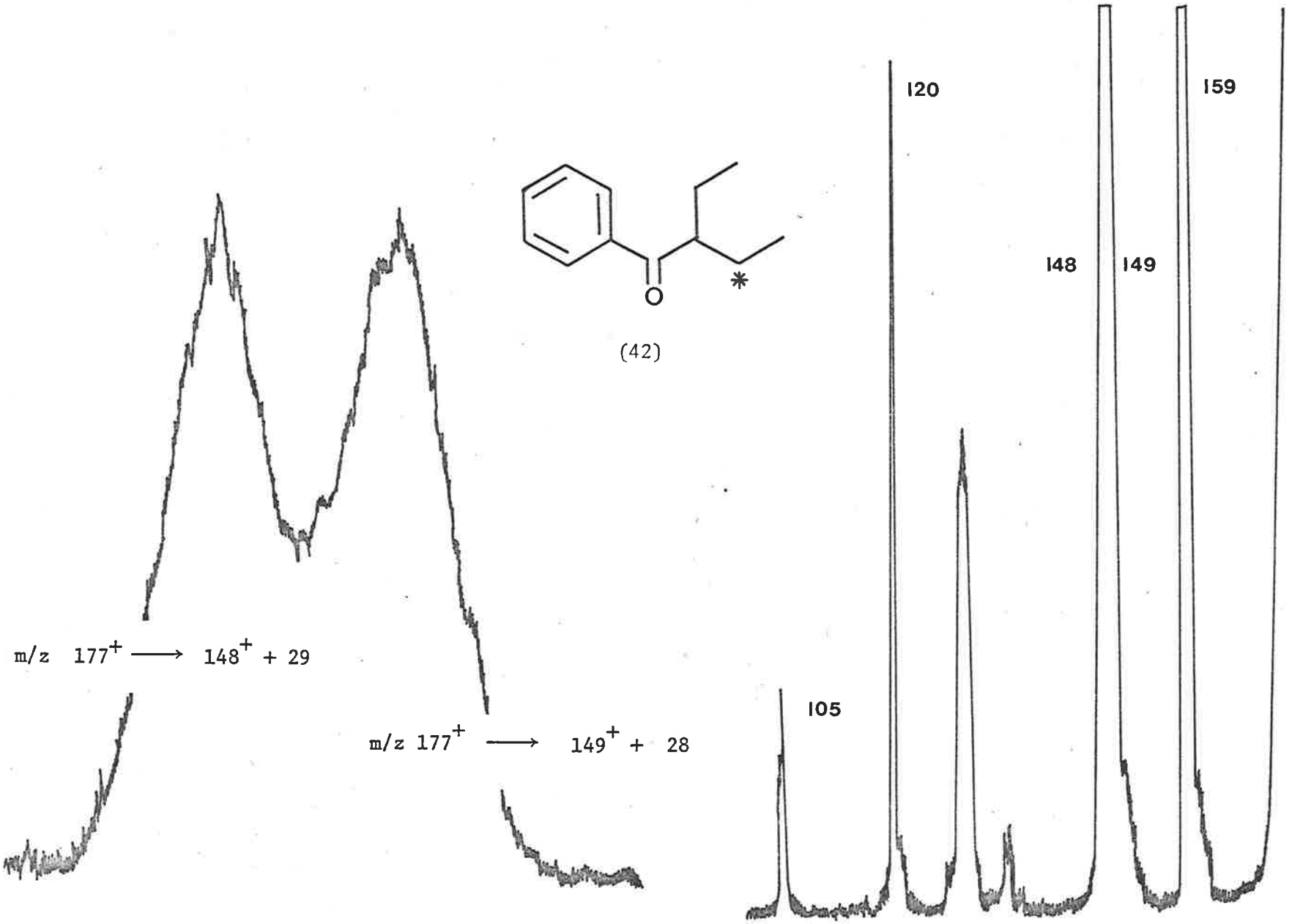

Figure 3-2

The metastable peak heights for the loss of (^{13}C)-ethylene and ethylene from the molecular ions of compounds (42) and (43) were measured using the microprocessor averaging technique described in the previous section. To ensure that the microprocessor was sampling the output voltages at the maxima of each peak, the metastable peaks were scanned slowly at a large detector gain and the centre of each determined geometrically. Re-scanning the peaks and checking the centre of each between successive data collection, ensured that the microprocessor was sampling at the peak maximum.

The ratio of the heights of the metastable peaks for the processes m/z $177^+ \rightarrow 149^+ +28$ and m/z $177^+ \rightarrow 148^+ +29$, (i.e., loss of ethylene versus loss of (^{13}C)-ethylene), where m/z 177 is the mass to charge ratio of the molecular ion of 4-(^{13}C)-2-ethylbutyrophenone (43), is shown in table 3-7.

Table 3-7

Compound	Metastable Ion Transition	Ratio ± SD[a]
4-(^{13}C),(43)	$177^+ \rightarrow 149^+ +28$ $177^+ \rightarrow 148^+ +29$	$\bar{\chi}$(29,000) = 1.019 ± 0.005
repeat		$\bar{\chi}$(51,000) = 1.018 ± 0.006[b]
3-(^{13}C),(42)	$177^+ \quad 149^+ +28$ $177^+ \quad 148^+ +29$	$\bar{\chi}$(56,000) = 1.041 ± 0.007

NOTES

(a) this is the ratio of the loss of ethylene to the loss of (^{13}C)-ethylene.
(b) determined on a separate occasion.

The reproducibility of this result for ketone (43) is also shown in table 3-7.

Similarly, the ratio of the heights of the metastable peaks for the processes m/z $177^+ \rightarrow 149^+ +28$ and m/z $177^+ \rightarrow 148^+ +29$, where m/z 177 is the mass to charge ratio of the molecular ion of 3-(^{13}C)-2-ethylbutyrophenone (42), was determined and is shown in table 3-7.

The increase in the certainty of these ratios when compared to the results obtained for the loss of (^{13}C)-ethylene and ethylene from 4-(^{13}C)-butyrophenone and butyrophenone respectively (intermolecular system), is probably due to the simplicity of the experimental procedure for intramolecular competitive reactions. In the case of the 2-ethylbutyrophenones (42) and (43), labelled and unlabelled ethylene are eliminated from the same molecular ion. As a result, the time interval between successive measurements of metastable peak height is minimized. Therefore, instrumental variables, in particular the sample pressure, are reduced in their effect on the peak height determinations.

There are two factors which need to be accounted for before the ratios in table 3-7 can be considered as accurate measures of ratios of ion abundances. The first correction to the peak height ratio was due to an instrumental factor. In La Trobe's mass spectrometer, a small baseline variance occurs on the high voltage (electric sector) side of metastable peaks. Since the metastable peaks for the McLafferty rearrangement from compounds (42) and (43) are unresolved, the peak due to loss of ethylene must be corrected for the presence of a peak 1.5V lower.

The correction required was determined by measuring the output voltage in the region of the metastable peak for the loss of ethylene from the molecular ion of butyrophenone at various electric sector

voltages. This, in effect, gave a plot of the height of the metastable peak versus the electric sector voltage. In this way, it was determined that there was a baseline variance of 1.1% of the metastable peak height at 1.5 volts higher than the voltage of the maximum.

The second factor involved the assumption, which is implicit in the above discussion; namely, peak heights are directly proportional to peak area (i.e., ion abundance). This assumption has validity providing that there is no difference between the widths of the peaks at half height, i.e., the kinetic energy release for the loss of ethylene and (^{13}C)-ethylene are the same in each compound. If this assumption is not true, then a correction is required to account for the difference in peak widths.

Since the peaks for the metastable transitions of interest here are unresolved, it was necessary to estimate their widths from the analogous metastable peaks due to the loss of ethylene from butyrophenone and (^{13}C)-ethylene from the carbon-13 labelled butyrophenones (35) and (36). These measurements were also performed on the La Trobe mass spectrometer. Scheme 3-15 sets out the reactions studied and the values of the metastable peak widths at 50% and 20% of the peak height. The peak widths are represented by ΔE in volts and the kinetic energy releases were calculated using equation 2-8. The ratios of the metastable peak widths of carbon-13 compounds (36) and (35) to the width of the peak for butyrophenone are shown in table 3-8.

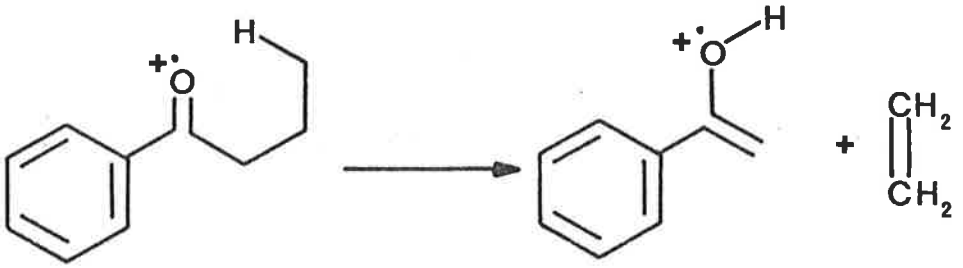

ΔE_{50} = 0.716 ± 0.004 volts.
ΔE_{20} = 1.118 ± 0.004 volts.

T_{50} = 22.65 ± 0.41 meV
T_{20} = 55.83 ± 0.44 mEv

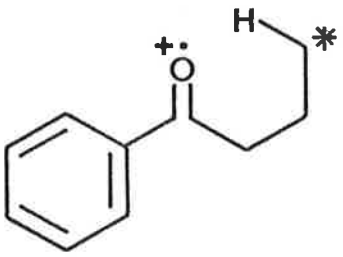

ΔE_{50} = 0.723 ± 0.007 volts.
ΔE_{20} = 1.132 ± 0.006 volts.

T_{50} = 22.80 ± 0.43 meV
T_{20} = 55.92 ± 0.57 meV

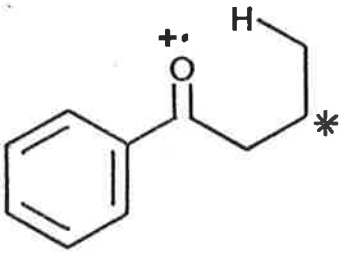

ΔE_{50} = 0.728 ± 0.008 volts.
ΔE_{20} = 1.141 ± 0.009 volts.

T_{50} = 23.17 ± 0.50 meV
T_{20} = 56.95 ± 0.92 meV

Scheme 3-15

Table 3-8

Ratio	50% Peak Height	20% Peak Height
$\Delta E(36)/\Delta E(2)$	1.010 ± 0.015	1.013 ± 0.009
$\Delta E(35)/\Delta E(2)$	1.017 ± 0.017	1.021 ± 0.012

Table 3-9 gives the uncorrected ratio of peak heights for loss of ethylene versus (^{13}C)-ethylene along with the corrected ratios due to baseline variance and peak width differences.

Table 3-9

Compound	Metastable Ion Transition	Ratio ± SD[a]
4-(^{13}C),(43)	$177^+ \rightarrow 149^+ +28$ $177^+ \rightarrow 148^+ +29$	$\bar{\chi}$ = 1.019 ± 0.005
correction due to differences in peak width ($\Delta E(36)/\Delta E(2)$)[b]		$\bar{\chi}$ = 1.006 ± 0.014
correction due to baseline variance (1.1%)		$\bar{\chi}$ = 0.995 ± 0.014
3-(^{13}C),(42)	$177^+ \rightarrow 149^+ +28$ $177^+ \rightarrow 148^+ +29$	$\bar{\chi}$ = 1.041 ± 0.007
correction due to differences in peak width ($\Delta E(35)/\Delta E(2)$)[b]		$\bar{\chi}$ = 1.020 ± 0.019
correction due to baseline variance (1.1%)		$\bar{\chi}$ = 1.009 ± 0.019

NOTES

(a) this is the ratio of the loss of ethylene to the loss of (^{13}C)-ethylene.
(b) see table 3-7.

The largest peak width correction ratio (see table 3-7) was used to estimate the true peak height ratio. As a result, the reduction in the peak height ratio may have been over-estimated.

Another approach to estimating the parameters of the overlapping metastable peaks (such as peak width and height etc.), is to attempt lineshape analysis. To evaluate the validity of this approach, deconvolution of the metastable peaks for loss of the ethylenes from compound (42) was undertaken.

It must be emphasized that lineshape analysis of the metastable peaks was attempted using *only a single scan* of these peaks. The required microprocessor-spectrometer interfacing for multiple scanning and peak shape averaging was not available at the time the experiments were performed. As a result, instrumental factors (such as pressure variations and the signal to noise ratio) have not been minimized which may lead to errors in estimating the peak parameters. However, the gross details of the differences between the metastable peaks are expected to be observed by this method.

The computer program used† involved a non-linear weighted least-square method of fitting the digitized metastable peak data to gaussian, lorentzian and mixed gaussian-lorentzian lineshapes. From the variabilities of the calculated parameters (peak height, position and width) it was clear that the metastable peaks were gaussian in shape. Table 3-10 lists the ratios of the peak heights and widths for the metastable peaks for the McLafferty rearrangement from compound (42).

---

† The deconvolution program was written by Dr. T. Kurucsev, who also performed the calculations.

Table 3-10

Compound	Ratio, Peak Widths[a]	Ratio, Peak Heights[b]
3-(^{13}C),(42)	1.075 ± 0.02	1.037 ± 0.007

NOTES

(a) ratio of loss of (^{13}C)-ethylene to ethylene.
(b) ratio of loss of ethylene to (^{13}C)-ethylene.

It is clear from table 3-10 that the ratios of the peak heights and peak widths are of the same order of magnitude as the ratios obtained previously (see tables 3-7 and 3-8 respectively). However, it is also clear that the ratio of peak widths has been overestimated by the deconvolution technique. If this ratio were used to correct the peak height ratio, an inverse carbon-13 kinetic isotope effect would result.

Based on the above results, the use of lineshape analysis for extracting small differences between the areas of metastable peaks, appears encouraging. It seems essential, however, that the experimental metastable peak lineshape should consist of the average of a number of scans. In this way, the reliability of peak widths and heights would be expected to increase markedly.

(f) Deuterium Labelled 2-Ethylbutyrophenones

As discussed previously in the study of carbon-13 labelled butyrophenones, the observation of an isotope effect, while indicating bonding charges at the isotopic position in the transition state, does not enable direct conclusions to be made about the operating mechanism. Clearly, isotopic substitution at other positions may indicate whether the reaction proceeds by one of a number of alternative mechanisms.

As a consequence, the carbon-13 studies of 2-ethylbutyrophenones necessitate the investigation of the effects of deuterium substitution on the 1,5-hydrogen migration.

The compounds 4-($^2H_3$)-2-ethylbutyrophenone, (4-($^2H_3$)-2-ethyl-1-phenyl-1-butanone)(44), 4-($^2H_3$)-2-ethyl-*p*-methoxybutyrophenone, (4-($^2H_3$)-2-ethyl-1-(4-methoxyphenyl)-1-butanone)(45) and 4-($^2H_3$)-2-ethyl-*p*-cyanobutyrophenone, (4-($^2H_3$)-2-ethyl-1-(4-cyanophenyl)-1-butanone)(46) were prepared and the isotope effects for the 1,5-hydrogen migration were measured. Their synthesis involved alkylating the substituted butyrophenones (2), (6) and (7), with 1-($^2H_3$)-2-iodoethane according to the method of Brown[289,290]. The synthetic route is summarized in scheme 3-16.

Measurements of the deuterium isotope effect for the McLafferty rearrangement from the molecular ions of compounds (43) - (46) were made for both the ion source and first FFR reactions. The instrument used in these measurements was the Hitachi Perkin-Elmer RMU-7D mass

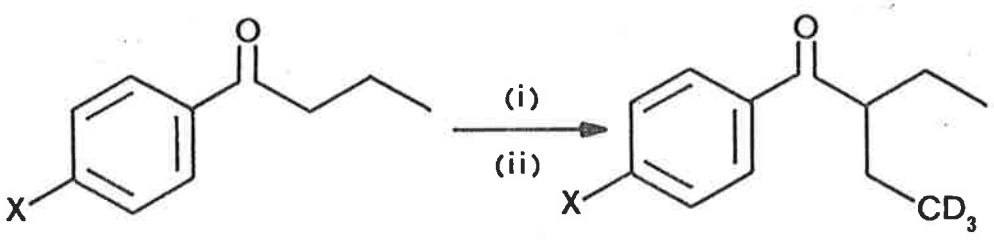

X = H (2)
CH_3O (6)
CN (7)

X = H (44)
CH_3O (45)
CN (46)

(i) KH/THF
(ii) CD_3CH_2I

Scheme 3-16

spectrometer. The first FFR metastable ion reactions were measured using the electric sector defocusing technique discussed in Chapter 2. Table 3-11 summarizes the deuterium isotope effects obtained for these compounds.

Table 3-11

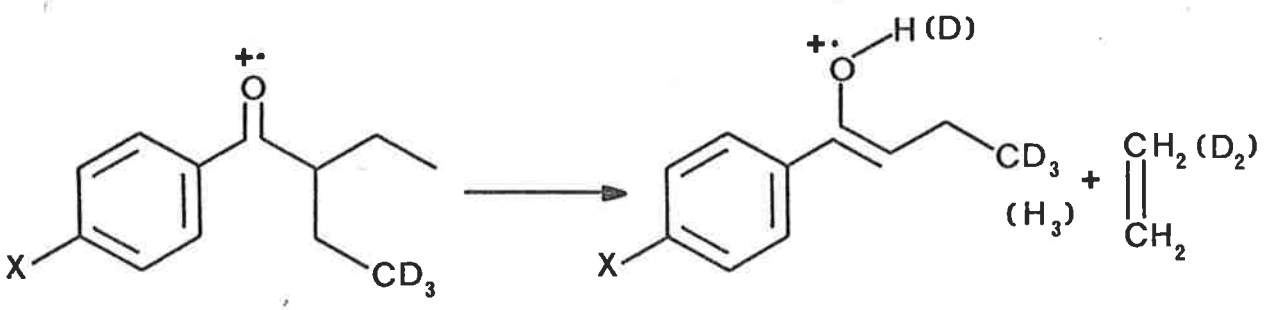

p-X-2-Ethylbutyrophenone	σ_p^{+a}	$k_H/k_D \pm SD^b$ ion source	$k_H/k_D \pm SD^b$ first FFR
p-OCH_3 (45)	-0.78	1.44 ± 0.02	1.63 ± 0.07
p-H (44)	0.0	1.65 ± 0.01	1.58 ± 0.07
p-CN (46)	0.66	1.72 ± 0.01	1.75 ± 0.03

NOTES

(a) Brown's σ_p^+ value[270]
(b) standard deviation.

The ion source and field free region reactions of compounds (44) - (46) indicate that hydrogen and deuterium randomization processes do not occur prior to the McLafferty rearrangement and 1,5-hydrogen transfer occurs in a site-specific manner. A similar result was stated earlier for 4-($^2H_3$)-butyrophenone (23).

To obtain further information on whether the McLafferty rearrangement in this system is stepwise or concerted, the secondary

isotope effect for loss of 3-($^2H_2$)-ethylene from 3-($^2H_2$)-2-ethylbutyrophenone, (3-($^2H_2$)-2-ethyl-1-phenyl-1-butanone)(47) was measured. The synthesis of compound (47) required the preparation of 1-($^2H_2$)-1-iodoethane. This was achieved by the reduction of phenyl acetate with lithium aluminium deuteride, followed by converting the hydroxyl group to an iodo group using trimethylsilyl iodide[297,298]. The potassium enolate anion of butyrophenone was prepared in tetrahydrofuran using potassium hydride and was then alkylated with 1-($^2H_2$)-1-iodoethane[289,290]. The synthetic sequence is summarized in scheme 3-17.

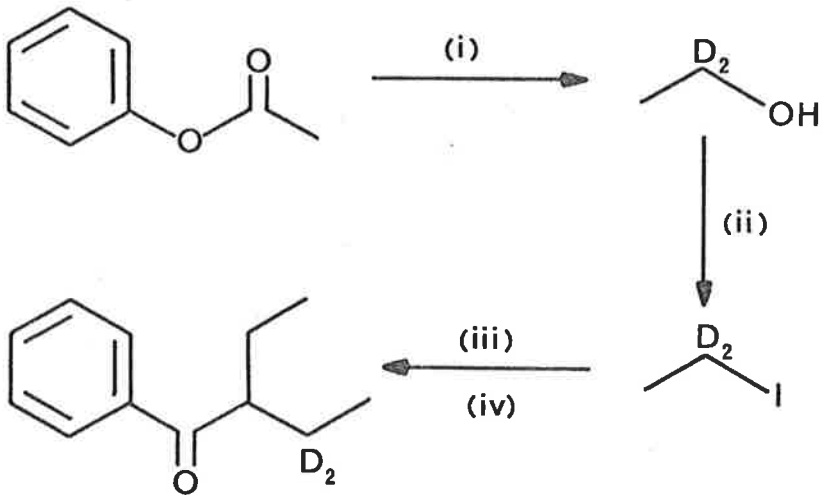

(47)

(i) LAD/Et_2O
(ii) $(CH_3)SiI/CHCl_3$
(iii) KH/THF
(iv) butyrophenone

Scheme 3-17

The deuterium secondary isotope effect was measured for the loss of ethylene versus ($^2H_2$)-ethylene from the molecular ion of ketone (47) in the first FFR of the Hitachi Perkin-Elmer RMU-7D mass spectrometer. The isotope effect obtained is shown in table 3-12.

Table 3-12

Instrument	Deuterium Isotope Effect ($k_H/k_D \pm SD$)
RMU-7D	1.16 ± 0.02
La Trobe	1.15 ± 0.02

The isotope effect measurement for the fragmentation of ketone (47), was repeated using the La Trobe mass spectrometer and is also shown in table 3-12.

(g) Trapping Experiments

If the McLafferty rearrangement in butyrophenone and related systems, proceeded by means of a stepwise mechanism, then it should be possible to trap the intermediate radical by an intramolecular process. Wagner and Liu[299] adopted this approach in their studies of the Norrish type II photoelimination in alkyl aryl ketones. They found that with the photoelimination of 2-allylbutyrophenone, 2-phenyl-2-norbornanol was produced. This indicates that the diradical formed from the initial 1,5-hydrogen migration has a sufficient lifetime to undergo intramolecular cyclization thereby inhibiting the completion of the Norrish type II pathway.

The approach of Wagner and Liu was adopted in investigating the McLafferty rearrangement. The compounds proposed for this study were; 2-allylbutyrophenone, (2-ethyl-1-phenyl-4-penten-1-one)(48) and 4-cyclopropylbutyrophenone, (4-cyclopropyl-1-phenyl-1-butanone)(49).

2-Allylbutyrophenone (48) was prepared from N-(1-propylbenzylidene)cyclohexylamine by the method of Stork and Dowd[300]. The mass spectrum of the compound will be discussed in Chapter 5.

The synthesis of 2-cyclopropylbutyrophenone (49), however, proved to be problematic and all attempts at preparing this compound were unsuccessful. The simplest approach was deemed to be cyclopropanation of 1-phenyl-5-hexen-1-ol (50) using the Simmons-Smith reagent[301]. Compound (50) was prepared in 96% yield by alkylation of benzaldehyde with 1-pent-4-enemagnesium bromide as shown in scheme 3-18. Reaction of the alkene (50) with the Simmons-Smith reagent, prepared in situ from zinc dust, copper^{I} chloride and di-iodomethane, resulted in a mixture of eight products (50% unreacted starting material) as determined by GLC. This reaction was repeated using dimethoxyethane as the co-solvent to precipitate zinc^{II} iodide from the reaction mixture. The product mixture obtained from this reaction was again complex and contained 50% starting material. Dichlorocarbene, prepared by catalytic phase transfer also failed to add to alkene (50). Carbene, prepared from diazomethane and copper^{I} chloride did not react with the alkene (50); GLC analysis of the isolated product showed it to be unreacted starting material.

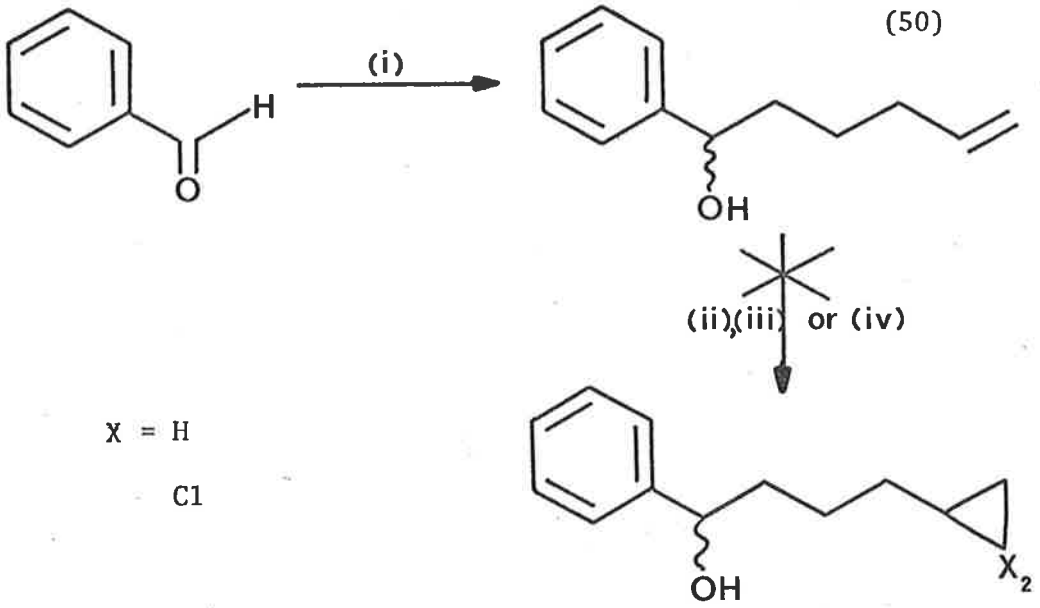

(i) 1-pent-4-enemagnesium bromide/Et_2O
(ii) $Zn/Cu^{I}Cl/CH_2I_2$
(iii) $CHCl_3$/KOH/triethylbenzylammonium chloride
(iv) $CH_2N_2/Cu^{I}Cl$

Scheme 3-18

CHAPTER 4

CALCULATIONS

In this chapter the results of calculations of isotope effects for the McLafferty rearrangement from various reactant and transition state models of the butyrophenone and 2-ethylbutyrophenone systems are presented. The calculations were performed in an attempt to provide precise information on the structure of the transition state for the McLafferty rearrangement in these systems. For this information, it was necessary to conceptualize and paramaterize various physically realistic models of the systems in question and to calculate the isotope effect occurring on isotopic substitution of various atoms in these models. Comparison of the calculated isotope effects with those obtained experimentally, should enable predictions to be made about the likely structure of the transition state. Further, any quantitative information on the transition state structure will necessarily facilitate the choice between the mechanisms proposed for the reaction. This approach to the structure of the transition state has been used on a number of occasions[302-309].

BEBOVIB-IV Calculations

The calculations were performed using the CDC 6400 series CYBER 173 computer at the University of Adelaide, computing centre. The program used for these calculations was a modified version of BEBOVIB-IV[310], which was made available by Professor L.B. Sims, University of Arkansas. It was written in FORTRAN-IV and required only slight modification to run on the CDC computer.

Briefly, BEBOVIB-IV calculates molecular masses and moments of inertia from the input structural parameters. Vibrational frequencies are calculated from bonding parameters (bond length and bond order) and force constants, both of which are determined by the

operator by modelling known systems. Isotope effects are evaluated using the relationships derived from absolute rate theory by Bigeleisen and Mayer (equations 1-6 to 1-11, Chapter 1).

The geometry of reactant and transition state models was specified in terms of an easy-to-use spherical polar coordinate system; coordinates of atoms were defined by bond lengths (r_{ij}) in Angstroms and the polar (θ) and azimuthal ($\emptyset$) angles in degrees. Coordinates of each atom were specified with respect to a right-handed cartesion coordinate system. Originally, the origin of this system was centred at some atom and the coordinates of the remaining atoms were specified by a series of translations and/or rotations of the coordinate system from its original position. The format for the atom coordinate input data is well described in the information accompanying the program[310].

Generally, standard force constants[311-315] were used for the reactant model. Since the structural parameters and force constants for the transition state are unknown, they were calculated from those of the reactant using empirical relationships. A modified version of Paulings rule[316] was used to relate the bond distances of the transition state (r_{ij}) to those of the reactant (r_{ij}^{o}) by means of the bond order (n_{ij}) of the bond between atoms i and j. This is shown in equation 4-1.

$$r_{ij} = r_{ij}^{o} - 0.30 \ln (n_{ij}) \qquad \text{Equation 4-1}$$

Standard bond distances (r_{ij}^{o}) are used for the reactant[317]. The stretching force constants for the transition state model were calculated using the Pauling-Badger relationship as shown in equation 4-2.

$$F_{ij} = n_{ij} . F_{ij}^{o} \qquad \text{Equation 4-2}$$

The stretching force constant of the reactant is denoted by F_{ij}^{o}. It has been shown[318,319], that equation 4-2 is a good approximation for bonds involving the elements of the first three rows of the periodic table. Angle bending force constants were estimated for the transition state using equation 4-3[306],

$$F_{\alpha} = g_{\alpha} . (n_{ij} . n_{jk})^{\frac{1}{2}} . F_{\alpha}^{o}(\alpha) \qquad \text{Equation 4-3}$$

where the angle bending force constant is denoted by $F_{\alpha}^{o}(\alpha)$ and α is the angle subtended by the bonds joining atoms i, j and k. The term, g_{α}, is a hybridization factor and is given in equation 4-4[306].

$$g_{\alpha} = 1.39 + 1.17 . \cos(\alpha) \qquad \text{Equation 4-4}$$

A simple valence force field (SVFF, diagonal potential energy matrix) was used for both reactant and transition state models. The imaginary (or zero) reaction coordinate frequency ($\nu_{L}^{\ddagger}$) was generated in the transition state model by introducing off-diagonal elements into the potential energy matrix. These elements represent the coupling of adjacent bond stretches and are termed interaction force constants. The interaction force constants, f_{ik}, are related to the stretching force constants by equation 4-5.

$$f_{ik} = A_{ik} . (F_{ij} . F_{jk})^{\frac{1}{2}} \qquad \text{Equation 4-5}$$

where A_{ik} are the proportionality constants or interaction coefficients. The interaction coefficients were evaluated by solving the determinant of the force constant matrix for the transition state. To ensure that the reaction coordinate corresponded to a zero or imaginary frequency, the determinant of the force constant matrix was set to less than, or equal to zero, as shown in equation 4-6.

$$|\underset{\sim}{F}_{ij}|\ \pi F_{ij} = D \leqslant 0 \qquad \text{Equation 4-6}$$

The term D is the barrier curvature parameter[319], the value of which determines shapes of potential energy surfaces at the transition state. Expansion of equation 4-6 leads to a complex expression containing, as the unknown variables, the interaction coefficients. In order to solve this expression, the simplifying assumption of equating the interaction coefficients was used.

Frequencies and principle moments of inertia were calculated for various isotopic reactant and transition state models using a version of the normal coordinate and vibrational analysis program of Gwinn[321,322]. Calculation of the isotope effect at each position was done according to the expressions of Bigeleisen and Mayer, given in the notation of Wolfsberg and Stern (equation 1-8, Chapter 1). The ratio of isotopic reaction coordinate frequencies ($\nu_{1L}^{\ddagger}/\nu_{2L}^{\ddagger}$) was evaluated directly from the frequencies calculated by the program (if $\nu_L^{\ddagger}$ is imaginary), or utilizing the Teller-Redlich product rule as shown in equation 1-14 (Chapter 1).

Models of Butyrophenone

As mentioned previously, the primary objective of the calculations was to devise various reactant and transition state models, having a basis in physical reality, which yield meaningful isotope effect data when compared to the experimental results. Considering the mechanisms that have been proposed for the McLafferty rearrangement from butyrophenones, the simplest is the stepwise process with 1,5-hydrogen migration as the rate determining step. This process involves the minimum atomic motion required to achieve a transition

state, the energy of which determines the rate of the overall process. In this situation, the reaction coordinate is defined by the motion of a hydrogen atom from carbon-4 of butyrophenone to the carbonyl oxygen, concomitant with geometry changes at carbon-4 due to hybridization changes.

(a) 1,5-Hydrogen Migration as the Rate Determining Step.

That part of the stepwise mechanism which is of interest here, can be represented as shown in scheme 4-1.

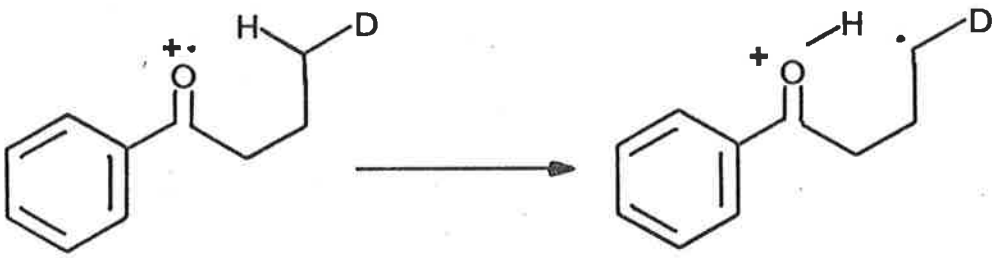

Scheme 4-1

To simplify the calculations, 15-atom cut-off models[323] were used for both the reactant and the transition state. This procedure required "cutting through" the aromatic ring and ignoring all atoms greater than two atoms removed from the carbonyl carbon. The validity of this method has been investigated by Sims and co-workers[302]. Problems associated with this procedure for cyclic transition states are being studied by the group at Arkansas[324].

Figures 4-1 and 4-2 are geometric representations of the 15-atom cut-off models of the reactant and the transition state respectively, used in the initial calculations. In these models, C_1-C_2-C_3 and C_4-O_5 are coplanar as are C_4-O_5 and C_{12}-H_{15}. The aromatic ring is represented by atoms C_1-C_2-C_3, the remaining atoms of this system

BUTYROPHENONE

REACTANT MODEL

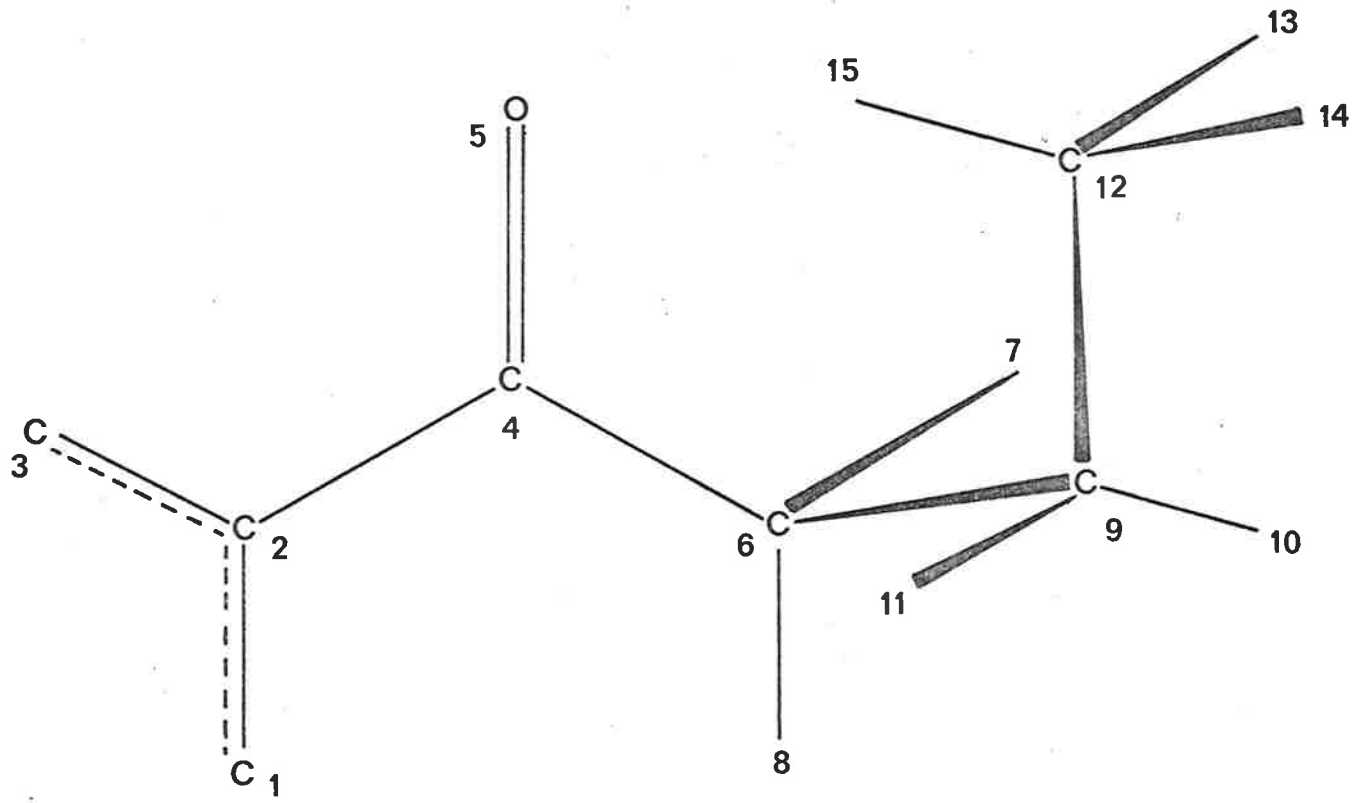

Figure 4-1

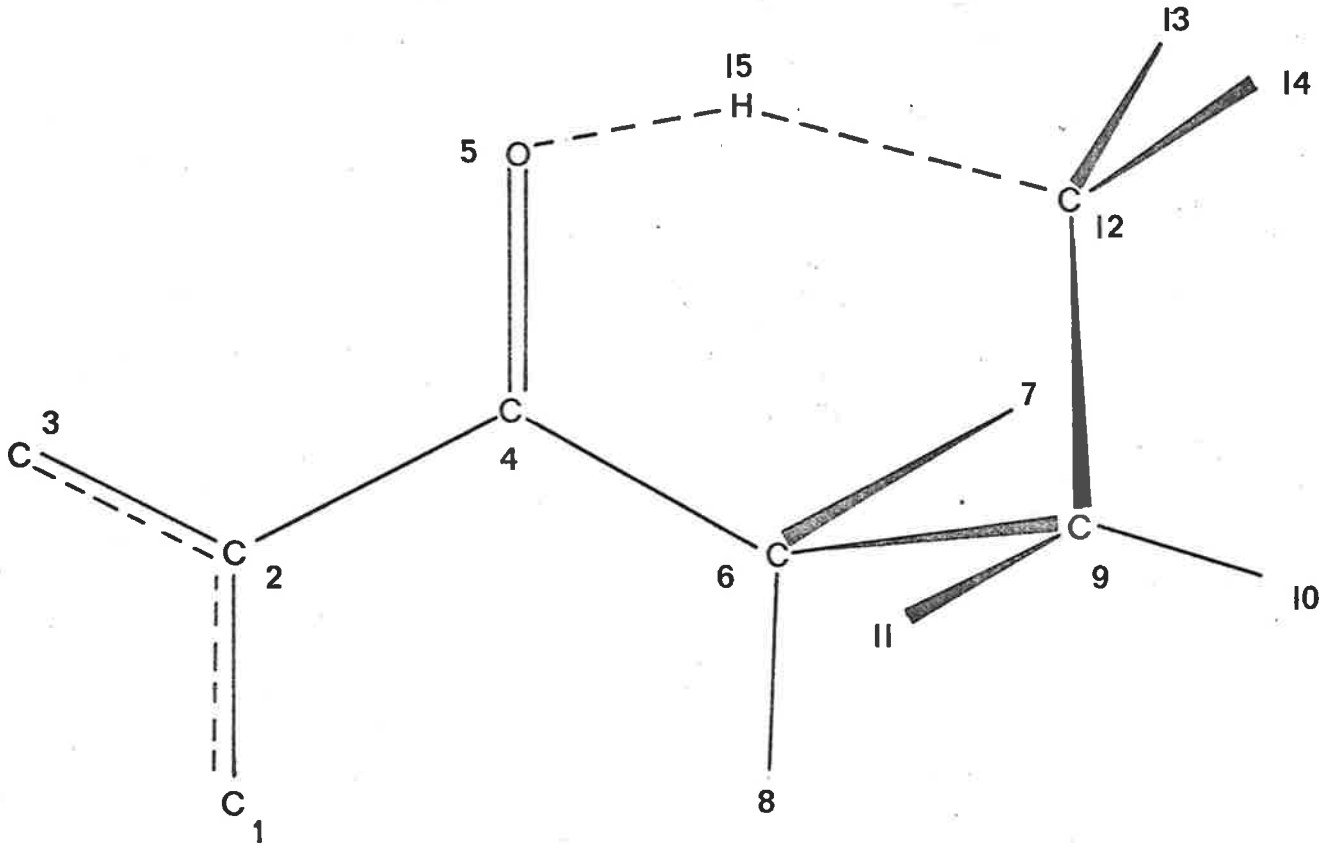

Figure 4-2

being redundant due to the cut-off procedure.

The confirmation about the C_6-C_9 and C_9-C_{12} bonds is staggered by 30°. This is predicted to be the most stable conformation while maintaining the coplanarity of C_4-O_5 and C_{12}-H_{15}. Newman projections[325] of the atoms around C_4, C_6, C_9 and C_{12} are shown in figure 4-3.

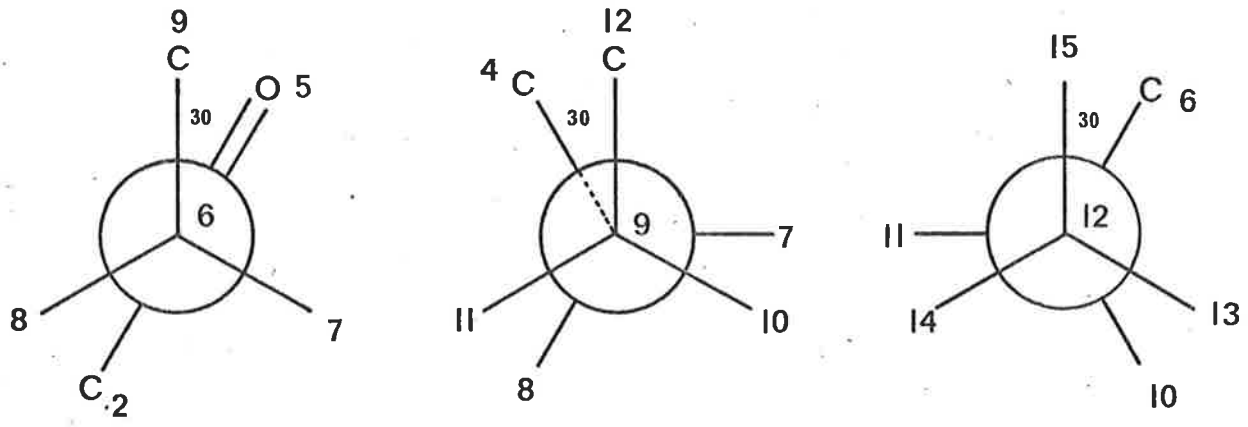

$C_6 \rightarrow C_4$ $C_9 \rightarrow C_6$ $C_{12} \rightarrow C_9$

Figure 4-3

Most of the geometry elements described above were retained for the transition state models. A series of models were devised in which H_{15} was transferred from C_{12} to O_5 by altering the bond orders of bonds H_{15}-C_{12} ($n_{15,12}$) and H_{15}-O_5 ($n_{15,5}$), such that $n_{15,12} + n_{15,5} = 1.0$ at all times. Since C_{12} undergoes a hybridization change from sp^3 to sp^2 during the course of 1,5-hydrogen migration, the conformation of atoms around C_{12} was altered in a linear fashion to account for this. Figure 4-4 indicates the angle changes occurring at C_{12} as the reaction proceeds.

A kinematically complete set of 44 internal coordinates for the reactant model and 50 internal coordinates for the transition state models were defined according to the rules of Decius[326] and are

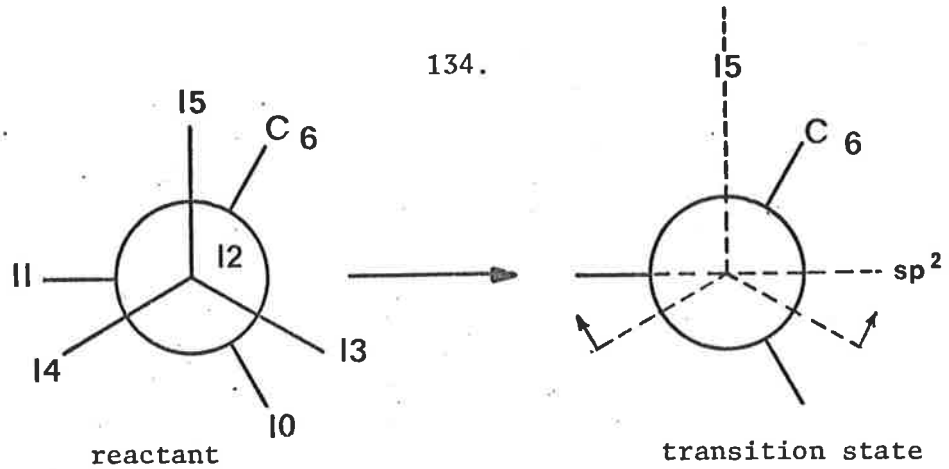

reactant
$n_{15,12} = 1,0$
$n_{15,5} = 0,0$

transition state
$n_{15,12} = x$
$n_{15,5} = t-x$

Figure 4-4

shown in table 4-1. In this table, Δr represents the bond stretching internal coordinates, $\Delta\alpha$ the angle bending, $\Delta\delta$ the out of plane wag and $\Delta\tau$ the torsion internal coordinate.

Table 4-2 lists the bond lengths, bond angles and force constants that were used for each type of internal coordinate. Changes in these parameters required to produce the transition state models are also shown in table 4-2. The torsional force constant of the transition state, $R_{50} = \Delta\tau_{4,5}$ (shown in table 4-2 as $\Delta\tau$(C-O) = 0.473 m dyne.Å/rad^2) was determined from the carbonyl stretching frequency of acetophenone[327]. This force constant is dependent on the bond order of the carbonyl group and the hybridization of its atoms (in this case sp^2). Equation 4-7, describes the empirical relationship which corrects the torsional force constant for ethane (F_τ^o = 0.072 m.dyneÅ/rad^2)[313] for the bond order n_{ij}, and the change in hybridization of each atom h_i, h_j.

$$F_\tau = h_i.h_j.(n_{ij})^4.F_\tau^o \qquad \text{Equation 4-7}$$

The hybridization factors were calculated by means of equation 4-8, where β is the tetrahedral angle; α_i and α_j are 109.5° for tetrahedral centres, 120.0° for sp^2 centres and 180.0° for sp centres[306,310].

Table 4-1

Internal Coordinates for Models of Butyrophenone[a].

$R_1 = \Delta r_{1,2}$[b]	$R_{26} = \Delta\alpha_{8,6,9}$
$R_2 = \Delta r_{2,3}$	$R_{27} = \Delta\alpha_{6,9,10}$
$R_3 = \Delta r_{2,4}$	$R_{28} = \Delta\alpha_{6,9,11}$
$R_4 = \Delta r_{4,5}$	$R_{29} = \Delta\alpha_{6,9,12}$
$R_5 = \Delta r_{4,6}$	$R_{30} = \Delta\alpha_{10,9,11}$
$R_6 = \Delta r_{6,7}$	$R_{31} = \Delta\alpha_{10,9,12}$
$R_7 = \Delta r_{6,8}$	$R_{32} = \Delta\alpha_{11,9,12}$
$R_8 = \Delta r_{6,9}$	$R_{33} = \Delta\alpha_{9,12,13}$
$R_9 = \Delta r_{9,10}$	$R_{34} = \Delta\alpha_{9,12,14}$
$R_{10} = \Delta r_{9,11}$	$R_{35} = \Delta\alpha_{9,12,15}$
$R_{11} = \Delta r_{9,12}$	$R_{36} = \Delta\alpha_{13,12,14}$
$R_{12} = \Delta r_{12,13}$	$R_{37} = \Delta\alpha_{13,12,15}$
$R_{13} = \Delta r_{12,14}$	$R_{38} = \Delta\alpha_{14,12,15}$
$R_{14} = \Delta r_{12,15}$	$R_{39} = \Delta\gamma_{1,3,4,2}$
$R_{15} = \Delta\alpha_{1,2,3}$[b]	$R_{40} = \Delta\gamma_{2,5,6,4}$
$R_{16} = \Delta\alpha_{1,2,4}$	$R_{41} = \Delta\tau_{2,4}$[b]
$R_{17} = \Delta\alpha_{3,2,4}$	$R_{42} = \Delta\tau_{4,6}$
$R_{18} = \Delta\alpha_{2,4,5}$	$R_{43} = \Delta\tau_{6,9}$
$R_{19} = \Delta\alpha_{2,4,6}$	$R_{44} = \Delta\tau_{9,12}$
$R_{20} = \Delta\alpha_{5,4,6}$	$R_{45} = \Delta r_{15,5}$[c]
$R_{21} = \Delta\alpha_{4,6,7}$	$R_{46} = \Delta\alpha_{4,5,15}$[c]
$R_{22} = \Delta\alpha_{4,6,8}$	$R_{47} = \Delta\alpha_{5,15,12}$[c]
$R_{23} = \Delta\alpha_{4,6,9}$	$R_{48} = \Delta\tau_{5,15}$[c]
$R_{24} = \Delta\alpha_{7,6,9}$	$R_{49} = \Delta\tau_{15,12}$[c]
$R_{25} = \Delta\alpha_{7,6,8}$	$R_{50} = \Delta\tau_{4,5}$[c]

NOTES

(a) The internal coordinates are defined according to the atom numbering in figure 4-1 and 4-2.
(b) Internal coordinate symbols are defined in the text.
(c) Unique to the transition state model.

Table 4-2

Structural Parameters and Force Constants for 4-($^2H_1$)-Butyrophenone. Loss of Ethylene by a stepwise process. 1,5 Hydrogen Migration as the Rate Determining Step.

Coordinate		Reactant Model		Transition State Models	
		r_i^o [a]	F_{ij}^o [b]	r_i	F_{ii}
Δr	$(C_{Ar}\text{-}C_{Ar})$ [c]	1.362 [d]	9.431 [e]	1.362	9.431
Δr	$(C_{Ar}\text{-}C)$	1.537	5.0	1.537	5.0
Δr	(C-O)	1.236 [d]	10.128 [e]	1.236	10.128
Δr	$(C_{sp2}\text{-}C)$	1.537	5.0	1.537	5.0
Δr	(C-C)	1.537	4.5	1.537	4.5
Δr	(C-H)	1.094	5.0	1.094-0.31n.n(C-H)	5.0.n(C-H)
Δr	(O-H) [f]			0.957-1n.n(O-H)	7.8.n(C-H)
		Angle	F^o_{bend} [g]	Angle	F_{bend}
$\Delta\alpha$	$(C_{Ar}\text{-}C_{Ar}\text{-}C_{Ar})$ [h]	120.0	1.310	120.0	1.310
$\Delta\alpha$	$(C_{Ar}\text{-}C_{Ar}\text{-}C)$	120.0	1.072	120.0	1.072
$\Delta\alpha$	$(C_i\text{-}C_j\text{-}C_k)$	120.0	0.84	120.0	0.84
$\Delta\alpha$	$(C_i\text{-}C_j\text{-}C_k)$	109.5	1.0	109.5	1.0
$\Delta\alpha$	$(C_i\text{-}C_h\text{-}H_k)$	109.5	0.65	i	$0.65(n_{ij}\cdot n_{jk})^{\frac{1}{2}}g\alpha$
$\Delta\alpha$	$(H_i\text{-}C_j\text{-}H_k)$	109.5	0.55	i	$9.55(n_{ij}\cdot n_{jk})^{\frac{1}{2}}g\alpha$
$\Delta\alpha$	$(C_4\text{-}O_5\text{-}H_{15})$ [f]			$12.7+11.2n_{5,15}$	$0.75(n_{4,5}\cdot n_{5,15})^{\frac{1}{2}}g\alpha$
$\Delta\alpha$	$(O_5\text{-}H_{15}\text{-}C_{12})$ [f]			$127.9-2.5n_{5,15}$	$0.75(n_{5,15}\cdot n_{15,12})^{\frac{1}{2}}g\alpha$
$\Delta\delta$ [j]		–	0.2	–	0.2
$\Delta\tau$(C-C) [k]		–	0.72	–	0.072
$\Delta\tau$(C-O) [f]				–	0.473
$\Delta\tau$(O-H) [f]				–	0.072
$\Delta\tau$(C-H) [f]				–	0.072

NOTES:

(a) standard bond lengths in Å
(b) standard force constants in m.dyne/Å[311-315]
(c) bond stretching internal coordinates
(d) calculated using Pauling's rule (see text)
(e) calculated using equation 4-2 (see text)
(f) applicable to transition state models only
(g) standard force constants in m.dyne Å/rad^2
(h) angle bending internal coordinates
(i) angles are input in accordance with geometry changes due to sp^3-sp^2 hybridization changes
(j) out-of-plane wag internal coordinates
(k) torsion/internal coordinates

$$h_i = [\beta.\sin(\alpha_i)/\alpha_i.\sin(\beta)]^2 \qquad \text{Equation 4-8}$$

The calculated isotope effects are insensitive to moderate changes in the magnitude of torsional force constants. However, equations 4-7 and 4-8 give estimates of these force constants, corrected for hybridization and bond order effects, which are physically reasonable[306].

The bond lengths for $\Delta r(C_{Ar}\text{-}C_{Ar})$, $\Delta r(C_{Ar}\text{-}C)$ and $\Delta r(C\text{-}O)$ in table 4-2 were calculated on the basis of Pauling's rule (equation 4-1) using bond orders of 1.67[328], 1.00 and 2.0 with a standard bond length of 1.537Å. Force constants for these internal coordinates were calculated from equation 4-2 using standard force constants of 5.8, 5.0 and 5.3 m.dyne/Å respectively.

The deuterium and carbon-13 isotope effects that were calculated for the 1,5-hydrogen migration using these models are shown in table 4-3. Calculations were performed at reaction temperatures of 333.2, 298.2 and 283.2°K in order to determine the temperature dependence of the isotope effect values. The carbon-13 isotope effects are listed for a temperature of 283.2°K since their temperature variation was found to be minimal (0.6% difference for a 50°K increase in temperature).

Evaluation of equation 4-6, which includes the interaction force constant f_{ik}, yielded an interaction coefficient of 1.0 (D=0). This coefficient represents the coupling of the internal coordinates R_{14} and R_{15}. The ratio $\nu_{1L}^{\ddagger}/\nu_{2L}^{\ddagger}$ for each of the isotopic models used (table 4-3), was evaluated as 1.00. This represents a flat-topped potential energy barrier to reaction.

(b) Para-Substituted Butyrophenones.

In an attempt to imitate the variation in deuterium isotope effect observed with changing para-substituent in butyrophenone

Table 4-3

Kinetic Isotope Effects for the Stepwise Process from 4-($^2H_1$)-Butyrophenone.

H-Transfer, Rate Determining Step[a].

$n_{5,15}$[c]	$n_{12,15}$	H_{15}-D[b] T=333.2, 298.2, 283.2[d]			C_{12}-^{13}C[e]	C_9-^{13}C	C_6-^{13}C	C_4-^{13}C
0.1	0.9	1.168	1.176	1.179	0.998	1.000	0.999	0.998
0.3	0.7	1.647	1.745	1.796	1.002	1.000	1.000	0.997
0.5	0.5	1.811	1.946	2.015	1.011	1.000	1.000	0.997
0.7	0.3	1.570	1.650	1.689	1.023	1.001	1.000	0.997
0.9	0.1	1.074	1.081	1.083	1.036	1.001	1.000	0.996

NOTES

(a) the calculations assume an interaction coefficient A_{ik} = 1.0 for internal coordinates R_{14} and R_{45}.
(b) H_{15} is replaced by D.
(c) bond order between atoms 5 and 15.
(d) temperatures in ^oK
(e) carbon-13 isotope effects were calculated at the same temperatures as the deuterium isotope effects. Only the effects at T=283.2^oK are listed.

(Chapter 3), the isotope effects were calculated for the *p*-methoxy and *p*-cyanobutyrophenone. The effect of changing substituent was represented by altering the force constants for the carbonyl group with respect to the unsubstituted compound. Carbonyl group stretching frequencies were obtained from the literature[327] for *p*-methoxy and *p*-cyanoacetophenone. Assuming that the bond order of the carbonyl group of acetaldehyde was 2.0 (ν_{max} = 1730.0 cm^{-1})[308], the bond orders of the substituted acetophenone carbonyl groups were calculated on the basis of the diatomic approximation. The bond order assumption for acetaldehyde is likely to be reasonable when one considers that only slight perturbation of this value is likely to result from hyperconjugation due to the α-methyl group.

Since the sum of bond orders for bonds C_2-C_4 and C_4-O_5 is 3.0, then the order of the C_2-C_4 can be directly calculated. Table 4-5 lists the bond orders for bonds C_2-C_4 and C_4-O_5 for compounds *p*-methoxybutyrophenone and *p*-cyanobutyrophenone.

Table 4-4

	p-Methoxybutyrophenone			*p*-Cyanobutyrophenone		
	n_{ij}	F_{ij} [a]	F_τ [b]	n_{ij}	F_{ij}	F_τ
$n_{2,4}$	1.107	5.535	—	1.073	5.365	—
$n_{4,5}$	1.893	10.033	0.456	1.927	10.212	0.490

NOTES

(a) bond stretching force constant in m.dyne/Å
(b) torsional force constant in m.dyne.Å/rad^2

As a result, the bond stretching internal coordinates R_3 ($=\Delta r_{2,4}$) and R_4 ($=\Delta r_{4,5}$) were evaluated in terms of bond lengths and force constants using equations 4-1 and 4-2 respectively. Standard bond

lengths and force constants were assumed in each case.

Similarly, the torsional force constants were calculated using the carbonyl bond orders in table 4-4 and the torsional force constant of ethane (F_τ^o = 0.072 m.dyne.Å/rad^2)[313] using equations 4-7 and 4-8. The bond stretch and torsional force constants are also listed in table 4-4.

Calculated deuterium isotope effects for the substituted butyrophenones are given in table 4-5 for temperatures of 333.2, 298.2 and 283.2^{o}K. Comparison of the values with those given in table 4-3 for the unsubstituted compound, indicate that moderate changes in the carbonyl force constants due to substitutent changes have very little effect on the isotope effect. It is clear that the calculated isotope effect values are relatively insensitive to the magnitude of the force constants. Since kinetic isotope effects are determined by relative changes in structure and force constants between the reactant and transition state, the actual structural parameters and force constants assumed for the reactant do not greatly affect the calculated isotope effects. Any physically reasonable value for these parameters; such as derived from the stretching frequency data described above, can be used to obtain a meaningful isotope effect values.

(c) Equilibrium Isotope Effects.

As discussed in Chapter 3, there are two possibilities for the stepwise McLafferty rearrangement from butyrophenones. Firstly, the 1,5-hydrogen migration may be the rate determining step, followed by rapid carbon-carbon bond cleavage. In this case, a primary kinetic deuterium isotope effect will be observed by isotopic labelling at carbon-4 of butyrophenone. Calculation of isotope effects for this

Table 4-5

Deuterium Isotope Effects for the Stepwise Process from 4-($^2H_1$)-*p*-Methoxybutyrophenone and 4-($^2H_1$)-*p*-Cyanobutyrophenone. H-Transfer, Rate Determining Step[a].

		p-CH_3O[b]			*p*-CN[c]		
$n_{5,15}$	$n_{12,15}$	T=333.2	298.2	283.2[d]	T=333.2	298.2	283.2
0.1	0.9	1.171	1.179	1.182	1.164	1.171	1.174
0.3	0.7	1.652	1.751	1.801	1.639	1.739	1.788
0.5	0.5	1.818	1.952	2.026	1.803	1.934	2.004
0.7	0.3	1.576	1.658	1.676	1.561	1.638	1.661
0.9	0.1	1.080	1.088	1.094	1.066	1.071	1.097

NOTES

(a) the calculations assume an interaction coefficient A_{ik} = 1.0 for the internal coordinates R_{14} and R_{45}.
(b) 4-($^2H_1$)-*p*-methoxybutyrophenone
(c) 4-($^2H_1$)-*p*-cyanobutyrophenone
(d) temperatures in ^oK

process have been discussed in sections (a) and (b) above.

A second possibility is that the carbon-carbon bond cleavage may be the rate determining step preceeded by a rapid 1,5-hydrogen migration. Deuterium labelling at carbon-4 of butyrophenone may then lead to the observation of an equilibrium isotope effect. Naturally, the observation of such an effect is dependent on the rapidity of the hydrogen transfer (and of the reverse transfer process) and the lifetime of the intermediate formed. In an attempt to quantify the equilibrium isotope effect for hydrogen transfer in butyrophenone, the reactant and intermediate were modelled, and isotope effects calculated. Clearly, the structure, geometry and force field of the intermediate in this pathway are unknown. In general, this is also true of all transition states that are envisaged for these systems, and, to an extent, the reactants. The calculations, therefore, have a heuristic element and must be considered in this light. Figure 4-5 is geometric representation of the intermediate involved in this pathway.

The reactant model used for these calculations was the same as that described in sections (a) and (b) above. Table 4-1 describes the internal coordinates (R_1-R_{44}), table 4-2 describes the structural parameters and force constants and figure 4-1 is a geometrical representation.

The set of internal coordinates for the intermediate ion include most of those listed in table 4-1. Those that do not apply in this case are; $R_{14}(=\Delta r_{12,15})$, R_{35} $(=\Delta\alpha_{9,12,15})$, R_{37} $(=\Delta\alpha_{13,12,15})$ and R_{38} $(=\Delta\alpha_{14,12,15})$. Internal coordinates, unique to the intermediate, which replace those removed from the reactant set are shown in table 4-6.

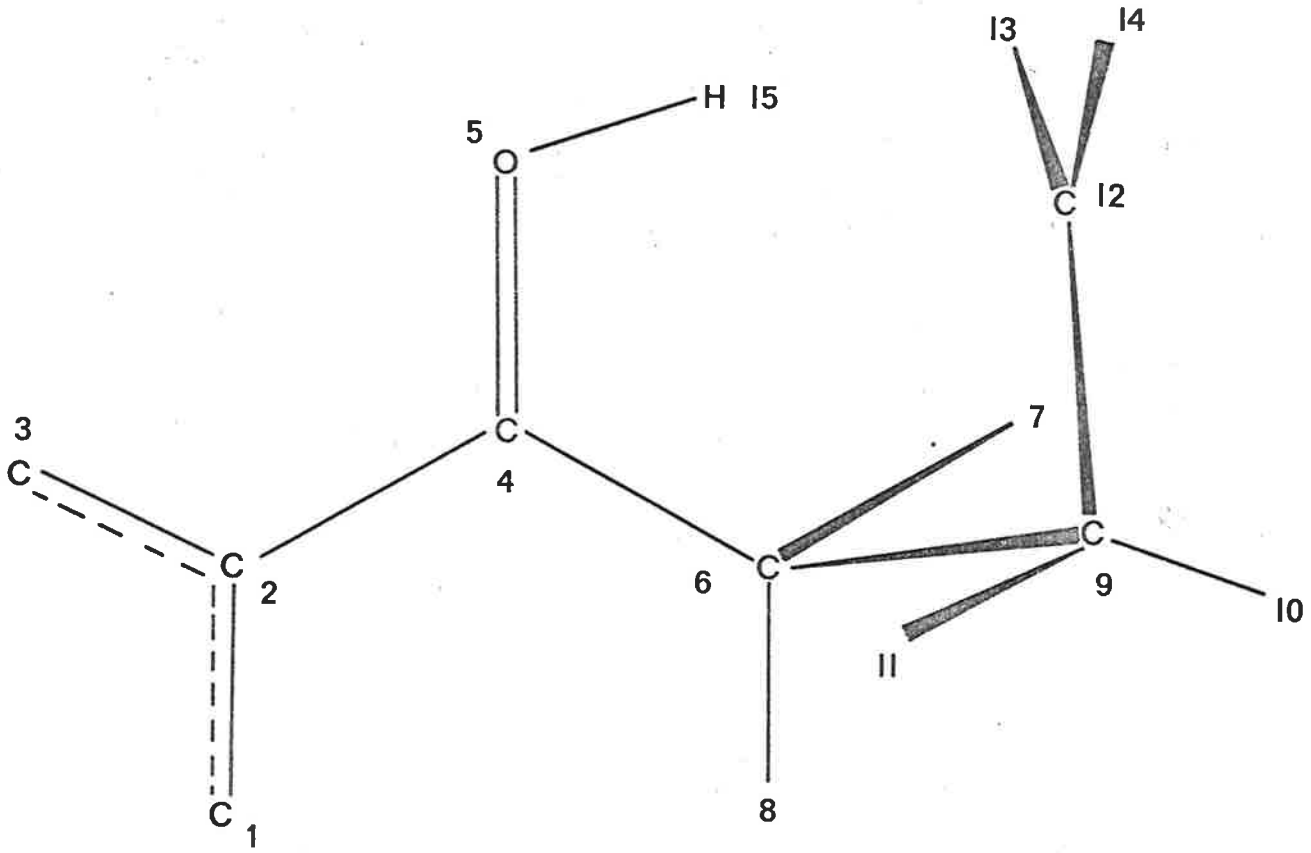

Figure 4-5

Table 4-6

Replacement Internal Coordinates for the Intermediate Ion

$$R_{14} = \Delta r_{5,15}$$

$$R_{35} = \Delta\alpha_{4,5,15}$$

$$R_{37} = \Delta\tau_{4,5}$$

$$R_{38} = \Delta\delta_{9,13,14,12}$$

Standard force constants were used for this model and are shown in table 4-2. The carbonyl torsion (R_{37}) was set initially at 0.072 m.dyne.Å/rad^2 which is considered as the lower limit (ethane torsion). Calculations were also performed with a carbonyl torsion of 0.511 m.dyne.Å/rad^2,[329] the value for ethylene, which is assumed to approximate the upper limit for this internal coordinate.

Since there are no coupled vibrations in the intermediate, no interaction force constants were used. This contrasts the requirement of an interaction coefficient in transition state models to define a reaction coordinate.

The results of these calculations are presented in table 4-7. Clearly, the calculated deuterium isotope effect is highly sensitive to changes in the carbonyl torsional force constant. This is to be expected due to the magnitude of the change in force constant. It is also clear from these calculations, that the limits placed on the equilibrium isotope effect are of the order of k_H/k_D = 0.8-1.2 which are determined to a large extent by the value given to the carbonyl torsion.

Table 4-7

Equilibrium Isotope Effects for the Stepwise Mechanism in which Carbon-Carbon Bond Cleavage is the Rate Determining Step.

F_τ [a]	H_{15}-D T=333.2, 298.2, 283.2 [b]			C_{12}-^{13}C [c]	C_9-^{13}C	C_6-^{13}C	C_4-^{13}C
0.072	1.131	1.175	1.196	1.034	1.002	1.000	0.998
0.511	0.837	0.824	0.818	1.035	1.002	1.000	0.997

NOTES

(a) torsional force constant in m.dyne. Å/rad^2
(b) temperature in ^oK
(c) carbon-13 isotope effects were calculated at T=333.2, 298.2, 283.2^oK. Only the T=283.2^oK results are listed.

Models of 2-Ethylbutyrophenone

(a) Stepwise Mechanism of Ethylene Loss.

Since the 2-ethylbutyrophenone system was a necessary extension of the experimental work begun with butyrophenone, calculation of isotope effects was also attempted using models of this system. Again, the aim of these calculations was to delineate as far as possible, the structure of the transition state for the McLafferty rearrangement from this compound by comparing the theoretical isotope effect with the value gained by measurement. As discussed previously in section (a), the simplest of the mechanistic alternatures to attempt to imitate theoretically, is the stepwise process with 1,5-hydrogen migration as the rate determining step. Scheme 4-2 details that part of the stepwise process which is of interest.

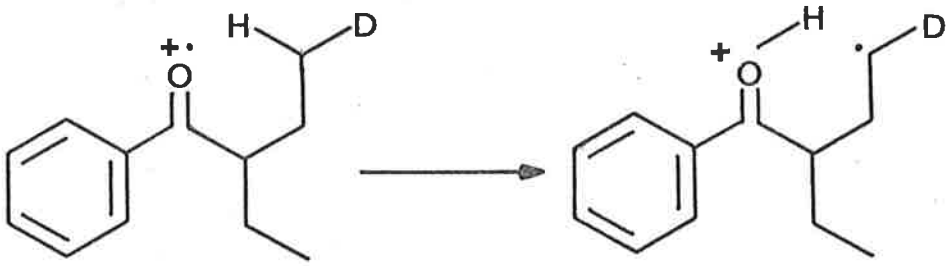

Scheme 4-2

Figures 4-6 and 4-7 are geometric representations of the 21-atom cut-off models of the reactant and the transition state used in the initial calculations. In these models, tetrahedral geometry was assumed for C_6, C_8, C_{11}, C_{15} and C_{18}. The geometry around C_2 and C_4 was assumed to be trigonal planar. The reactant model has a plane of symmetry containing atoms C_1, C_2, C_3, C_4, O_5, C_6 and H_7 and bisecting the angle subtended by bonds C_{15}-C_6 and C_6-C_8.

2-ETHYLBUTYROPHENONE

REACTANT MODEL

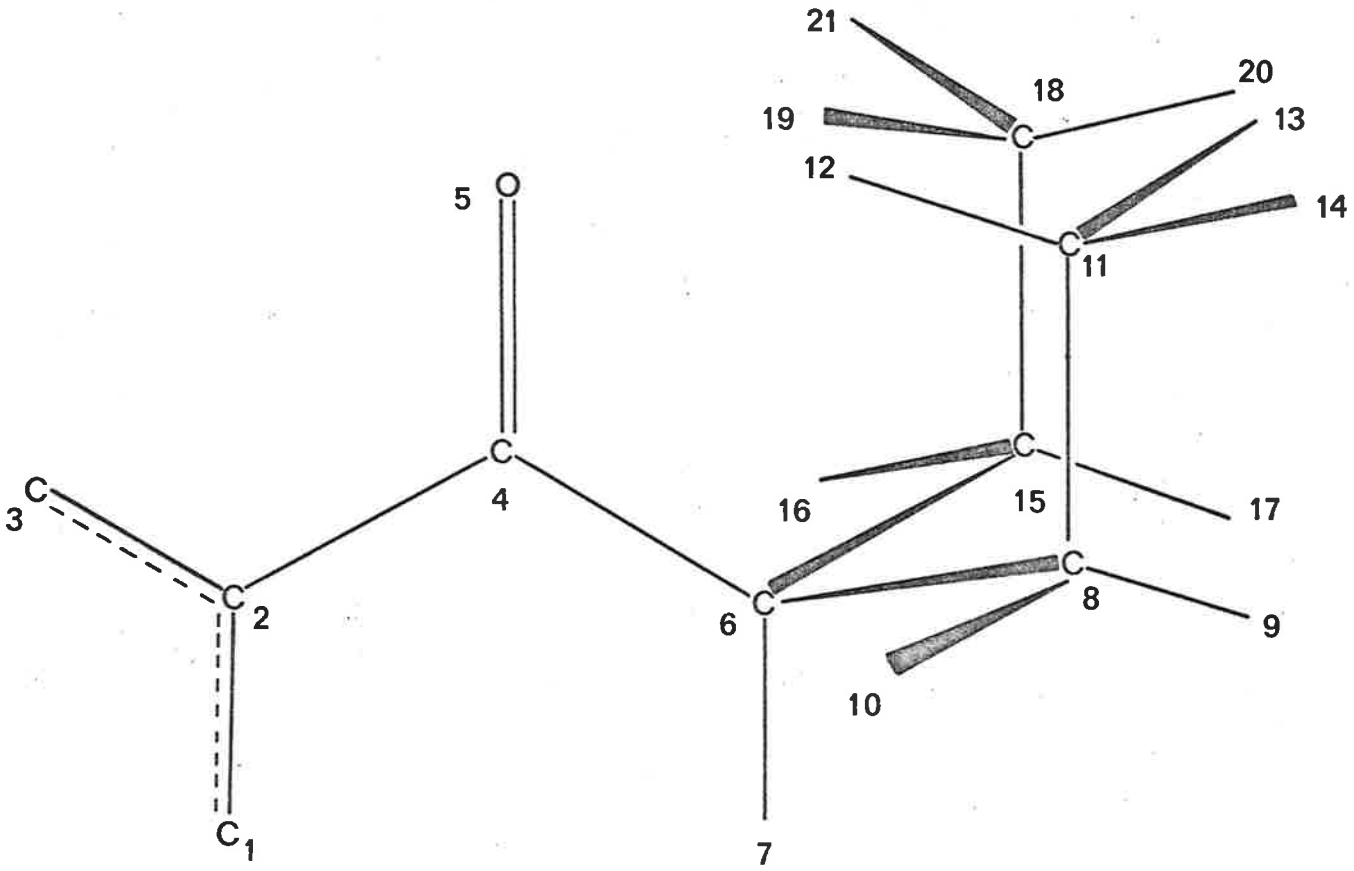

Figure 4-6

1,5-HYDROGEN MIGRATION

TRANSITION STATE MODEL

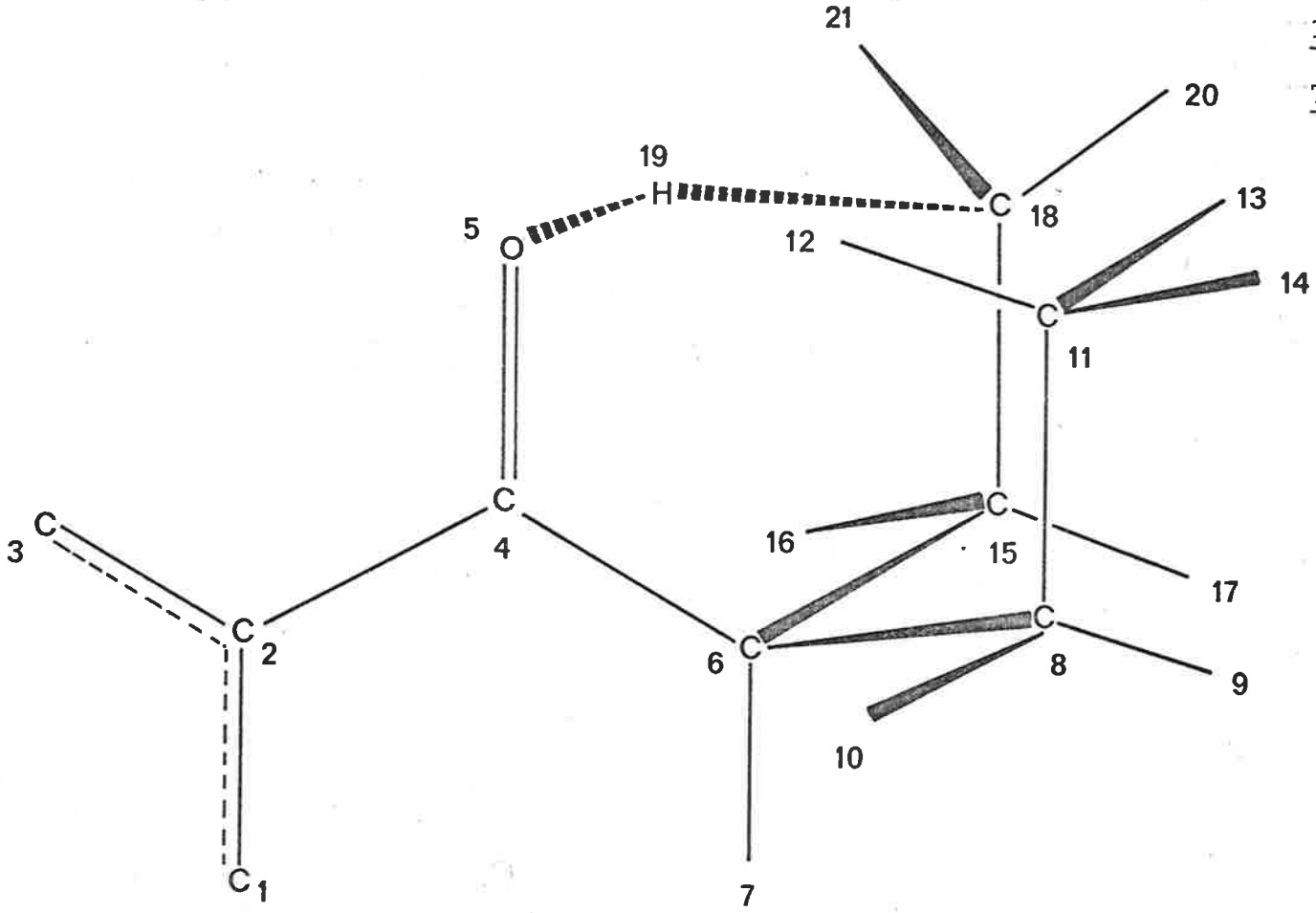

Figure 4-7

Naturally, this symmetry element is destroyed in the transition state due to the migration of H_{19}. Atoms C , C_2 and C_3, as with the butyrophenone models, represent the aromatic ring; the remaining atoms of this group are redundant due to the cut-off procedure. The conformation of the bonds around the C_6-C_8, C_8-C_{11}, C_6-C_{15} and C_{15}-C_{18} bonds is staggered by 30 degrees as with the butyrophenone models. The conformation of the entire molecule is defined in detail by the Newman projections in figure 4-8.

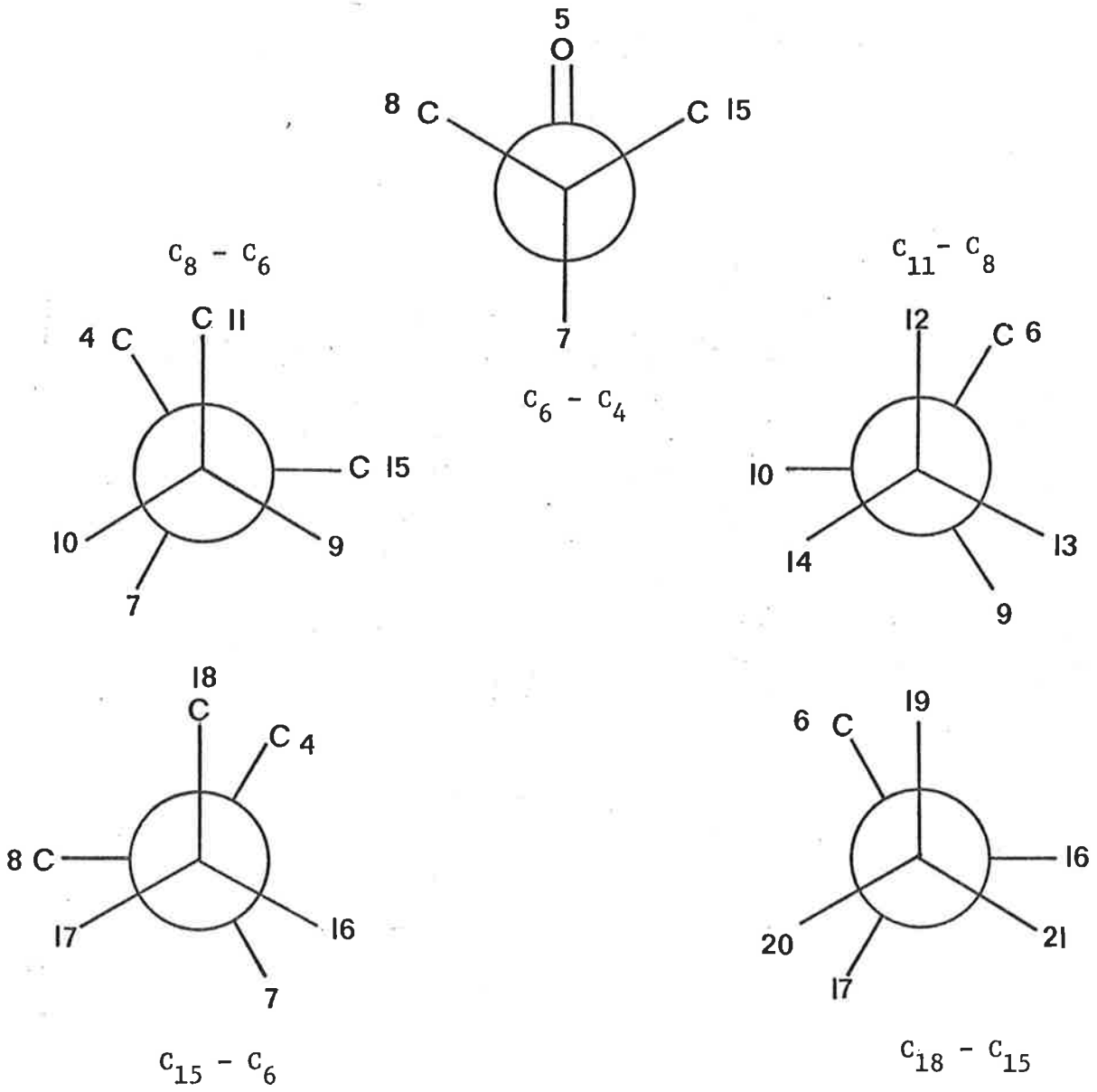

Figure 4-8

Transition state models were devised in which H_{19} was progressively transferred from C_{18} to O_5. This was achieved by changing the bond orders of bonds O_5-H_{19} and H_{19}-C_{18} according to the following relationship; if $n_{19,18} = x$ then $n_{5,19} = x-1$. Since the transfer of H_{19} requires that the hybridization of C_{18} change from sp^3 to sp^2, the geometry about this atom was changed from tetrahedral to trigonal planar in a linear fashion.

A kinematically complete set of 64 internal coordinates for the reactant model and 70 internal coordinates for the transition state models were defined according to the rules of Decius[325]. Table 4-8 lists the internal coordinates for the reactant and transition state models of 2-ethylbutyrophenone.

Table 4-9 summarizes the bond lengths, bond angles and force constants for each type of internal coordinate (bond stretch, angle bend, out-of plane wag and torsion). Changes in these parameters required to formulate the transition state models are also shown in table 4-9. The torsional force constant for the carbonyl group, R_{68} ($=\Delta\tau_{4,5}$) was determined from the stretching frequency of acetophenone as described previously (equations 4-7 and 4-8, section (a)). The bond length for internal coordinate $\Delta r(C_{Ar}\text{-}C_{Ar})$ was determined by Pauling's rule (equation 4-1) using a standard bond length of 1.537Å and a bond order of 1.67. Similarly, the bond length Δr(C-O) in table 4-9 was determined from Pauling's Rule with a standard bond length of 1.43Å and a bond order of 2.0. Force constants for $\Delta r(C_{Ar}\text{-}C_{Ar})$ and Δr(C-O) were evaluated using equation 4-2 with standard force constants of 5.8 m.dyne/Å and 5.3 m.dyne/Å respectively. The bond orders for these calucalations were the same as those used in the bond length estimations.

Table 4-8

Internal Coordinates for 2-Ethylbutyrophenone Models

$R_1 = \Delta r_{1,2}$
$R_2 = \Delta r_{2,3}$
$R_3 = \Delta r_{2,4}$
$R_4 = \Delta r_{4,5}$
$R_5 = \Delta r_{4,6}$
$R_6 = \Delta r_{6,7}$
$R_7 = \Delta r_{6,8}$
$R_8 = \Delta r_{8,9}$
$R_9 = \Delta r_{8,16}$
$R_{10} = \Delta r_{8,11}$
$R_{11} = \Delta r_{11,12}$
$R_{12} = \Delta r_{11,13}$
$R_{13} = \Delta r_{11,14}$
$R_{14} = \Delta r_{6,15}$
$R_{15} = \Delta r_{15,16}$
$R_{16} = \Delta r_{15,17}$
$R_{17} = \Delta r_{15,18}$
$R_{18} = \Delta r_{18,19}$
$R_{19} = \Delta r_{18,20}$
$R_{20} = \Delta r_{18,21}$
$R_{21} = \Delta\alpha_{1,2,3}$
$R_{22} = \Delta\alpha_{1,2,4}$
$R_{23} = \Delta\alpha_{3,2,4}$
$R_{24} = \Delta\alpha_{2,4,5}$
$R_{25} = \Delta\alpha_{2,4,6}$
$R_{26} = \Delta\alpha_{5,4,6}$
$R_{27} = \Delta\alpha_{4,6,7}$
$R_{28} = \Delta\alpha_{4,6,8}$
$R_{29} = \Delta\alpha_{4,6,15}$
$R_{30} = \Delta\alpha_{7,6,15}$
$R_{31} = \Delta\alpha_{7,6,8}$
$R_{32} = \Delta\alpha_{8,6,15}$
$R_{33} = \Delta\alpha_{6,8,9}$
$R_{34} = \Delta\alpha_{6,8,10}$
$R_{35} = \Delta\alpha_{6,8,11}$
$R_{36} = \Delta\alpha_{9,8,10}$
$R_{37} = \Delta\alpha_{9,8,11}$
$R_{38} = \Delta\alpha_{10,8,11}$
$R_{39} = \Delta\alpha_{8,11,12}$
$R_{40} = \Delta\alpha_{8,11,13}$
$R_{41} = \Delta\alpha_{8,11,14}$
$R_{42} = \Delta\alpha_{12,11,13}$
$R_{43} = \Delta\alpha_{12,11,14}$
$R_{44} = \Delta\alpha_{13,11,14}$
$R_{45} = \Delta\alpha_{6,15,16}$
$R_{46} = \Delta\alpha_{6,15,17}$
$R_{47} = \Delta\alpha_{6,15,18}$
$R_{48} = \Delta\alpha_{16,15,17}$
$R_{49} = \Delta\alpha_{16,15,18}$
$R_{50} = \Delta\alpha_{17,15,18}$
$R_{51} = \Delta\alpha_{15,18,19}$
$R_{52} = \Delta\alpha_{15,18,20}$
$R_{53} = \Delta\alpha_{15,18,21}$
$R_{54} = \Delta\alpha_{19,18,20}$
$R_{55} = \Delta\alpha_{19,18,21}$
$R_{56} = \Delta\alpha_{20,18,21}$
$R_{57} = \Delta\delta_{1,3,4,2}$
$R_{58} = \Delta\delta_{2,5,6,4}$
$R_{59} = \Delta\tau_{2,4}$
$R_{60} = \Delta\tau_{4,6}$
$R_{61} = \Delta\tau_{6,8}$
$R_{62} = \Delta\tau_{8,11}$
$R_{63} = \Delta\tau_{6,15}$
$R_{64} = \Delta\tau_{15,18}$
$R_{65} = \Delta r_{5,19}{}^{a}$
$R_{66} = \Delta\alpha_{4,5,19}{}^{a}$
$R_{67} = \Delta\alpha_{5,19,18}{}^{a}$
$R_{68} = \Delta\tau_{4,5}{}^{a}$
$R_{69} = \Delta\tau_{5,19}{}^{a}$
$R_{70} = \Delta\tau_{19,18}{}^{a}$

NOTES

(a) internal coordinates for the transition state only.

Table 4-9

Structural Parameters and Force Constants for 4-($^2H_1$)-2-Ethylbutyrophenone. Loss of Ethylene by a Stepwise Process. 1,5-Hydrogen Migration as the Rate Determining Step.

Coordinate		Reactant Model		Transition State Models	
		r_i^o [a]	F_{ij}^o [b]	r_{ij}	F_{ij}
Δr	$(C_{Ar}\text{-}C_{Ar})$ [c]	1.383 [d]	9.686 [e]	1.383	9.686
Δr	$(C_{Ar}\text{-}C)$	1.537	5.0	1.537	5.0
Δr	(C-O)	1.222 [d]	10.6 [e]	1.222	10.6
Δr	$(C_{sp2}\text{-}C)$	1.537	5.0	1.537	5.0
Δr	(C-C)	1.537	4.5	1.537	4.5
Δr	(C-H)	1.094	5.0	1.094-0.31n.n(C-H)	5.0.n(C-H)
Δr	(O-H) [f]	—	—	0.957-0.31n.n(O-H)	7.5.n(O-H)
		Angle	F^o_{bend} [g]	Angle	F_{bend}
$\Delta\alpha$	$(C_{Ar}\text{-}C_{Ar}\text{-}C_{Ar})$ [h]	120.0	1.345	120.0	1.345
$\Delta\alpha$	$(C_{Ar}\text{-}C_{Ar}\text{-}C)$	120.0	1.041	120.0	1.041
$\Delta\alpha$	$(C_i\text{-}C_j\text{-}C_k)$	120.0	0.81	120.0	0.81
$\Delta\alpha$	$(C_i\text{-}C_j\text{-}C_k)$	109.5	1.0	109.5	1.0
$\Delta\alpha$	$(C_i\text{-}C_j\text{-}H_k)$	109.5	0.65	i	$0.65(n_{ij}.n_{jk})^{\frac{1}{2}}g\alpha$
$\Delta\alpha$	$(H_i\text{-}C_j\text{-}H_k)$	109.5	0.55	i	$0.55(n_{ij}.n_{jk})^{\frac{1}{2}}g\alpha$
$\Delta\alpha$	$(C_4\text{-}O_5\text{-}H_{19})$ [f]	—	—	$103.2+3.4.n_{5,19}$	$0.75(n_{4,5}.n_{5,19})^{\frac{1}{2}}g\alpha$
$\Delta\alpha$	$(O_5\text{-}H_{19}\text{-}C_{18})$ [f]	—	—	$135.4+11.1.n_{5,19}$	$0.75(n_{5,19}.n_{19,18})^{\frac{1}{2}}g\alpha$
$\Delta\delta$ [j]		—	0.2	—	0.2
$\Delta\tau$	(C-C) [k]	—	0.072	—	0.072
$\Delta\tau$	(C-O) [f]			—	0.473
$\Delta\tau$	(O-H) [f]			—	0.072
$\Delta\tau$	(C-H) [f]			—	0.072

NOTES:

(a) standard bond lengths in Å
(b) standard force constants in m.dyne/Å
(c) bond stretching internal coordinates
(d) calculated using Pauling's rule (see text)
(e) calculated using equation 4-2 (see text)
(f) applicable to transition state models only
(g) standard force constants in m.dyne Å/rad^2
(h) angle bending internal coordinates
(i) angles are input in accordance with geometry changes due to sp^3-sp^2 hybridization changes.
(j) out-of-plane wag internal coordinates
(k) torsional internal coordinates

The deuterium and carbon-13 isotope effects that were calculated using the models described above are given in table 4-10. Calculations were performed at temperatures of 383.0, 333.0 and 283.0°K to ascertain the temperature variation of the isotope effects. Again, the carbon-13 results are quoted for a temperature of 283.0°K since they were found to be relatively temperature independent.

The value of the interaction coefficient, A_{ik}, used was 1.0 (D=0). This value was used to couple the internal coordinates R_{18} and R_{65} leading to an asymmetric motion of H_{19} from C_{18} to O_5. All of the values for the ratio $\nu_{1L}^{\ddagger}/\nu_{2L}^{\ddagger}$ for each of the isotopic models shown in table 4-10, were calculated to be 1.00. This represents a flat-topped potential energy barrier to reaction.

(b) Secondary Isotope Effects on the Stepwise Process.

In accordance with the measurement of a secondary isotope effect for the McLafferty rearrangement from 3-($^2H_2$)-2-ethylbutyrophenone (47) (Chapter 3), calculations were carried out using BEBOVIB-IV in an attempt to reproduce this effect. Again, the initial calculations were performed using models which were devised for the stepwise mechanism involving 1,5-hydrogen migration as the rate determining step.

The models that were used in this investigation were identical to those used in section (a) for the compound labelled at carbon-4 (C_{18}). Figures 4-6, 4-7 and 4-8 describe in detail the geometry and conformation of the reactant and transition state models for this investigation. In this case the isotope effects were calculated using models in which the hydrogens at C_{15} were replaced with deuterium.

Table 4-11 lists the results for these calculations. The interaction coefficient used in these calculations had the effect

Table 4-10

Kinetic Isotope Effects for the Stepwise Process from 4-($^2H_1$)-2-Ethylbutyrophenone H-Transfer, Rate Determining Step[a].

$n_{5,19}$[c]	$n_{19,18}$	H_{19}-D[b] T=383.0, 333.0, 283.0[d]	C_{18}-^{13}C[e]	C_{15}-^{13}C	C_6-^{13}C	C_4-^{13}C
0.1	0.9	1.221 1.240 1.262	0.997	1.000	1.000	0.998
0.3	0.7	1.719 1.871 2.027	1.001	1.000	1.000	0.997
0.5	0.5	1.865 2.063 2.313	1.010	1.000	1.000	0.997
0.7	0.3	1.553 1.652 1.836	1.022	1.001	1.000	0.996
0.9	0.1	0.969 0.956 1.033	1.035	1.001	1.000	0.996

NOTES

(a) the calculations assume an interaction coefficient A_{ik} = 1.0 for internal coordinates R_{18} and R_{65}.
(b) H_{19} is replaced with D.
(c) bond order between atoms 5 and 19.
(d) temperatures in ^oK.
(e) carbon-13 isotope effects were calculated at the same temperatures as the deuterium isotope effects. Only the effects at T=283.2^oK are listed.

Table 4-11

Kinetic Isotope Effects for the Stepwise Process from 3-($^2H_2$)-2-Ethylbutyrophenone H-Transfer, Rate Determining Step[a].

$n_{5,19}$[b]	$n_{19,18}$	H_{16},H_{17}-D_2 T=333.2, 283.2[c]	C_{18}-^{13}C[d]	C_{15}-^{13}C	C_6-^{13}C	C_4-^{13}C
0.1	0.9	1.000 1.000	0.997	1.000	1.000	0.998
0.3	0.7	1.000 1.000	1.000	1.000	1.000	0.997
0.5	0.5	1.000 1.000	1.009	1.000	1.000	0.997
0.7	0.3	1.000 1.000	1.022	1.001	1.000	0.996
0.9	0.1	1.000 1.001	1.035	1.001	1.000	0.996

NOTES

(a) the calculations assume an interaction coefficient A_{ik} = 1.000 for internal coordinates R_{18} and R_{65}.
(b) bond order between atoms 5 and 19
(c) temperature in ^oK
(d) carbon-13 isotope effects were calculated at T=333.2 and 283.2^oK. Only the T=283.2^oK results are listed.

of coupling coordinates R_{18} and R_{65} and was given the value of 1.00 as described previously. Carbon-13 isotope effect values quoted in table 4-11 are those obtained at a temperature of 283.2°K; those calculated at 333.2°K were omitted due to reasons previously explained.

It is clear from table 4-11, and not entirely unexpected, that the rate of 1,5-hydrogen migration in this system is largely unaffected by isotopic substitution at C_{15}. Clearly, the bonding changes that occur for this process do not affect the hybridization at C_{15}. The effects of hyperconjugation or induction have not been included in the transition state models for this calculation, but it is expected that differences in rates on deuterium substitution should be very small[16].

So far, the calculations have employed models of the reactant and the transition state which have been derived from a consideration of the stepwise mechanism with 1,5-hydrogen transfer as the rate determining step. An alternative stepwise mechanism involves carbon-carbon bond cleavage as the slowest step in process. This is shown in scheme 4-3 in which the protonated carbonyl is derived from 1,5-hydrogen migration of 2-ethylbutyrophenone.

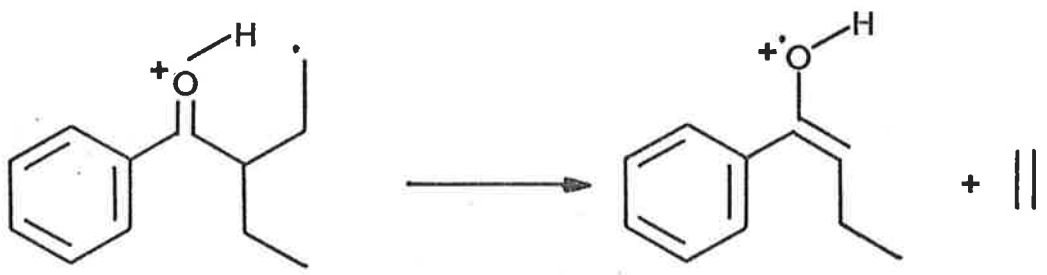

Scheme 4-3

Clearly, this system of intermediate and transition state requires the construction of model systems which are different to those described previously for 2-ethylbutyrophenone.

Figures 4-9 and 4-10 are geometric representations of the protonated carbonyl intermediate and the transition state 21-atom cut-off models for the C_6-C_{15} bond cleavage mechanism. In the model of the intermediate, tetrahedral geometry was assumed for the atoms around C_6, C_8, C_{11} and C_{15}. Trigonal planar geometry was assumed for atoms C_2, C_4 and C_{18}. The plane containing atoms H_{21}-C_{18}-H_{20} is perpendicular to the plane containing C_6-C_{15}-C_{18}. This geometry element was included to ensure that there is maximum p-orbital overlap between the orbital containing the free radical at C_{18} and the C_6-C_{15} bond which is breaking. The conformation of the bonds around the C_6-C_8, C_8-C_{11} and C_6-C_{15} bonds is identical to that of the reactant model described previously in section (a) (figures 4-6 and 4-8). The conformation of bonds about C_{15}-C_{18} is shown in figure 4-11 by means of a Newman projection.

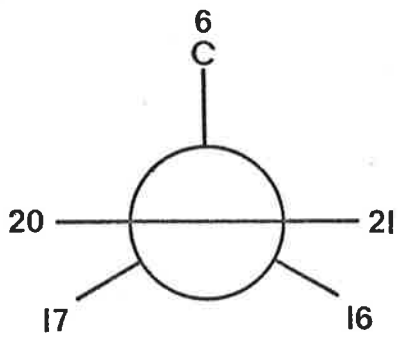

C_{18} - C_{15}

Figure 4-11

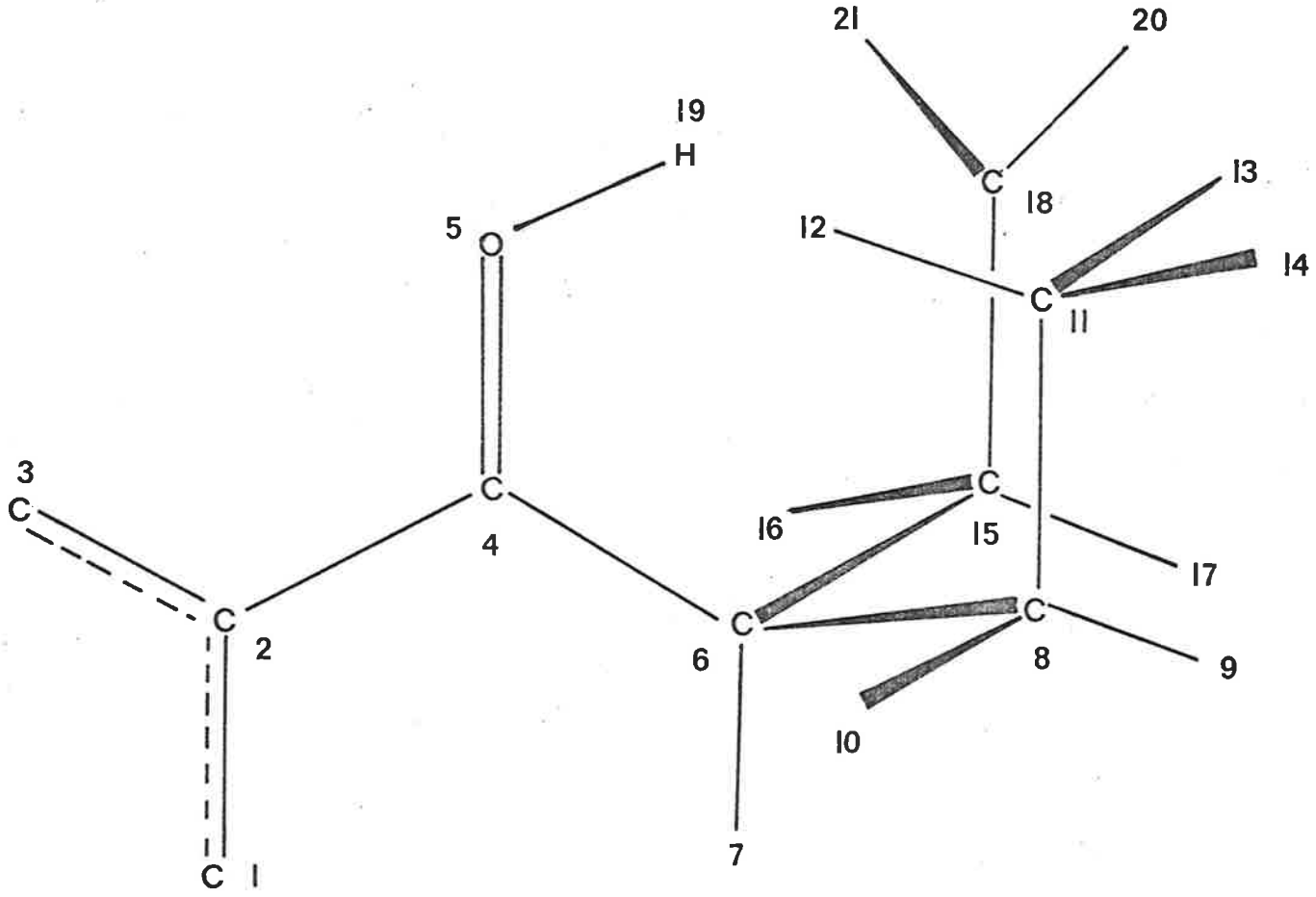

Figure 4-9

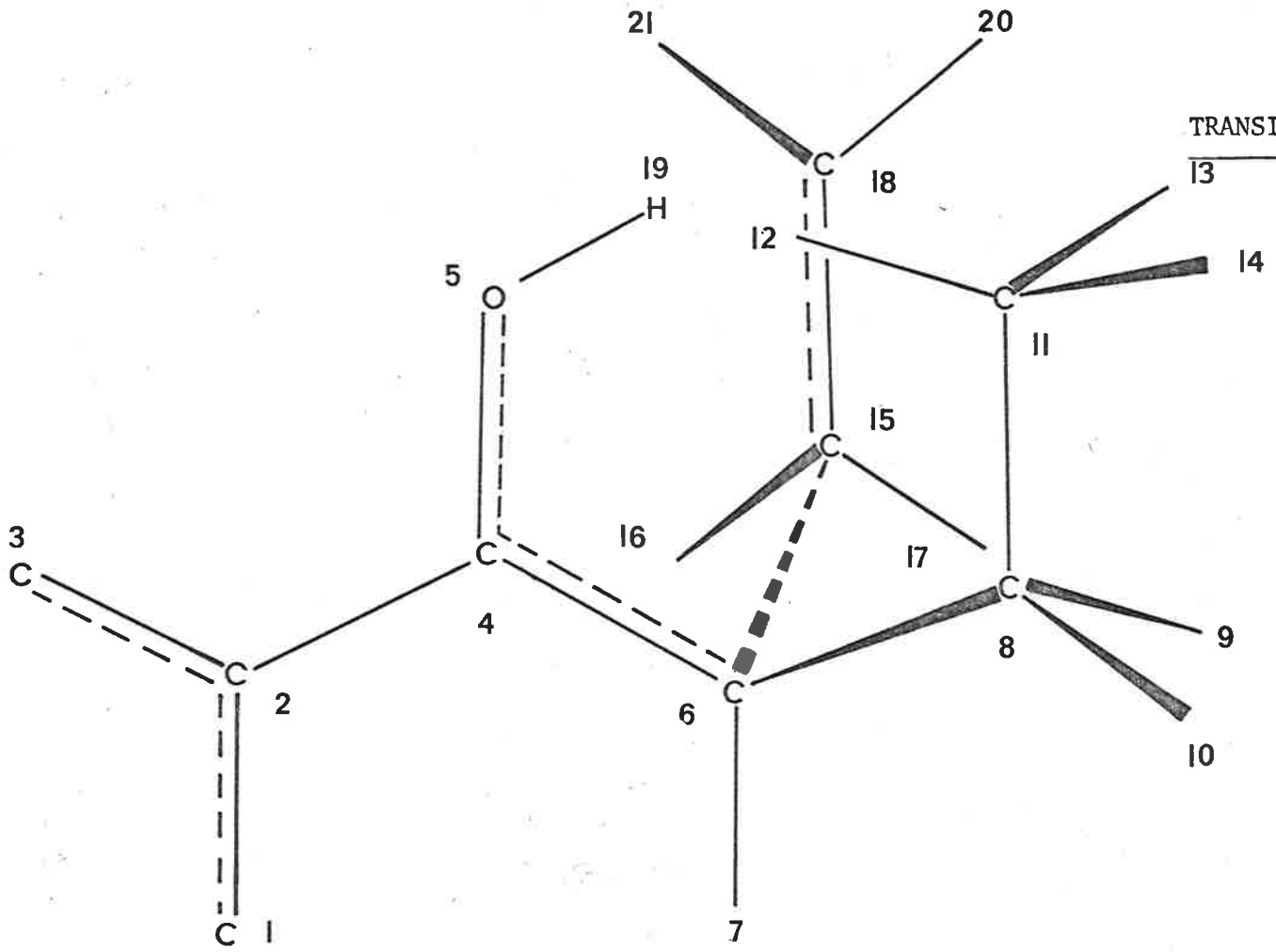

C_6-C_{15} CLEAVAGE

TRANSITION STATE MODEL

Figure 4-10

The angle subtended by bonds C_4-O_5 and O_5-H_{19} was set at 114.5° on the basis of the results from *ab initio* molecular orbital calculations of $CH_3CH_2COH^{+\cdot}$ by Radom and co-workers[330].

A series of transition state models were devised in which the bond order of the C_6-C_{15} bond was decreased in the usual manner; namely, 0.9, 0.7, 0.5, 0.3 and 0.1. Concurrently with decreasing C_6-C_{15} bond order, the bond order of the C_{15}-C_{18} was increased in the following manner; 1.1, 1.3, 1.5, 1.7, 1.9, to simulate the overlap of the p-orbital centre on C_{18} with that forming at C_{15}. The hybridization changes at C_6 and C_{15} (sp^3 to sp^2) were accounted for by linearly changing the geometry about these centres from tetrahedral to trigonal planar. As a consequence, the angles subtended by the bonds C_4-C_6 and C_6-H_7, C_6-H_7 and C_6-C_8, C_{18}-C_{15} and C_{15}-H_{16}, and C_{18}-C_{15} and C_{15}-H_{17} were altered from 109.5° to 120.0° (product value). With regard to this change in hybridization, the bonds subtended by C_4-C_6 and C_6-C_{15}, and H_{16}-C_{15} and C_{15}-C_6 were reduced in a linear fashion from 109.5° to 90.0° (product value).

A kinematically complete set of 64 internal coordinates for the 21-atom cut-off models of the intermediate and the transition state were defined according to the rules of Decius[325]. Most of these coordinates are represented in table 4-8 with the following changes; R_{18} ($=\Delta r_{18,19}$) is replaced with R_{18} ($=\Delta r_{5,19}$), R_{51} ($=\Delta\alpha_{15,18,19}$) is replaced with R_{51} ($=\Delta\alpha_{19,5,4}$), R_{54} ($=\Delta\alpha_{19,18,20}$) is replaced with R_{54} ($=\Delta\gamma_{21,22,15,18}$) and R_{55} ($=\Delta\alpha_{19,18,21}$) is replaced with R_{55} ($=\Delta\tau_{4,5}$).

Table 4-9 summarizes the bond lengths, bond angles and force constants for each type of internal coordinate (bond stretch, angle bend, out of plane wag and torsion). Changes in these parameters

required to define the transition state models in terms of bond orders, are also shown in this table. Two of the entries in table 4-9 need modification to account for the differences in the system described above. The first of these is the transition state bond length and force constant for Δr (C_{15}-C_{18}). The bond length, r_{ij}, was changed according to the relationship in equation 4-9

$$r_{ij} = 1.537 - 0.3 \ln.n_{15,18} \qquad \text{Equation 4-9}$$

The force constant, F_{ij}, was changed according to the relationship in equation 4-10

$$F_{ij} = 4.5.n_{15,18} \qquad \text{Equation 4-10}$$

Secondly, the internal coordinate described by $\Delta\alpha(O_5\text{-}H_{19}\text{-}C_{18})$ does not apply in this case.

The deuterium and carbon-13 isotope effects calculated using these models are listed in table 4-12. Calculations were performed at temperatures of 333.2 and 283.2^{o}K. The carbon-13 results are quoted at a temperature of 283.2^{o}K as before. Evaluation of the interaction coefficient by solving the determinant of the force field matrix when, D, the curvature parameter, is zero (equation 4-6) gave a value of 0.618. The matrix was composed of the SVFF matrix with off-diagonal elements coupling the internal coordinates R_4 and R_5, R_5 and R_{14}, and R_{14} and R_{17}. Clearly, an isotope effect is operative for this mechanism when C_{15} is labelled with deuterium.

Table 4-12

Kinetic Isotope Effects for the Stepwise Process from 3-($^2H_2$)-2-Ethylbutyrophenone

C_6-C_{15} Cleavage, Rate Determining Step[a,b].

$n_{6,15}$[c]	$n_{15,18}$	H_{16},H_{17}-D_2 T=333.2, 283.2[d]		C_{18}-^{13}C[e]	C_{15}-^{13}C	C_6-^{13}C	C_4-^{13}C
0.9	1.1	1.024	1.027	1.002	1.024	1.022	1.027
0.7	1.3	1.134	1.182	1.011	1.016	1.041	1.008
0.5	1.5	1.272	1.368	1.013	1.023	1.037	1.006
0.3	1.7	1.380	1.518	1.018	1.031	1.032	1.006
0.1	1.9	1.516	1.709	1.030	1.043	1.029	1.008

NOTES

(a) the "reactant" species in these calculations is the intermediate resulting from 1,5-hydrogen transfer.
(b) the calculations assume an interaction coefficient A_{ik} = 0.618 for internal coordinates R_4 and R_5, R_5 and R_{14} and R_{14} and R_{17}.
(c) bond order between atoms 6 and 15.
(d) temperatures in ^oK
(e) carbon-13 isotope effects were calculated at T=333.2 and 283.2^oK. Only the T=283.2^oK results are listed.

(c) Concerted Process

The calculations described above have been concerned with models derived from the stepwise mechanisms of the McLafferty rearrangement. The concerted model can be considered as several orders of magnitude more complex than previous models since it requires that both 1,5-hydrogen migration and carbon-carbon bond cleavage occur at the same time. Transition state models for this process must therefore account for the motion of all of the atoms in the cyclic six-membered arrangement. Motions involved include both reduction and increase in bond distances due to increasing and decreasing bond orders respectively. As a result, the individual atoms involved in this transition state must move in a variety of directions in a synchronous fashion. Models which are prepared to describe the concerted process must take into account all of these motions and those due to hybridization changes.

The reactant model for this process is identical to that described in section (a) below (figure 4-6). Figure 4-12 is a geometrical representation of the 21-atom cut-off transition state model for the concerted reaction from 2-ethylbutyrophenone. Bonds which charge their bond orders in the transition state models are; C_4-O_5 ($n_{4,5}$ 2.0-1.0), C_4-C_6 ($n_{4,6}$ 1.0-2.0), C_6-C_{15} ($n_{6,15}$ 1.0-0.0) C_{15}-C_{18} ($n_{15,18}$ 1.0-2.0), C_{18}-H_{19} ($n_{18,19}$ 1.0-0.0) and H_{19}-O_5 ($n_{19,5}$ 0.0-1.0); where the bond orders in parentheses are the reactant and product values respectively. In each model, the bond orders described above are charged in a linear fashion such that $n_{4,5} + n_{4,6} + n_{6,15} + n_{15,18} + n_{18,19} + n_{19,5} = 6.0$.

The geometry about C_6, C_{15} and C_{18} was altered in a linear fashion from tetrahedral to trigonal planar in accord with the

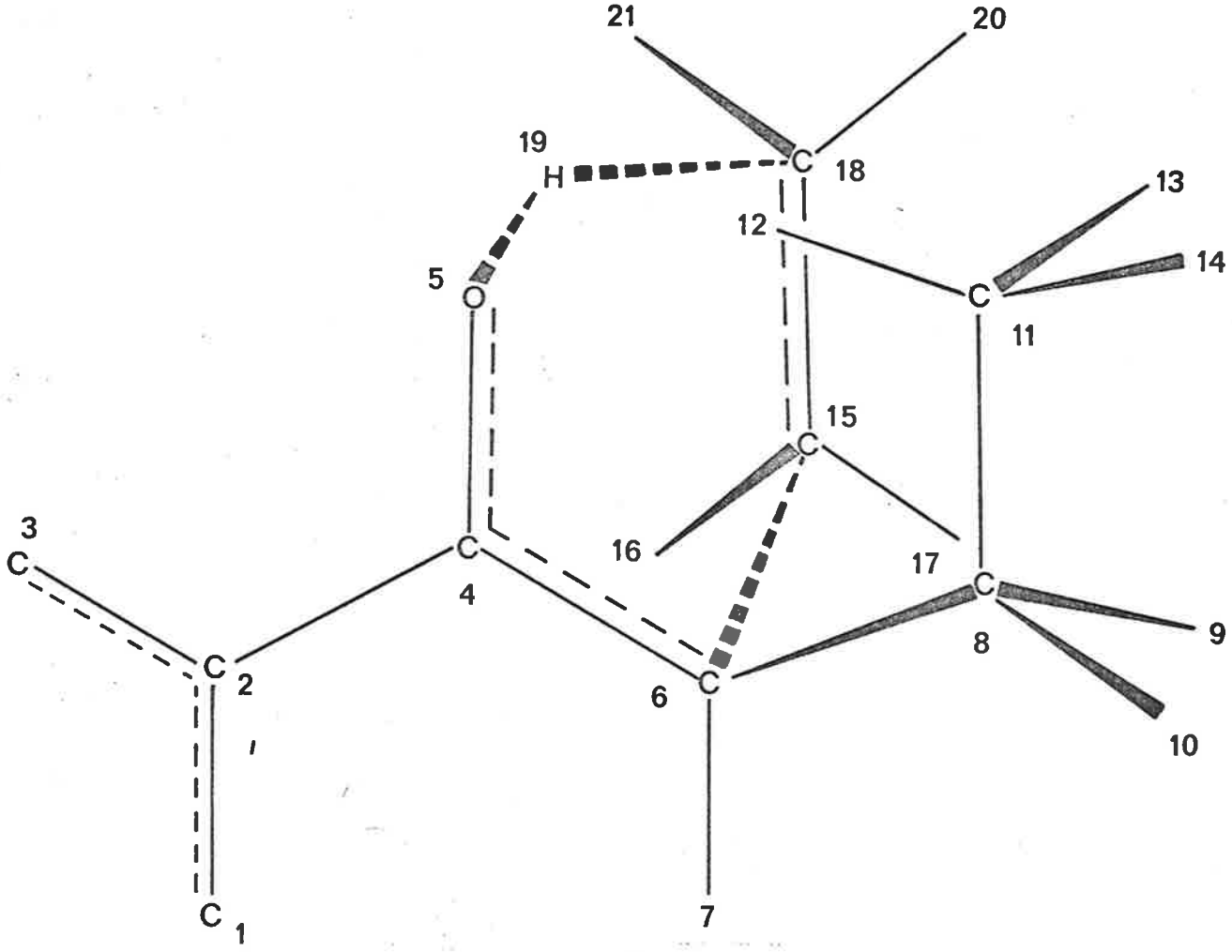

Figure 4-12

CONCERTED TRANSITION STATE MODEL

changes in hybridization occurring at these centres. Consequently, the angles subtended by the bonds C_4-C_6 and C_6-C_{15}, C_4-C_6 and C_6-H_7, C_6-H_7 and C_6-C_8, C_{18}-C_{15} and C_{15}-H_{17}, C_{18}-C_{15} and C_{18}-H_{20}, and C_{15}-C_{18} and C_{18}-H_{21} were altered from 109.5° to 120.0° (product value). Simultaneously with these angle changes, the angles subtended by the bonds C_4-C_6 and C_6-C_{15}, H_{16}-C_{15} and C_6-C_{15}, and H_{19}-C_{18} and C_{18}-C_{15} were reduced in a linear fashion from 109.5° to 90.0° (product value).

A kinematically complete set of 70 internal coordinates for the 21-atom cut-off models of the transition state are shown in table 4-8. As before, table 4-9 summarizes the bond lengths, bond angles and force constants for each type of internal coordinate.

It is clear from the above discussion, that the transition state models for the concerted reaction incorporates most of the features of both 1,5-hydrogen migration and carbon-carbon bond cleavage models described previously.

The results of the calculations utilizing the concerted models are presented in table 4-13. As before, the calculations were performed at reaction temperatures of 333.2 and 283.2°K, and the carbon-13 isotope effects are quoted at a temperature of 283.2°K. Evaluation of the interaction coefficient by means previously described (D=0), yielded 1.0. This represents coupling of the internal coordinates R_4 and R_5, R_5 and R_{14}, R_{14} and R_{17}, R_{17} and R_{18}, R_{18} and R_{65}, and R_{65} and R_4.

The final transition state model ($n_{4,5}$ = 1.1 etc.), has a geometric problem in that the transferring hydrogen is strongly bound to O_5 ($n_{9,5}$ = 0.9) but is being pulled away by the leaving

Table 4-13

Kinetic Isotope Effects for the Concerted Process

from 4-($^2H_1$)-2-Ethylbutyrophenone[a]

$n_{4,5}$[b]	$n_{4,6}$	$n_{6,15}$	$n_{15,18}$	$n_{18,19}$	$n_{19,5}$	H_{19}-D T=333.2, 283.2[c]		C_{18}-^{13}C[d]	C_{15}-^{13}C	C_6-^{13}C	C_4-^{13}C
1.9	1.1	0.9	1.1	0.9	0.1	1.217	1.216	1.011	1.021	1.022	1.041
1.7	1.3	0.7	1.3	0.7	0.3	1.436	1.466	1.002	1.016	1.022	1.036
1.5	1.5	0.5	1.5	0.5	0.5	1.427	1.447	1.014	1.027	1.022	1.040
1.3	1.7	0.3	1.7	0.3	0.7	1.183	1.180	1.019	1.030	1.023	1.047

NOTES

(a) interaction coefficient, $A_{ik} = 1.0$ coupling coordinates described in text.
(b) bond order
(c) temperature in ^oK
(d) values quoted at T=283.2^oK

ethylene unit. As a result, the calculated O_5-H_{19} distance is greater than expected leading to erroneous calculated isotope effects. Little can be done about this effect without adjusting bond orders as a counteraction. Table 4-14 lists the deuterium isotope effects calculated for the loss of ethylene from 3-($^2H_2$)-2-ethylbutyrophenone. These results were obtained using the concerted model described above, and represent secondary isotope effects for the process.

Table 4-14

Secondary Kinetic Isotope Effects for the Concerted Process

from 3-($^2H_2$)-2-Ethylbutyrophenone[a]

$n_{4,5}$[b]	$n_{4,6}$	$n_{6,15}$	$n_{15,18}$	$n_{18,19}$ *	$n_{19,5}$	H_{16},H_{17}-D T-333.2, 283.2[c]
1.9	1.1	0.9	1.1	0.9	0.1	1.014 1.018
1.7	1.3	0.7	1.3	0.7	0.3	1.052 1.064
1.5	1.5	0.5	1.5	0.5	0.5	1.110 1.138
1.3	1.7	0.3	1.7	0.3	0.7	1.203 1.259
1.1	1.9	0.1	1.9	0.1	0.9	1.391 1.520

NOTES

(a) interaction coefficient, A_{ik} = 1.0 coupling coordinates R_4 and R_5, R_5 and R_{14}, R_{14} and R_{17}, R_{17} and R_{18}, R_{18} and R_{65}, and R_{65} and R_4

(b) bond order

(c) temperatures in ^oK

RRKM Calculations

BEBOVIB-IV calculates isotope effects on specified chemical processes by evaluating partition functions for reactant and transition state model species. As was discussed previously, this program utilizes the equations of absolute rate theory in their Bigeleisen and Mayer formulation. Chapter 1 discusses in detail, the basis of these equations and their fundamental assumptions.

Using absolute rate theory to describe chemical processes requires the assumption of a Maxwell-Boltzmann distribution for the species involved. However, mass spectral processes are concerned with, in the main, unimolecular reactions of isolated ionic species (ion-molecule reactions and collision induced fragmentation are not considered in this context). The internal energy of these ions is determined during the initial ionization process and, in the absence of intermolecular energy exchange, is constant (excepting for unimolecular reaction and radiative transitions). Clearly, there is no mechanism for achieving a Maxwell-Boltzmann energy distribution in a system of isolated ions in the gas phase.

From the results presented in earlier sections of this chapter, isotope effects calculated by means of BEBOVIB-IV are highly sensitive to the degree of hydrogen transfer in the transition state. As the degree of hydrogen transfer in the transition state models becomes increasingly asymmetrical (reactant-like or product-like), the calculated isotope effect falls from the maximum value (symmetrical case). This result is in complete accord with the predicted variability of kinetic isotope effects with transition state geometry based on Westheimer's theory (Chapter 1).

The effects of substituents on the experimentally observed deuterium isotope effect for the butyrophenone system (Chapter 3) can be rationalized in terms of their influence on the degree of hydrogen transfer in the transition state. To mimic substituent effects of this kind by calculational methods, one must therefore rely on a procedure which is sensitive to geometrical differences between transition state models; BEBOVIB-IV fulfils this requirement. Due to the absence of a Maxwell-Boltzmann distribution, the value of the kinetic isotope effect calculated using this method may well be quite different from that expected using energy distribution independent calculations (such as RRKM calculations), and experimentally determined values. In a qualitative sense, however, BEBOVIB-IV can be expected to provide information which, when compared with the experimental results, will aid in determining which of the proposed mechanisms is operative in the process under study.

Another problem that was encountered while considering methods of calculating isotope effects was the effective reaction temperature The vibrational reaction temperature for the McLafferty rearrangement from butyrophenones is not known. The calculated values presented in preceding sections suggest however, that variations in the reaction temperature do not alter the kinetic isotope effect markedly. This small temperature effect has been observed previously[309]. The observation of small kinetic isotope effects and small temperature variations in these calculated values suggest that corrections due to tunnelling are small and can be ignored.

Calculations based on RRKM theory have been performed in order to ascertain whether the results of the BEBOVIB-IV calculations are

reliable in a quantitative sense. However, it is well known that RRKM calculations are relatively insensitive to changes in the transition state geometry[331]. As an example, RRKM calculations of the rate of isomerization of 1,1-dichlorocyclopropane to 2,3-dichloropropene using various transition state models, gives much the same value[332]. The calculated data were virtually indistinguishable even when the frequency pattern of one transition state model having no particular physical significance, was included.

The RRKM program that was used in these calculations was written by Dr. K.D. King, University of Adelaide . A description of the calculational method is found elsewhere[333] (see also Chapter 2). The molecular system that was studied was the 21-atom cut-off model of 1,5-hydrogen transfer in 2-ethylbutyrophenone described previously. Table 4-14 shows the molecular parameters using in these calculations.

The grouped and averaged frequency pattern and moments of inertia were obtained from the BEBOVIB-IV calculations of the symmetrical hydrogen transfer model ($n_{18,19} = n_{19,5} = 0.5$). The symmetry factor represents pathway degeneracy for the process specified.

Values for the deuterium kinetic isotope effect for various critical energies (ϵ_o) are shown in table 4-15. Figure 4-13 is a plot of the calculated isotope effects versus the critical energy.

Since the complete thermochemistry for the 2-ethylbutyrophenone molecular ion and the butyrophenone enol radical cation are not known, data from the McLafferty rearrangement from 2-pentanone will be considered. The IP_v of 2-pentanone has been determined by photoionization spectroscopy to be 9.37 eV[220]. Appearance potential

Table 4-14

	Reactant Model	Transition States	
		H-Transfer	D-Transfer
Frequencies[a]	3040 (11)	2893 (11)	2942 (11)
	1779 (4)	1781 (4)	1716 (4)
	1519 (6)	1517 (6)	1507 (6)
	1423 (5)	1359 (5)	1340 (5)
	1197 (4)	1155 (4)	1156 (4)
	1041 (3)	986 (3)	1009 (3)
	936 (3)	879 (3)	893 (3)
	811 (4)	765 (4)	724 (4)
	559 (3)	575 (3)	597 (3)
	444 (1)	533 (1)	525 (1)
	390 (2)	439 (2)	439 (2)
	302 (2)	363 (2)	357 (2)
	219 (2)	269 (2)	262 (2)
	186 (1)	204 (1)	202 (1)
	160 (1)	194 (1)	186 (1)
	133 (1)	170 (1)	162 (1)
	73 (1)	121 (1)	123 (1)
	61 (2)	76 (2)	76 (2)
	41 (1)	59 (1)	59 (1)
$I_A I_B I_C$[b]	2.94	2.93	2.98
σ[c]	1.00	0.50	1.00
collision diameter[d]	7.0	—	—

NOTES

(a) frequencies in cm^{-1}, degeneracies in parentheses
(b) overall moment of inertia in $(g.cm^2)^3 \times 10^{128}$
(c) symmetry number
(d) collision diameter in Å.

Table 4-15

Critical Energy (eV)	k_H/k_D
3.24	1.257
2.99	1.292
2.74	1.334
2.49	1.382
2.24	1.441
2.00	1.515
1.75	1.609
1.50	1.735
1.25	1.913
1.00	2.186
0.76	2.480
0.51	3.566
0.26	6.286

measurements by photoionization spectroscopy yield a value of 10.07 eV for the formation of the McLafferty product ion (enol form of acetone) from 2-pentanone[220]. Simplistically then, the critical energy for the reaction is of the order of 1.0 eV.

Using this result, one can estimate that the critical energy for loss of ethylene from the 2-ethylbutyrophenone molecular ion is between 1.0 - 2.0 eV. From table 4-15, the range of calculated isotope effect values corresponding to this range in critical energies is k_H/k_D 1.515 - 2.186. Comparison of these values with the deuterium isotope effects calculated using BEBOVIB-IV (table 4-10) indicates that the results from BEBOVIB-IV calculations are at least semi-quantitative.

Figure 4-14

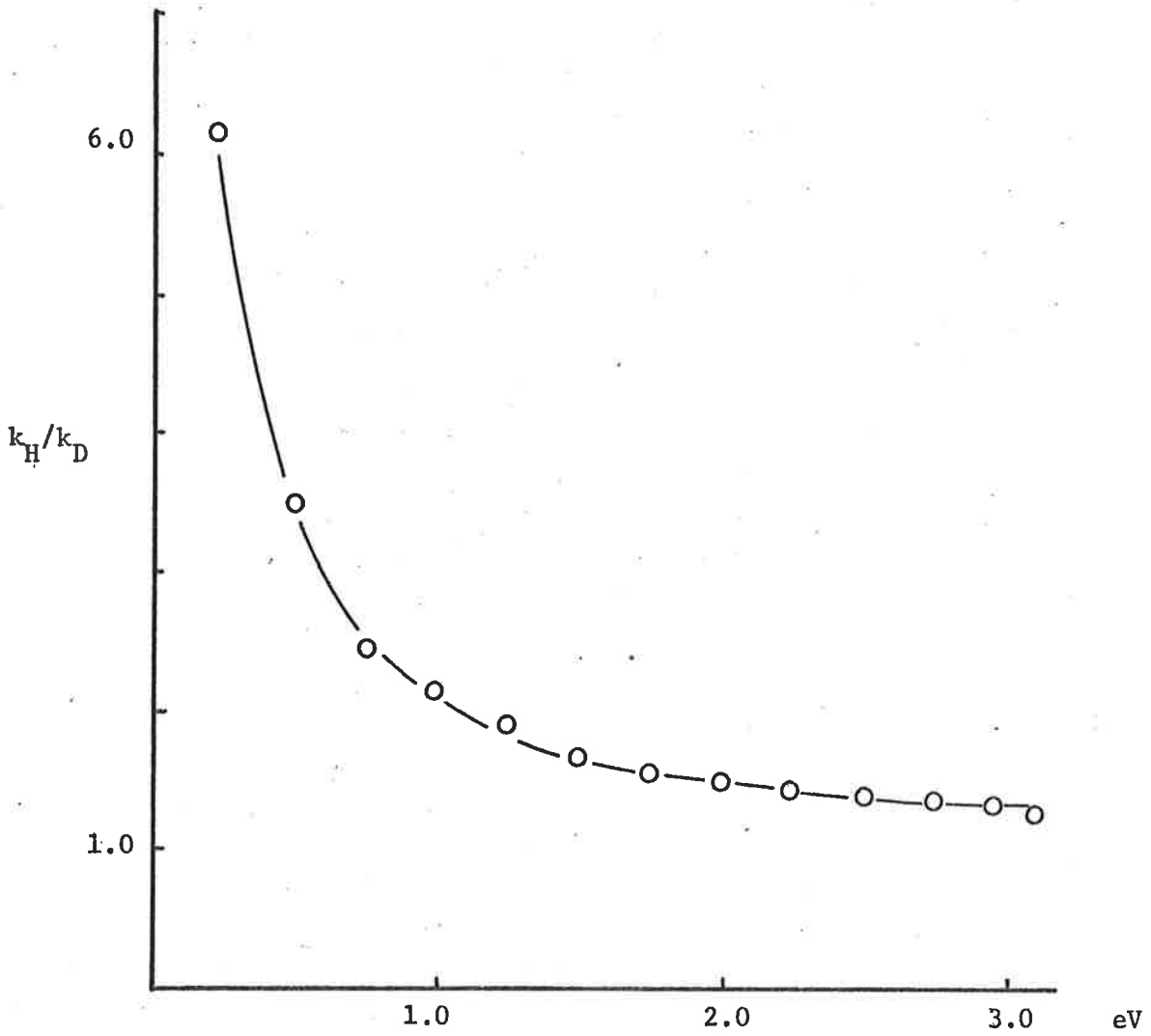

CHAPTER 5

DISCUSSION OF RESULTS AND CONCLUSIONS

INTRODUCTION

As emphasized previously, Chapters 3 and 4 contain the results of the experimental work and the calculations respectively. In this chapter, the experimental and calculational results will be discussed, in terms of the various mechanisms proposed for the McLafferty rearrangement. Where necessary, the results presented in the previous chapters will be summarized (usually in graphical form) as an aid to the discussion.

Scheme 5-1 reiterates the stepwise and concerted mechanisms proposed for the McLafferty rearrangement from the molecular ion of butyrophenones. Briefly, the basic difference between the mechanisms is the presence of an intermediate in the stepwise process. The concerted mechanism involves breaking and forming bonds and the motion of atoms or groups in a synchronous manner. Similar motions occur in the stepwise mechanism but at different times in the overall reaction process; the intermediate can be said to separate the mechanisms in time and space.

The rate determining step of the stepwise mechanism may be either 1,5-hydrogen migration (step (i)) or 3,4-bond cleavage (step (ii)). If step (i) is rapid when compared to step (ii) and the intermediate is of sufficiently long lifetime, an equilibrium situation may develop between the reactant and the intermediate.

Much of the work described in this thesis is concerned with attempting to define structural and electronic parameters of the transition state for the McLafferty rearrangement. The experimental work described previously can be viewed as an attempt to probe the electronic nature of the reaction: Westheimer's theory, although

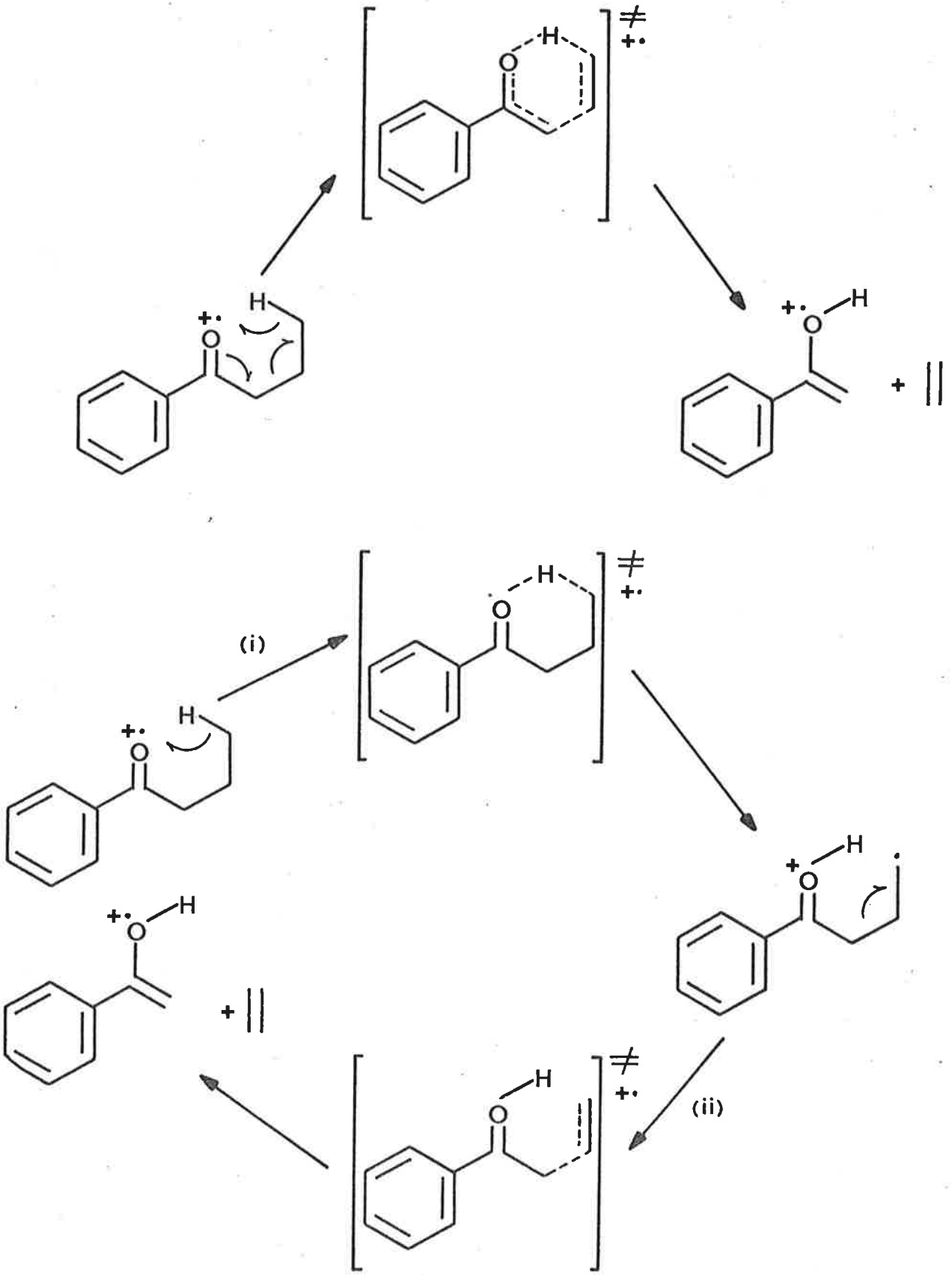

Scheme 5-1

often discussed in terms of transition state symmetry, is based on the electronic properties of this species. Naturally, any attempt to separate electronic and structural factors when considering motion of species on potential energy surfaces is futile; structural changes for molecules, necessitates changes in potential energy. In this light, the preparation of calculational models detailed in Chapter 4, can be seen not only as a means of probing structural aspects of the reaction, but also as investigations of its electronic nature.

KINETIC ENERGY RELEASES

The initial investigations involved determining the effect of substituent changes on the kinetic energy release for the loss of ethylene from para substituted butyrophenones (table 3-1). Figure 5-1 is a plot of the T_{50} values versus Brown's σ_p^+ values. It is clear from Figure 5-1 that the kinetic energy release for the loss of ethylene from substituted butyrophenones is small (<27 meV)[334]. The composite nature of the kinetic energy release (due to $\epsilon_{excess} = \epsilon^{\ddagger} + \epsilon_o^r$, see Figure 2-6) has been discussed previously (Chapter 2). Since these measurements were made on first FFR metastable ion transitions, it is expected that the contribution of $\epsilon^{\ddagger}$ to the kinetic energy release will be small. One can therefore conclude that ϵ_o^r will be the major contributor to T although this is tentative on the grounds that T itself is small.

Since the thermochemistry for this system is not known, ϵ_{excess} cannot be estimated. Without this parameter, it is difficult to define the proportion of ϵ_o^r partitioned into external degress of freedom; i.e., overall rotational and translational degrees of freedom of products. As a result, since T is small, the value of

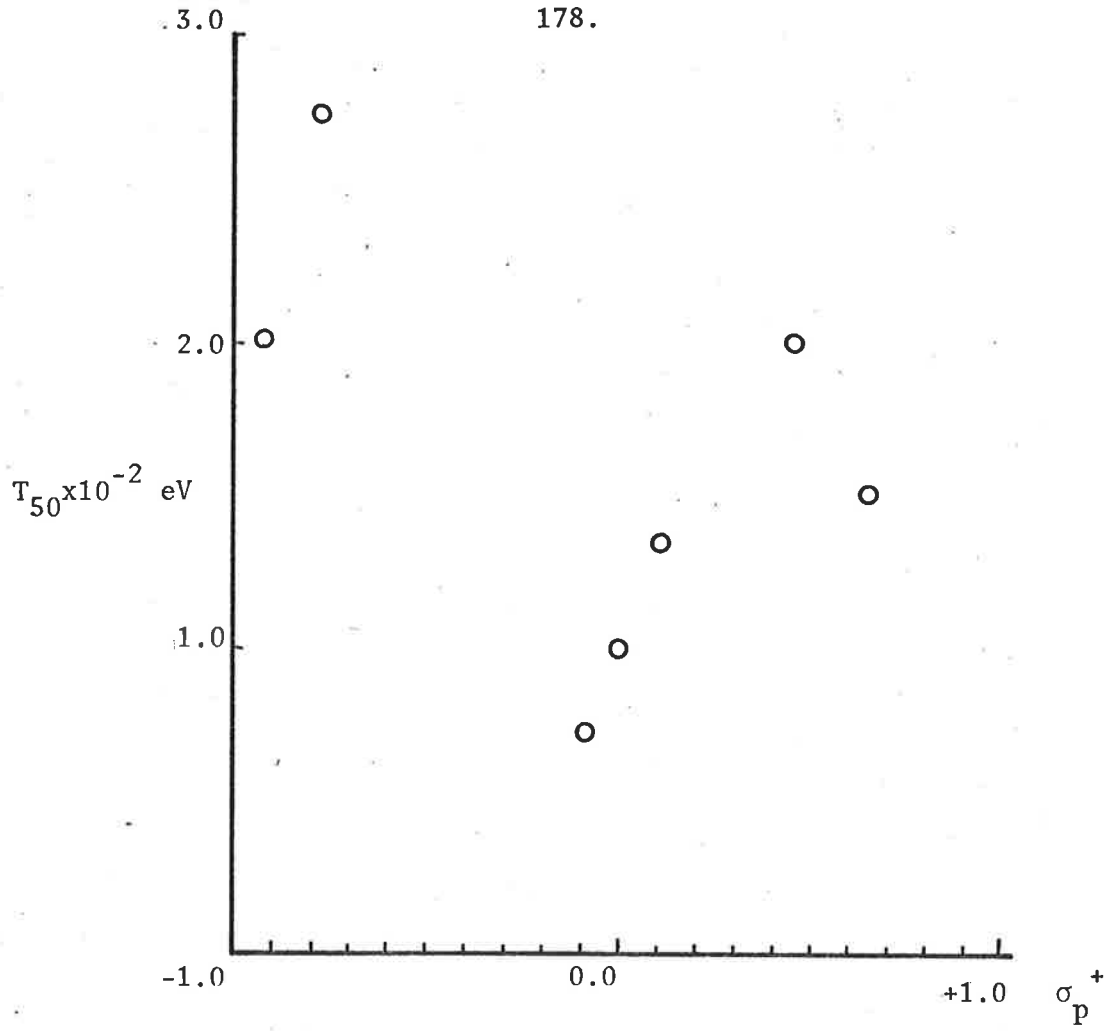

Figure 5-1

ε_o^r is either small or if not, then much of the reverse activation energy is channelled into the vibrational modes rather than translational (and rotational) modes of the products. Effectively, if T is large then clearly ε_o^r must also be large; however, the converse need not apply.

Since ε_{excess} cannot be estimated without knowledge of the thermochemistry for the reaction, the effect of the substituents on the kinetic energy release for the process is difficult to evaluate. It is apparent from Figure 5-1 that the correlation of T values with the σ_p^+ value for the substituent is poor. This may be due at least in part, to the composite nature of T_{50} as discussed previously (deriving from both $\varepsilon^{\ddagger}$ and ε_o^r). It is highly likely that an

improvement in the correlation will result if T/ϵ_{excess} is evaluated and compared with σ_p^+.

INTERMEDIATE LIFETIME STUDIES

As discussed previously, the major difference between the stepwise and concerted mechanisms for the McLafferty rearrangement is the presence of an intermediate in the former case. Differentiation between various mechanistic alternatives has often been based on the detection of intermediates in the proposed reaction pathways. However, all attempts at "trapping" the intermediate in the stepwise mechanism for this rearrangement failed.

The ICR experiments detailed in Chapter 3 indicated that if this intermediate is formed, then it must have a lifetime $<3x10^{-3}$ sec, since it was not detected by deuteron transfer reactions. The only species that was observed by transfer of a deuterium to 3,5-dimethylpyridine was the ion at m/z 121; the enol ion of acetophenone, produced by the McLafferty rearrangement from 4-($^2H_3$)-butyrophenone (23). Observation of this reaction implies that if the McLafferty rearrangement produces an intermediate of sufficient lifetime, detection is possible utilizing the ICR technique.

Another form of trapping experiment based on the work by Wagner and co-workers on the Norrish type II photo-elimination, was also attempted[299]. The presence of a carbon radical centre in the stepwise intermediate enables the possibility of reaction from this site which leads to products differing from those from the McLafferty rearrangement. 2-Allylbutyrophenone (48) was prepared in an attempt to trap the intermediate carbon radical by opening an alternative reaction pathway (thereby preventing the completion of the McLafferty

rearrangement). The predicted alternative pathway for compound (48) is shown in scheme 5-2[299].

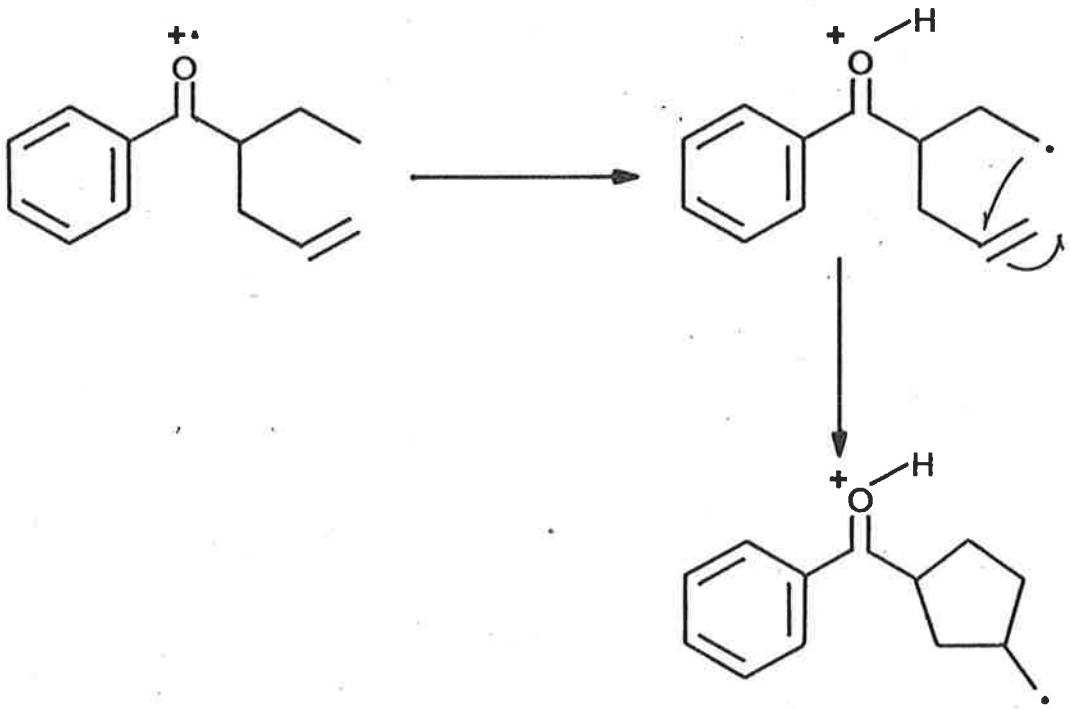

Scheme 5-2

The rate of cyclization of 5-hexen-1-yl radical and related systems is known to be $k = 10^5 sec^{-1}$ [336]. Observation of the loss of ethylene in the mass spectrum of this compound (Appendix 1) implies that if the stepwise intermediate is formed its lifetime is shorter than $\sim 10^{-5}$ sec.

Since the rate of cyclopropylcarbinyl radical ring opening is $k = 1.3 \times 10^8 sec^{-1}$ [337], trapping of the stepwise intermediate was attempted with 2-cyclopropylbutyrophenone (49). However, all synthetic attempts to this compound were unsuccessful.

Clearly, the inability to detect the stepwise intermediate by

the means described above does not deny its existence. Even though the existence of this species may be fleeting, its presence naturally precludes the possibility of the concerted mechanism.

ISOTOPE EFFECTS IN THE BUTYROPHENONE SYSTEM

The effect of substituents on the deuterium isotope effect for 1,5-hydrogen migration is apparent from Figure 5-2. Isotope effects for the ion source reactions versus the σ_p^+ value for the substituent are shown in Figure 5-2(a). Figure 5-2(b) depicts the isotope effect versus σ_p^+ value for the first FFR reaction. The values for the deuterium isotope effects for reaction in both regions of the mass spectrometer are contained in table 3-2.

It is evident that a deuterium isotope effect occurs for the McLafferty rearrangement from substituted butyrophenones. The observation of this effect for this process in other systems has been mentioned previously (Chapter 3).

In general, the deuterium isotope effect for the first FFR is larger than for the ion source reaction. This is in accord with our understanding of the energetic requirements of ions in various sections of the mass spectrometer. Metastable ions are species of lower energy than their unstable counterparts which decompose in the ion source. The magnitude of the isotope effect, being a function of ion internal energy[335], reflects this difference between the reaction occurring in the ion source and field free regions.

The scatter of data in Figure 5-2(a) may be related to the effect of ion internal energy on the isotope effect as discussed above. Due to instrumental factors, only those metastable ions which

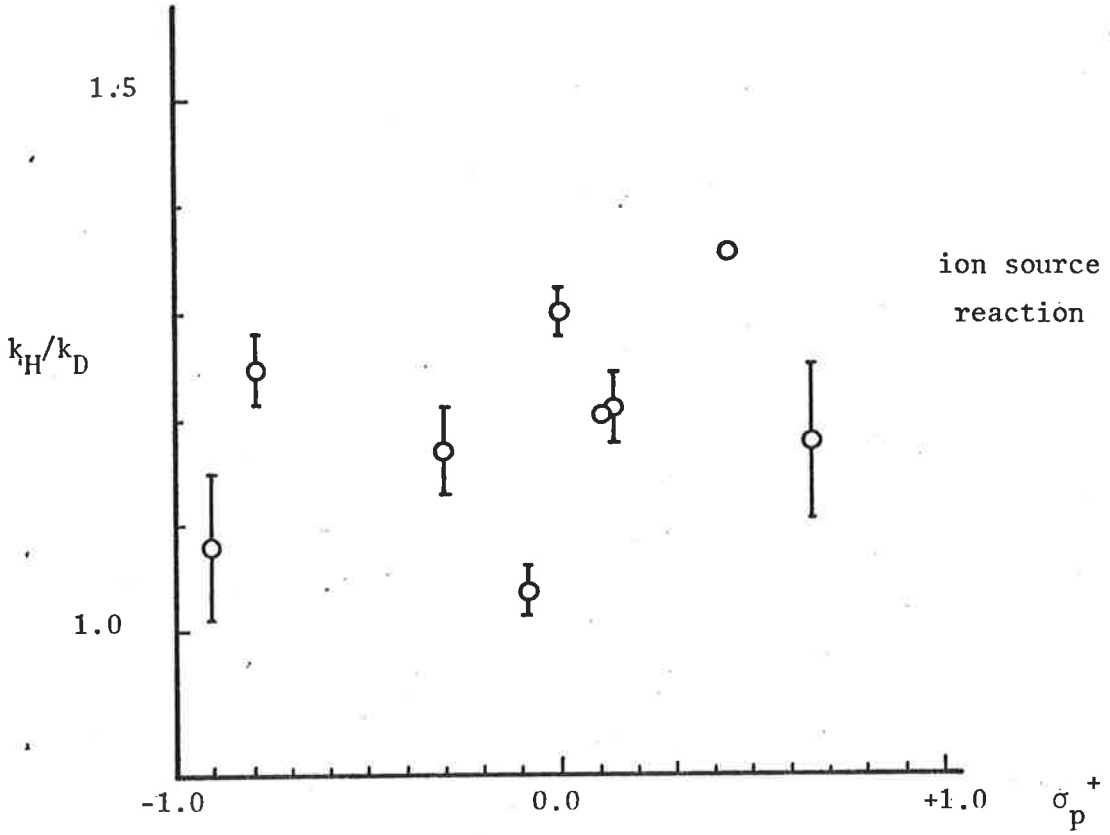

Figure 5-2(a)

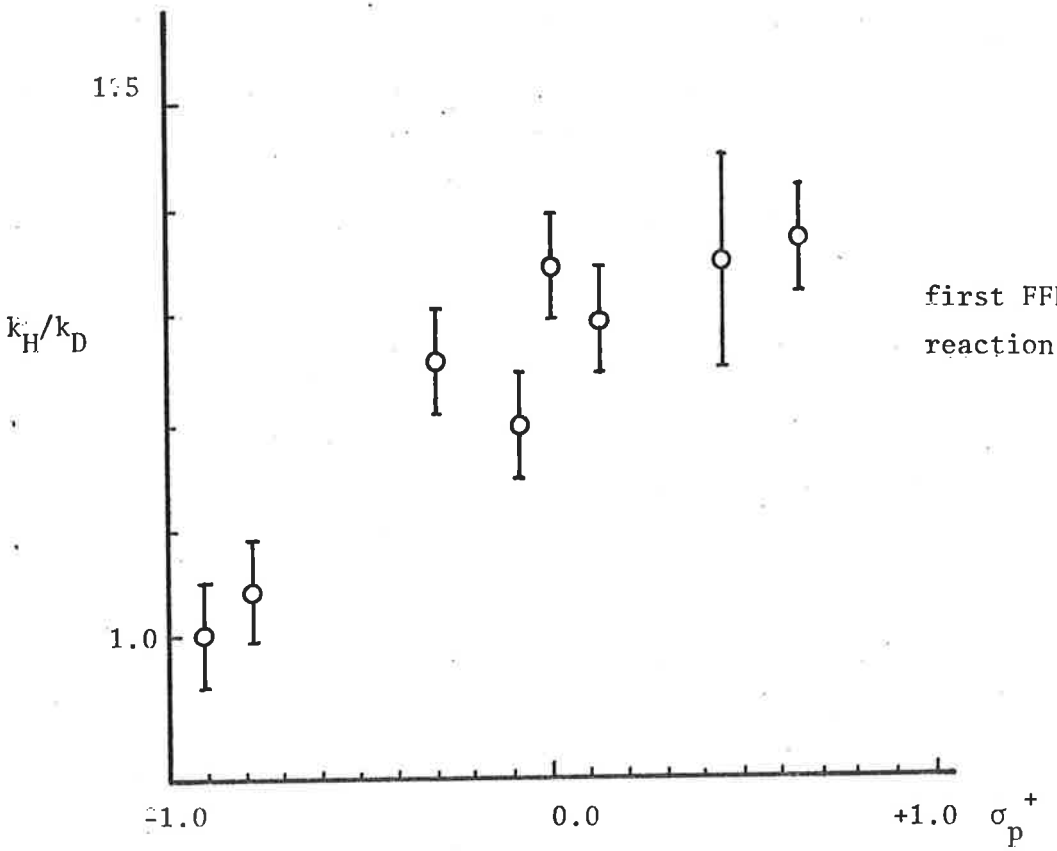

Figure 5-2(b)

decompose within a narrow region of the mass spectrometer are observed. As a result, the spectrometer selects metastable ions with a defined range of internal energy. On this basis, the reactions giving rise to the results plotted in Figure 5-2(b) are of ions with a defined energy content. Ion source reactions on the other hand, occur from ions with widely varying internal energy. Isotope effects are expected to reflect this spread in energy content. The internal energy distribution for source ions may also be biased by various reactions peculiar to the various substituted butyrophenones.

The magnitude of the deuterium isotope effect obtained in this study fall within the range cited previously (k_H/k_D = 0.7-2.17) for the McLafferty rearrangement in other systems (Chapter 3). The low value for this effect in this and other systems may be due to a number of reasons. Firstly, comparison of isotope effects for 1,5-hydrogen migration in radical cations generated in both solution and the gas phase, with similar processes in neutral molecules suggests that the low effect observed may be due to the nature of the radical cation[255-257] (Chapter 3). Differences between the reactions of charged and neutral species can be interpreted on the basis of their energetic requirements. If the degree of hydrogen transfer in each case is different then by Westheimer's theory (Chapter 1) the magnitude of the isotope effect will be related to this difference. Clearly, if the transition state for hydrogen transfer in radical cations is asymmetric (reactant or product like) compared to the reaction in netural species, the isotope effect will be reduced.

Secondly, the balance of forces to the transferring isotope

in the symmetrical case, required to achieve the maximum isotope effect cannot be achieved when the transfer is non-linear. As a result, the symmetrical stretching vibration ($\nu_R^{\ddagger}$) is isotopically sensitive leading to a reduction in the expected maximum in the isotope effect for the process. Calculations based on non-linear symmetrical hydrogen transfer transition states[89-91] indicate that isotope effects are reduced as the angle subtended by the partial bonds to the hydrogen isotope decreases (Chapter 1). In the case of a six membered transition state, such as for 1,5-hydrogen migration, the angle subtended by the bonds to the isotope is 120^{o} (considering the system to be a regular hexagon). The maximum isotope effect for such a situation (symmetrical transfer) is calculated to be $k_H/k_D \sim 4$[89]. The similarities between the transition state for loss of ethylene from the molecular ion of butyrophenone and the situations discussed above are clear. Considering this, it is not unexpected that the deuterium isotope effect for this process is of smaller magnitude than similar processes for neutral species.

The effect of the substituents on the deuterium isotope effect for the reaction is apparent from Figure 5-2(b). Electron donating substituents (negative σ_p^+) decrease the isotope effect relative to electron withdrawing substituents (positive σ_p^+) which increase this effect. The correlation coefficient for the straight line $y = 1.26 + 0.24x$, where x is the σ_p^+ values and y is the value of the isotope effect, is 0.92 (1% level of significance for 6 degrees of freedom).

The trend in isotope effect observed in these studies should be compared with the trend observed by McLafferty and Wachs with log (z/z_o) values for the rearrangement from butyrophenones

(Chapter 3)[249]. From their work, it is clear that as the electron withdrawing capabilities of the substituent in butyrophenone increases (negative to positive σ_p^+ values), the activation energy for the reaction decreases, i.e., log (z/z_o) increases. Combining this result with the trend in isotope effects observed, leads to the conclusion that the transition state for the McLafferty rearrangement from butyrophenones is product-like; i.e., the reaction is endothermic. This conclusion is based on the fundamentals of Westheimer's theory; as the asymmetry of the transition state increases, the isotope effect falls from its maximum value which occurs in symmetric case. In the case of an endothermic reaction, as the activation energy is decreased the potential energy surface becomes more symmetrical. Clearly, with a reactant-like situation, decreasing the activation energy increases the exothermicity of the reaction and thereby decreases the isotope effect.

Calculational models of the reactant and transition state for 1,5-hydrogen migration of butyrophenone were prepared in an attempt to reproduce the deuterium isotope effect observed experimentally. The models are described in Chapter 4 (Figures 4-1 and 4-2) and the results of the calculations are presented in table 4-3. Figure 5-3 describes the atom numbering for these systems. Figure 5-4 is a plot of the calculated deuterium isotope effect versus the bond order of the forming oxygen-hydrogen bond $(n_{5,15})$.

The results of the calculations are consistent with those measured assuming a product-like transition state. Calculations using various models were attempted. The molecular geometry having a basis in physical reality and giving meaningful isotope effects was the 30^o staggered model described in Chapter 4. Models employing a planar six-membered, cyclic transition state suggested

BUTYROPHENONE

REACTANT MODEL

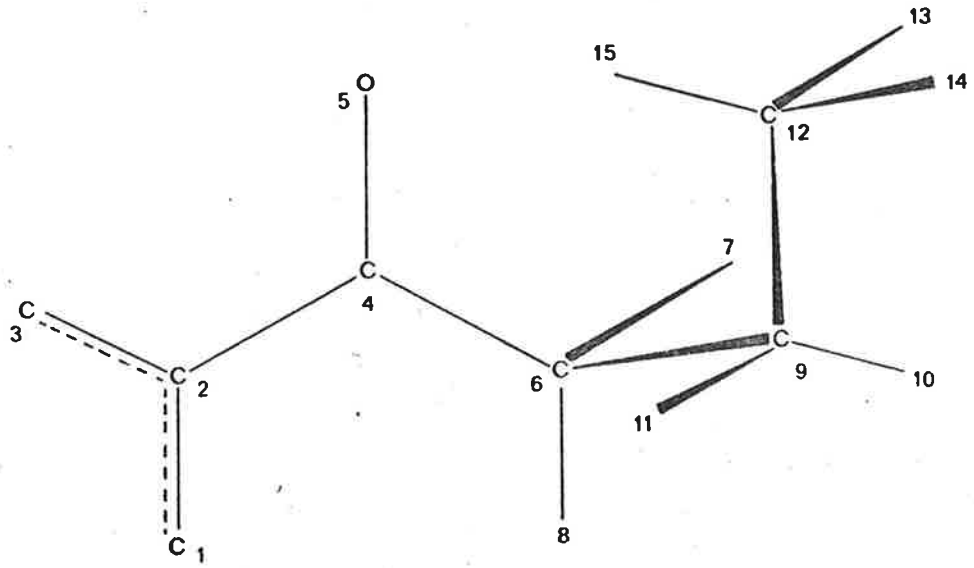

2-ETHYLBUTYROPHENONE

REACTANT MODEL

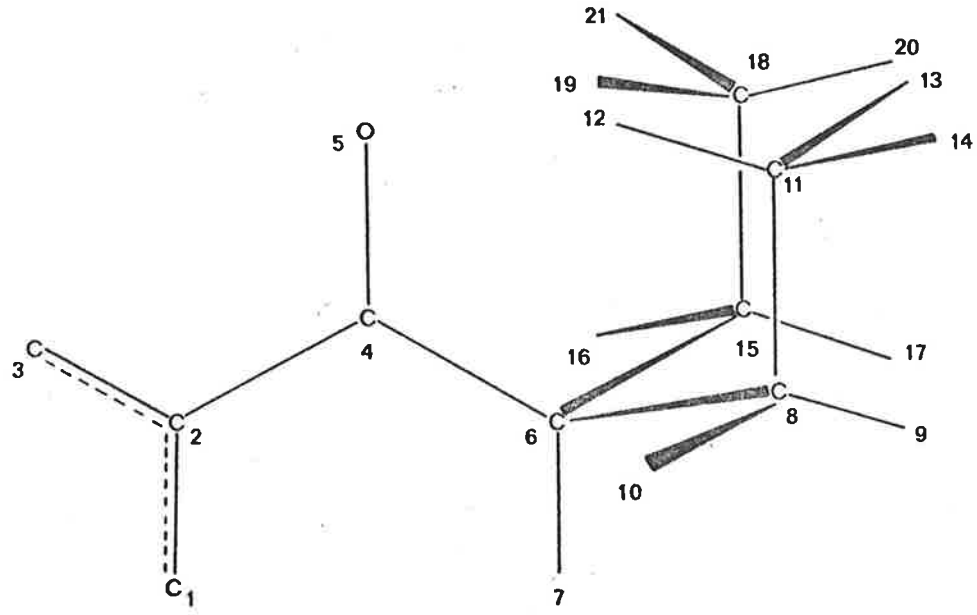

Figure 5-3

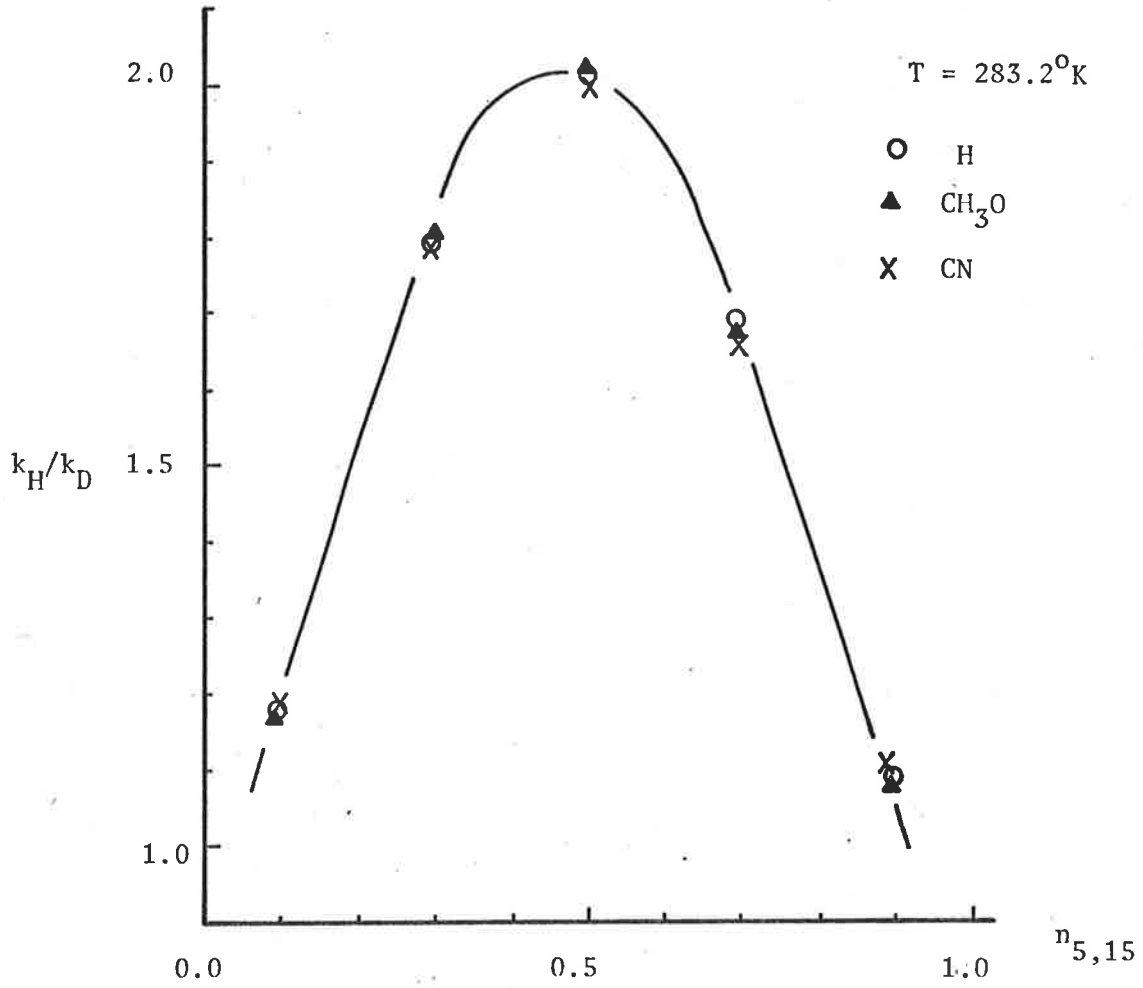

Figure 5-4

by molecular orbital calculations[215], produced deuterium isotope effects which were below unity for all of the transition state models. In the planar case, the transferring hydrogen approached the migrating terminus too closely as the bond order $n_{5,15}$ was increased.

Carbon-13 isotope effects calculated using the 1,5-hydrogen transfer model (table 4-3), suggest that isotopic substitution at positions C_{12} and C_4 will lead to the observation of an isotope effect for the process. The isotope effect at C_{12} increases from k_1/k_2 0.998-1.036 with increasing transition state asymmetry (toward a product-like situation). However, the effect predicted at C_4

is constant ($k_1/k_2 \sim 0.997$). Both of these results are expected on the basis of bonding changes which occur with this model. Since the bonding changes at C_9 and C_6 are expected to be minimal in this model, there should be no (or negligible) isotope effects at these positions. This prediction is corroborated by the results in table 4-3.

The effect of altering the carbonyl frequencies of the reactant and transition state models in accord with para substituent charges is also shown in Figure 5-3. Clearly, the effect of the substituents on the observed deuterium isotope effect is not through changes in the carbonyl stretching frequency. The substituent effect is more likely to be on the symmetry of the transition state. If this is the case, the increase in measured deuterium isotope effect with the electron withdrawing capability of the substituent, will be due to the increase in the symmetry of hydrogen transfer.

Simplistically, the observation of a deuterium isotope effect on the 1,5-hydrogen migration implicates this step as part of the rate determining step for the overall process. However as discussed previously, if 1,5-hydrogen migration is rapid and not part of the rate determining step, an equilibrium situation may develop. This may result in the observation of an equilibrium isotope effect.

Calculational estimates of the equilibrium deuterium isotope effect for 1,5-hydrogen migration (assuming that carbon-carbon bond breakage is the rate determining step), predict that its value should lie between K_H/K_D 0.82 and 1.20 at 283.2^{o}K (table 4-7) for butyrophenone. The lower value is calculated using a carbonyl

torsion similar to the torsion of ethylene; where as the upper values utilize the torsion of ethane. Clearly, the more realistic value for the carbonyl torsion is close to that of ethylene. As a result, the expected equilibrium isotope effect for this process is estimated to be around K_H/K_D 0.82. The magnitude of the experimental value (1.35, first FFR) indicates that it is unlikely that it represents an equilibrium isotope effect. Higher values of the measured isotope effect for electron withdrawing substituents indicate that it is probable that the 1,5-hydrogen migration is a kinetic situation.

Since the measured isotope effects (table 3-2, Figure 5-2) are greater than expected for β secondary isotope effects for carbon-carbon bond cleavage ($k_H/k_D < 1.15$)[16], it is highly likely that these results represent primary kinetic effects. In this case, step (i) in scheme 5-1 describes motions of atoms which are involved in the rate determining step. In accord with this result, the alternatives for the mechanisms proposed for this rearrangement include, (i) stepwise with 1,5-hydrogen migration as the rate determining step or (ii) concerted (scheme 5-1). Clearly, to determine which of these options is correct (or at least the closest approximation to physical reality), one should attempt to measure an isotope effect for atoms involved in other aspects of the rearrangement. In effect, carbon-13 labelling of each carbon involved in the six-membered transition state will give isotope effects if and only if the concerted mechanism is operative (intra and inter – molecular cases). There are two qualifications to observing carbon isotope effects. Firstly, the bonding charges occurring at a particular atom (bond breakage and formation) may in fact cause the

total bonding to this atom to be unchanged in the transition state[43]. Cancelling of opposing effects will result in either very small or no isotope effect at this position: bonding changes as a pre-requisite for the observation of an isotope effect has been emphasized in Chapter 1. Secondly, the bonding changes at the atom may be so small that the isotope effect may fall within the experimental error[43].

The system chosen for initial carbon-13 isotope effect studies was butyrophenone (Chapter 3). The nature of this experiment required competive *intermolecular* rate comparisons. Experimental problems associated with this type of study have been dealt with fully in Chapter 3.

The major problem apart from the experimental difficulties, was the presence of an isotope effect on the ionization potential for the isotopic molecules. This effect was detected by measuring the isotopic ratio for the ions undergoing α-cleavage from the molecular ions of butyrophenone and 4-(^{13}C)-butyrophenone (36) (table 3-6). Since the isotopic atom is far removed from the reaction site, its effect on the rate of this reaction would only be secondary (for carbon isotopes, this would be undetectable). The ratio of product ion abundances for the reaction from butyrophenone and 4-(^{13}C)-butyrophenone (36) should be equal to the ratio of molecular ion abundances if there were no differences in the internal energy distribution on ionization. The ratios are k_1/k_2 = 1.045±0.13 where k_1 is the rate constant for the lighter and k_2 the heavier isotope, and $M_1^{+\cdot}/M_2^{+\cdot}$ = 1.054±0.06 respectively. Rate increases for α-cleavage from the carbon-13 labelled butyrophenone most likely results from the higher mean internal energy of this compound due to its lower zero point energy.

Potentially, the measurement of the intensities of product ions formed with rates which are isotope independent (e.g., α-cleavage in the above example), can be used to correct for the isotope effect on the ionization process. However, due to the experimental difficulties (pressure fluctuations) encountered in the intermolecular comparative rate studies, and inaccuracies inherent in correcting peak height ratios for effects such as differences in ionization potentials, it was decided to use the intramolecular approach in these measurements. Intramolecular comparative rate studies by their very nature, would minimize the experimental difficulties and would negate the effects of the isotope on the ionization process. The system studied was isotopically labelled 2-ethylbutyrophenone.

ISOTOPE EFFECTS IN THE 2-ETHYLBUTYROPHENONE SYSTEM

The results for the measurement of loss of ethylene and (^{13}C)-ethylene from 4-(^{13}C)-2-ethylbutyrophenone (43) and 3-(^{13}C)-2-ethylbutyrophenone (42) are shown in table 3-7. The ratios in table 3-7 were corrected for the instrumental factor (baseline variance) and the differences in peak height due to un-equal kinetic energy releases for the labelled and un-labelled compounds (35) and (36). The differences between the isotopic ratios for compound (43) and (42) are significant. In each case the correction was overestimated; i.e., the largest correction factor was used in each case. Table 3-9 lists the corrected ratios for loss of ethylene versus loss of (^{13}C)-ethylene from compounds (42) and (43). The ratios are reproduced in table 5-1.

Table 5-1

Compound	Metastable Ion Transition	Ratio ± SD[a]
4-(^{13}C), (43)	$177^+ \rightarrow 149^+ + 28$ $177^+ \rightarrow 148^+ + 29$	$\bar{x}$=0.995±0.014
3-(^{13}C), (42)	$177^+ \rightarrow 149^+ + 28$ $177^+ \rightarrow 148^+ + 29$	$\bar{x}$=1.009±0.019

NOTES

(a) this is the ratio of the loss of ethylene to loss of (^{13}C)-ethylene.

It is clear from the results in table 5-1, that the carbon-13 isotope effect for compound (42) is greater than for compound (43). The isotope effects are small, as expected from consideration of the effects of internal energy on these parameters[335]. Their magnitude may also reflect the complexity of the bond forming and breaking processes in the cyclic transition state[43]. *In my view, there can be no doubt that a carbon-13 isotope effect is occurring for the loss of ethylene from 3-(^{13}C)-2-ethylbutyrophenone.*

The deuterium isotope effects that were measured for the 1,5-hydrogen migration step in substituted 2-ethylbutyrophenones are shown in table 3-11. Figure 5-5(a) is a plot of k_H/k_D versus Brown's σ_p^+ value for the ion source reaction of these compounds and figure 5-5(b) is a similar plot for the first FFR reaction. As before, the presence of an electron donating substitutent in the para position has a diminitive effect on the observed isotope effect when compared to electron withdrawing substituents. This effect has been discussed previously for the para substituted

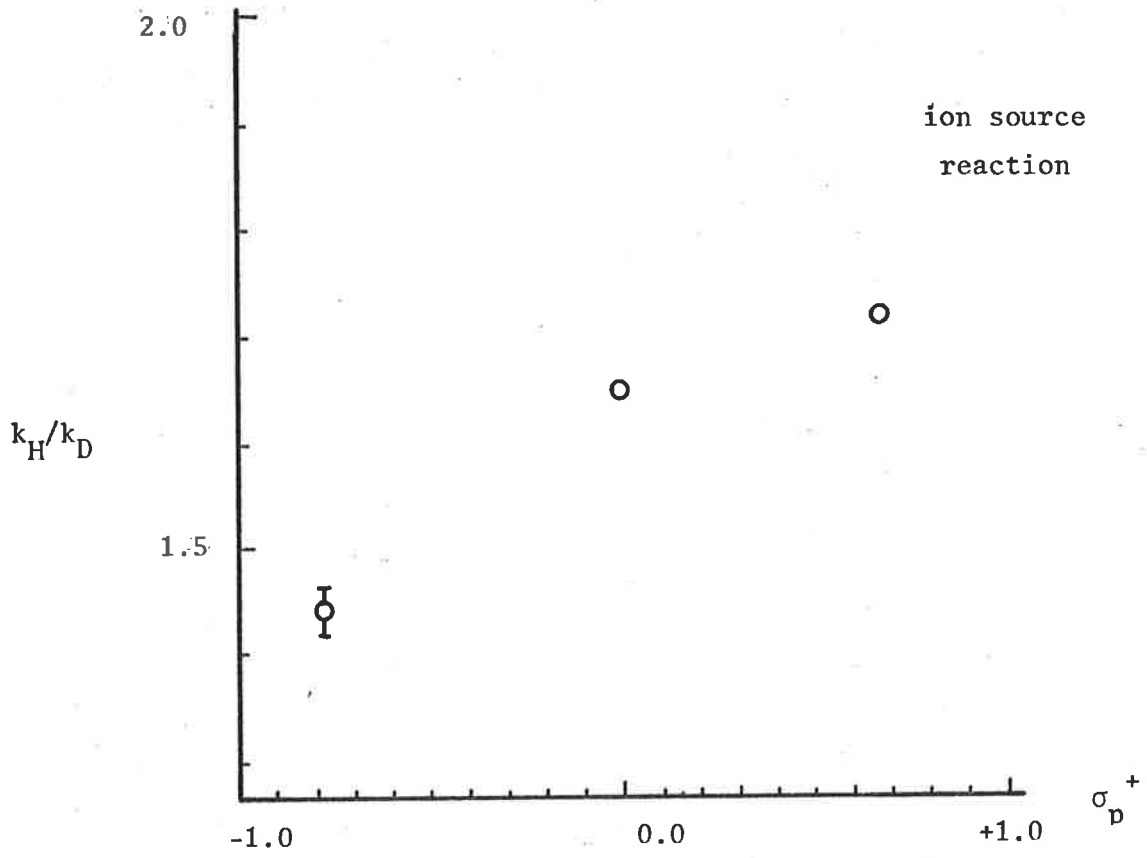

Figure 5-5(a)

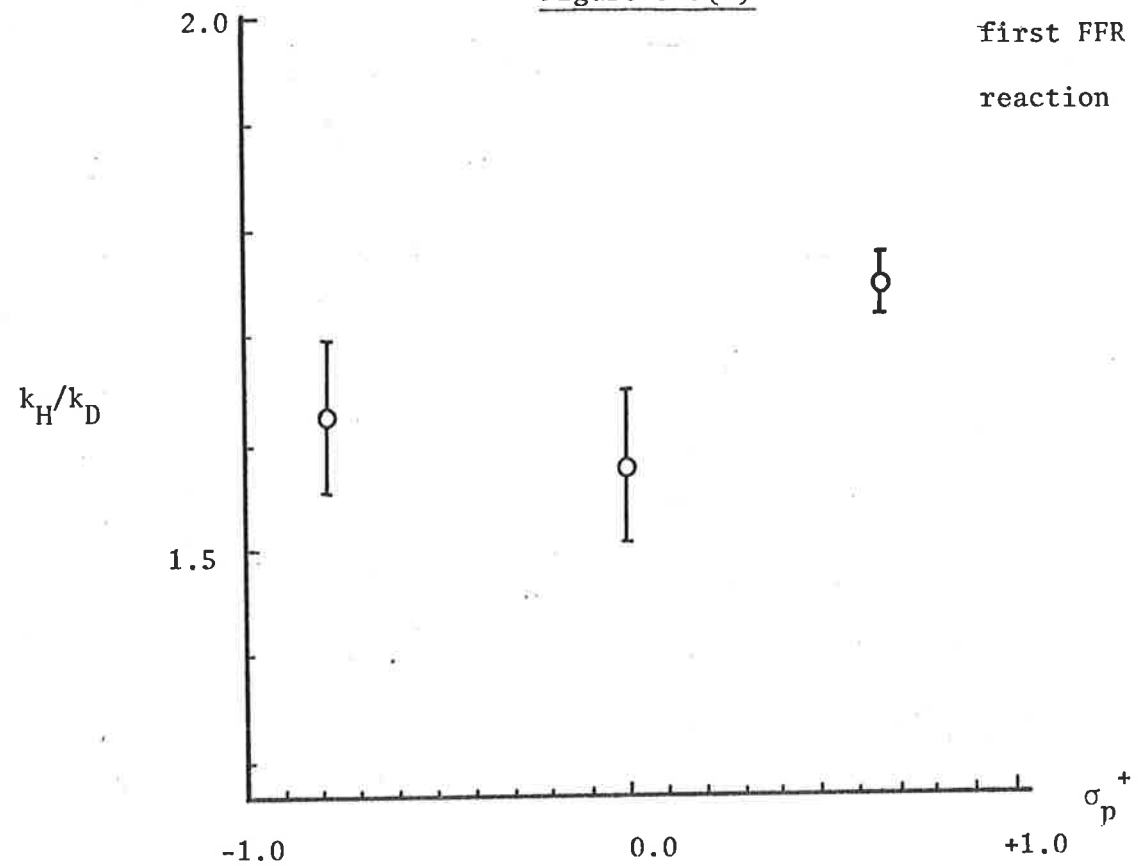

Figure 5-5(b)

butyrophenones. The magnitude of the deuterium isotope effect observed in this system is greater than would be expected if 1,5-hydrogen migration were an equilibrium process. The equilibrium isotope effect expected has been calculated for butyrophenone models (K_H/K_D ~0.82 at 283.2°K). The isotope effect observed therefore represents differences in rates of reaction on isotopic substitution i.e. a kinetic isotope effect.

Reactant and transition state models for 1,5-hydrogen migration in 2-ethylbutyrophenone were prepared and the deuterium and carbon-13 isotope effects calculated (Chapter 4). Figures 4-6 and 4-7 are diagramatic representations of these models and table 4-10 lists the results of the calculations. Figure 5-6 is a plot of the calculated deuterium isotope effect versus increasing bond order of the oxygen-hydrogen bond ($n_{5,19}$), (Figure 5-3).

The carbon-13 isotope effects calculated using this model are shown in table 4-10. In a similar manner to the stepwise models of butyrophenone, carbon-13 substitution at C_{18} and C_4 result in isotope effects on the rate of reaction. Labelling at C_{18} produces isotope effects ranging from k_1/k_2 0.997 - 1.035 for transition state models varying from reactant to product-like. The isotope effect at C_4 is again relatively constant; k_1/k_2 ~0.997. Isotopic substitution at C_{15} and C_6 do not produce isotope effects on the reaction rate in accordance with the absence of bonding changes at these positions.

Further evidence for the involvement of carbon-carbon bond cleavage in the rate determining step comes from the observation of a secondary deuterium isotope effect for the McLafferty rearrangement from 3-($^2H_2$)-2-ethylbutyrophenone (47). The isotope effect

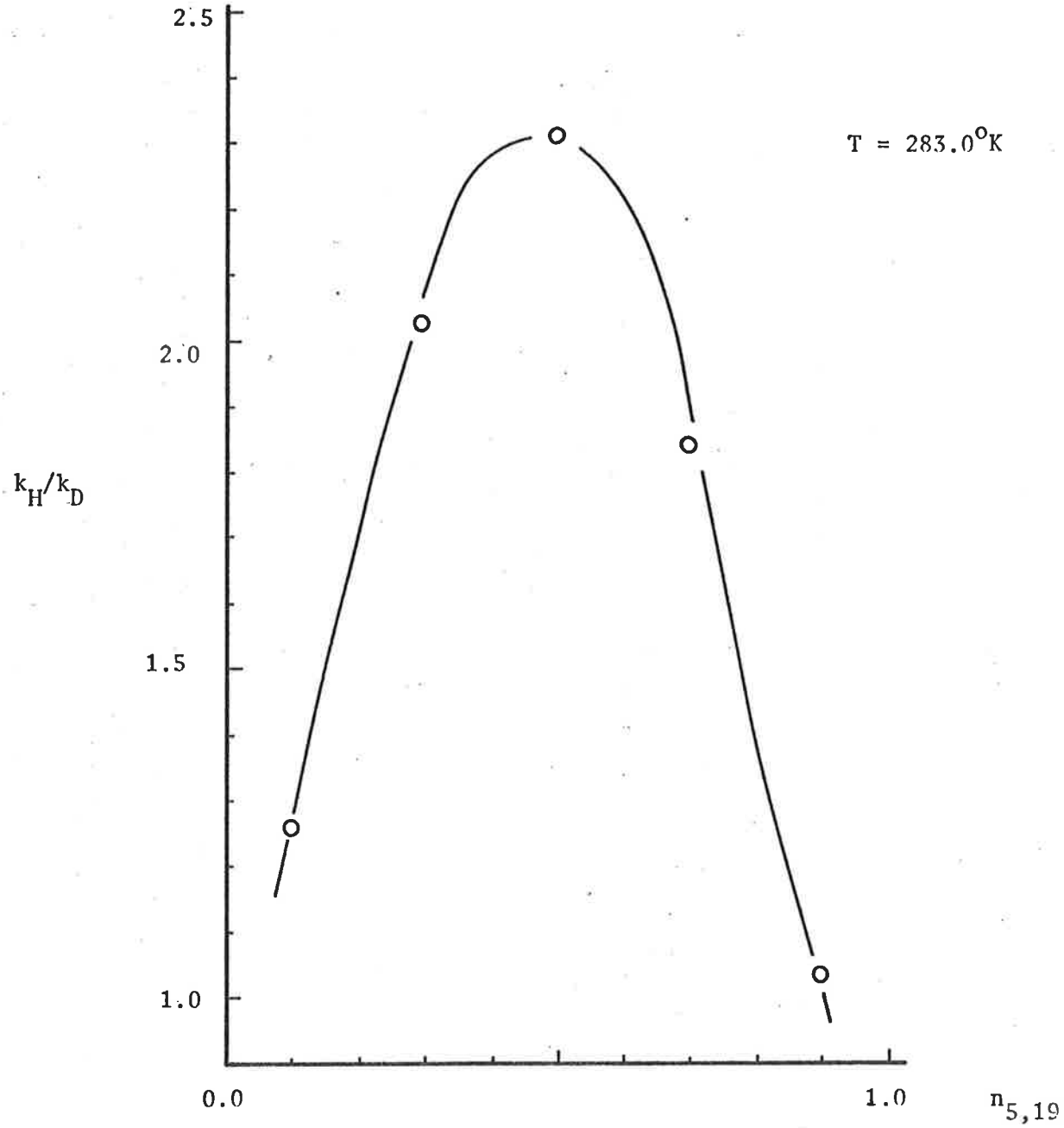

Figure 5-6

observed was $k_H/k_D = 1.16 \pm 0.02$ (first FFR of the RMU-7D mass spectrometer; table 3-12). This effect is of the same magnitude as α-secondary isotope effects[16], but is too large for a β-secondary effect; i.e. it is apparent from the magnitude of the observed secondary effect that bonding changes (re-hybridization, see Chapter 1) are occurring which are consistent with the involvement of carbon-carbon bond cleavage in the rate determining step of the process.

The conclusions discussed above for the secondary isotope effect are corroborated by calculations using various stepwise models of 3-($^2H_2$)-2-ethylbutyrophenone (47). Results from models describing 1,5-hydrogen migration as the rate determining step, indicate that no isotope effect is expected by replacing H_{16} and H_{17} with deuterium ($k_H/k_D = 1.000$ for all transition state models; see table 4-11).

Models based on carbon-carbon (C_{15}-C_6) bond cleavage as the rate determining step however, predict that an isotope effect will be observed for 3-($^2H_2$)-2-ethylbutyrophenone (47) (table 4-12). Figure 5-7 reproduces these results in graphical form to emphasize the monotonic increase in the α-secondary isotope effect with the product-like nature of the transition state. The increase in this effect is entirely expected since the degree of hybridization change at C_{15} increases with the increasing product-like nature of the transition state.

The results from calculations of isotope effects using the concerted model of loss of ethylene from 2-ethylbutyrophenone will now be discussed. Models (reactant and transition state) used in the concerted process are shown in Figures 4-6 and 4-12. Calculated

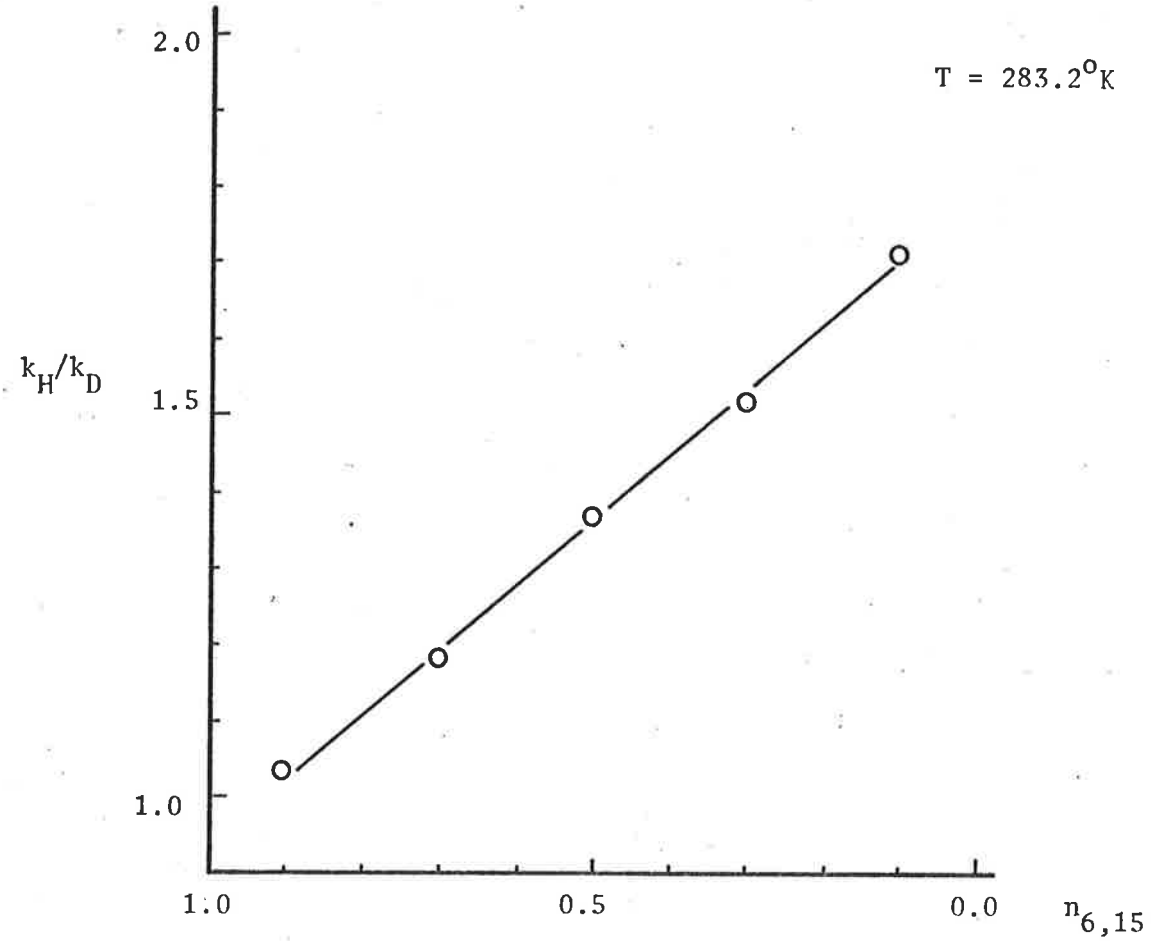

Figure 5-7

isotope effects are listed in table 4-13 and plotted in Figure 5-8 against the bond order of the forming oxygen-hydrogen bond ($n_{5,19}$). It is apparent from these results that the deuterium isotope effect passes through a maximum at around $n_{5,19}$ = 0.4. Again, this behaviour is predictable on the basis of Westheimer's theory. The carbon-13 isotope effects calculated using this model are also shown in table 4-12. Calculation of carbon-13 isotope effects at C_{18}, C_{15}, C_6 and C_4 indicates that bonding changes occur at all of these positions in the concerted model. The calculated values at C_{18} (k_1/k_2 1.011 - 1.019) and C_{15} (k_1/k_2 1.021 - 1.047) are different from the values calculated by means of the 1,5-hydrogen

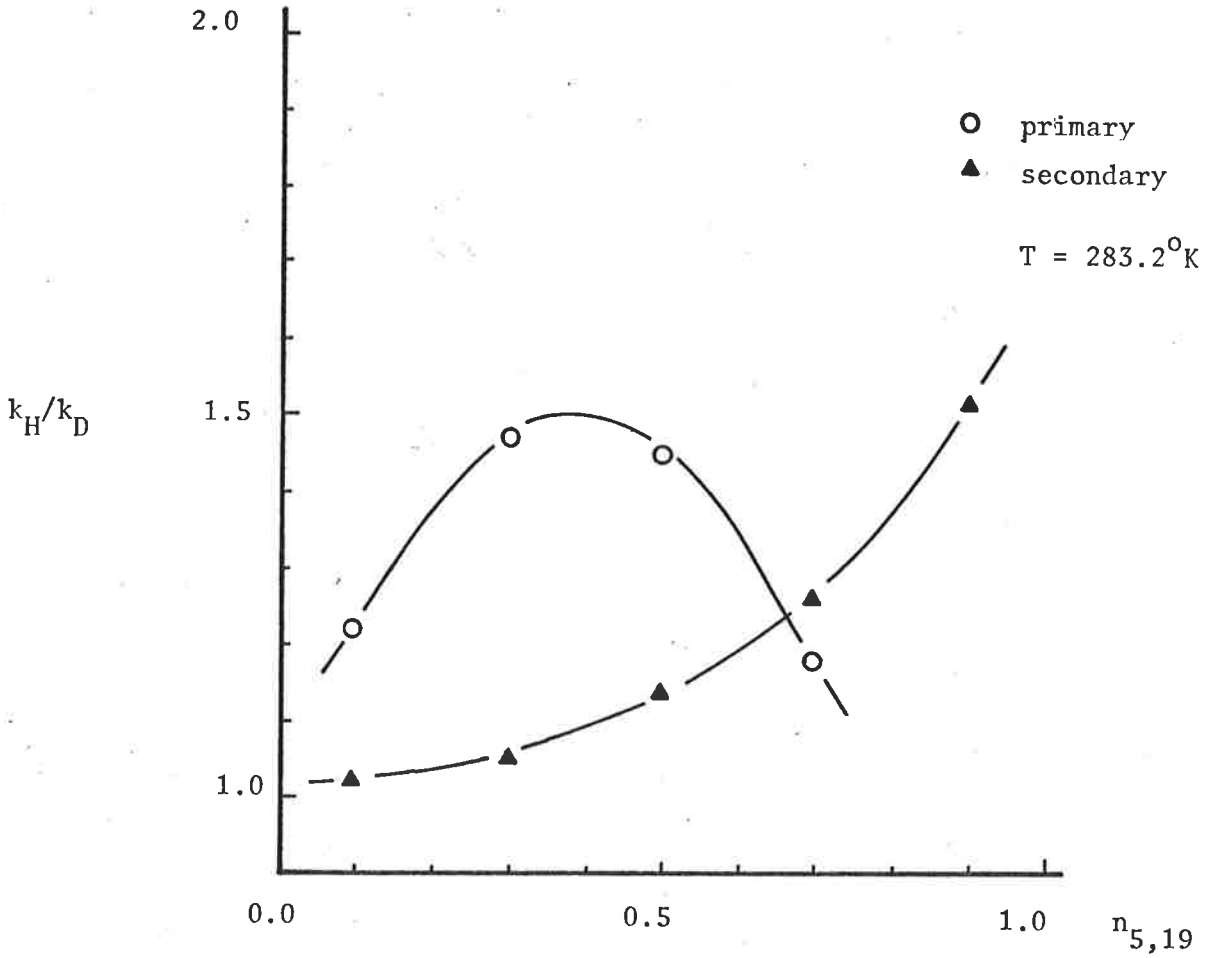

Figure 5-8

transfer stepwise models of 2-ethylbutyrophenone, and similar to the carbon-carbon bond cleavage model. Significantly, they are also similar to the carbon-13 isotope effects observed experimentally.

Secondary isotope effects for 3-($^2H_2$)-2-ethylbutyrophenone were also calculated using the concerted model (table 4-14). These results are also shown in Figure 5-6. Again there is an increase in the secondary effect with increasing product-like nature of the transition state as expected.

The magnitudes of the primary isotope effects calculated using

the concerted model, are less than those obtained from the stepwise model. Since both models were similar, this result would not have been predicted.

In the 1,5-hydrogen transfer stepwise model, the interaction coefficient used in the calculations was A_{ik}=1.0; clearly, no other coefficient could be used since only two bonds are interacting. However, in the concerted model, all interaction coefficients were A_{ik}=1.0 and no adjustment was made to allow for greater interactions between particular bonds. This may account for the lower deuterium isotope effect values, since increasing the interaction coefficient between the bonds to the transferring isotope will most certainly raise the magnitude of the effect.

CONCLUSIONS

The observation of a deuterium kinetic isotope effect for 1,5-hydrogen migration in substituted butyrophenones (which includes 2-ethylbutyrophenones) and the observation of a carbon-13 isotope effect in 3-(^{13}C)-2-ethylbutyrophenone (42) suggests that the McLafferty rearrangement in these systems may proceed by a concerted mechanism. The α-secondary isotope effect in 3-($^{2}H_2$)-2-ethylbutyrophenone (47) provides further evidence that carbon-carbon bond cleavage is part of the rate determining step.

Correlation between experimental and theoretical results has been achieved using models based on the concerted mechanism. Some of the experimental results are mimicked by calculations using various stepwise models. However, the concerted model reproduces all of the experimental data in, at least a semi-quantitative fashion.

There is a further mechanism which fits the available evidence that must be considered. The argument may be developed in the following way.

There is always the possibility that an isotope effect may be observed for a non-rate determining step, although this statement contradicts many of the standard texts (for example see ref. 6). This situation is exemplified in pathways involving equilibrium steps prior to the rate determining step. In an intramolecular case, reaction may involve the choice between isotopes in equivalent positions, thereby leading to the possibility of isotope effects. *Clearly, this choice is present whether the reaction step is rate determining or not.* However, if the activation energy for this step is small relative to the activation energy of the rate determining step, and if the decomposing species has sufficient energy to react, the differing isotopes will be removed in a ratio which approaches the statistical ratio.

As the activation energy for the initial step increases in relation to that of the rate determining step, the effect of the differences in zero point energies will become more pronounced, thus resulting in the possibility of an isotope effect. If the activation energy of the initial step is large, but that step is still not rate determining, there will be a finite probability of observing an isotope effect for the non-rate determining step. *The limiting situation will be when the activation energies for both steps are of similar magnitude in which case kinetic isotope effects will be observed for each step.* In the cases considered above, the isotope effect will be expected to increase as the activation energy for the initial step increases.

The situations described above are clearly stepwise and differ from the concerted process only by the presence of an intermediate. The occurrence of such stepwise mechanisms cannot be excluded on the available experimental evidence. The probability of the activation energies for 1,5-hydrogen migration and carbon-carbon bond cleavage being the same must be small, therefore the occurrence of the limiting stepwise situation described above is unlikely. An estimate of the isotope effects (deuterium and carbon-13) for the limiting stepwise case can be gained for each step from a combination of the results obtained from calculations utilizing both of the stepwise models (e.g., see tables 4-10, 4-12 and 4-13). These results indicate that there is little difference in the calculated isotope effects for both the limiting stepwise and concerted processes.

Identification of the intermediate proposed for the stepwise mechanisms by means of "trapping" experiments was unsuccessful. Naturally, this may well be due to the non-existence of such a species in the McLafferty rearrangement. On the other hand, these experiments cannot be taken to disprove the intermediacy of such a species.

Finally, it is clear from the details of the experimental procedure for the measurement of both deuterium and carbon-13 isotope effects (Chapter 3), that this technique allows for the investigation of the mechanisms of many mass spectral processes. An "order of magnitude" improvement in the accuracy of these measurements is possible by introducing rapid scanning, peak averaging and deconvolution techniques to extract small differences in peak areas.

Utilization of carbon-14 and oxygen-18 isotopic labelling would also have enormous advantages in situations where instrumental energy resolution is a problem.

CHAPTER 6

EXPERIMENTAL

GENERAL

Mass spectra (MS) were recorded on a modified[338] Hitachi Perkin-Elmer RMU-7D mass spectrometer operating at an electron beam energy of 70 eV and an accelerating potential of 3.6 kV, unless otherwise stated. Samples were introduced into the ion source by means of an all glass, heated inlet system maintained at a temperature of around 150°C. Typically, the source pressure was $5x10^{-6}$ torr and the first field free region pressure was $5x10^{-7}$ torr. Metastable ion transitions in the first field free region were investigated by means of the electric sector defocusing technique described in Chapter 2. Mass spectral data are quoted as the m/z value, followed by its intensity (%) relative to the base peak of the spectra and lastly its structural assignment, where possible.

The carbon isotope effect measurements, some of the kinetic energy release measurements and the recording of mass analysed, ion kinetic energy (MIKE) spectra were made using the new "grand-scale" reverse sector mass spectrometer designed and built by Dr. P.J. Derrick and his colleagues at La Trobe University, Bundoora, Victoria[295,296]. This instrument employs a magnetic sector with a radius of 78 cm., the first field free region is 112 cm. in length, the pressure of the field free region is of the order of $1x10^{-8}$ torr and the operating electron energy is 70eV.

Ion cyclotron resonance (ICR) mass spectra were recorded using a Dynaspec ICR9 spectrometer operating in the magnetic field modulation mode. Typical operating conditions for the square three-section cell were,

$\omega_c/2\pi$ = 153.7 kHz.

emission current = 0.2 μA.

ion current = 10^{-12} - 10^{-11}A.

ion transit time = 2-3 x 10^{-3} sec.

pressure = 10^{-6} - 10^{-5} torr.

Ion transit times were obtained directly by means of a device based on that originally described by McMahon and Beauchamp[339]. The sample inlet system for the instrument consists of a direct-probe for solids and a dual inlet port for the introduction of liquids and gases. Cyclotron ejection experiments were peformed as described in the literature[276,340].

Infrared (IR) spectra were recorded using a Unicam SP200 or a Jasco IRA-1 grating infrared spectrophotometer and were calibrated with reference to the 1602 cm^{-1} band of polystyrene. Absorption band positions are quoted in wavenumbers (cm^{-1}) and their intensities expressed as follows: s, strong; m, medium; w, weak; sh, shoulder; br, broad. The spectra were recorded either as nujol mulls, as liquid films or as solutions, using sodium chloride plates. Data are given in the following order; absorption band wavenumber (cm^{-1}), relative intensity and structural assignment.

Proton magnetic resonance (PMR) spectra were recorded at a magnetic field of 60 MHz using either a Varian T-60 or Jeol PMX-60 spectrometer. The spectra were obtained as either carbon tetrachloride or deuterochloroform solutions of the sample containing tetramethylsilane (10% V/V) as an internal reference. Data are given in the following order; chemical shift in p.p.m. (δ), multiplicity, first order coupling constant (J) expressed in Hertz, relative intensity as the number of protons and the structural

assignment.

Melting points were determined using a Kofler hot-stage melting point apparatus under a Reichert microscope and are uncorrected.

Microanalyses were performed by the Australian Microanalytical Service, Melbourne, Victoria.

Gas liquid chromatography (GLC) was carried out using a Pye 104 chromatograph with nitrogen as a carrier gas. Sample detection was by means of flame ionization. Unless otherwise stated, the flow-rate of the carrier gas was maintained at 40 ml./min. Columns used were constructed of glass and had the following supports and dimensions;

A. 5% FFAP on Varaport 30 (100/120) (1mx5mm)

B. 15% OVIOI on Chromasorb W (60/80) (3mx8mm)

C. 15% SE30 on Chromasorb A (40/60) (1mx5mm)

D. 20% FFAP on Varaport 30 (100/120) (3mx8mm).

High pressure liquid chromatography (HPLC) was performed on a Spectra Physics Chromatronix 3500 chromatograph using a Lichrosorb SI60 column of 10μ particle size and dimensions 250mm x 10mm.

In purification by column chromatography, Spence aluminium oxide or Sorbsil silica gel were used as adsorbants. Preparative thin layer chromatography (TLC) was carried out using glass plates coated with a 1:1 mixture of Merck Kieselgel G and HF254. Analytical TLC was carried out on either Merck aluminium oxide 60 F254 neutral (type E) or silicagel 60F254 plates.

Light petroleum refers to the hydrocarbon fraction of b.p. 60-70^{o}C and petroleum ether refers to the hydrocarbon fraction of b.p. 30-40^{o}C. In this text, ether refers to diethyl ether.

Butyllithium was prepared in hexane using 1-chlorobutane by the method of Gilman and co-workers[341]. The solution was stored at -5°C and the molarity determined by titrating diphenyl acetic acid according to the method of Kofron and Baclawski[342].

ATTEMPTED ALKYLATION OF 4-SUBSTITUTED BENZONITRILES

The following general procedure, described for the preparation of 1-(4-methylphenyl)-1-butanone (1), was used in the preparation of 1-phenyl-1-butanone (2) and 1-(4-chlorophenyl)-1-butanone (3). This method is an adaption of the procedure described by Amstutz[262].

Propylmagnesium bromide was prepared in the usual manner[343] from 1-bromopropane (2.0g; 16.3 mmol) and magnesium (0.4g; 16.7 mmol) in anhydrous ether (20 ml) under an atmosphere of nitrogen. The Grignard reagent thus prepared was added slowly (0.25h) to a stirred solution of 4-methylbenzonitrile (1.0g; 8.5 mmol) in anhydrous tetrahydrofuran (10ml). The reaction mixture was maintained under an atmosphere of nitrogen, stirred and heated under reflux for 12h. Hydrolysis of the mixture was effected by the successive addition of water (5ml), saturated ammonium chloride solution (1 ml) and dilute hydrochloric acid (2M; 10 ml). After stirring the resulting mixture for 1h., the separated aqueous phase was extracted with ether (4 x 20 ml). The combined organic layers were dried with magnesium sulphate and the solvents removed *in vacuo*. Analytical TLC (silica gel; benzene) indicated the presence of 4-methylbenzonitrile (Rf 0.9) and 1-(4-methylphenyl)-1-butanone (Rf 0.5). Distillation (b.p. 59°C (block)/0.05 mm.Hg; lit[344]. 251.5°C/758 mm.Hg) gave 1-(4-methylphenyl)-1-butanone (0.6g, 40%) as a colourless oil.

The above procedure was used to synthesize 1-(4-chlorophenyl)-1-butanone from 4-chlorobenzonitrile (1.0g; 7.4 mmol) and 1-phenyl-1-butanone from benzonitrile (0.2g; 15.3 mmol). In both cases analytical TLC (silica; benzene) indicated that the reaction was incomplete even after heating under reflux for 24h.; the major

component of the product mixture being starting material.

OXETANE

This compound (b.p. 48-54°C; lit.[269] 48°C) was prepared in 20% yield (1.0g) from (3-bromopropyl)acetate (15.0g; 83.0 mmol) by the method of Noller[269]. (3-Bromopropyl)acetate was prepared in 80% yield (15.0g) by acetylation of 1-bromo-3-propanol (14.4g; 0.10 mol) with acetyl chloride (8.1g; 0.11 mol) in anhydrous pyridine (100 ml) according to the method described by Vogel[345].

1-($^2H_1$)-3-PROPANOL (11)

Preparation of this compound was achieved by the reduction of oxetane (5.0g; 86.0 mmol) with lithium aluminium deuteride (99 atom %D; 1.7g; 40.0 mmol) in anhydrous ether (50 ml) according to the method of Searles, Pollart and Lutz[268]. Distillation of the crude product, obtained from the addition of wet ether to the reaction mixture until the excess lithium aluminium deuteride had been destroyed and removal of the ether *in vacuo*, yielded 1.2g (70%) of 1-($^2H_1$)-3-propanol (11) (b.p. 96-98°C/760 mm Hg; lit.[346] 97.2°C/760 mm Hg).

PMR ($CDCl_3$): δ 0.89, triplet of triplets, 7.0, 1.0 Hz., 2H, ($\underline{CH_2}^2H$-)
1.60, quinlet, 7.0 Hz., 2H, (C-$\underline{CH_2}$-C)
2.62, singlet, 1H, (-$\underline{OH}$)
3.60, triplet, 7.0 Hz, 1H, (C-$\underline{CH_2}$-O)

PREPARATION OF 1-BROMO-3-($^2H_1$)-PROPANE (10)

1-Bromo-3-($^2H_1$)-propane (10) (b.p. 71-73°C; lit.[267] 71°C) was prepared in 70% yield (2.9g) from the reaction of 1($^2H_1$)-3-propanol

(2.0 g; 33.0 mmol) with phosphorus tribromide (3.3g; 12.0 mmol) by the method of Noller and Dinsmore[267].

PREPARATION OF 4-($^2H_1$)-1-(4-SUBSTITUTED PHENYL)-1-BUTANONES

The general procedure which follows was used to prepare initially the isotopically un-labelled and then the deuterium labelled ketones. The isotopically un-labelled ketones prepared were; 1-(4-methylphenyl)-1-butanone (1), 1-phenyl-1-butanone (2), 1-(4-chlorophenyl)-1-butanone (3), 1-(4-bromophenyl)-1-butanone (4), 1-(4-fluorophenyl)-1-butanone (5), 1-(4-methoxyphenyl)-1-butanone (6) and 1-(4-cyanophenyl)-1-butanone (7). Similarly, the isotopically labelled ketones prepared were; 4-($^2H_1$)-1-(4-methylphenyl)-1-butanone (13), 4-($^2H_1$)-1-(4-chlorophenyl)-1-butanone (16), 4-($^2H_1$)-1-(4-bromophenyl)-1-butanone (17), 4-($^2H_1$)-1-(4-fluorophenyl)-1-butanone (14), 4-($^2H_1$)-1-(4-methoxyphenyl)-1-butanone (12), 4-($^2H_1$)-1-(4-cyanophenyl)-1-butanone (18) and 4-($^2H_1$)-1-phenyl-1-butanone (15). The procedure is detailed for the preparation of 4-($^2H_1$)-1-(4-methoxyphenyl)-1-butanone.

3-($^2H_1$)-Propylmagnesium bromide was prepared from 1-bromo-3-($^2H_1$)-propane(10) (0.33g; 2.6 mmol) and magnesium (0.06g; 2.6 mmol) in anhydrous ether (10 ml) under an atmosphere of nitrogen[343]. This was added, in a dropwise manner, to a stirred anhydrous ether (20 ml) solution of 4-methoxybenzaldehyde (0.3g; 2.2 mmol) at 0°C, under an atmosphere of nitrogen. On completion of the addition, the reaction mixture was stirred at 20°C for 1h. Hydrolysis was effected by the successive addition of water (5 ml) and dilute hydrochloric acid (2M; 5 ml). The separated aqueous phase was

extracted with ether (3 x 20 ml) and the combined organic phases washed with water (10 ml) and dried with magnesium sulphate. The organic solvent was removed *in vacuo* yielding a viscous yellow oil whose IR (film) indicated the presence of an absorption band at 3400 cm^{-1} (b; O-H stretch) and the absence of absorption bands for the aldehydic carbonyl stretch. The benzylic alcohol was oxidized as follows without purification or further characterization.

A dichloromethane solution of 4-($^2H_1$)-1-(4-methoxyphenyl)-1-butanol was added in one portion to a vigorously stirred suspension of pyridinium chlorochromate (0.72g; 3.3 mmol) and sodium acetate (0.50g) in dichloromethane (20 ml)[264]. The reaction mixture was stirred at 20°C for 3h., diluted with ether (100 ml) and filtered through a short Florisil column. The filtrate was washed successively with dilute hydrochloric acid (2M, 10 ml) and water (10 ml) then dried with magnesium sulphate. Removal of the solvents *in vacuo* yielded the crude ketone which was purified by preparative TLC (silica; 20% ethyl acetate, 80% benzene; Rf 0.6) and finally distilled (b.p. 93-97° (block)/0.5 mm Hg.; lit.[347] 162-163°C/20 mm Hg.). The yield of 4-($^2H_1$)-1-(4-methoxyphenyl)-1-butanone (12) was 80% (0.32g), based on the starting aldehyde.

The compounds, 1-(4-chlorophenyl)-1-butanone (16) and 1-(4-bromophenyl)-1-butanone (17) were oxidized by titrating a stirred solution of the ketone in acetone (20 ml) with a standard solution of chromium trioxide and sulphuric acid in water (Jones reagent)[348].

Table 6-1 lists the isotopically un-labelled ketones prepared by this method. The table summarizes the method of purification of the ketones and lists some of their physical properties.

Table 6-1

compound	purification	b.p.(°C/mm Hg.) or m.p.(°C) expt.	lit.	yield(%)	reference
(1) *p*-methyl	1:4, ether: light petroleum[a]	59(block)/0.05	251.5/758	50	344
(3) *p*-chloro	1:9, dichloromethane: light petroleum[b]	95(block)/1.2	253-254/760	50	349
(4) *p*-bromo	1:9, ether: light petroleum[b]	80(block)/0.7	149-151/13	57	350
(5) *p*-fluoro	4:6, ether: light petroleum[a]	48(block)/0.05	230-232/760	86	351
(6) *p*-methoxy	1:4, ethylacetate: benzene[a]	120(block)/1.2	162-163/20	76	347
(7) *p*-cyano	3:7, light petroleum: ether[a]	40-42[c]		50	

NOTES

(a) purification by preparative TLC using silica gel plates.
(b) purification by column chromatography using aluminium oxide.
(c) melting point.

Table 6-2

compound	purification[a]	expt. b.p.(°C/mm Hg.) or m.p.(°C)	yield
(13) *p*-methyl		95(block)/1.2	50
(16) *p*-chloro		65(block)/0.8	50
(17) *p*-bromo	1:9, ether: light petroleum[b]	105(block)/1.2	60
(14) *p*-fluoro		75(block)/0.8	80
(12) *p*-methoxy		95(block)/0.5	80
(18) *p*-cyano	1:19, ether: light petroleum[c]	41-43[d]	85
(15) *p* -H	benzene[b]	82(block)/0.8 (142/50)[e]	70

NOTES

(a) if different from Table 6-1.
(b) purification by preparative TLC using silica gel plates.
(c) purification by column chromatography using aluminium oxide.
(d) melting point.
(e) literature boiling point[352].

Table 6-2 lists the deuterium labelled prepared by the method detailed above.

1-(4-Cyanophenyl)-1-butanone was a new compound. The microanalytical, PMR, IR and MS data are shown below.

Formula: $C_{11}H_{11}NO$ m.p. 40-42°C

Analysis: requires C = 76.27 H = 6.40 N = 8.09 %

found C = 76.40 H = 6.47 N = 7.99 %

PMR ($CDCl_3$): δ 1.02; triplet; 6.0Hz.; 3H; ($\underline{CH_3}$-)

1.75; quintet; 7.0Hz.,6.0Hz.;2H; (-$\underline{CH_2}$-CH_3)

3.0; triplet; 7.0Hz; 2H; (-CO-$\underline{CH_2}$-)

IR(nujol): ν_{max} = 2220 cm^{-1}; (w); (-C≡N)
1670 cm^{-1}; (s,sh); (C=O)
1600 cm^{-1}; (s); (aromatic)
1570 cm^{-1}; (m); (aromatic)
1505 cm^{-1}; (m); (aromatic).

MS: m/z 173; 18%; $(M)^{+\cdot}$

145; 20%; $(M-C_2H_4)^{+\cdot}$

130; 100%; $(M-C_3H_7)^{+\cdot}$

102; 35%; $(m/z\ 130-CO)^{+}$

75; 6% $(m/z\ 102-HCN)^{+}$

The PMR, IR and MS data for each of the compounds listed in tables 6-1 and 6-2 were analysed in terms of the individual structural characteristics of each compound. Typically, the PMR spectra of the deuterium labelled compounds (12)-(18) showed broadening of the methyl resonance (approx. δ1.0) characteristic of deuterium incorporation. The deuterium coupling was of the order of 1.0Hz. The IR spectra of the deuterium labelled ketones showed an absorption in the region ν_{max} 2160 cm^{-1}, indicating the

presence of a C-$^{2}H_{1}$ stretching vibration. MS analysis indicated that the deuterium incorporation in each compound was ≥99%.

PREPARATION OF 4-($^{2}H_{1}$)-1-(4-HYDROXYPHENYL)-1-BUTANONE (19)

This compound was prepared in 60% yield (0.11g) by heating 4-($^{2}H_{1}$)-1-(4-methoxyphenyl)-1-butanone (12) (9.20g; 1.1 mmol) with anhydrous pyridine hydrochloride (0.60g; 5.2 mmol) at 140°C for 6h. This procedure follows that described by Prey[265]. The crude product was purified by preparative TLC (silica gel; 1:4, ethyl acetate: benzene) and recrystallized from an acetone-petroleum ether mixture to a constant melting point (m.p. 88-90°C; lit.[353] 91°C). The PMR ($CDCl_3$), IR (nujol) and MS data were obtained and analysed to ascertain the nature and purity of compound (19).

PREPARATION OF 4-(4-($^{2}H_{1}$)-BUTYRYL)BENZAMIDE (9)

4-Butyrylbenzamide (9) was prepared in 91% yield (0.20g) from 1-(4-cyanophenyl)-1-butanone (0.20g; 1.2 mmol) by heating with a mixture of hydrogen peroxide solution (3%; 5.6g; 4.9 mmol) and a potassium hydroxide solution (25% w/v; 1.8g; 8.0 mmol), according to the method of Buck and Ide[266]. Recrystallization of the crude product from acetone, light petroleum yielded pure 4-butyrylbenzamide, m.p. 177-178°C.

Formula:	$C_{11}H_{13}NO_2$			m.p. 177-178°C	
Analysis:	required	C=69.09	H=6.85	N=7.33	%
	found	C=69.27	H=6.75	N=7.27	%

PMR ($^2H_6$-acetone): δ 1.00; triplet; 7.0Hz; 3H; (CH_3-)

1.85 quintet; 2.0Hz; ($-CH_2-CH_2-CH_3$)

2.10; broad singlet; 2H; ($-NH_2$)

3.10; triplet; 6.0Hz; 2H; ($-CO-CH_2-$)

8.13; singlet; 4H; (aromatic)

IR (nujol): ν_{max} 3420 cm^{-1}; (m, sh); (N-H)

3160 cm^{-1}; (w, br); (N-H)

1680 cm^{-1}; (s); (C=O)

1640 cm^{-1}; (m, br); (amide 1 and 2 bands)

MS: m/z 191; 29%; $(M)^{+\cdot}$

163; 7%; $(M-C_2H_4)^{+\cdot}$

148; 100% $(M-C_3H_7)^+$

120; 8% $(m/z\ 148-CO)^+$

103; 19%; $(m/z\ 120-NH_3)^+$

75; 6% $(m/z\ 103-CO)^+$

4-(4-($^2H_1$)-Butyryl)benzamine (20) (m.p. 177-178°C) was prepared in 80% yield (0.18g) in the same manner as described above for ketone (9). The PMR, IR and MS were analysed to determine the purity of this compound.

ATTEMPTED PREPARATIONS OF 1-(4-NITROPHENYL)-1-BUTANONE

METHOD(1): ALKYLATION OF 4-NITROBENZOYL CHLORIDE

Anhydrous cadmium chloride (2.0g; 10.8 mmol) was added in portions to a refluxing ethereal solution of propylmagnesium bromide under an atmosphere of nitrogen. Propylmagnesium bromide was prepared in the usual manner[343] from bromopropane (2.66g; 21.6 mmol)

and magnesium (0.58g; 23.8 mmol) in anhydrous ether (20ml). The resulting mixture was sitrred and heated under reflux until it gave a negative result for the Gilman test for Grignard reagents[354]. The ether was removed from the reaction mixture and anhydrous benzene (20 ml) added.

4-Nitrobenzoyl chloride (m.p. 72-74°C; lit.[355] 75°C) was prepared in 82% yield (4.54g) by treating sodium 4-nitrobenzoate (5.0g; 28.2 mmol) with oxalylchloride (5.0g; 39.4 mmol) by the method of Adams and Ulich[273].

A solution of 4-nitrobenzoyl chloride (1.0g; 5.4 mmol) in anhydrous benzene (20 ml) was added slowly (0.5h) to the benzene solution of dipropylcadmium maintained under an atmosphere of nitrogen. The reaction mixture was stirred at 5°C for 1h and then at 20°C for 12h. This follows the procedure outlined by Cason[272,356]. Hydrolysis of the reaction mixture was effected by the successive addition of water (10 ml) and dilute hydrochloric acid (2M; 5 ml). The separated aqueous phase was extracted with benzene (2 x 20 ml) and the combined organic extracts washed with dilute sodium hydroxide solution (5%; 10 ml) and water (10 ml). The benzene solution was dried with magnesium sulphate and the solvent removed *in vacuo* yielding a red oil. Preparative TLC (silica gel; 1:1, ether: light petroleum) of the distilled red oil (b.p. 145°C(block)/3.5 mm Hg) resulted in the isolation of two major products. The PMR and IR spectral data of both compounds indicated that the desired product had not been produced and neither compound was further

characterized†.

METHOD (2): ALKYLATION OF 2-BROMO-1-(4-NITROPHENYL)-1-ETHANONE (21)

A solution of 9-borabicyclo[3.3.1]nonane (9BBN) in tetrahydrofuran (0.9M) was prepared from a standard tetrahydrofuran solution of diborane[357] (0.9M; 108.7 ml; 0.1 mol) and cyclooctadiene (10.89; 0.1 mol) by the method of Knights and Brown[358,359].

2-Bromo-1-(4-nitrophenyl)-1-ethanone (21) was prepared in 61% yield (4.5g) from copper^{II} bromide (11.2g; 50.1 mmol) and 4-nitroacetophenone (5.0g; 30.2 mmol) by the method of King and Ostrum[360].

9-Ethyl-9-borabicyclo[3.3.1]nonane (22) was prepared by bubbling anhydrous ethylene into a tetrahydrofuran solution of 9BBN (0.9M; 11.0 ml; 10.0 mmol) at 0^{o}C for 3h. A solution of 2-bromo-1-(4-nitrophenyl)-1-ethanone (21) in anhydrous *tert*-butyl alcohol (20 ml) and anhydrous tetrahydrofuran (2 ml), was added to the cooled solution of 9-ethyl-9BBN (22) prepared above. Freshly prepared potassium *tert*-butoxide (0.85g; 10.0 mmol) in anhydrous *tert*-butyl alcohol (20 ml) was added to the reaction mixture over 0.75h. The reaction mixture was stirred at 0^{o}C for 1h. and at 20^{o}C for a further 3h. Both the reaction and work-up procedures follow that described by Brown and co-workers[274,275].

Removal of the organic solvents, after the work-up procedure, yielded a dark red oil, shown by analytical TLC (silica gel; 1:1,

---

† The above reaction procedure for preparing 1-(4-nitrophenyl)-1-butanone was repeated using benzoyl chloride. The PMR and IR indicated that 1-phenyl-1-butanone had been produced (~60% yield).

ethyl acetate: benzene) to consist of five components. Isolation of each of the components was achieved by preparative TLC (silica gel; 1:1, ethyl acetate: benzene). PMR and IR data indicated that none of the components were the required product, and no further structural characterization was carried out.

The above reaction procedure was carried out, on 1/10th of the above scale, with potassium 2,4,6-tri-(*tert*-butyl)phenoxide (0.3g; 1.0 mmol) in place of potassium *tert*-butoxide, with no improvement on the complexity of the product mixture[361].

1-($^2H_3$)-3-PROPANOL

METHOD (1): ALKYLATION OF ETHYLENE OXIDE

The preparation of 1-propanol was attempted by the reaction of ethylene oxide (6.16g; 140.0 mmol) with methylmagnesium iodide, prepared from iodomethane (9.9g; 70.0 mmol) and magnesium (1.7g; 70.0 mmol) in anhydrous ether (50 ml)[343]. This is the method of Huston and D'Arcy[278]. The procedure was repeated several times and the crude products obtained after work up of the reaction mixture were analysed by GLC using column A at a temperature of 110°C. Occasionally, the yield of 1-propanol was low and the amount of polymeric material high. Due to the fickle nature of this reaction another synthetic route to 1-($^2H_3$)-3-propanol was attempted.

METHOD (2): ALKYLATION OF ACETIC ACID

Propionic acid was prepared in 30% yield (as determined by GLC analysis using column A at a temperature of 120°C) by an adaption of the method of Pfeffer and Silbert[279] and Creger[280].

Lithium isopropylcyclohexylamide† was prepared by the dropwise addition of butyllithium in hexane (1.8M; 4.6ml; 8.3 mmol) to an anhydrous tetrahydrofuran solution (20 ml) of isopropylcyclohexylamine (1.17g; 8.3 mmol) at 0°C, under an atmosphere of nitrogen. The resulting solution was stirred at 0°C for 0.5h, cooled to -78°C and acetic acid (0.25g; 4.3 mmol) was added, dropwise. After stirring the reaction mixture for 0.5h at -78°C, hexamethylphosphoramide (1.83g; 8.3 mmol) was added,followed by iodomethane (0.59g; 4.3 mmol). After stirring at -78°C for 0.5h, the reaction mixture was warmed to 20°C and stirred for a further 3h. The work-up procedure follows that described by Pfeffer and Silbert[279].

METHOD (3): ALKYLATION OF *tert*-BUTYL ACETATE

tert-Butyl acetate (b.p. 95-98°C; lit.[281] 97-98°C), was prepared from acetic anhydride (100 ml) anhydrous *tert*-butyl alcohol (100 ml) and anhydrous zinc chloride (0.3g) in 50% yield by the method of Vogel[281].

tert-Butyl 3-($^2H_3$)-propionate (25) (b.p. 95-100°C; lit.[362] 118°C/760 mm Hg was prepared in 94% yield (2.6g) from *tert*-butyl acetate (2.4g; 2.1 mmol) and ($^2H_3$)-iodomethane (98 atom% D; 3.0g; 2.1 mmol) according to the method of Rathke and Lindert[282]. The base used in the alkylation was lithium isopropylcyclohexylamide

---

† References 279 and 280 use lithium di-isopropylamide as the base for forming the dianion of the acid to be alkylated. A trial reaction using the procedure described above, excepting that the reaction temperature was maintained at 0°C, gave none of the required product as determined by GLC analysis (column A, at a temperature of 120°C).

prepared from butyllithium in hexane (1.8M; 1.3 ml; 2.4 mmol) and isopropylcyclohexylamine (0.33g; 2.4 mmol)†. Tetrahydrofuran was distilled from the reaction mixture and the residue diluted with ether. The ethereal solution was extracted with dilute sulphuric acid (10%), until no cloudiness occurred when the acid wash was neutrallized, washed with saturated sodium bicarbonate solution (2 x 10 ml) and dried with potassium carbonate. Analysis of the ethereal solution by GLC using column A at a temperature of 55°C and column C at a temperature of 100°C indicated that *tert*-butyl 3-($^2H_3$)-propionate (25) had been formed in quantitative yield.

tert-Butyl propionate (b.p. 117-118°C), used for comparison purposes in GLC analyses, was prepared in 60% yield (17.0g) from propionyl chloride (20.0g; 0.22 mol), *tert*-butyl alcohol (16.0g; 0.22 mol) and N,N-dimethylaniline (28.0g; 0.23 mol) by the method of Vogel[281].

tert-Butyl 3-($^2H_3$)-propionate (25) (2.6g; 20.0 mmol) was reduced by lithium aluminium hydride (1.63g; 43.0 mmol) in anhydrous ether under an atmosphere of nitrogen. The reaction mixture was stirred and heated under reflux for 10h, then cooled to 0°C and excess lithium aluminium hydride and organometallic salts decomposed by the addition of wet ether. Distillation gave 1-($^2H_3$)-3-propanol (b.p. 92-98°C; lit.[363] 97.2°C) in 65% yield (0.8g).

---

† The addition of hexamethylphosphoramide (0.53g; 2.4 mmol) as a cosolvent did not have any effect on the yield of alkylated product and so was omitted from the procedure.

1-BROMO-3-($^2H_3$)-PROPANE (24)

This compound was prepared in 14% isolated yield by reacting 1-($^2H_3$)-3-propanol (0.8g; 12.7 mmol) with phosphorus tribromide (1.24g; 4.6 mmol) according to the method of Noller and Dinsmore[267]. Purification of the crude 1-bromo-3-($^2H_3$)-propane was achieved by preparative GLC using column D at a temperature of 70°C.

4-($^2H_3$)-1-PHENYL-1-BUTANONE (23)

This compound (b.p. 82-85°C(block)/0.8 mm Hg; lit[352] 142°C/ 50 mm Hg.) was prepared by oxidation of 4-($^2H_3$)-1-phenyl-1-butanol using pyridinium chlorochromate (0.55g; 2.6 mmol) and sodium acetate (0.1g; 1.4 mmol) in dichloromethane (20 ml)[264]. 4-($^2H_3$)-1-phenyl-1-butanol was prepared from benzaldehyde (0.18g; 1.7 mmol) and 3-($^2H_3$)-propylmagnesium bromide made from 1-bromo-3-($^2H_3$)-propane (0.22g; 1.7 mmol) and magnesium (0.05g; 1.9 mmol) in anhydrous ether (10 ml)[343]. The procedure used is described for the preparation of the 4-($^2H_1$)-1-(4-substituted phenyl)-1-butanones. The yield of 4-($^2H_3$)-1-phenyl-1-butanone (23) was 77% (0.2g). MS analysis indicated deuterium incorporation of 98%.

4-($^2H_1$)-1-HYDROXY-1-PHENYL-1-BUTANONE (29)

The starting point in this synthetic sequence is the esterification of 4-benzoylbutanoic acid. 4-Benzoylbutanoic acid (m.p. 113-114°C; lit.[286] 116°C) was prepared in 90% yield by the Friedel-Crafts acylation of benzene with succinic anhydride according to the method of Somerville and Allen[364]. The acid (20.0g; 0.11 mol) was converted to ethyl 4-benzoylbutyrate by heating under reflux in anhydrous ethanol (100 ml) containing a catalytic amount of 4-toluenesulphonic acid

(0.1g), for 24h. Analytical TLC (silica gel; 3:7, ether: light petroleum), PMR ($CDCl_3$) and IR (film) indicated that the reaction produced the ethyl ester in quantitative yield and it was used without purification.

Ethyl 4,4-ethylenedioxy-4-phenylbutyrate (32) was prepared in 100% yield (crude) by heating a benzene solution of ethyl 4-benzoylbutyrate (25.0g; 0.11 mol) and 1,2-dihydroxyethane (24.0g; 0.39 mol) containing a catalytic amount of 4-toluenesulphonic acid (0.1g), under reflux with continuous water separation.

The ethylene acetal ester (32) (27.5g; 0.11 mol) was reduced to 4-hydroxy-1-phenyl-1-butanone ethylene acetal (31) by lithium aluminium hydride (6.4g; 0.17 mol) in anhydrous ether (100 ml) under an atmosphere of nitrogen. After refluxing the ethereal solution for 3h, the reaction mixture was cooled to 0°C and water (6.4 ml), sodium hydroxide solution (15%; 6.4 ml) and water (19.2 ml) were successively added. Analysis of the crude product, after removal of the ether, by TLC (silica gel; ether), PMR ($CDCl_3$) and IR (film) indicated that none of the ethylene acetal ester (32) remained. The detailed procedure for the synthetic steps to this point are described by Ward and Sherman[286].

4-Hydroxy-1-phenyl-1-butanone ethylene acetal (31) (24.0g; 0.11 mol) was oxidized to 4,4-ethylenedioxy-4-phenyl-butanal (30) using pyridinium chlorochromate (36.2g; 0.17 mol) in dichloromethane (100 ml) by the method of Corey and Suggs[264]. Removal of the solvents after work-up produced a light yellow oil. Distillation 0.2 mm Hg.) gave pure 4,4-ethylenedioxy-4-phenyl-butanal (30) in 78% yield (18.0g).

PMR($CDCl_3$): δ 2.25; (multiplet); 4H; ($-CH_2-CH_2-CO-$)

3.67; (multiplet); 4H; ($-O-CH_2-CH_2-O-$)

7.25; (multiplet); 5H; (aromatic)

9.50; (singlet); 1H; ($-CO-H$)

IR (film): ν_{max} 2860 cm^{-1}; (w); (CHO)

2780 cm^{-1}; (w); (CHO)

1730 cm^{-1}; (s); (CO)

1040 cm^{-1}; (s); (C-O-C)

4,4-Ethylenedioxy-4-phenyl-butanal (30) (4.0g; 19.4 mmol) was reduced with lihtium aluminium deuteride (99 atom % D; 0.3g; 7.1 mmol) in anhydrous ether (100 ml) under an atmosphere of nitrogen. After heating under reflux for 1h., the reaction mixture was cooled to 0°C and water (0.3 ml), sodium hydroxide solution (15%; 0.3 ml) and water (0.9 ml) were successively added while stirring vigorously. The white suspension was filtered from the ethereal solution and washed with ether (2 x 20 ml). Removal of the ether *in vacuo* after drying the solution with magnesium sulphate, yielded 4.1g of crude 4-($^2H_1$)-4-hydroxy-1-phenyl-1-butanone ethylene acetal. The IR (film) of this product showed the absence of the aldehydic carbonyl stretching frequency (ν_{max} 1730 cm^{-1}) and the presence of a weak absorption band at ν_{max} 2140 cm^{-1} (C-^2H stretch) and a broad band at ν_{max} 3400 cm^{-1} (O-H stretch).

Removal of the ethylene acetal function was achieved by stirring a solution of 4-($^2H_1$)-4-hydroxy-1-phenyl-1-butanone ethylene acetal (4.1g; 19.6 mmol) in tetrahydrofuran (50 ml) and water (20 ml) containing 4-toluenesulphonic acid (0.5g), for 48h at 20°C. The tetrahydrofuran, water solution was diluted with a potassium carbonate

solution (10%; 10 ml) and extracted with ether (5 x 20 ml). The combined organic extracts were washed with saturated sodium chloride solution (10 ml) and water (2 x 10 ml) and dried with magnesium sulphate. Removal of the organic solvents *in vacuo*, and distillation (b.p. 130-135°C(block)/0.1 mm Hg; lit.[365] m.p. 32-33°C) gave pure 4-($^2H_1$)-4-hydroxy-1-phenyl-1-butanone (29) in 88% yield (based on the starting aldehyde (30)) (2.8g).

4-BROMO-4-($^2H_1$)-1-PHENYL-1-BUTANONE (26)

1-($^2H_1$)-4-Oxo-4-phenylbutyl 4-toluenesulphonate (28) (1.9g) was prepared from 4-($^2H_1$)-4-hydroxy-1-phenyl-1-butanone (29) (1.0g; 0.1 mmol) and 4-toluenesulphonyl chloride (2.3g; 12.2 mmol) in anhydrous pyridine (20 ml) in 98% yield, by standard methods[285].

4-Bromo-4-($^2H_1$)-1-phenyl-1-butanone (26) (b.p. 95°C (block)/0.1 mm Hg; lit.[366] 157°C/15.0 mm Hg) was prepared in 94% yield (0.14g) from 1-($^2H_1$)-4-oxo-4-phenylbutyl 4-toluenesulphonate (28) (0.2g; 0.6 mmol) and anhydrous lithium bromide (0.1g; 1.0 mmol) in anhydrous hexamethylphosphoramide (10 ml), by the method of Beckwith and Moad[284].

4-CHLORO-4-($^2H_1$)-1-PHENYL-1-BUTANONE (27)

This compound was prepared in 90% yield (0.1g) from 1-($^2H_1$)-4-oxo-4-phenylbutyl 4-toluenesulphonate (28) (0.2g; 0.6 mmol) and anhydrous lithium chloride (0.04g; 1.0 mmol) in anhydrous hexamethylphosphoramide (10 ml) by the method of Beckwith and Moad[284].

ATTEMPTED SYNTHESIS OF ^{13}C-1-PHENYL-1-BUTANONES (33)-(36)

The following methods were used in the attempted synthesis of 1-(^{13}C)-1-phenyl-1-butanone (33), 2-(^{13}C)-1-phenyl-1-butanone (34), 3-(^{13}C)-1-phenyl-1-butanone (35), 4-(^{13}C)-1-phenyl-1-butanone (36).

METHOD (1):

Acetophenone (0.5g; 4.2 mmol) was alkylated using potassium *tert*-butoxide (1.5g; 4.2 mmol) and iodoethane (0.7g; 4.2 mmol) in dimethylsulphoxide (7.6 ml) by the method of Heiszwolf and Kloosterziel[287]. The crude products obtained after work-up, were separated by preparative TLC (silica gel; 3:17, ether: light petroleum). The components of the product mixture with R_f 0.3 and R_f 0.4 were found by PMR ($CDCl_3$) analysis to be acetophenone (50%) and 1-phenyl-1-butanone (10%) respectively. The component at R_f 0.5 was identified as 2-ethyl-1-phenyl-1-butanone (37) (40%) by PMR ($CDCl_3$), IR (film) and MS analysis. Distillation of the crude product (b.p. 60^{o}C (block)/0.05 mm Hg; lit.[367] 117-118^{o}C/7 mm Hg) gave pure 2-ethyl-1-phenyl-1-butanone.

METHOD (2):

The attempted alkylation of acetophenone (0.5g; 4.2 mmol) with bromoethane (0.46g; 4.2 mmol) was carried out in a heterogeneous mixture of dichloromethane (10 ml) and an aqueous sodium hydroxide solution (50%; 10 ml) containing triethylbenzyl ammonium chloride (0.1g) as the phase transfer catalyst. This follows the procedure of Jończyk, Serafin and Makosza[368] and Makosza[288].

Analysis of the reaction mixture by TLC (silica gel; 3:17, ether: light petroleum) indicated that stirring at 20^{o}C for 24h effects no reaction. After stirring at 80^{o}C for 48h, GLC analysis using

column C at a temperature of 170°C indicated that 1-phenyl-1-butanone had formed in 10% yield. The remainder of the volatile material was determined to be acetophenone.

The above procedure was repeated using diethylsulphate (1.0g; 6.5 mmol) as the alkylating agent. Starting material was detected, by GLC analysis using column C at a temperature of 170°C, after 72h. at 80°C.

The catalytic phase transfer alkylation of acetophenone (0.5g; 4.2 mmol) as described above, was repeated using tetrabutylammonium hydrogen sulphate (1.43g; 4.2 mmol)[369] and iodoethane (1.32g; 8.4 mmol). Analysis of the reaction mixture by GLC using column C at a temperature of 170°C indicated that there were three components; acetophenone (55%), 1-phenyl-1-butanone (25%) and 2-ethyl-1-phenyl-1-butanone (20%).

METHOD (3):

Acetophenone (0.25g; 2.1 mmol) was alkylated, according to the method of Brown[289,290], using potassium hydride (50% in paraffin; 0.2g; 2.1 mmol) in anhydrous tetrahydrofuran (10 ml) and iodoethane (0.33g; 2.1 mmol). The results of this experiment are listed in table 6-3.

In an attempt to optimize the yield of 1-phenyl-1-butanone by this method, a variety of reaction conditions were employed. The results of these experiments are listed in table 6-3. In each case, analysis of the product mixture was by GLC using column C at a temperature of 170°C or column A at a temperature of 150°C.

Table 6-3

	Equivalents				Products (%)		
Comments	Acetophenone	Iodoethane	Solvent	Temperature(^{o}C)	Acetophenone	monoalk	dialk
normal[a]	1.0	1.0	THF[b]	-78	44	19	37
normal	1.5	1.0	THF	-78	40	21	39
reverse[a]	1.1	3.0	DMF[c]	0.0	14	11	75

NOTES

(a) normal addition is the addition of iodoethane to the potassium enolate
reverse addition is the addition of the potassium enolate to iodoethane.
(b) THF - tetrahydrofuran
(c) DMF - dimethylformamide

METHOD (4):

[1-(Phenylvinyl)oxy]trimethylsilane (39) was prepared in 60% yield (3.7g) from acetophenone (3.8g; 32.0 mmol), potassium hydride (50% in paraffin; 2.6g; 32.0 mmol) and trimethylsilyl chloride (5.2g; 48.0 mmol) in anhydrous tetrahydrofuran (100 ml) by the method of Brown[289]. Distillation (b.p. 102-106°C/20 mm Hg) of the crude product after removal of the solvent yielded pure silyl enol ether (39). Identification of this compound was made by comparison of the PMR ($CDCl_3$) and IR (film) spectra with those published in the literature[370].

Using 2,2́ -bipyridyl (0.01g) as an indicator[291], [1-(phenylvinyl) oxy]trimethylsilane (39) (0.24g; 1.3 mmol) in anhydrous tetrahydrofuran (5 ml) was added in a dropwise fashion, to a stirred solution of methyllithium (1.3M; 1.0 ml; 1.3 mmol) in anhydrous tetrahydrofuran at -78°C. When the colour of the solution had changed from purple to yellow (indicator), iodoethane (0.2g; 1.3 mmol) was added in one portion. The reaction mixture was stirred for 1h. at -78°C and then at 20°C for a further 1h. Saturated ammonium chloride solution (10 ml) was added to the reaction mixture and the separated aqueous phase extracted with ether (3 x 10 ml). Drying of the ethereal solution with magnesium sulphate and removal of the solvent *in vacuo* yielded a colourless oil. GLC analysis of the oil with column A at a temperature of 170°C, indicated that the products of the reaction were acetophenone (81%), 1-phenyl-1-butanone (12%) and 2-ethyl-1-phenyl-1-butanone (7%).

METHOD (5):

Lithium di-isopropylamide was prepared at -78°C by the addition of butyllithium, in hexane (2.2M; 0.8 ml; 1.7 mmol), to an anhydrous

tetrahydrofuran (20 ml) solution of di-isopropylamine (0.17g; 1.7 mmol) under an atmosphere of nitrogen. After stirring the resultant solution for 1h. at -78°C, acetophenone (0.2g; 1.7 mmol) in anhydrous tetrahydrofuran (5 ml) was added dropwise, and the solution stirred for a further 0.5h. Iodoethane (0.27g; 1.7 mmol) was added in one portion and the solution was allowed to warm slowly to 20°C. Saturated ammonium chloride solution (10 ml) was added and the resulting mixture extracted with ether (3 x 20 ml). The ethereal extracts were washed successively with dilute hydrochloric acid (2M; 10 ml) and water (10 ml) and then dried with magnesium sulphate. GLC analysis using column C at a temperature of 170°C indicated that the ethereal solution contained acetophenone (48%), 1-phenyl-1-butanone (26%) and 2-ethyl-1-phenyl-1-butanone (26%).

^{13}C LABELLED 1-PHENYL-1-BUTANONES (33)-(36)

The method described below was used to prepare the following ^{13}C-labelled compounds (yield); 1-(^{13}C)-1-phenyl-1-butanone (33) (60%), 2-(^{13}C)-1-phenyl-1-butanone (34) (65%), 3-(^{13}C)-1-phenyl-1-butanone (35) (63%) and 4-(^{13}C)-1-phenyl-1-butanone (36) (65%). Each of the ketones prepared were purified by HPLC eluting with a 1:4, ether: hexane solvent mixture and detected using a UV detection system. The general method is described for the preparation of 3-(^{13}C)-1-phenyl-1-butanone (35).

Acetophenone dimethylhydrazone (40)† was prepared in quantitative

† The ^{13}C-labelled acetophenone dimethylhydrazones were prepared in an identical manner to the un-labelled hydrazone using 0.21g of 1-(^{13}C)-1-phenyl-1-ethanone (91.8 atom %^{13}C) and 0.21g of 2-(^{13}C)-1-phenyl-1-ethanone (91.3 atom % ^{13}C).

yield (2.7g) by heating under reflux for 24h. a solution of acetophenone (2.0g; 16.7 mmol) and N,N-dimethylhydrazine (4.0g; 66.7 mmol) in anhydrous ethanol (20 ml) under an atmosphere of nitrogen[292]. Distillation (b.p. 95-100°C (block)/3.0 mm Hg; lit.[292] 55-56°C/0.15 mm Hg) yielded pure acetophenone dimethylhydrazone whose PMR ($CDCl_3$), IR (film) and MS data were consistent with the hydrazone structure.

Preparation of α-lithiated acetophenone dimethylhydrazone (0.16g; 1.0 mmol) was achieved by adding the hydrazone to a tetrahydrofuran solution of lithium di-isopropylamide at 0°C. The lithium di-isopropylamide solution was prepared from butyllithium, in hexane (1.3M; 0.9 ml; 1.2 mmol), and di-isopropylamine (0.12g; 1.2 mmol) in anhydrous tetrahydrofuran (50 ml) at 0°C. 1-(^{13}C)-1-Iodoethane (91.1 atom % ^{13}C; 0.19g; 1.2 mmol)† was added in one portion to the stirred solution of the lithium salt of the hydrazone. The reaction procedure and method of workup follows that described by Corey and Enders[293]. 3-(^{13}C)-1-Phenyl-1-butanone dimethylhydrazone (41) formed in this manner, was used without further purification.

3-(^{13}C)-Phenyl-1-butanone (35) was generated from the dimethylhydrazone (41) prepared above, by stirring in a tetrahydrofuran (10 ml) and water (10 ml) solution with copper^{II} acetate (0.2g; 1.3 mmol) according to the method of Corey and Knapp[294].

---

† To prepare 4-(^{13}C)-1-phenyl-1-butanone (36), 1-(^{13}C)-2-iodoethane (90.6 atom % ^{13}C) was used.

4-AND 3-(^{13}C)-2-ETHYL-1-PHENYL-1-BUTANONES (43), (42)

These compounds were prepared from 4-(^{13}C)-1-phenyl-butanone (36) (0.04g; 0.3 mmol) and 3-(^{13}C)-1-phenyl-1-butanone (35) (0.04g; 0.3 mmol) respectively, using potassium hydride (50% in paraffin; 0.04g; 0.5 mmol) and iodoethane (0.17g; 1.0 mmol) by the method of Brown[289,290].

Purification of the ketones (42) and (43) was achieved by preparative TLC (silica gel; 3:17, ether: light petroleum) followed by distillation: compound (42), 90°C (block)/0.1 mm Hg; compound (43), 70°C (block)/0.05 mm Hg; lit.[367] 117-118°C/7 mm Hg. The yield of 4-(^{13}C)-2-ethyl-1-phenyl-1-butanone (43) was 50% (0.02g) and of 3-(^{13}C)-2-ethyl-1-phenyl-1-butanone (42) was 55% (0.03g).

4-($^{2}H_3$)-2-ETHYL-1-(4-SUBSTITUTED PHENYL)-1-BUTANONES (44)-(46)

The compounds 4-($^{2}H_3$)-2-ethyl-1-phenyl-1-butanone (44), 4-($^{2}H_3$)-2-ethyl-1-(4-methoxyphenyl)-1-butanone (43) and 4-($^{2}H_3$)-2-ethyl-1-(4-cyanophenyl)-1-butanone (46) were prepared from 1-phenyl-1-butanone (2) (0.15g; 1.0 mmol), 1-(4-methoxyphenyl)-1-butanone (6) (0.15g; 0.9 mmol) and 1-(4-cyanophenyl)-1-butanone (7) (0.15g; 1.0 mmol) respectively, using potassium hydride (50% in paraffin; 0.08g; 1.0 mmol) and 1-($^{2}H_3$)-2-iodoethane (0.2g; 1.2 mmol) by the method of Brown[289,290]. Purification of the ketones (44), (45) and (46) was achieved by preparative TLC (silica gel; 3:17, ether: light petroleum) and distillation. The yields of ketones (44), (45) and (46) were 70% (0.13g), 50% (0.1g) and 55% (0.11g) respectively.

3-($^2H_2$)-2-ETHYL-1-PHENYL-1-BUTANONE (47)

1-($^2H_2$)-1-Ethanol was prepared in 60% yield (1.1g) by the reduction of phenyl acetate (5.0g; 36.8 mmol) with lithium aluminium deuteride (99 atom % D; 2.2g; 55.2 mmol) in anhydrous ether (25 ml) under an atmosphere of nitrogen.

1-($^2H_2$)-1-Iodoethane was prepared in anhydrous chloroform (10 ml) from 1-($^2H_2$)-1-ethanol (1.1g; 22.9 mmol) using trimethylsilyl iodide (9.2g; 45.8 mmol) in 40% yield (1.4g) according to the method of Jung and co-workers[297,298].

The preparation of 3-($^2H_2$)-2-ethyl-1-phenyl-1-butanone (47) involved the alkylation of the potassium enolate of 1-phenyl-1-butanone (0.15g; 1.0 mmol) with 1-($^2H_2$)-1-iodoethane (0.2g; 1.2 mmol) in anhydrous tetrahydrofuran (20 ml) under an atmosphere of nitrogen according to the method of Brown[289,290]. Distillation of the crude ketone (47) (b.p. 90°C (block)/0.1 mm Hg; lit.[367] 117-118°C/7 mm Hg) yielded the pure compound in 65% yield (0.12g).

2-ETHYL-1-PHENYL-4-PENTEN-1-ONE (48)

This compound was prepared from N-(1-propylbenzylidene)cyclohexylamine by the method of Stork and Dowd[300,299].

Purification was achieved by distillation (b.p. 73-76°C/0.1 mm Hg; lit.[371] 115°C/5.0 mm Hg) followed by preparative TLC (silica gel; benzene) and finally bulb to bulb distillation.

ATTEMPTED PREPARATION OF 4-CYCLOPROPYL-1-PHENYL-1-BUTANONE (49)

METHOD (1):

1-Phenyl-5-hexen-1-ol (50) (b.p. 125-130°C/1.0 mm Hg) was prepared by the dropwise addition of an ethereal solution (5 ml) of benzaldehyde (2.0g; 18.9 mmol) to a stirred solution (50 ml) of

1-pent-4-enemagnesium bromide in ether at 20°C. The Grignard reagent was prepared in the usual manner from 1-bromo-4-pentene (3.4g; 22.8 mmol) and magnesium (0.6g; 25.0 mmol) in anhydrous ether (50 ml)[343]. After stirring for 1h. at 20°C, the reaction mixture was heated under reflux for a further 1h. On cooling, saturated ammonium chloride solution (10 ml) was added. The aqueous phase was separated and extracted with ether (3 x 20 ml). The ethereal extracts were combined and washed successively with saturated sodium chloride solution (10 ml) and water (10 ml), and dried with magnesium sulphate. Removal of the ether *in vacuo* and distillation of the resulting oil (b.p. 125-130°C/1.0 mm Hg) gave 1-phenyl-5-hexen-1-ol (50) in 96% yield (3.2g).

1-Phenyl-5-hexen-1-ol (50) (0.4g; 2.3 mmol) was characterized as its ketone, 1-phenyl-5-hexen-1-one which was obtained by pyridinium chlorochromate oxidation using the method of Corey and Suggs[264]. Distillation of the crude product (b.p. 130-135°C(block)/ 6.0 mm Hg; lit[372] b.p. 122°C/80 mm Hg) gave 1-phenyl-5-hexen-1-one in 82% yield (0.33g). PMR ($CDCl_3$), IR (film) and MS data were consistent with the structural characteristics of this compound.

The Simmons-Smith reagent was prepared in anhydrous ether (20 ml) from zinc dust (1.49g; 22.8 mmol), copper^{I} chloride (0.27g; 27.3 mmol) and di-iodomethane (1.85g; 69.0 mmol) by refluxing for 0.5h under an atmosphere of nitrogen[301]. 1-Phenyl-5-hexen-1-ol (50) (0.4g; 22.7 mmol) in anhydrous ether (5 ml) was added dropwise and the reaction mixture heated under reflux for 72h. Addition of saturated ammonium chloride solution (10 ml), extraction of the separated aqueous phase with ether (3 x 10 ml) washing the organic phase with saturated sodium carbonate solution (2 x 10 ml), drying

with magnesium sulphate and removal of the ether *in vacuo* yielded the crude product. GLC analysis using Column D at a temperature of 160°C, indicated a complex mixture of eight components; the major component being 1-phenyl-5-hexen-1-ol (50).

The above procedure was repeated using dimethoxyethane (5 ml) as a cosolvent. GLC analysis using column D at a temperature of 165°C indicated that a complex mixture containing 40% starting material was formed. The reaction mixture was not further characterized.

METHOD (2)

1-Phenyl-5-hexen-1-ol (50) (0.1g; 0.6 mmol) was added to a stirred heterogeneous mixture of chloroform (10 ml) and sodium hydroxide solution (20%; 10 ml), containing triethylbenzyl-ammonium chloride (0.05g; 0.2 mmol). Analytical TLC (silica gel; 3:7; ether: petroleum ether) indicated only starting material after stirring for 12h. at 25°C.

The reaction mixture was heated to 60°C and stirred for 48h. Analytical TLC indicated that the major component was starting material.

METHOD (3)

An ethereal solution of diazomethane was generated from N-nitrosourea by standard methods[373] and used without distillation. To this solution, 1-phenyl-5-hexen-1-ol (50) (0.2g; 1.2 mmol) and a catalytic amount of copper^{I} chloride (<0.05g) was added. After the evolution of nitrogen had ceased, the ether solution was washed with saturated sodium chloride (10 ml) solution and dried with

potassium carbonate. The ether was removed *in vacuo* yielding a light yellow oil. Analytical TLC (silica gel; 1:4; ether: petroleum ether) of the crude product showed it to be mainly starting material (>90%).

APPENDIX 1

MASS SPECTRA

Positive Ion Spectra

All peaks greater than 5% of the base peak (arbitrarily 100%) and certain others of diagnostic value are listed below.

1-(4-METHYLPHENYL)-1-BUTANONE (1)

m/z	65	91	119	120	134	147
%	20	46	100	8	5	8
m/z	162					
%	8					

1-PHENYL-1-BUTANONE (2)

m/z	51	77	105	106	120	148
%	18	48	100	7	6	18

1-(4-CHLOROPHENYL)-1-BUTANONE (3)

m/z	75	111	113	139	140	141
%	26	42	14	100	8	34
m/z	147	154	(156)	(182)	(184)	
%	20	7	(2.5)	(1.5)	(0.5)	

1-(4-BROMOPHENYL)-1-BUTANONE (4)

m/z	50	75	76	77	147	155
%	11	20	24	5	28	25
m/z	157	183	184	185	186	198
%	25	100	9	100	9	6
m/z	200	(226)	(228)			
%	6	(2)	(2)			

1-(4-FLUOROPHENYL)-1-BUTANONE (5)

m/z	75	95	123	124	138	166
%	7	24	100	10	10	10
m/z	167					
%	5					

1-(4-METHOXYPHENYL)-1-BUTANONE (6)

m/z	77	92	107	135	136	150
%	17	12	6	100	8	5
m/z	178					
%	13					

1-(4-CYANOPHENYL)-1-BUTANONE (7)

m/z	75	102	130	131	145	173
%	6	35	100	9	20	18
m/z	174					
%	5					

1-(4-HYDROXYPHENYL)-1-BUTANONE (8)

m/z	39	65	93	121	122	136
%	16	29	22	100	7	7
m/z	164					
%	22					

4-BUTYRYLBENZAMIDE (9)

m/z	65	75	103	104	120	148
%	6	6	19	7	8	100
m/z	149	163	191	192		
%	10	7	29	6		

4-BROMO-4-($^2H_1$)-1-PHENYL-1-BUTANONE (26)

m/z	51	77	105	106	115	116
%	20	18	40	6	48	35
m/z	117	118	119	120	(120)	128
%	12	37	5	5	(4)	12
m/z	129	146	147	148	(225)	(227)
%	17	28	100	26	(<1)	(1)

4-CHLORO-4-($^2H_1$)-1-PHENYL-1-BUTANONE (27)

m/z	39	40	50	51	63	77
%	15	10	15	34	10	60
m/z	78	89	92	105	106	115
%	6	7	5	100	7	25
m/z	116	118	146	147	(183)	(185)
%	14	13	14	35	(1)	(<1)

4-($^{2}H_{1}$)-4-HYDROXY-1-PHENYL-1-BUTANONE (29)

m/z	51	77	78	105	106	108
%	20	55	9	100	10	5
m/z	120	121	122	133	(146)	(147)
%	40	35	5	5	(1)	(2)
m/z	(148)	(149)	165			
%	(3)	(1)	10			

2-ETHYL-1-PHENYL-1-BUTANONE (37)

m/z	39	41	43	51	55	77
%	6	7	7	16	5	42
m/z	105	106	148	176		
%	100	8	7	9		

ACETOPHENONE DIMETHYLAYDRAZONE (40)

m/z	42	43	44	46	50	51
%	37	20	55	22	20	52
m/z	52	77	78	79	103	104
%	10	100	35	10	30	42
m/z	105	106	188	119	132	147
%	13	13	30	10	30	26
m/z	162					
%	58					

4-($^2H_3$)-2-ETHYL-1-PHENYL-1-BUTANONE (44)

m/z	51	60	77	104	105	106
%	9	5	31	6	100	9
m/z	(149)	(151)	(179)			
%	(2)	(3)	(4)			

4-($^2H_3$)-2-ETHYL-1-(4-METHOXYPHENYL)-1-BUTANONE (45)

m/z	64	77	84	86	91	107
%	5	13	5	5	9	6
m/z	135	136	(179)	(181)	209	
%	100	10	(1)	(15)	5	

4-($^2H_3$)-1-(4-CYANOPHENYL)-2-ETHYL-1-BUTANONE (46)

m/z	73	74	75	76	102	103
%	6	9	9	8	34	24
m/z	104	130	131	174	(175)	176
%	5	100	19	9	(3)	16
m/z	204					
%	8					

3-($^2H_2$)-2-ETHYL-1-PHENYL-1-BUTANONE (47)

m/z	51	52	77	78	105	106
%	18	5	50	5	100	10
m/z	148	149	(150)	(178)		
%	5	5	(3)	(2)		

2-ETHYL-1-PHENYL-4-PENTEN-1-ONE (48)

m/z	41	51	55	67	77	78
%	12	17	9	5	72	9
m/z	91	105	106	120	159	160
%	6	100	14	6	10	13
m/z	173	188				
%	13	12				

1-PHENYL-5-HEXEN-1-OL (50)

m/z	39	44	49	53	55	56
%	50	55	30	45	45	20
m/z	57	67	68	84	85	
%	40	100	100	25	15	

1-PHENYL-5-HEXEN-1-ONE

m/z	39	41	51	52	77	78
%	67	45	55	7	93	20
m/z	105	106	120	174		
%	100	7	57	8		

REFERENCES

1. L.P. Hammett, *Physical Organic Chemistry*, McGraw-Hill, New York, 2nd edn., 1970.

2. L. Melander, *Isotope Effects on Reaction Rates*, Ronald Press, New York, 1960.

3. F.H. Westheimer, *Chem. Rev.*, 1961, 61, 265.

4. H.S. Johnston, *Gas Phase Reaction Rate Theory*, Ronald Press, New York, 1966.

5. R.L. Schowen, *Prog. Phys. Org. Chem.*, 1972, 9, 275.

6. A. Fry, *Chem. Soc. Rev.*, 1972, 1, 163.

7. M. Wolfsberg, *Acc. Chem. Res.*, 1972, 5, 225.

8. J. Bigéleisen, M.W. Lee and F. Mandel, *Annu. Rev. Phys. Chem.*, 1973, 24, 407.

9. R.P. Bell, *The Proton in Chemistry*, Chapman and Hall, 2nd edn., 1973.

10. W.A. Van Hook in *Isotope Effects in Chemical Reactions*, edited by J.C. Collins and N.S. Bowman, ACS Monograph 167, Van Nostrand Reinhold, New York, 1971.

11. E.K. Thornton and E.R. Thornton in *Isotope Effects in Chemical Reactions*, edited by J.C. Collins and N.S. Bowman, ACS Monograph 167, Van Nostrand Reinhold, New York, 1971.

12. R.P. Bell, *Chem. Soc. Rev.*, 1974, 3, 513.

13. R.A. More O'Ferrall in *Proton Transfer Reactions*, edited by E.F. Caldin and V. Gold, Halsted Press, a Division of John Wiley and Sons Inc., New York, N.Y., 1975.

14. E.A. Halevi, *Prog. Phys. Org. Chem.*, 1963, 1, 109.

15. A. Streitwieser, Jr., R.H. Jagow, R.C. Fahey and S. Suzuki, *J. Am. Chem. Soc.*, 1958, 80, 2326.

16. D.E. Sunko and S. Borčic in *Isotope Effects in Chemical Reactions*, edited by J.C. Collins and N.S. Bowman, ACS Monograph 167, Van Nostrand Reinhold, New York, 1971.

17. M. Born and J.R. Oppenheimer, *Annalen der Physik*, 1927, 84, 457.

18. A. Eyring and M. Polanyi, *Z. Phys. Chem., Abt. B.*, 1931, 12, 279.

19. S. Glasstone, K. Laidler and H. Eyring, *The Theory of Rate Processes*, McGraw-Hill, New York, 1941.

20. P. Pechukas in *Dynamics of Molecular Collisions*, Part B, edited by W.H. Miller, Plenum Press, New York, 1976.

21. B.C. Garrett and D.G. Truhlar, *J. Am. Chem. Soc.*, 1979, 101, 4534.

22. B.C. Garrett and D.G. Truhlar, *J. Am. Chem. Soc.*, 1980, 102, 2559.

23. B.H. Mahan, *J. Chem. Educ.*, 1974, 51, 709.

24. R.C. Tolman, *The Principles of Statistical Mechanics*, Oxford University Press, London, 1938.

25. R.D. Levine and R.B. Bernstein, *Molecular Reaction Dynamics*, Oxford University Press, New York, 1974; pp. 100-112.

26. H. Eyring, *J. Chem. Phys.*, 1935, 3, 107.

27. K.J. Laidler, *Reaction Kinetics*, Vol. 1, Pergamon Press, Oxford, 1963.

28. K. Müller, *Agnew. Chem., Int. Ed. Engl.*, 1980, 19, 1.

29. W.G. Richards and J.A. Horsley, *Ab Initio Molecular Orbital Calculations for Chemists*, Clarendon Press, Oxford, 1970.

30. A.R. Miller, *J. Am Chem. Soc.*, 1978, 100, 1984.

31. J. Bigeleisen and M. Göeppert-Mayer, *J. Chem. Phys.*, 1947, 15, 261.

32. J. Bigeleisen, *J. Chem. Phys.*, 1949, 17, 675.

33. J. Bigeleisen and M. Wolfsberg, *Adv. Chem. Phys.*, 1958, 1, 15.

34. M. Wolfsberg and M.J. Stern, *Pure Appl. Chem.*, 1964, 8, 225.

35. R.E. Weston and H.A. Schwarz, *Chemical Kinetics*, Prentice-Hall, Englewood Cliffs, N.J., 1972; p. 101.

36. O. Redlich, *Z. Phys. Chem., Abt. B.*, 1935, 28, 371 and E. Teller quoted by W.R. Angus, C.R. Bailen, J.B. Hale, C.K. Ingold, A.H. Leckie, C.G. Raisin, J.W. Thompson and C.L. Wilson, *J. Chem. Soc.*, 1936, 971.

37. G. Herzberg, *Infrared and Raman Spectra of Polyatomic Molecules*, Van Nostrand, New York, 1945.

38. P.E. Yankiwich and R.M. Ikeda, *J. Am. Chem. Soc.*, 1959, 81, 1532.

39. M.J. Stern and M. Wolfsberg, *J. Chem. Phys.*, 1966, 45, 2618.

40. R.A. More O'Ferrall in *Proton Transfer Reactions*, edited by E.F. Caldin and V. Gold, Halsted Press, a Division of John Wiley and Sons Inc., New York, N.Y., 1975; p. 220.

41. N.B. Slater, *J. Chem. Phys.*, 1961, 35, 445.

42. J. Bigeleisen and M. Wolfsberg, *J. Chem. Phys.*, 1953, 21, 1972.

43. A. Fry in *Isotope Effects in Chemical Reactions*, edited by J.C. Collins and N.S. Bowman, ACS Monograph 167, Van Nostrand Reinhold, New York, 1971.

44. K. Kuchitsu, *J. Chem. Phys.*, 1968, 49, 4456.

45. R.W. Wood and D.A. Rank, *Phys. Rev.*, 1935, 47, 792.

46. J.J. Rush, L.W. Schröeder and A.J. Melveger, *J. Chem. Phys.*, 1972, 56, 2793.

47. J.M. Williams and L.F. Schneemeyer, *J. Am. Chem. Soc.*, 1973, 95, 5780.

48. E.R. Thornton, *J. Org. Chem.*, 1962, 27, 1943.

49. R.P. Bell and D.M. Goodall, *Proc. R. Soc. London, Ser. A.*, 1966, 294, 273.

50. J.E. Dixon and T.C. Bruice, *J. Am. Chem. Soc.*, 1970, 92, 905.

51. F.G. Bordwell and W.J. Boyle, Jr., *J. Am. Chem. Soc.*, 1971, 93, 512.

52. D.J. Barnes and R.P. Bell, *Proc. R. Soc. London, Ser. A.*, 1970, 318, 421.

53. E.S. Lewis *Topics in Current Chemistry*, 1978, 74, 32.

54. E.S. Lewis and M.M. Butler, *J. Chem. Soc., Chem. Commun.*, 1971, 941.

55. E.S. Lewis and M.M. Butler, *J. Am. Chem. Soc.*, 1976, 98, 2257.

56. E.S. Lewis and M.M. Butler, *J. Org. Chem.*, 1971, 36, 2582.

57. E.S. Lewis and K. Ogino, *J. Am. Chem. Soc.*, 1976, 98, 2260.

58. W.A. Pryor and K.G. Kneipp, *J. Am. Chem. Soc.*, 1971, 93, 5584.

59. G.A. Russell in *Free Radicals*, edited by J.K. Kochi, Wiley-Interscience, New York, 1973.

60. K.B. Wiberg and L.H. Slaugh, *J. Am. Chem. Soc.*, 1958, 80, 3033.

61. E.S. Lewis and C.C. Shen, *J. Am. Chem. Soc.*, 1977, 99, 3055.

62. E.S. Lewis and S. Kozuka, *J. Am. Chem. Soc.*, 1973, 95, 282.

63. E.S. Lewis and S. Kozuka, *J. Am. Chem. Soc.*, 1976, 98, 2254.

64. E.S. Lewis and K. Ogino, *J. Am. Chem. Soc.*, 1976, 98, 2264.

65. E.S. Lewis and E.C. Nieh, *J. Am. Chem. Soc.*, 1976, 98, 2268.

66. R.P. Bell and B.G. Cox, *J. Chem. Soc., B.*, 1970, 194.

67. A.F. Cockerill, *J. Chem. Soc., B.*, 1967, 964.

68. R.P. Bell and B.G. Cox, *J. Chem. Soc., B.*, 1971, 783.

69. D.W. Earls, J.R. Jones and T.G. Rumney, *J. Chem. Soc., Faraday Trans. 1.*, 1972, 68, 925.

70. L. Melander and N-Å. Bergman, *Acta Chem. Scand.*, 1971, 25, 2264.

71. R.W. Alder, R. Baker and J.M. Brown, *Mechanism in Organic Chemistry*, Wiley-Interscience, a Division of John Wiley and Sons Ltd., London, 1971; p32.

72. D.J. Underwood and J.H. Bowie, *J. Chem. Soc., Perkin Trans. 2.*, 1977, 1670.

73. K.M. Wellman, M.E. Victoriano, P.C. Isolani and J.M. Riveros, *J. Am. Chem. Soc.*, 1979, 101, 2242.

74. G. Hammond, *J. Am. Chem. Soc.*, 1955, 77, 334.

75. J.M. Jasinski and J.I. Brauman, *J. Am. Chem. Soc.*, 1980, 102, 2906.

76. R.F.W. Bader, *Can. J. Chem.*, 1964, 42, 1822.

77. A.V. Willi and M. Wolfsberg, *Chem. Ind. (London)*, 1964, 2097.

78. R.P. Bell, *Discuss. Faraday Soc.*, 1965, 39, 16.

79. W.H. Saunders, Jr., *Chem. Ind. (London)*, 1966, 663.

80. R.A. More O'Ferrall and J. Kouba, *J. Chem. Soc., B*, 1967, 985.

81. W.J. Albery, *Trans. Faraday Soc.*, 1967, 63, 200.

82. A.W. Willi, *Helv. Chim. Acta.*, 1971, 54, 1220.

83. R.P. Bell, W.H. Sachs and R.L. Tranter, *Trans. Faraday Soc.*, 1971, 67, 1995.

84. E.L. Motell, A.W. Boone and W.H. Fink, *Tetrahedron*, 1978, 34, 1619.

85. J. Bigeleisen, *Pure Appl. Chem.*, 1964, 8, 217.

86. R.P. Bell, *Trans. Faraday Soc.*, 1961, 57, 961.

87. A.J. Kresge and Y. Chiang, *J. Am. Chem. Soc.*, 1969, 91, 1025.

88. R.A. More O'Ferrall, G.W. Koeppl and A.J. Kresge, *J. Am. Chem. Soc.*, 1971, 93, 1.

89. R.A. More O'Ferrall, *J. Chem. Soc., B*, 1970, 785.

90. W.H. Saunders, *J. Chem. Soc., Chem. Commun.*, 1973, 850.

91. F.S. Klein, A. Persky and R.E. Weston, Jr., *J. Chem. Phys.*, 1964, 41, 1799.

92. H. Dwart, D.A. Benko and M.E. Bromberg, *J. Am. Chem. Soc.*, 1978, 100, 7093.

93. A.A. Frimer, P.D. Bartlett, A.F. Boschung and J.G. Jewett, *J. Am. Chem. Soc.*, 1977, 99, 7977.

94. A.M. Katz and W.H. Saunders, Jr., *J. Am. Chem. Soc.*, 1969, 91, 4469.

95. W.A. Van Hook in *Isotope Effects in Chemical Reactions*, edited by J.C. Collins and N.S. Bowman, ACS Monograph 167, Van Nostrand Reinhold, New York, 1971; pp. 49-56.

96. E.K. Thornton and E.R. Thornton in *Isotope Effects in Chemical Reactions*, edited by J.C. Collins and N.S. Bowman, ACS Monograph 167, Van Nostrand Reinhold, New York, 1971; pp. 243-246.

97. E.S. Lewis in *Proton Transfer Reactions*, edited by E.F. Caldin and V. Gold, Halsted Press, a Division of John Wiley and Sons Inc., New York, N.Y., 1975.

98. M.D. Harmony, *Chem. Soc. Rev.*, 1972, 1, 211.

99. D. Fărcasiu, *J. Chem. Educ.*, 1975, 52, 76.

100. E. Wigner, *Z. Phys. Chem., Abt. B.*, 1932, 19, 203.

101. H.S. Johnston, *Gas Phase Reaction Rate Theory*, Ronald Press, New York, 1966; p 134.

102. R.P. Bell, *Proc. R. Soc. London, Ser. A.*, 1933, 139, 466.

103. R.P. Bell, *Trans. Faraday Soc.*, 1959, 55, 1.

104a. *Advances in Mass Spectrometry*, Vols., 1-7, Heyden and Son Ltd., London.

104b. *Mass Spectrometry, Specialist Periodical Reports*, Vols., 1-5, The Chemical Society, London.

105. A.L. Burlingame, C.H.L. Shackleton, I.Howe and O.S. Chizhov, *Anal. Chem.*, 1978, 50, 346R.

106. A.L. Burlingame, B.J. Kimble and P.J. Derrick, *Anal. Chem.*, 1976, 48, 368R.

107. A.L. Burlingame, R.E. Cox and P.J. Derrick, *Anal. Chem.*, 1974, 46, 248R.

108. A.L. Burlingame and G.A. Johanson, *Anal. Chem.*, 1972, 44, 337R.

109. D.H. Williams, *Acc. Chem. Res.*, 1977, 10, 280.

110. R.D. Bowen, D.H. Williams and H. Schwarz, *Angew. Chem., Int. Ed. Eng.*, 1979, 18, 451.

111. R.K. Boyd and J.H. Beynon, *Int. J. Mass Spectrom. Ion Phys.*, 1977, 23, 163.

112. T.W. Bentley in *Mass Spectrometry, Specialist Periodical Reports*, Vol. 5, R.A.W. Johnstone, Senior Reporter, The Chemical Society, London, 1979; p. 64.

113. C. Lifshitz in *Advances in Mass Spectrometry*, Vol. 7A, edited by N.R. Daly, Heyden and Son Ltd., London, 1978; p. 3.

114. W.J. Chesnavich and M.T. Bowers in *Gas Phase Ion Chemistry*, Vol. 1, edited by M.T. Bowers, Academic Press Inc., New York, 1979; p. 119.

115. J.L. Franklin in *Gas Phase Ion Chemistry*, Vol. 1, edited by M.T. Bowers, Academic Press Inc., New York, 1979; p. 273.

116. J.A. Pople, *Int. J. Mass Spectrom. Ion Phys.*, 1976, 19, 89.

117. D.H. Williams in *Advances in Mass Spectrometry*, Vol. 7B, edited by N.R. Daly, Heyden and Son, Ltd., London, 1978; p. 1157.

118. J.L. Holmes in *Mass Spectrometry*, Vol. 5, edited by A. Maccoll, MTP International Review of Science, Physical Chemistry, Series II, Butterworth, London, 1975.

119. J.L. Holmes in *Isotopes in Organic Chemistry*, Vol. 1, edited by E. Buncel and C.C. Lee, Elsevier Scientific Publishing Company, Amsterdam, 1975; p. 61.

120. K. Levsen and H. Schwarz, *Angew. Chem., Int. Ed. Eng.*, 1976, 15, 509.

121. T.A. Lehman and M.M. Bursey, *Ion Cyclotron Resonance Spectrometry*, John Wiley and Sons, Inc., New York, 1976.

122. A. McCormick in *Mass Spectrometry, Specialist Periodical Reports*, Vol. 5, R.A.W. Johnstone, Senior Reporter, The Chemical Society, London, 1979; pp. 135-139.

123. J.H.D. Eland in *Mass Spectrometry, Specialist Periodical Reports*, Vol. 5, R.A.W. Johnstone, Senior Reporter, The Chemical Society, London, 1979; pp. 91-98.

124. E.G. Johnson and A.O. Nier, *Phys. Rev.*, 1953, 91, 10.

125. W.A. Chupka, *J. Chem. Phys.*, 1959, 30, 191.

126. J.A. Hipple and E.U. Condon, *Phys. Rev.*, 1946, 69, 347.

127. K.R. Jennings, *J. Chem. Phys.*, 1965, 43, 4176.

128. J.H. Futrell, K.R. Ryan and L.W. Sieck, *J. Chem. Phys.*, 1965, 43, 1832.

129. M. Barber and R.M. Elliott, *12th Annual Conference on Mass Spectrometry and Allied Topics*, Committee E.14, A.S.T.M., Montreal, June 1964.

130. J.H. Beynon, R.M. Caprioli, W.E. Baitinger and J.W. Amy, *Int. J. Mass Spectrom. Ion Phys.*, 1969, 3, 313.

131. J.H. Beynon, J.W. Amy and W.E. Baitinger, *J. Chem. Soc., Chem. Commun.*, 1969, 723.

132. R.W. Kiser, R.E. Sullivan and M.S. Lupin, *Anal. Chem.*, 1969, 41, 1958.

133. J.H. Beynon, R.M. Caprioli and T. Ast, *Org. Mass Spectrom.*, 1971, 5, 229.

134. J.H. Beynon, R.G. Cooks, J.W. Amy, W.E. Baitinger and T.Y. Ridley, *Anal. Chem.*, 1973, 45, 1023A.

135. R.K. Boyd and J.H. Beynon, *Org. Mass Spectrom.*, 1977, 12, 163.

136. D.S. Millington and J.A. Smith, *Org. Mass Spectrom.*, 1977, 12, 264.

137. B. Munson, *Anal. Chem.*, 1977, 49, 772A.

138. P.J. Derrick in *Mass Spectrometry, Specialist Periodical Reports*, Vol. 4, R.A.W. Johnstone, Senior Reporter, The Chemical Society, London, 1977; pp. 132-145.

139. H.-R. Schulten in *Advances in Mass Spectrometry*, Vol. 7A, edited by N.R. Daly, Heyden and Son, Ltd., London, 1978; p. 83.

140. D.S. Simons, B.N. Colby and C.A. Evans, *Int. J. Mass Spectrom. Ion Phys.*, 1974, 15, 291.

141. D.I. Carroll, I. Dzidic, R.N. Stillwell, M.G. Horning and E.C. Horning, *Anal. Chem.*, 1974, 46, 706.

142. T. Baer in *Gas Phase Ion Chemistry*, Vol. 1, edited by M.T. Bowers, Academic Press, Inc., New York, 1979; pp. 153-196.

143. R.D. Macfarlane and D.F. Torgerson, *Science*, 1976, 191, 920.

144. J.H. Bowie and B.D. Williams in *Mass Spectrometry*, Vol. 5, edited by A. Maccoll, MTP International Review of Science, Physical Chemistry, Series II, Butterworths, London, 1975.

145. J. Franck, *Trans. Faraday Soc.*, 1925, 21, 536.

146. E.U. Condon, *Phys. Rev.*, 1928, 32, 858.

147. E. Lindholm in *Ion-Molecule Reactions*, Vol. 2, edited by J. Franklin, Plenum Press, New York, 1972; p. 457.

148. B. Brehm and E.van Puttkamer in *Advances in Mass Spectrometry*, edited by E. Kendrick, The Elsevier Publishing Company, Amsterdam, 1968; p.591.

149. J.B. Cumming and P. Kebarle, *Canad. J. Chem.*, 1978, 56, 1.

150. D. Smith and N.G. Adams in *Gas Phase Ion Chemistry*, Vol. 1, edited by M.T. Bowers, Academic Press, New York, 1979, p. 2.

151. H.M. Rosenstock, M.B. Wallenstein, A.L. Wahrhaftig and E. Eyring, *Proc. Natl. Acad. Sci.*, 1952, 38, 667.

152. R.A. Marcus, *J. Chem. Phys.*, 1952, 20, 352.

153. R.A. Marcus, *J. Chem. Phys.*, 1952, 20, 359.

154. R.A. Marcus and O.K. Rice, *J. Phys. and Colloid Chem.*, 1959, 30, 735.

155. O.K. Rice, *J. Phys. Chem.*, 1961, 65, 1588.

156. D.H. Williams and I. Howe, *Principles of Mass Spectrometry*, McGraw-Hill Book Company (UK) Ltd, London, 1972; pp. 46-74.

157. R.G. Cooks, J.H. Beynon, R.M. Caprioli and G.R. Lester, *Metastable Ions*, Elsevier Scientific Publishing Company, Amsterdam, 1973; pp. 217-254.

158. B.S. Rabinovitch and D.W. Setser, *Advan. Photochem.*, 1964, 3, 1.

159. P.J. Robinson and K.A. Holbrook, *Unimolecular Reactions*, John Wiley and Sons Inc., (Interscience Division), New York, 1972.

160. W.L. Hase in *Modern Theoretical Chemistry*, Part B, Plenum Press, New York, 1976.

161. W.J. Chesnavitch and M.T. Bowers, *J. Am. Chem. Soc.*, 1976, 98, 8301.

162. W.J. Chesnavitch and M.T. Bowers, *J. Am. Chem. Soc.*, 1977, 99, 1705.

163. J.L. Franklin in *Gas Phase Ion Chemistry*, Vol. 1, edited by M.T. Bowers, Academic Press, Inc., New York, 1979; pp. 276-277.

164. B. Brehm, R. Frey, A. Küstler and J.H.D. Eland, *Int. J. Mass Spectrom. Ion Phys.*, 1974, 13, 251.

165. B. Brehm, J.H.D. Eland, R. Frey and A. Küstler, *Int. J. Mass Spectrom. Ion Phys.*, 1973, 12, 197.

166. J.H.D. Eland, R. Frey, H. Schulte and B. Brehm, *Int. J. Mass Spectrom. Ion Phys.*, 1976, 21, 209.

167. J.H.D. Eland, R. Frey, A. Kuestler, H. Schulte and B. Brehm, *Int. J. Mass Spectrom. Ion Phys.*, 1976, 22, 155.

168. B. Brehm, J.H.D. Eland, R. Frey and H. Schulte, *Int. J. Mass Spectrom. Ion Phys.*, 1976, 21, 373.

169. J. Sunner and I. Szabo, *Int. J. Mass Spectrom. Ion Phys.*, 1977, 25, 241.

170. P.F. Knewstubb and N.W. Reed, *Int. J. Mass Spectrom. Ion Phys.*, 1970, 5, 361.

171. J.F. Elder, Jr., J.H. Beynon and R.G. Cooks, *Org. Mass Spectrom.*, 1976, 11, 415.

172. R. Stockbauer, *Int. J. Mass Spectrom. Ion Phys.*, 1977, 25, 89.

173. R. Stockbauer, H.M. Rosenstock, *Int. J. Mass Spectrom. Ion Phys.*, 1978, 27, 185.

174. F.W. McLafferty, T. Wachs, C. Lifshitz, G. Innorta and P. Irving, *J. Am. Chem. Soc.*, 1970, 92, 6867.

175. J.R. Gilbert and A.J. Stace, *Org. Mass Spectrom.*, 1975, 10, 1032.

176. J.R. Gilbert and A.J. Stace, *Int. J. Mass Spectrom. Ion Phys.*, 1974, 15, 311.

177. E.G. Jones, J.H. Beynon and R.G. Cooks, *J. Chem. Phys.*, 1972, 57, 2652.

178. J.H. Beynon, R.M. Caprioli, W.E. Baitinger and J.W. Amy, *Org. Mass Spectrom.*, 1970, 3, 661.

179. J.L. Holmes and A.D. Osborne, *Int. J. Mass Spectrom. Ion Phys.*, 1977, 23, 189.

180. J.R. Christie, P.J. Derrick and G.J. Rickard, *J. Chem. Soc., Faraday 2*, 1978, 74, 304.

181. M.G. Evans and M. Polanyi, *Trans. Faraday Soc.*, 1939, 35, 178.

182. J.C. Polanyi, *Acc. Chem. Res.*, 1972, 5, 161.

183. U. Löhle and Ch. Ottinger, *J. Chem. Phys.*, 1969, 51, 3097.

184. K.C. Smyth and T.W. Shannon, *J. Chem. Phys.*, 1969, 51, 4633.

185. G. Hvistendahl and D.H. Williams, *J. Chem. Soc., Perkin Trans. 2.*, 1975, 881.

186. D.H. Williams and G. Hvistendahl, *J. Am. Chem. Soc.*, 1974, 96, 6753.

187. D.H. Williams and G. Hvistendahl, *J. Am. Chem. Soc.*, 1974, 96, 6755.

188. G. Hvistendahl and D.H. Williams, *J. Chem. Soc., Chem. Commun.*, 1975, 4.

189. M.J.S. Dewar, *Disc. Faraday. Soc.*, 1977, 62, 197.

190. M.J.S. Dewar and H.S. Rzepa, *J. Am. Chem. Soc.*, 1977, 99, 7432.

191. J. Rigaudy and S.P. Klesney, *Nomenclature of Organic Chemistry; Sections A, B, C, D, E, F and H*, International Union of Pure and Applied Chemistry, Pergamon Press, 1979.

192. G.P. Happ and D.W. Stewart, *J. Am. Chem. Soc.*, 1952, 74, 4404.

193. A.J.C. Nicholson, *Trans. Faraday Soc.*, 1954, 50, 1067.

194. F.W. McLafferty, *Anal. Chem.*, 1956, 28, 306.

195. D.G.I. Kingston, J.T. Bursey and M.M. Bursey, *Chem. Rev.*, 1974, 2, 215.

196. S. Meyersen and J.D. McCollum, *Adv. Anal. Chem. Instrum.*, 1963, 2, 179.

197. H. Budzikiewicz, C. Djerassi and D.H. Williams, *Mass Spectrometry of Organic Compounds*, Holden-Day, Inc., San Francisco, 1967; pp. 155-162.

198. J.H. Bowie in *The Chemistry of Carbonyl Compounds*, Vol. 2, edited by J. Zabicky, Interscience, New York, N.Y., 1970.

199. J. Diekman, J.K. McLeod, C. Djerassi and J.D. Baldeschwieler, *J. Am. Chem. Soc.*, 1969, 91, 2069.

200. G. Eadon, J. Diekman and C. Djerassi, *J. Am. Chem. Soc.*, 1970, 92, 6205.

201. W. Carpenter, A.M. Duffield and C. Djerassi, *J. Am. Chem. Soc.*, 1968, 90, 160.

202. A.N.H. Yeo and D.H. Williams, *J. Am. Chem. Soc.*, 1969, 91, 3582.

* 203. A.H.H. Yeo, R.G. Cooks and D.H. Williams, *J. Chem. Soc., Chem. Commun.*, 1968, 1269.

204. D.J. McAdoo, D.N. Witiak and F.W. McLafferty, *J. Am. Chem. Soc.*, 1977, 99, 7265.

205. F.M. Benoit and A.G. Harrison, *Org. Mass Spectrom.*, 1976, 11, 1056.

206. S. Hammerum, unpublished results.

207. R.P. Morgan and P.J. Derrick, *J. Chem. Soc., Chem. Commun.*, 1974, 836.

208. P.J. Derrick, A.M. Falick and A.L. Burlingame, *J. Am. Chem. Soc.*, 1974, 96, 615.

209. P.J. Derrick, A.M. Falick, S. Lewis and A.L. Burlingame, *J. Phys. Chem.*, 1979, 83, 1567.

210. C. Djerassi, G. von Mutzenbecher, J. Fajkos, D.H. Williams and H. Budzikiewicz, *J. Am. Chem. Soc.*, 1065, 87, 817.

211. D.H. Williams and C. Djerassi, *Steroids*, 1964, 3, 259.

212. C. Djerassi and L. Tökés, *J. Am. Chem. Soc.*, 1966, 88, 536.

213. L. Tökés, R.T. LaLonde and C. Djerassi, *J. Org. Chem.*, 1967, 32, 1020.

214. A.F. Thomas and B. Willhalm, *Helv. Chim. Acta.*, 1967, 50, 826.

215. F.P. Boer, T.W. Shannon and F.W. McLafferty, *J. Am. Chem. Soc.*, 1968, 90, 7239.

216. J.D. Henion and D.G.I. Kingston, *J. Am. Chem. Soc.*, 1974, 96, 2532.

217. J.K. Crandall and D.R. Paulson, *J. Org. Chem.*, 1968, 33, 991.

218. J. March, *Advanced Organic Chemistry: Reactions, Mechanisms and Structure*, second edition, McGraw-Hill Kogakusha, Ltd., 1977; p. 72.

219. W.J. Bauma, D. Poppinger and L. Radom, *J. Am. Chem. Soc.*, 1977, 99, 6443.

220. E. Murad and M.G. Inghram, *J. Chem. Phys.*, 1964, 40, 3263.

221. T.W. Bentley and R.A.W. Johnstone, *Advan. Phys. Org. Chem.*, 1970, 8, 151.

222. C.C. Van de Sande and F.W. McLafferty, *J. Am. Chem. Soc.*, 1975, 97, 4613.

223. C.C. Van de Sande and F.W. McLafferty, *J. Am. Chem. Soc.*, 1975, 97, 4617.

224. K. Levsen and H. Schwarz, *J. Chem. Soc., Perkin 2*, 1976, 1231.

225. S.K. Pollack and W.J. Hehre, *J. Am. Chem. Soc.*, 1977, 99, 4845.

226. J.L. Holmes, J.K. Terlouw and F.P. Lossing, *J. Phys. Chem.*, 1976, 80, 2860.

227. J.L. Holmes and F.P. Lossing, *Org. Mass Spectrom.*, 1979, 14, 512.

228. J.L. Holmes and F.P. Lossing, *J. Am. Chem. Soc.*, 1980, 102, 3732.

229. J.L. Holmes and F.P. Lossing, *J. Am. Chem. Soc.*, 1980, 102, 1591.

230. A.F. Thomas, B. Willhalm and J.H. Bowie, *J. Chem. Soc. B.*, 1967, 392.

231. D.J. McAdoo, F.W. McLafferty and J.S. Smith, *J. Am. Chem. Soc.*, 1970, 92, 6343.

232. F.W. McLafferty, D.J. McAdoo, J.S. Smith and R. Kornfeld, *J. Am. Chem. Soc.*, 1971, 93, 3720.

233. J.H. Beynon, R.M. Caprioli and R.G. Cooks, *Org. Mass Spectrom.*, 1974, 9, 1.

234. J.L. Holmes in *Mass Spectrometry*, Vol. 5, edited by A. Maccoll, MTP International Review of Science, Physical Chemistry, Series II, Butterworth, London, 1975; pp. 235-240.

235. J.L. Holmes in *Isotopes in Organic Chemistry*, edited by E. Bancel and C.C. Lee, Elsevier, Amsterdam, 1975; pp. 86-87.

236. T.A. Molenaar-Langeveld, N.M.M. Nibbering, R.P. Morgan and J.H. Beynon, *Org. Mass Spectrom.*, 1978, 13, 172.

237. J. Diekman, J.K. McLeod, C. Djerassi and J.D. Baldeschwieler, *J. Am. Chem. Soc.*, 1969, 91, 2069.

238. S. Meyerson, C. Fenselau, J.L. Young, W.R. Lardis, E. Selke and L.C. Leitch, *Org. Mass Spectrom.*, 1970, 3, 689.

239. D.G.I. Kingston, H.P. Tannenbaum, G.B. Baker, J.R. Dimmock and W.G. Taylor, *J. Chem. Soc., C.*, 1970, 2574.

240. J.R. Hass, M.M. Bursey, D.G.I. Kingston and H.P. Tannenbaum, *J. Am. Chem. Soc.*, 1972, 94, 5095.

241. D.B. Bigley and J.C. Thurman, *Tetrahedron Lett.*, 1967, 2377.

242. K.J. Laidler, *Chemical Kinetics*, McGraw-Hill, New York, 1950; p.66.

243. R.G.W. Norrish, *Trans. Faraday Soc.*, 1937, 33, 1521.

244. G.R. McMillan, J.G. Calvert and J.N. Pitts, Jr., *J. Am. Chem. Soc.*, 1964, 86, 3602.

245. P.J. Wagner and G.S. Hammond, *J. Am. Chem. Soc.*, 1966, 88, 1245.

246. E.J. Baum, J.K.S. Wan and J.N. Pitts, Jr., *J. Am. Chem. Soc.*, 1966, 88, 2652.

247. P.J. Wagner, *Acc. Chem. Res.*, 1971, 4, 168.

248. P.J. Wagner, P.A. Kelso and R.G. Zepp, *J. Am. Chem. Soc.*, 1972, 94, 7480.

249. F.W. McLafferty and T. Wachs, *J. Am. Chem. Soc.*, 1967, 89, 5043.

250. M.M. Bursey and F.W. McLafferty, *J. Am. Chem. Soc.*, 1967, 89, 1.

251. F.W. McLafferty, *J. Chem. Soc., Chem. Commun.*, 1968, 956.

252. R. Gooden and J.I. Brauman, *J. Am. Chem. Soc.*, 1977, 99, 1977.

253. M.S. Kim, R.C. Dunbar and F.W. McLafferty, *J. Am. Chem. Soc.*, 1978, 100, 4600.

254. M.S. Kim and F.W. McLafferty, *J. Phys. Chem.*, 1978, 82, 501.

255. M.M. Green, J.M. Moldawan, M.W. Armstrong, T.L. Thompson, K.J. Sprague, A.J. Hass and J.J. Artus, *J. Am. Chem. Soc.*, 1976, 98, 849.

256. M.M. Green, J.G. McGrew II and J.M. Moldowan, *J. Am. Chem. Soc.*, 1971, 93, 6700.

257. M.M. Green, J.M. Moldowan and J.G. McGrew II, *J. Org. Chem.*, 1974, 39, 2166.

258. M.M. Green, G.J. Mayotte, L. Meites and D. Forsyth, *J. Am. Chem. Soc.*, 1980, 102, 1466.

259. D.H. Williams, H. Budzikiewicz and C. Djerassi, *J. Am. Chem. Soc.*, 1964, 86, 284.

260. C. Djerassi and J.K. McLeod, *Tetrahedron Lett.*, 1966, 2183.

261. J.K. McLeod and C. Djerassi, *J. Am. Chem. Soc.*, 1967, 89, 5182.

262. E.D. Amstutz, *J. Am. Chem. Soc.*, 1949, 71, 3836.

263. M.S. Kharasch and O. Reinmuth, *Grignard Reactions of Nonmetallic Substances*, Constable and Company, Ltd., London, 1954; p. 769.

264. E.J. Corey and J.W. Suggs, *Tetrahedron Lett.*, 1975, 2647.

265. V. Prey, *Ber. Dtsch. Chem. Ges.*, 1941, 74, 1219.

266. J.S. Buck and W.S. Ide, *Org. Synth. Coll. Vol.*, 1943, 2, 44.

267. C.R. Noller and R. Dinsmore, *Org. Synth., Coll. Vol.*, 1943, 2, 358.

268. S. Searles, Jr., K.A. Pollart and E.F. Lutz, *J. Am. Chem. Soc.*, 1957, 79, 948.

269. C.R. Noller, *Org. Synth., Coll. Vol.*, 1955, 3, 835.

270. H.C. Brown and Y. Okamoto, *J. Am. Chem. Soc.*, 1958, 80, 4979.

271. M.S. Kharasch and O. Reinmuth, *Grignard Reactions of Nonmetallic Substances*, Constable and Company Ltd., London, 1954; pp. 1237-1243.

272. D.A. Shirley, *Org. React.*, 1954, 8, 28.

273. R. Adams and L.H. Ulich, *J. Am. Chem. Soc.*, 1920, 42, 599.

274. H.C. Brown and M.M. Rogić, *J. Am. Chem. Soc.*, 1969, 91, 2146.

275. H.C. Brown, M.M. Rogić, H. Nambu and M.W. Rathke, *J. Am. Chem. Soc.*, 1969, 91, 2147.

276. J.L. Beauchamp and J.T. Armstrong, *Rev. Sci. Instrum.*, 1969, 40, 123.

277. J.L. Beauchamp, L.R. Anders and J.D. Baldeschwieler, *J. Am. Chem. Soc.*, 1967, 89, 4569.

278. R.C. Huston and H.M. D'Arcy, *J. Org. Chem.*, 1953, 18, 16.

279. P.E. Pfeffer and L.S. Silbert, *J. Org. Chem.*, 1970, 35, 262.

280. P.L. Creger, *J. Am. Chem. Soc.*, 1967, 89, 2500.

281. A.I. Vogel, *A Textbook of Practical Organic Chemistry*, Longmans, London, 1964; p. 384.

282. M.W. Rathke and A. Lindert, *J. Am. Chem. Soc.*, 1971, 93, 2318.

283. *Handbook of Chemistry and Physics*, edited by R.C. West, CRC Press, Ohio, 1974; pp. F207-F211.

284. A.L.J. Beckwith and G. Moad, *J. Chem. Soc., Perkin Trans 2*, 1975, 1726.

285. L.F. Fieser and M. Fieser, *Reagents for Organic Synthesis*, John Wiley and Sons, Inc., New York, 1967; p. 1180.

286. H.P. Ward and P.D. Sherman, Jr., *J. Am. Chem. Soc.*, 1968, 90, 3812.

287. G.J. Heiszwolf and H. Kloosterziel, *Rec. Trav. Chim. Pays-Bas.*, 1970, 89, 1152.

288. M. Makosza in *Modern Synthetic Methods*, edited by R. Scheffold, Assn. of Swiss Chemists, 1976; pp. 49-58.

289. C.A. Brown, *J. Org. Chem.*, 1974, 39, 1324.

290. C.A. Brown, *J. Org. Chem.*, 1974, 39, 3913.

291. H.O. House, *Modern Synthetic Reactions*, W.A. Benjamin, Inc., California, 1972, 2nd edn.; p. 551.

292. G.R. Newkome and D.L. Fishel, *J. Org. Chem.*, 1966, 31, 677.

293. E.J. Corey and D. Enders, *Tetrahedron Lett.*, 1976, 3.

294. E.J. Corey and S. Knapp, *Tetrahedron Lett.*, 1976, 3667.

295. M.G. Darcy, D.E. Rogers and P.J. Derrick, *Int. J. Mass Spectrom. Ion Phys.*, 1978, 27, 335.

296. P.J. Derrick in *Advances in Mass Spectrometry*, Vol. 7A, edited by N.R. Daly, Heyden and Son, Ltd., London, 1978; p. 143.

297. M.E. Jung and P.L. Ornstein, *Tetrahedron Lett.*, 1977, 2659.

298. M.E. Jung, M.A. Mazurek and R.M. Lim, *Synthesis*, 1978, 588.

299. P.J. Wagner and K-C. Lin, *J. Am. Chem. Soc.*, 1974, 96, 5952.

300. G. Stork and S.R. Dowd, *J. Am. Chem. Soc.*, 1963, 85, 2178.

301. H.E. Simmons, T.L. Cairns, S.A. Vladuchick and C.M. Hoiness, *Org. React.*, 1973, 20, 1.

302. L.B. Sims, A. Fry, L.T. Netherton, J.C. Wilson, K.D. Reppond and S.W. Crook, *J. Am. Chem. Soc.*, 1972, 94, 1364.

303. G.W. Burton, L.B. Sims, J.C. Wilson and A. Fry, *J. Am. Chem. Soc.*, 1977, 99, 3371.

304. G.W. Burton, L.B. Sims and D.J. McLennan, *J. Chem. Soc., Perkin Trans. 2*, 1977, 1763.

305. G.W. Burton, L.B. Sims and D.J. McLennan, *J. Chem. Soc., Perkin Trans. 2*, 1977, 1847.

306. D.E. Lewis, L.B. Sims, H. Yamataka and J. McKenna, submitted for publication (1980).

307. H. Yamataka, J.C. Wilson, L.B. Sims, A. Fry and D.E. Lewis, submitted for publication (1980).

308. J.L. Hogg, J. Rodgers, I. Korach and R.L. Schowen, *J. Am. Chem. Soc.*, 1980, 102, 79.

309. G. Klass, D.J. Underwood and J.H. Bowie, *Aust. J. Chem.*, 1980 in press.

310. L.B. Sims, G.W. Burton and D.E. Lewis, *BEBOVIB-IV*, Q.C.P.E. Program No. 337, 1977.

311. E.B. Wilson, Jr., J.C. Decius and P.C. Cross, *Molecular Vibrations*, McGraw-Hill Book Company, New York, N.Y., 1955; pp. 175-176.

312. G. Gerzberg, *Molecular Spectra and Structure, Part II: Infrared and Raman Spectra of Polyatomic Molecules*, D. Van Nostrand, Princeton, N.J., 1945.

313. J.H. Schachtschneider and R.G. Snyder, *Spectrochim. Acta*, 1963, 19, 117.

314. R.G. Snyder and J.H. Schachtschneider, *Spectrochim. Acta*, 1969, 30, 290.

315. R.G. Snyder and J.H. Schachtschneider, *Spectrochim. Acta*, 1965, 21, 169.

316. L. Pauling, *J. Am. Chem. Soc.*, 1947, 69, 542.

317. *Table of Interatomic Distances and Configurations in Molecules and Ions*, Special Publications, Nos. 11 and 18, The Chemical Society, London, 1958, 1965.

318. H.S. Johnston, *Gas Phase Reaction Rate Theory*, Ronald Press, New York, N.Y., 1966; Chapter 4.

319. D.R. Herschback and V.W. Laurie, *J. Chem. Phys.*, 1961, 35, 458.

320. W.E. Buddenbaum and P.E. Yankwich, *J. Phys. Chem.*, 1967, 71, 3136.

321. W.D. Gwinn, *J. Chem. Phys.*, 1971, 55, 477.

322. H.L. Sellers, L.B. Sims, L. Schafer and D.E. Lewis, *J. Mol. Struct.*, 1977, 41, 149.

323. M.J. Stern and M. Wolfsberg, *J. Chem. Phys.*, 1966 45, 4105.

324. L.B. Sims, private communication.

325. J. March, *Advanced Organic Chemistry: Reactions, Mechanisms and Structure*, second edition, McGraw-Hill Kogakusha, Ltd., Tokyo, 1977; pp. 124-128.

326. J.C. Decius, *J. Chem. Phys.*, 1949, 17, 1315.

327. M. Berthelot and C. Lawrence, *Canad. J. Chem.*, 1975, 53, 993.

328. C.A. Coulson, *Valence*, 2nd edn., Oxford University Press, London, 1961; p. 269.

329. S.R. Hartshorn and V.J. Shriner, *J. Am. Chem. Soc.*, 1972, 94, 9002.

330. W.J. Bouma, J.K. MacLeod and L. Radom, *J. Am. Chem. Soc.*, 1980, 102, 2246.

331. P.J. Robinson and K.A. Holbrook, *Unimolecular Reactions*, John Wiley and Sons Inc., (Interscience Division), New York, 1972; pp. 160-161, 171-182.

332. K.A. Holbrook, J.S. Palmer, K.A.W. Parry and P.J. Robinson, *Trans. Faraday Soc.*, 1970, 66, 869.

333. K.D. King, and R.D. Goddard, *J. Am. Chem. Soc.*, 1975, 97, 4504.

334. R.G. Cooks, J.H. Beynon, R.M. Caprioli and G.R. Lester, *Metastable Ions*, Elsevier Scientific Publishing Company, Amsterdam, 1973; p. 108.

335. R.G. Cooks, J.H. Beynon, R.M. Caprioli and G.R. Lester, *Metastable Ions*, Elsevier Scientific Publishing Company, Amsterdam, 1973; pp. 101-104.

336. D.J. Carlsson and K.U. Ingold, *J. Am. Chem. Soc.*, 1968, 90, 7047.

337. B. Maillard, D. Forrest and K.U. Ingold, *J. Am. Chem. Soc.*, 1976, 98, 7024.

338. J.H. Bowie and S. Hart, *Int. J. Mass Spectrom. Ion Phys.*, 1974, 13, 319.

339. T.B. McMahon and J.L. Beauchamp, *Rev. Sci. Instrum.*, 1971, 42, 1632.

340. J.H. Bowie and B.D. Williams, *Aust. J. Chem.*, 1974, 27, 1923.

341. H. Gilman, J.A. Beel, C.G. Brannen, M.W. Bullock, G.E. Dunn and L.S. Miller, *J. Am. Chem. Soc.*, 1949, 71, 1499.

342. W.G. Kofron and L.M. Baclawski, *J. Org. Chem.*, 1976, 41, 1879.

343. M.S. Kharasch and O. Reinmuth, *Grignard Reactions of Nonmetallic Substances*, Constable and Company, Ltd., London, 1954; chapter 2.

344. I. Tsukervanik and I. Terent'eva *Zh. Obshch. Khim.*, 1940, 10, 1405.

345. L.F. Fieser, *J. Am. Chem. Soc.*, 1953, 75, 4400.

346. J.A.V. Butler, D.W. Thomson and W.H. MacLennan, *J. Chem. Soc.*, 1933, 674.

347. S. Skraup and F. Nielen, *Ber. Dtsch. Chem. Ges.*, 1924, 57, 1294.

348. L.F. Fieser and M. Fieser, *Reagents for Organic Synthesis*, Vol. 1, John Wiley and Sons, Inc., New York, 1967; pp. 142-143.

349. G.T. Morgan and W.J. Hickinbottom, *J. Chem. Soc.*, 1921, 119, 1885.

350. H. Oelschlager, *Annalen der Chemie*, 1961, 641, 81.

351. Ng.Ph. Buu - Hoi, Ng.Hoān, P. Jacquignon, *Recueil das Travaux Chimiques des Pays-Bas*, 1949, 68, 781.

352. S.F. Birch, R.A. Dean, F.A. Fidler and R.A. Lowry, *J. Am. Chem. Soc.*, 1949, 71, 1362.

353. W.H. Perkin, *J. Chem. Soc.*, 1889, 55, 548.

354. H. Gilman and L.L. Heck, *J. Am. Chem. Soc.*, 1930, 52, 4949.

355. G.T.O. Martin and J.R. Partington, *J. Chem. Soc.*, 1936, 1175.

356. J. Cason, *J. Am. Chem. Soc.*, 1946, 68, 2078.

357. H.C. Brown, *Organic Synthesis via Boranes*, John Wiley and Sons, New York, 1975; p. 18.

358. E.F. Knights and H.C. Brown, *J. Am. Chem. Soc.*, 1968, 90, 5280.

359. H.C. Brown, *Organic Synthesis via Boranes*, John Wiley and Sons, New York, 1975; p.32.

360. L.C. King and G.K. Ostrum, *J. Org. Chem.*, 1964, 29, 3459.

361. H.C. Brown, N. Nambu and M.M. Rogić, *J. Am. Chem. Soc.*, 1969, 91, 6855.

362. J.W. Lynn and J. English, Jr., *J. Org. Chem.*, 1951, 16, 1546.

363. S.A. Mumford and J.W.C. Phillips, *J. Chem. Soc.*, 1950, 75.

364. L.F. Somerville and C.F.H. Allen, *Org. Synth., Coll. Vol.*, 1943, 2, 81.

365. C.V. Vhelintzev and E.D. Osetrova, *C.R. (Dokl.) Acad. Sci. URSS*, 1935, 3, 251.

366. G. Baddeley and R. Williamson, *J. Chem. Soc.*, 1956, 4647.

367. B.E. Hudson, Jr., and C.R. Hauser, *J. Am. Chem. Soc.*, 1941, 63, 3163.

368. A. Jończyk, B. Serafin and M. Makosza, *Tetrahedron Lett.*, 1971, 1351.

369. A. Brändström and U. Jungen, *Tetrahedron Lett.*, 1972, 473.

370. J. Klein and A. Medlik-Balan, *J. Org. Chem.*, 1976, 41, 3307.

371. C. Cherrier and J. Metzger, *C.R. Acad. Sci.*, 1948, 226, 797.

372. P.J. Wagner and A.E. Kemppainen, *J. Am. Chem. Soc.*, 1972, 94, 7495.

373. F. Arndt, *Org. Syn., Coll. Vol.*, 1943, 2, 461.